Engineering Materials

Kapil Gupta *Editor*

Micro and Precision Manufacturing

Springer

Engineering Materials

The “Engineering Materials” series provides topical information on innovative, structural and functional materials and composites with applications in optical, electronical, mechanical, civil, aeronautical, medical, bio and nano engineering. The individual volumes are complete, comprehensive monographs covering the structure, properties, manufacturing process and applications of these materials. This multidisciplinary series is devoted to professionals, students and all those interested in the latest developments in the Materials Science field.

More information about this series at http://www.springer.com/series/4288

Kapil Gupta
Editor

Micro and Precision Manufacturing

Springer

Editor
Kapil Gupta
Department of Mechanical and Industrial
Engineering Technology
University of Johannesburg
Johannesburg
South Africa

ISSN 1612-1317 ISSN 1868-1212 (electronic)
Engineering Materials
ISBN 978-3-319-68800-8 ISBN 978-3-319-68801-5 (eBook)
https://doi.org/10.1007/978-3-319-68801-5

Library of Congress Control Number: 2017954465

Printed on acid-free paper

This Springer imprint is published by Springer Nature
The registered company is Springer International Publishing AG
The registered company address is: Gewerbestrasse 11, 6330 Cham, Switzerland

Preface

Micro-manufacturing and precision manufacturing entail the use of sophisticated techniques in order to attain special manufacturing requirements, such as precision machining and finishing of various DTM, bio and smart materials; micro-manufacturing of mechanical components; machining of intricate shapes and features; and precision finishing of engineered products. To accomplish the aforementioned tasks, a number of conventional and advanced processes are strategically exploited. Therefore, knowledge of working principle, process mechanism, and control and accuracy of these processes is essential for their successful implementation.

This book consists of a total of eight chapters emphasizing novel aspects, current trends and latest developments in micro- and precision manufacturing. Chapter "Machining of Microshapes and Features" details manufacturing of micro-shapes and features by various conventional and advanced processes. Chapter "Electrochemical Methods of Micropart's Manufacturing" describes mechanism and working of electrochemical machining for micro-parts manufacturing. Chapter "Precision Photochemical Machining" is dedicated to precision photochemical machining. Chapter "Nano-Machining, Nano-Joining and Nano-Welding" highlights the development of nano-manufacturing with focus on nano-machining, joining and welding. Ultraprecision finishing techniques for fabrication of optical components are discussed in Chapter "Fabrication of Optical Components by Ultraprecision Finishing Processes". Chapter "Condition Monitoring in Micro-Injection Moulding" discusses the important aspects of condition monitoring in micro-injection moulding. Chapter "Surface Finish Improvement of Additive Manufactured Metal Parts" sheds light on some post-finishing methods for additive manufactured metal parts. Chapter "Precision Coatings" is an impressive note on precision coatings and highlights their principle and applications for various engineered parts.

This book is intended to facilitate the industrial, research and academic community by ensuring knowledge enrichment in theoretical and research aspects of the techniques used to fulfil various micro- and precision manufacturing requirements.

I thank all the authors for their valuable contribution.

Johannesburg, South Africa Kapil Gupta
June 2017

Contents

About the Editor

Dr. Kapil Gupta is a Senior Lecturer in the Department of Mechanical and Industrial Engineering Technology at the University of Johannesburg, South Africa. His research interests include advanced machining processes, sustainable manufacturing, microfabrication, precision engineering and gear technology.

Machining of Microshapes and Features

Asma Perveen and Carlo Molardi

Abstract Accelerated trend of miniaturization and thereby increasing use of microfeatures and microparts have tremendously encouraged scientists and engineers to develop new techniques for their precision fabrication. Considering that, this chapter introduces various machining techniques for microfeature fabrication, their capabilities, salient features and associated surface integrity aspects. It also reviews the past work and highlights recent technological development in this area.

Keywords Microholes · Laser machining · Electro discharge machining · Electrochemical discharge machining

1 Introduction

Increasing demand for developing micromachining technology to fabricate microfeatures and microshapes has been attracting the interest of researchers to fulfil the specific requirements of aerospace, biomedical, electronics and automotive industries [1, 2]. Downscaling trend of processes, machines, metrology in order to satisfy the current needs of smaller, thinner and lighter products with accuracy and precision appears to push the established technologies towards miniaturization. Manufacturing of engineered parts and components with feature size ranging from 1 to 999 μm is known as micromanufacturing [1, 2]. In order to satisfy current needs, innovative micromachining processes other than the improvement in the existing machining technologies have become crucial. Nevertheless, this journey of

A. Perveen (✉)
Department of Mechanical Engineering, Nazarbayev University,
53 Kabanbay Batyr Ave., Astana 010000, Republic of Kazakhstan
e-mail: asma.perveen@nu.edu.kz

C. Molardi
Department of Electrical and Electronics Engineering,
Nazarbayev University, 53 Kabanbay Batyr Ave., Astana 010000
Republic of Kazakhstan

K. Gupta (ed.), *Micro and Precision Manufacturing*, Engineering Materials,
https://doi.org/10.1007/978-3-319-68801-5_1

product miniaturization imposes technical constrains on individual machining technique in terms of machinability, shape complexity and surface integrity. Fabrication techniques such as photolithography, focus ion beam and electron beam lithography are considered to be the most prevalent micromachining techniques in terms of their process capacity to fabricate micro-/nanosize features. However, such methods require high expenditure for equipment and maintenance and also lack of capability to fabricate complex 3D geometries. Conventional micromachining and finishing techniques are capable of generating surfaces with nanofinish. Nevertheless, size limitations of cutting tool required for micromachining of complex microfeatures impede their effective cutting due to the presence of cutting forces. Among the tool-based machining processes, micro-EDM and micro-ECM show significant promising capability due to their non-contact phenomena. Negligible process force makes possible the fabrication of electrodes which could be used to fabricate microshapes and intricate features. On the other hand, it is also attractive to employ laser techniques to fabricate microfeatures which might eliminate the usage of master micromold. Challenges and limitations imposed by individual micromachining technologies directed the interest of researchers towards the development of hybrid micromachining processes. Hybrid process developed by combining two individual processes offers enhanced benefits arising from both individual processes with reduced negative effects caused by application of each process separately.

There have been many attempts to develop the low-cost macromachining processes for applications requiring micro- and nanofeatures. As of today, considerable research efforts have been enforced towards the course of machine tools development, on-machine micro-/nanometrology for efficient process control and expansion of processes for micro-/nanomachining techniques. Therefore, this chapter attempts to focus on the growing applications of microshapes and features and associated challenges in machining them. Following that, this chapter also introduces various machining techniques for their successful fabrication.

One of the most widely used microfeature is microholes which are essentially required in micronozzles, microdies, fluidic filters, grids, inkjet printer nozzles, fuel injection nozzles, optical apertures, high-pressure orifices, micropipettes, pneumatic sensors and manipulators and biomedical filters [2–5]. Although fabrication of simple microholes is not that difficult, machining of holes having irregular cross section involves more complicated steps. Holes having some internal features or internal size larger than hole opening and with reverse tapered holes and grooves require not only the modifications of the tool geometry but also the advancements of the process itself [3–5].

3D array microfeatures with variable cross sections can be used as tools for micro-ECM process for making cavities [6], fabricating through holes for the purpose of interfacing devices in MEMS by passing wires and as tools in micromilling applications [7]. Microelectrode and microhole array are typically useful in fabricating microholes (50 μm diameters on 600-μm thin plates) in the nozzles for spraying purpose for biotechnology applications [8]. Microrods of harder materials with high aspect ratio can also be useful as a component in various MEMS applications, as shaft for microrobot/microactuator, as microneedle for syringe, as a tool for fabricating high aspect ratio holes without burr and as mechanical punch to perforate thin foils [9–11].

The next section details the fabrication of aforementioned microshapes and features by various conventional and advanced techniques.

2 Details on Fabrication Techniques for Microshapes and Features

2.1 Micromachining

Micromachining is defined as the machining process in which the thicknesses of the material layer removed by single pass of the cutting edge ranges from 1–999 μm. Material removal mechanism involved in cutting is mostly by shearing or plastic deformation. Nanofinished surface with submicron profile accuracy can be obtained using small scale of material removal with well-defined tool geometry. Micromechanical machining comprises of microcutting methods, i.e. microturning, micromilling, microdrilling that employ defined cutting edges and microgrinding that uses undefined cutting edges [12].

2.1.1 Micromilling

Micromilling is basically scaled-down version of macromilling which implies downscaling of machine tools, cutting tools and cutting parameters. Despite their similarity in kinematics, process physics and mechanism, micro- and macromilling processes differ significantly in many aspects [13]. Due to run-out error of tool which happens at microscale level, micromilling suffers greatly from lack of accuracy unlike conventional milling [14]. Higher ratio of tool run-out to tool diameter in case of micromilling causes one of the cutting edges to be active at a same time, and as a result, variation of force increases greatly. Eventually, tool chipping occurs even with low force of mN values. The principle stress reaches to maximum value causing the tool to fail [15].

Cardos et al. [16] conducted investigation on Al–Cu–Bi–Pb age-hardened alloy by fabricating microfeatures and studied surface roughness. A cemented carbide end milling tool with 800 μm diameter was used with feed rate variation of 2–8 μm/flute and tool rotation of 6500 rpm. Micromilling operation was conducted using three machining strategies such as constant overlap spiral cutting (Fig. 1a), parallel spiral cutting and parallel zigzag cutting. Constant overlap strategy generated best result among the three strategies as shown in Fig. 1b.

Unpredictable tool failure has always been a key issue in micromilling. As per the research results, variation of tool geometry plays an important role in tool wear. Feng et al. [18] conducted a comparative study of two-flute Δ-type and D-type end mills made of tungsten carbide on brass. Mesa arrays with triangular and square base used in biomedical applications were fabricated using cutting velocity of

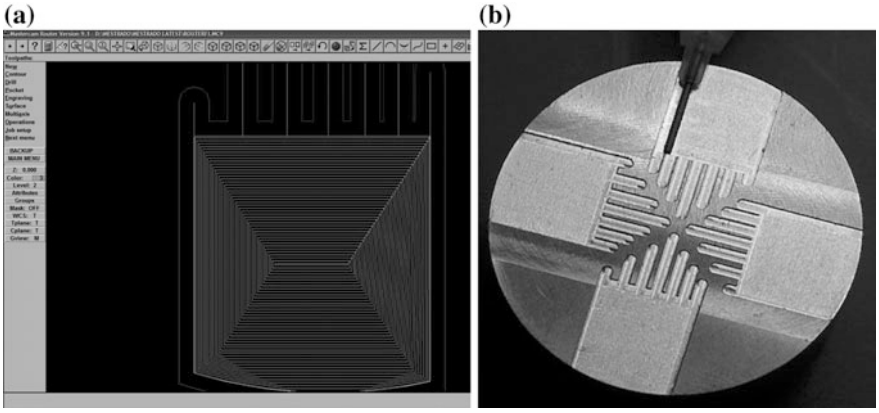

Fig. 1 Machining strategies using feed rate of 6 µm/tooth: **a** constant overlap spiral; **b** photograph of a micromilled surface on aluminium samples using 0.8-mm-diameter end mill [16, 17] (with kind permission from 'Taylor & Francis', 'Russian Academy of Science')

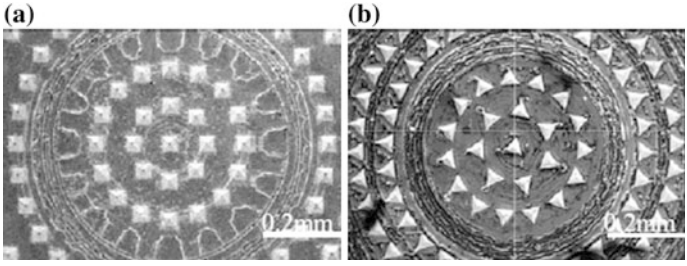

Fig. 2 Micromachining of biomedical parts [18] (with kind permission from 'IOP Science')

40,000 rpm, depth of cut 30 µm and feed rate 60 mm/min. D-type end mills contribute to the successful fabrication of width of walls and channel down to 80 µm as shown in Fig. 2. Moreover, follow contour instead of layer-by-layer strategy also generates better surface roughness. As per the experimental study as well as FEM analysis, D-type micro-end mill shows more compatibility for micromachining.

Convex lens array of 4 × 4 on brass was also fabricated with the help of single crystal diamond end mill by Kawai et al. [19]. Machined lens has pitch of 290 µm and diameter and height, respectively, of 236 and 16 µm. Generated lens have roughness value of 448 µm. For micromechanical applications, structures such as moulds and masks were also manufactured on polymethyl methacrylate (PMMA) using microend mill. Stepped surfaces were machined on the sidewall (Fig. 3a). Each step has altitude of 4 µm, and the narrowest step at bottom has 2 µm width. The wall existed on the top of the structure has width of 8 µm. Because of the repetitive cutting passes, side forces were minimized which in turn allowed the

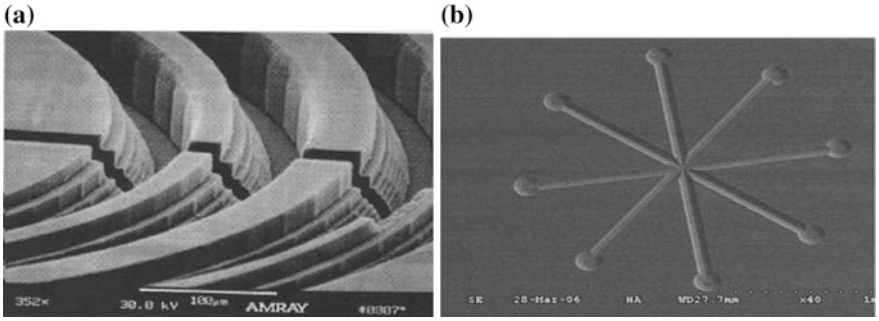

Fig. 3 **a** Stepped structures on PMMA fabricated by micro end mill [20] (with kind permission from 'Elsevier'). **b** Eight reservoir microreactors on PMMA [21] (with kind permission from 'Wiley')

fabrication of the thin walls [20]. Other than using micro-end mills, ball end mill of 9 μm nose radius was also exploited to fabricate microreactor with eight reservoirs on PMMA (Fig. 3b). The reservoir fabricated was of 150 μm diameter, 60 μm of width and 50 μm of depth (for both channel and reservoir) [21].

2.1.2 Microturning

As per the literature, several electronic and optical processes such as electron beam direct writing, direct laser writing, holographic process can be utilized for fabrication of anti-reflective structured surfaces, microlens arrays, optical microstructures. Nevertheless, complicated shape like sinusoidal wave patterns with greater accuracy does not seem so easy to fabricate using those processes. Diamond turning exhibits its superiority over optical and electronic technique when it comes to the fabrication of complicated part with wavelength value in the range of micrometres. With the assistance of fast tool servo (FTS), diamond turning can produce 3D freeform surface for optical image with better tolerance in the form of geometry as well as roughness [9, 22, 23].

Gao et al. [23] manufactured angle grid surface for surface encoder used in multiaxis positioning by combining diamond turning with FTS where piezoelectric actuator controls the movement of tool with several nanometre accuracies. This surface fabricated on aluminium alloy has sinusoidal wave patterns of 100 μm wavelength and 100 nm amplitudes on both x-axis and y-axis. Alignment of tool centre with the centre of spindle was carefully done, as it is paramount for the accurate production of sinusoidal surface. Fabrications start from outer circle and end at the workpiece centre, and it takes almost 13 h in a temperature-controlled room. Fabricated grid with tool compensation and result of three evaluations are shown in Fig. 4. Profile accuracy for three evaluations shows similar order of magnitude which indicates the successful fabrication of sinusoidal wave patterns with error compensation reduced to nanometre level [23].

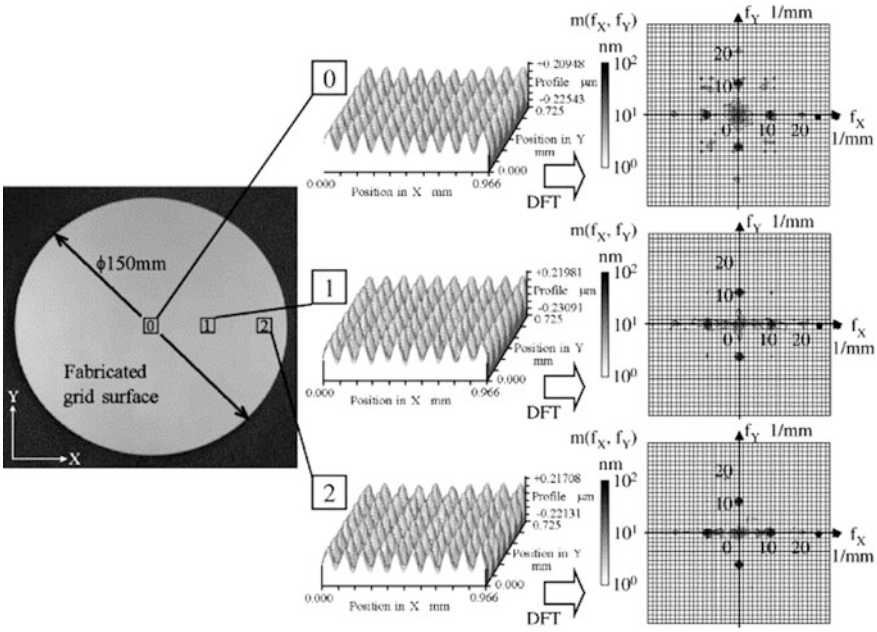

Fig. 4 Fabrication and evaluation results of the sinusoidal grid surface [22] (with kind permission from 'Elsevier')

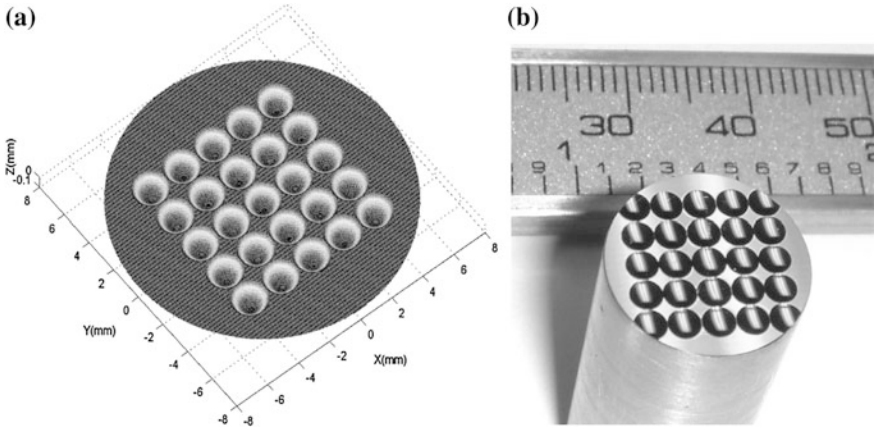

Fig. 5 **a** Microlens array design. **b** Machined freeform microlens array (larger units in millimetres) (with kind permission from 'OSA')

Yi et al. [24] implemented simple slow tool servo to manufacture microlens array of 5 × 5 and diffractive optical elements using three-axis ultraprecision turning machine (Fig. 5). Fabrication was done in two steps. Depth of cut for rough and finish cutting used was, respectively, 10 and 2 μm. Diamond cutter with nose

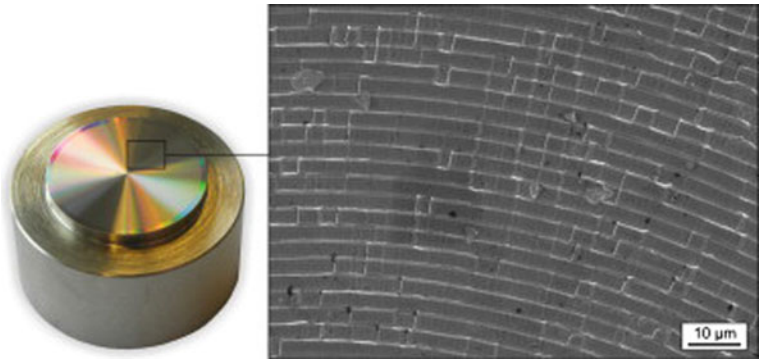

Fig. 6 Holographic microstructures machined on nickel silver using nanofast servo-assisted turning [25] (with kind permission from 'Elsevier')

radius of 250 µm, rake angle of 0° and clearance angle of 10° was used for fabrication. Surface roughness measured for this microarray was found to be 34.5 nm (measured length 0.70 mm) which is considered satisfactory for the optical applications. Therefore, this method can be used without any need of post-processing. Figure 6 shows the holographic microstructure generated on nickel silver sample using nanofast tool servo [25].

2.1.3 Microdrilling

Printed circuit board (PCB) known as mother of most of the electrical appliances plays an important role for transmission as it connects electronics components with the use of fine wire. These connections via wire on different layers are normally done using microscale high-density holes (either through or blind). Through holes are useful for single, double-sided, or multilayer boards. Blind holes are mostly found in high-density interconnecting boards. Microdrilling is identified as the appropriate method to machine these holes in PCBs. Mechanical microdrill of 0.2–0.3 mm size is already commercially available, and it could go down to 0.1 mm or below as well. However, fabrication of hole with 0.05–0.10 mm size requires the drill machine with significantly higher spindle speed. Therefore, drilling machine having spindle speed of 350,000 rpm is getting more popularity. Other than spindle speed, drilling depth, material hardness, spindle run-out, rigidity and drill design also affect the drilled hole quality [26]. Figure 7 shows microhole array fabricated on PCB with the help of 0.1- and 0.15-mm-diameter drill bit.

Microdrilling of monocrystalline silicon has also been conducted. But in this attempt, the microhole was ended up with fracture at the entrance side of hole. In order to prevent this kind of fracture, clearance angle for the tool was proposed to be greater than 0°. Egashira et al. [27] investigated on microhole drilling of monocrystalline silicon. For this hole fabrication, D shape tool with cutting radius

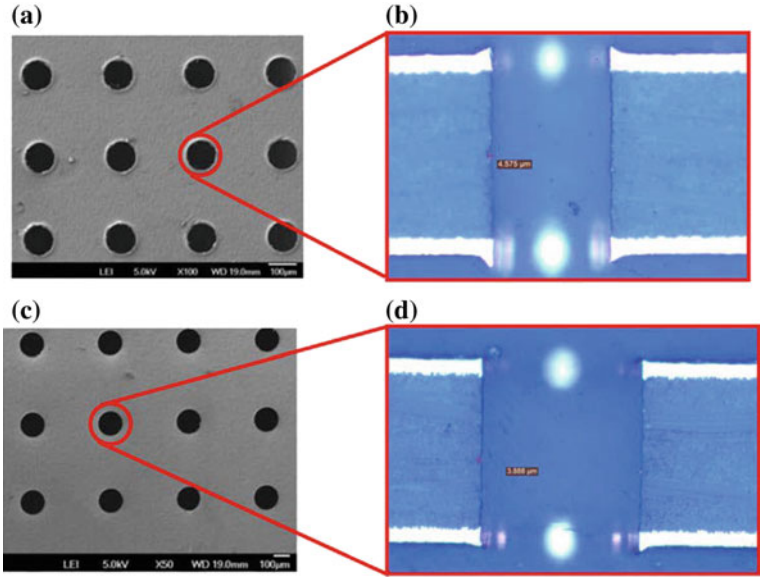

Fig. 7 Holes fabricated by **a** 0.1- and **b** 0.15-mm drill bites **c** enlarged view of microhole (0.1 mm drill) **d** enlarged view of microhole (0.15 mm drill) [26] (with kind permission from 'Emerald Group Publishing Limited')

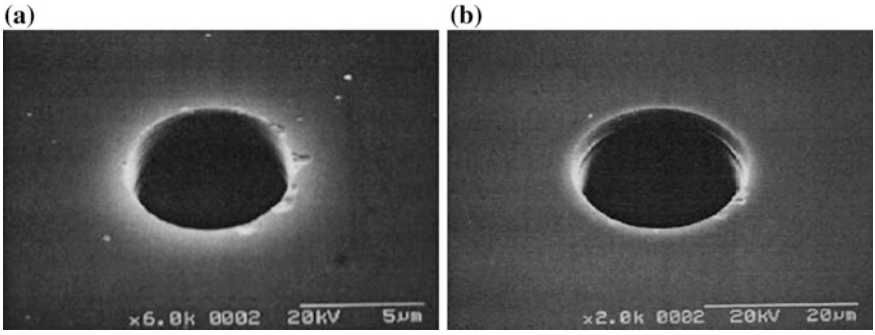

Fig. 8 **a** Microhole having diameter and depth of 6.7 µm and 10 µm, respectively, (feed rate = 0.03 µm/s). **b** Microhole having diameter and depth of 22 µm and 90 µm (feed rate = 0.1 µm/s) [27] (with kind permission from 'Elsevier')

of 0.5 µm was manufactured using wire electrodischarge grinding (WEDG). Figure 8a shows the fabricated hole of 6.7 µm size using 6-µm-size microdrill and feed rate of 0.03 µm/s, whereas Fig. 8b shows deep microhole with more than 4 aspect ratios fabricated at feed rate of 0.1 µm/s.

2.2 Electrochemical Machining

Electrolysis-based metal dissolution removes material in electrochemical machining [28]. In ECM process, workpiece as anode and tool electrode as cathode are immerged in the electrolyte; due to applied voltage between anode and cathode, current is generated and passed between anode and cathode. Eventually, material from the workpiece is removed according to the tool shape [29, 30]. Although the mechanism for ECM and micro-ECM is similar, dissolution zone for micro-ECM needs to be localized in order to assure dimensional accuracy [10]. Micro-ECM also requires the electrode size to be smaller, ultrashort pulses, smaller voltage and current value [31]. Different types of micro-ECM available are micro-ECM drilling, micro-ECM using mask, micro-ECM milling and die-sinking micro-ECM. [1].

Micro-ECM is quite useful for the applications related to microstructure fabrications such as microholes and microchannels used in microdies and micronozzles. Due to anodic dissolution and evolution of gas at cathode, ECM experiences zero tool wear [5, 6]. Eventually, several holes can be fabricated using the same tool due to its reusing characteristics. However, due to ultrashort pulse, lower voltage and lower current value, material removal rate in micro-ECM is significantly lesser than micro-EDM [2, 31, 32]. Therefore, generated surface appears significantly smooth as well as burr free without any microcracks and heat-affected zones [1, 21, 33]. However, micro-ECM can cause distorted machined shape due to the larger dissolution zone even with low process power [34, 35].

Schuster et al. [36] proposed the use of short pulse voltage for the fabrication of submicron size optical structures and successfully fabricated 3D structures with submicron size as well as of high aspect ratio on gold (Au). This method offers relatively straightforward fabrication of structure having high aspect ratios and several microns of depth. Pulse voltage of 10 ns along with LiCl/dimethyl sulfoxide electrolytes increases the precision level to submicron scale. Figure 9 shows the micro-ECM fabricated microstructures on gold.

ECM was also used to fabricate microholes with spiral ribs for internal cooling. Initially, hole was fabricated by wire EDM. Spiral ribs on the hole were created

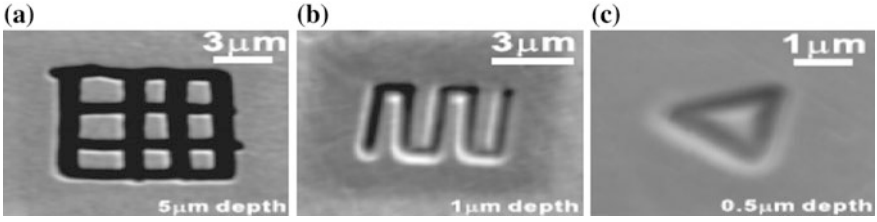

Fig. 9 Microstructures machined on Au using 1 M LiCl/DMSO solution. The applied machining parameters are: a 4.2 V, 20 ns pulses, rest potential $\Phi_{Au} = 0.05$ V; b 5.6 V, 10 ns pulses, rest potential $\Phi_{Au} = 0.05$ V; c 5.6 V, 11 ns pulses, rest potential $\Phi_{Au} = 0$ V [36] (with kind permission from 'Elsevier')

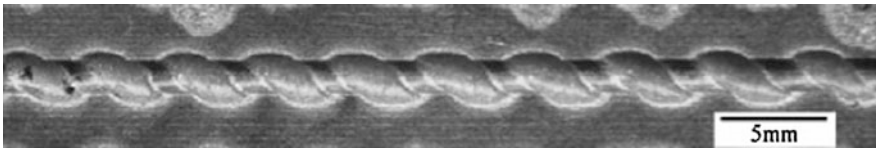

Fig. 10 Spiral duct cooling passage processed by ECM [37] (with kind permission from 'Springer')

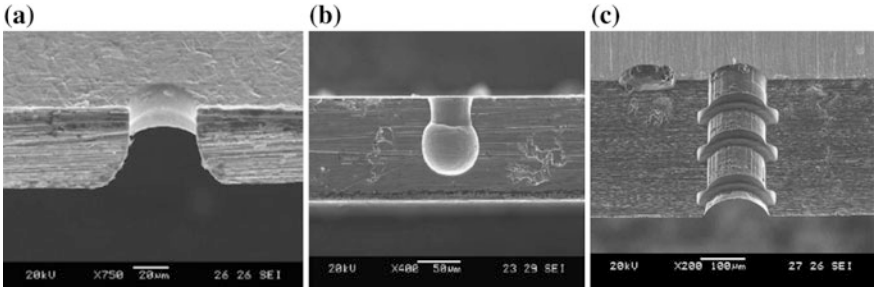

Fig. 11 **a** Cross-sectional view of reverse tapered hole [38]. **b** Microcavity machined by controlled dissolution time of 5 min. **c** Microhole with grooved array [38] (with kind permission from 'Elsevier')

using ECM process in the second step with the help of shaped tool [37]. Figure 10 shows the spiral shape hole (with average deviation of <8.5% and shape duplication of 0.07–0.1 mm) machined by ECM in 10 min. Wang et al. [37] suggested to use pulse power, narrow initial gap, lower voltage and lower electrolytic concentration to machine high-accuracy microfeatures by ECM. With the help of insulated electrode and pulse voltage of 6 V, reversed tapered hole was successfully fabricated on 50-µm-thick stainless steel plate (as shown in Fig. 11a) by Jo et al. [38]. In addition, spherical cavities were also fabricated at controlled dissolution time (see Fig. 11b). In order to fabricate these kinds of microcavities, insulated electrode was made to go downward to make few micrometre depth of cylindrical hole first with the pulse on time of 30 ns, and then, electrode was held at that position with the pulse on time of 150 ns. Figure 11c shows microhole having diameter of 130 µm with grooved array. Fabrication of such repeatable structure-like arrayed microhole using single disc shape tool without any tool wear gives ECM certain advantages over other processes [38].

2.3 Electrodischarge Machining

Being an electrothermal process, EDM can remove material from conductive as well as semi-conductive material. EDM has the capabilities of machining both circular and non-circular holes, as well as complex profiles/structures. As per the literature,

several varieties of EDM process such as die-sinking EDM, wire EDM, wire EDG have been practised by the machining community. Moreover, micro-EDM, microwire EDM and micro-WEDG have been extensively used with the downscaling of EDM power, electrode and axis movement resolution. Both the micro-EDM and macro-EDM have greater potential, and yet research work is ongoing to improve the process capabilities. Recently, some researchers also reported on nanopulse EDM. During EDM process, voltage is applied across the tool workpiece terminals; when the gap between cathode and anode is appropriate, electric field breaks down the dielectric properties of the EDM oil and series of spark starts to move between cathode and anode depending on the polarity. Now, each of the sparks removes material from both the tool and workpiece, resulting in the formation of crater on the machined surface. Dielectric flush helps to remove the generated debris away and prepares for the next cycle [39, 40].

Micro-EDM is widely exploited in machining of simple microholes as well as complex micromoulds. Process mechanism of micro-EDM is similar as EDM. However, micro-EDM is mainly dedicated for the microscale fabrication of microfeatures, which also requires the fabrication of microscale electrodes. The discharge energy for micro-EDM is less than 100 μJ, and eventually, the crater size is reduced to less than 500 μm [34, 41]. In order to facilitate short pulse duration for micro-EDM, RC generator is preferred over transistor generator [1]. Apart from that, to achieve precise dimensional accuracy of fabricated features using micro-EDM, it also requires the precise movement of the machine axis [41]. Microwire EDM utilizes small-scale diameter wire (100–20 μm) in order to facilitate the machining of smaller cutting width as well as inner corner. WEDM has their huge applications in the fabrication of micromechanical device as well as microstamping tool. Gear with module 0.1 was fabricated using 30-μm-diameter wire with the help of WEDM (Fig. 12a) [41]. Application of micro-EDM for batch production is also possible. Weng et al. [42] machined 16 pieces of electrode array on tungsten electrode using wire EDM (Fig. 11b). Later on, using those electrodes, microslots were fabricated on copper plate using micro-EDM (Fig. 12c). Other than

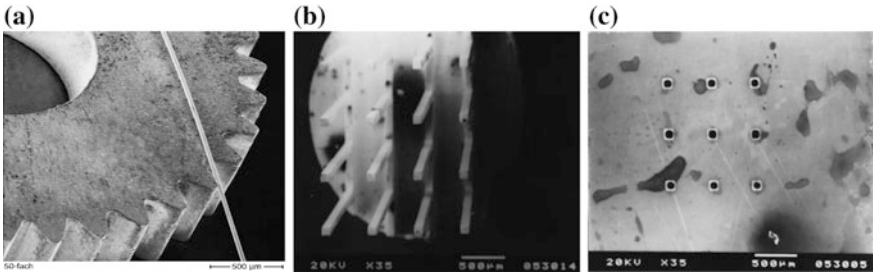

Fig. 12 **a** Gear with module 0.1 machined by micro-WEDM using wire electrode of 30 μm diameter [41] (with kind permission from 'Elsevier') **b** Multielectrodes of diameter of 100 μm and length of 5 mm fabricated by wire EDM. **c** Microslots fabricated on copper using multielectrodes with positive polarity [42] (with kind permission from 'Springer')

using micro-WEDM, micro-EDM can also be used for fabricating gear cluster on WC–Co super hard alloy (thickness of 70 μm) using electrode arrays [11].

Microdie-sinking EDM is also effectively used for the fabrication of microinjection moulding and hot embossing dies. This process transfers the reverse shape of electrode to the work part. Microelectrode of 500 μm diameter was utilized to create simple shape like blind hole with 5 μm depth on WC using die-sinking micro-EDM [39].

Microchannel with 15 aspect ratios and 50 μm width can be machined using micro-EDM technique which is useful for manufacturing of forming tool with microchannel for microfluidic applications. As shown in Fig. 13, microcavity in hot-forming tool was fabricated using 0.1-mm-diameter pin which was manufactured by electrical discharge dressing [43, 44].

Recent development in the area of scanning algorithm increases the process capability of the micro-EDM milling for the fabrication of 3D complex features. A small pyramid having 50 μm height was fabricated using micro-EDM milling (Fig. 14a). Figure 14b shows the fabricated two and half dimensional

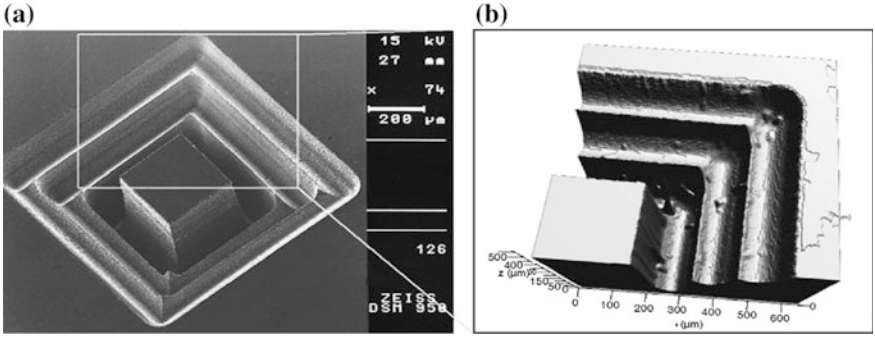

Fig. 13 Microcavity machined on hot-forming tool by EDM milling, using tool diameter of 0.1 mm [41] (with kind permission from 'Elsevier')

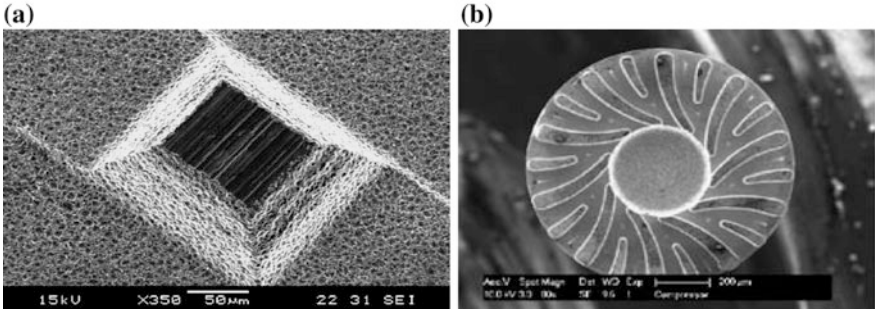

Fig. 14 **a** Small pyramid machined using micro-EDM milling [150 μm (L) × 140 μm (W) × 50 μm (H)] [5] (with kind permission from 'Elsevier') **b** Top view of a microcompressor machined on a 1-μm-diameter cylinder [45] (with kind permission from 'Springer')

microcompressor on a cylinder of 1 mm diameter made of stainless steel. Centre hole of 300 μm diameter was drilled using commercial electrode, and blades were fabricated using micro-EDM milling with the help of same tool after its diameter is reduced using WEDG [5, 45].

2.4 Laser Machining

Lasers offer an excellent beam quality and pledge significant advantages and improvements in microscale high-precision material processing. Nevertheless, it is not only a matter of beam quality that makes the lasers' technology so attractive, but also several other benefits such as high efficiency, moderate price, flexibility to work with different materials, easy integration and installation are offered by this process. With respect to traditional approaches, lasers interact with materials in a complete contact-less and wear-less fashion, with huge benefits on machining precision. Besides these, lasers have the capability to pursue high-power industrial macromachining using mainly continuous wave lasers, as well as ultraprecision micromachining by exploiting the high-energy, short-pulsed operation.

With regard to the last-mentioned operation, the possibility to tune pulse duration from microsecond to femtosecond, to tune the pulse repetition rate from a single shot to megahertz and to choose emission wavelength ranging from mid-IR (CO_2 lasers) to UV region (excimer lasers) makes lasers suitable to process a wide range of materials including silicon, ceramic, glass, metals, compounds and polymers. Although the choice of an appropriate laser source is fundamental, it is also necessary to employ specialized components in order to obtain the desired geometry [46]. Currently micromachining is developed using two different technological approaches: direct laser writing (DLW) by using a 2D galvanometer scan head and mask projection technique (MP) by using a fixed mask, as shown in Fig. 15a, b [47]. The first is suitable for creating every kind of 3D surface, with some limitations given by the precision of the galvanometer head used for directing the beam and some limitations on material manufacturability caused by the high intensity of the required laser. The second is much more suitable for high-precision photolithography as the laser beam is well homogenized and directed on the target. Besides, it is possible to duplicate the same model for many times without losing precision.

By means of high-energy pulses, characterized by short pulse duration, it is possible to reach ablation threshold and obtain remarkable structures on silicon for printed circuits or for other applications such as printer nozzle, biomedical catheter, hole drilling, thin-film scribing, microelectromechanical system (MEMS) and microfluidic. Figure 16a–f presents some examples of this kind of precise microfeature machined by lasers.

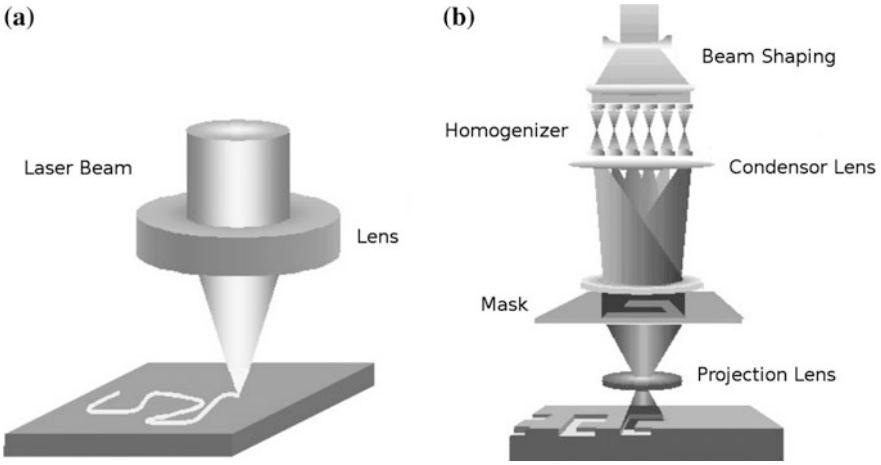

Fig. 15 **a** Direct laser writing (DLW). **b** Mask projection (MP) [47] (with kind permission from 'SPIE')

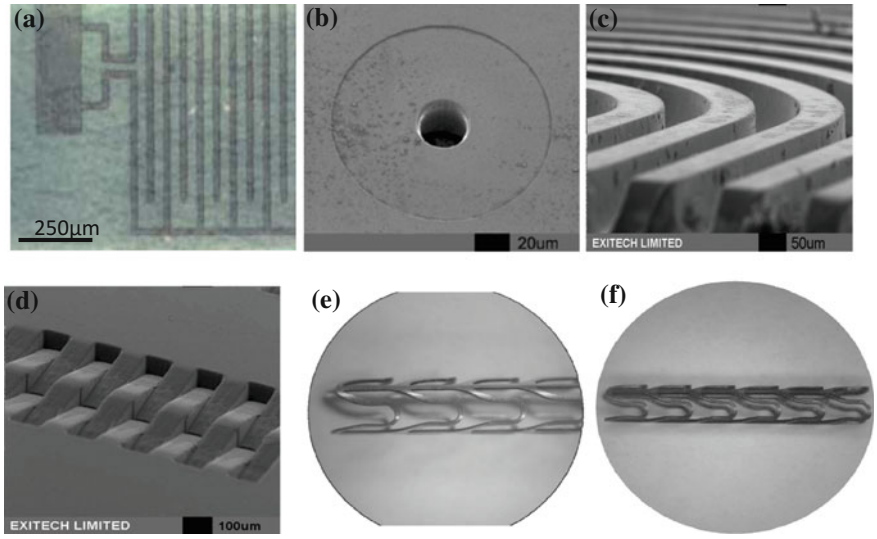

Fig. 16 **a** Indium–tin–oxide printed circuit using a Q-switched Nd:YAG laser [47], **b** printer nozzle drilled on a olyimide substrate using an excimer laser [47] (with kind permission from 'SPIE') **c**, **d** channels and ramps for microfluidic purpose carved on polyester using KrF excimer laser [47, 48] (with kind permission from 'SPIE'), **e** A 316L stainless steel cardiovascular stent cut with fibre laser and **f** cut with YAG laser [47, 49] (with kind permission from 'Elsevier')

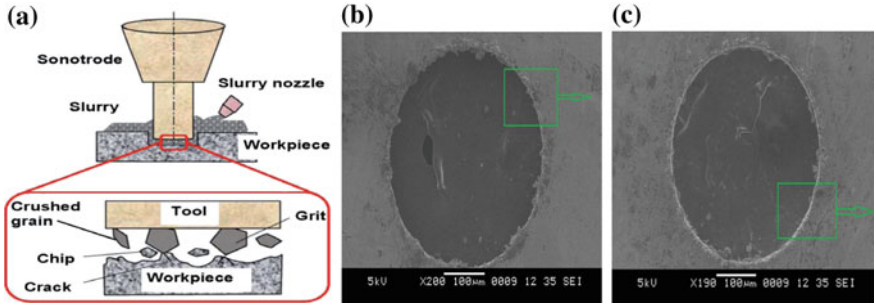

Fig. 17 **a** Working principle of ultrasonic machining [54]. (With kind permission from 'Elsevier') **b** SEM image of entry of microhole. **c** Exit of microhole [58] (with kind permission from 'Elsevier')

2.5 *Ultrasonic Machining*

Fabrication of microfeature on glass or brittle material needs special machining strategies. Microultrasonic machining is one of such promising techniques useful for high aspect ratio microfeatures fabrication without any damage to the workpiece. Microhole is the most common feature fabricated by this process [34, 50]. Microhole of 5 μm on silicon was drilled by using micro-USM which can meet the requirement of integrated circuit package containing device with microdimension [51]. Principle of micro-USM is similar as conventional USM. Material removal in micro-USM is mainly done by the combination of abrasion and cavitation erosion. Mechanical action/abrasion is induced by the ultrasonic vibration (frequency 20 kHz) of the tool to the abrasive particles, whereas cavitation erosion is mainly because of the change of pressure created by ultrasonic vibration in the fluid close to work zone [52, 53].

The working principle of USM system is given in Fig. 17a [54]. Micro-USM has the capability to drill holes, machine slot and other 3D features [55]. Microholes with dimension lower than 10 μm were comfortably machined on quartz, glass, silicon and alumina [50, 51, 56]. Micro-USM has also been used for precise 3D cavity generation [57]. Kuriakose et al. [58] successfully fabricated microhole on 20-μm-thick Zr–Cu–Ti metallic glass using micro-USM (Fig. 17b, c). Hollow cylindrical tool made of stainless steel was used for microhole drilling with varying grit size abrasive.

2.6 *Hybrid Machining*

One of earliest attempt on hybrid machining was made by Takahata and Takeo [59] where micro-ECM/lapping is combined with EDM to further enhance the surface integrity of machined surface [59]. In addition to electrolytic dissolution, Al_2O_3

grains contained in the electrolyte solution also remove material due to the polishing effect of grains which result in mirror-like surface with 32 nm after 120 s of machining. Simultaneous electrodischarge/electrochemical machining (SEDCM) with layer-by-layer material removal was also attempted [33], where low-resistive deionized water between electrode and workpiece acts as both dielectric and slightly conductive electrolyte. Short voltage pulses cause material removal in terms of crater and following that voltage pulses initiates a weak electrochemical reaction due to lower conductivity of deionized water. As a result, anodic dissolution causes the surface roughness to be reduced [33].

Figure 18 shows three-dimensional microcavities fabricated by micro-EDM milling and SEDCM milling. For SEDCM, short pulse with 500 kHz frequency and 30% duty ratio were used. Material is removed by 0.2 µm depth at each layer using feed rate 50 µm/s; however, for last 5 µm depth, feed rate of 10 µm/s was used. It is clearly visible from the figure that SEDCM milling has the process capability better than EDM milling [60].

Hybrid machining combining ECDM and grinding using PCD tool was also investigated. The idea is to take advantage of ECDM which facilitates high material removal and microgrinding which offers higher surface quality. Figure 19 shows the microstructure fabricated using this combined technique. ECDM process was used to generate the microstructure roughly using WC electrode of 40-µm tool.

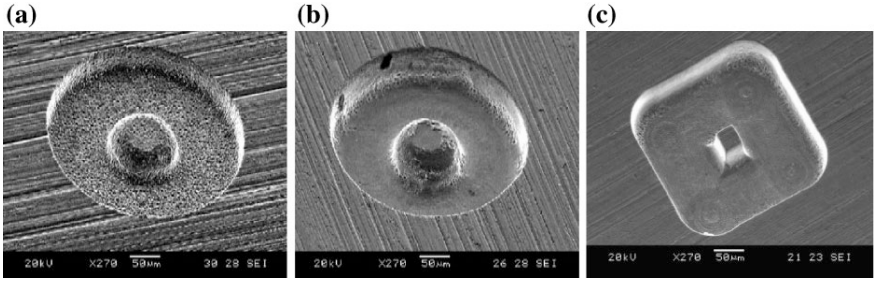

Fig. 18 3D microcavities fabricated by **a** micro-EDM milling and **b** SEDCM milling; **c** microfeatures machined by SEDCM milling at feed rate: 10 µm/s [60] (with kind permission from 'Elsevier')

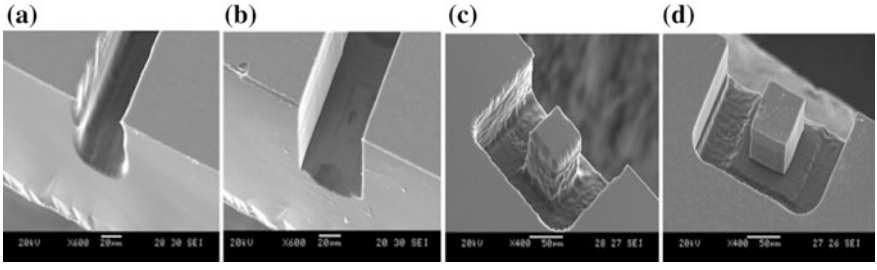

Fig. 19 Microstructures fabricated by a, c ECDM and b, d combined ECDM and grinding by a PCD tool [61] (with kind permission from 'Springer')

Pulse voltage of 23 V was applied across the electrode and work part with the tool rotation of 300 rpm and feed rate of 3 μm/s. Subsequent microgrinding was conducted using PCD tool which reduced the surface roughness significantly [61].

These examples show that hybrid micromachining techniques can be efficiently used for machining of complicated microstructures with better surface quality on glass materials.

3 Summary

Current trend of machining is moving towards miniaturization due to the huge industrial demand of downscaled products. In this chapter, the important industrial applications which require the microscale machining processes are highlighted. Underpinning concepts of these major micromachining techniques and their potential capabilities are also summarized in the light of the applications. In addition, hybrid micromachining process combining two different micromachining processes is also found to have greater potential as it makes use of advantages arising from both processes. However, hybrid process combining more than two processes is still in infancy and should be the focus of future research. Moreover, most of these micromachining technologies are still in exploration phase; therefore, more research work is essential to be conducted to elevate the technology readiness level for direct industrial applications.

References

1. Kapil Gupta NK, Jain RF Laubscher (2015) Spark-erosion machining of miniature gears: a critical review. Int J Adv Manuf Technol 80(9–12):1863–1877. doi:10.1007/s00170-015-7130-2
2. Masuzawa T (2000) State of the art of micromachining. CIRP Ann Manufact Technol 49 (2):473–488
3. Masuzawa T, Okajima K, Taguchi T, Fujino M (2002) EDM-lathe for micromachining. CIRP Ann Manufact Technol 51(1):355–358
4. Egashira K, Tsuchiya H, MIYAZAKI M (2005) EDM of reverse-tapered micro holes. In: International conference on leading edge manufacturing in 21st century, pp 757–760
5. Asad A, Masaki T, Rahman M, Lim H, Wong Y (2007) Tool-based micro-machining. J Mater Process Technol 192:204–211
6. Kim BH, Park BJ, Chu CN (2006) Fabrication of multiple electrodes by reverse EDM and their application in micro ECM. J Micromech Microeng 16(4):843
7. Fleischer J, Masuzawa T, Schmidt J, Knoll M (2004) New applications for micro-EDM. J Mater Process Technol 149(1–3):246–249
8. Penache C, Gessner C, Brauning-Demian A, Scheffler P, Spielberger L, Hohn O, Schossler S, Jahnke T, Gericke KH, Schmidt-Boecking HW (2002) Microstructured electrode arrays: a source of high-pressure nonthermal plasma. pp 17–25
9. Takeuchi Y, Suzukawa H, Kawai T, Sakaida Y (2006) Creation of ultra-precision microstructures with high aspect ratios. CIRP Ann Manufact Technol 55(1):107–110

10. Csala V, Szalay T, Farkas B, Markos S (2015) Application benchmark of three micro hole machining processes for manufacturing the nozzle of a medical water jet machine. Acta Polytechnica Hungarica 12(2):53–69
11. Takahata K, Gianchandani YB (2002) Batch mode micro-electro-discharge machining. J Microelectromech Syst 11(2):102–110
12. Masuzawa T, Tönshoff H (1997) Three-dimensional micromachining by machine tools. CIRP Ann Manuf Technol 46(2):621–628
13. Huo D (2013) Micro-cutting: fundamentals and applications. Wiley, New Jersey
14. Dhanorker A, Ozel T (2008) Meso/micro scale milling for micro-manufacturing. Int J Mechatron Manuf Syst 1(1):23–42
15. Fang F, Liu K, Kurfess T, Lim G (2006) Tool-based micro machining and applications in MEMS. In: MEMS/NEMS, Springer, Heidelberg, pp 678–740
16. Cardoso P, Davim JP (2010) Optimization of surface roughness in micromilling. Mater Manuf Processes 25(10):1115–1119
17. Cardoso P, Davim JP (2012) A brief review on micromachining of materials. Rev Adv Mater Sci 30(1):98–102
18. Fang F, Wu H, Liu X, Liu Y, Ng S (2003) Tool geometry study in micromachining. J Micromech Microeng 13(5):726
19. Kawai T, Sawada K, Takeuchi Y (2001) Ultra-precision micro structuring by means of mechanical machining. In: Technical digest. MEMS 2001. 14th IEEE international conference on micro electro mechanical systems (Cat. No.01CH37090), 25–25 Jan 2001. pp 22–25
20. Friedrich C, Coane P, Vasile M (1997) Micromilling development and applications for microfabrication. Microelectron Eng 35(1–4):367–372
21. Yi AY, Lu W, Farson DF, Lee LJ (2008) Overview of polymer micro/nanomanufacturing for biomedical applications. Adv Polym Technol 27(4):188–198
22. Gao W, Araki T, Kiyono S, Okazaki Y, Yamanaka M (2003) Precision nano-fabrication and evaluation of a large area sinusoidal grid surface for a surface encoder. Precis Eng 27(3):289–298
23. Dow TA, Miller MH, Falter PJ (1991) Application of a fast tool servo for diamond turning of nonrotationally symmetric surfaces. Precis Eng 13(4):243–250
24. Yi AY, Li L (2005) Design and fabrication of a microlens array by use of a slow tool servo. Opt Lett 30(13):1707–1709
25. Meier A (2015) Diamond turning of diffractive microstructures. Precis Eng 42:253–260
26. Liang X, Li B, Fu L, Wu X, Shi H, Peng T, Xu B (2015) Mechanical drilling of PCB micro hole and its application in micro ultrasonic powder molding. Circ World 41(2):87–94
27. Egashira K, Mizutani K (2002) Micro-drilling of monocrystalline silicon using a cutting tool. Precis Eng 26(3):263–268
28. McGeough JA (1974) Principles of electrochemical machining. Chapman and Hall Halsted Press Division, Wiley, London New York
29. Kalpakjian S, Schmid S (2014) Manufacturing processes for engineering materials 5th edn. agenda 12:1
30. Bhattacharyya B, Munda J, Malapati M (2004) Advancement in electrochemical micro-machining. Int J Mach Tools Manuf 44(15):1577–1589
31. Schuster R, Kirchner V, Allongue P, Ertl G (2000) Electrochemical micromachining. Science 289(5476):98–101
32. Kozak J, Rajurkar KP, Makkar Y (2004) Selected problems of micro-electrochemical machining. J Mater Process Technol 149(1):426–431
33. Masuzawa T, Kuo C-L, Fujino M (1994) A combined electrical machining process for micronozzle fabrication. CIRP Ann Manuf Technol 43(1):189–192
34. Masuzawa T (2000) State of the art of micromachining. CIRP Ann Manuf Technol 49 (2):473–488
35. Crichton I, McGeough J, Munro W, White C (1981) Comparative studies of ecm, edm and ecam. Precis Eng 3(3):155–160
36. Ma X, Schuster R (2011) Locally enhanced cathodoluminescence of electrochemically fabricated gold nanostructures. J Electroanal Chem 662(1):12–16

37. Wang M, Peng W, Yao C, Zhang Q (2010) Electrochemical machining of the spiral internal turbulator. Int J Adv Manuf Technol 49(9–12):969–973
38. Jo CH, Kim BH, Chu CN (2009) Micro electrochemical machining for complex internal micro features. CIRP Ann Manuf Technol 58(1):181–184
39. Kunieda M, Lauwers B, Rajurkar K, Schumacher B (2005) Advancing EDM through fundamental insight into the process. CIRP Ann Manuf Technol 54(2):64–87
40. Gupta K, Chaubey SK, Jain NK (2014) Exploring wire-EDM for manufacturing the high quality meso-gears published in Procedia Materials Science, vol 5. Elsevier, 1755–1760, In: Proceedings of international conference on advances in manufacturing and materials engineering (ICAMME 2014), Surathkal, India, 27–29 March 2014
41. Uhlmann E, Piltz S, Doll U (2005) Machining of micro/miniature dies and moulds by electrical discharge machining—recent development. J Mater Process Technol 167(2):488–493
42. Weng F-T, Her M-G (2002) Study of the Batch Production of Micro Parts Using the EDM Process. Int J Adv Manuf Technol 19(4):266–270
43. Rajurkar K, Yu Z (2000) 3d micro-edm using cad/cam. CIRP Ann Manuf Technol 49(1):127–130
44. Yu Z, Masuzawa T, Fujino M (1998) Micro-EDM for three-dimensional cavities-development of uniform wear method. CIRP Ann Manuf Technol 47(1):169–172
45. Liu K, Lauwers B, Reynaerts D (2010) Process capabilities of Micro-EDM and its applications. Int J Adv Manuf Technol 47(1–4):11–19
46. Lasagni FA, Lasagni AF (2011) Fabrication and characterization in the micro-nano range: new trends for two and three dimensional structures, vol 10. Springer Science & Business Media
47. Gower M, Rizvi N (2000) Applications of laser ablation to microengineering. In: Proc SPIE, pp 452–460
48. Rizvi NH (1999) Production of novel 3D microstructures using excimer laser mask projection techniques. In: Design, test, and microfabrication of MEMS/MOEMS, International Society for Optics and Photonics, pp 546–552
49. Meng H, Liao J, Zhou Y, Zhang Q (2009) Laser micro-processing of cardiovascular stent with fiber laser cutting system. Opt Laser Technol 41(3):300–302
50. Egashira K, Masuzawa T, Fujino M, Sun X-Q (1997) Application of USM to micromachining by on-the-machine tool fabrication. Int J Electr Mach 2:31–36
51. Egashira K, Masuzawa T (1999) Microultrasonic machining by the application of workpiece vibration. CIRP Ann Manuf Technol 48(1):131–134
52. Kremer D, Saleh S, Ghabrial S, Moisan A (1981) The state of the art of ultrasonic machining. CIRP Ann Manuf Technol 30(1):107–110
53. McGeough JA (2001) Micromachining of engineering materials, CRC Press
54. Zhang C, Rentsch R, Brinksmeier E (2005) Advances in micro ultrasonic assisted lapping of microstructures in hard–brittle materials: a brief review and outlook. Int J Mach Tools Manuf 45(7):881–890
55. Moronuki N, Saito Y, Kaneko A (2006) Vibration micro-machining of low-melting temperature glass. Int J Manuf Technol Manage 9(1–2):18–33
56. Choi HJ, Lee SW, Lee BG (2003) Micro-hole machining using ultrasonic vibration. In: Key engineering materials, Trans Tech Publication, pp 29–34
57. Yu Z, Rajurkar KP, Tandon A (2004) Study of 3D micro-ultrasonic machining. Trans ASME-B-J Manuf Sci Eng 126(4):727–732
58. Kuriakose S, Patowari PK, Bhatt J (2017) Machinability study of Zr-Cu-Ti metallic glass by micro hole drilling using micro-USM. J Mater Process Technol 240:42–51
59. Takahata K, Takeo S (1997) Fine surface finishing method for 3-dimensional micro structures. IEICE Trans Electron 80(2):291–296
60. Nguyen MD, Rahman M, San Wong Y (2012) Enhanced surface integrity and dimensional accuracy by simultaneous micro-ED/EC milling. CIRP Ann Manuf Technol 61(1):191–194
61. Cao XD, Kim BH, Chu CN (2013) Hybrid micromachining of glass using ECDM and micro grinding. Int J Precis Eng Manuf 14(1):5–10

Electrochemical Methods of Micropart's Manufacturing

Sebastian Skoczypiec

Abstract This chapter introduces basics of electrochemical micromachining (ECMM). In this process, no mechanical contact between tool and workpiece occurs, and machinability is not connected with material mechanical properties, and therefore, it is an attractive technology, especially when shaping 3-D sculptured surfaces in difficult-to-cut materials. However, the key problem in ECMM is to localize dissolution to achieve satisfactory accuracy. In this chapter, specificity of electrochemical micromachining and recent trends in this area are presented. The conditions of electrochemical dissolution are discussed, and the possibilities of shaping accuracy increase are indicated in details. The special attention is paid to the results of application of voltage pulses and integration with other technologies in hybrid and sequential machining.

Keywords Electrochemical · Electrodischarge · Hybrid machining · Laser · Micromachining

Electrochemical machining (ECM) is an anodic electrochemical dissolution process in which material is removed by electrochemical dissolution when applying constant or pulse voltage between tool (cathode) and workpiece (anode) [1]. Through the thin gap (<<0.5 mm) between tool and workpiece, an electrolyte flows. Due to the presence of electrolyte in interelectrode gap, the electric charge is transported by ions, whereas by electrons in outer circuit. The electrochemical reactions on the electrode–electrolyte borders are mainly responsible for the change of conduction from electronic to ionic. One of these reactions is dissolution of workpiece material, which takes place according to Faraday's law. The dissolved material and other electrochemical reaction products are transported outside the gap by forced flow of the electrolyte.

S. Skoczypiec (✉)
Institute of Production Engineering, Faculty of Mechanical Engineering,
Cracow University of Technology, al. Jana Pawła II 37, 31-864 Kraków, Poland
e-mail: skoczypiec@mech.pk.edu.pl

K. Gupta (ed.), *Micro and Precision Manufacturing*, Engineering Materials,
https://doi.org/10.1007/978-3-319-68801-5_2

Since the fifties of the last century, ECM has been becoming an effective method for producing a wide variety of parts for the defense, aerospace, automotive, and medical industries. As regards to the micromachining application, the following advantages of this process can be mentioned: (i) no tool wear, (ii) high productivity, (iii) excellent surface quality. Therefore, recent advances in machining accuracy and precision prove that ECM becomes an attractive technology for precise micromachining. However, in order to make ECM suitable for such application, it is necessary to develop modified machining system which should provide high localized machining with gap width below 100 μm.

1 Specificity of Electrochemical Micromachining (ECMM)

Microfabrication through electrochemical action includes cathodic processes (i.e., electrodeposition, electroplating, electroforming, through-mask electroplating), anodic processes (i.e., electrochemical micromachining, electroetching, electropolishing), or open circuit processes (chemical polishing, chemical milling, chemical etching). Majority of these technologies are adapted to manufacture planar (2-D) structures, and only electrochemical micromachining (ECMM) is suitable for manufacturing 3-D complex surfaces. In ECMM, the allowance can be removed by tool shape reproduction in the machined surface (referred as electrochemical sinking, Fig. 1a) [2]. The major problem in sinking is to design and produce electrode tool with sophisticated shape. The electrode preparation cost is high, and

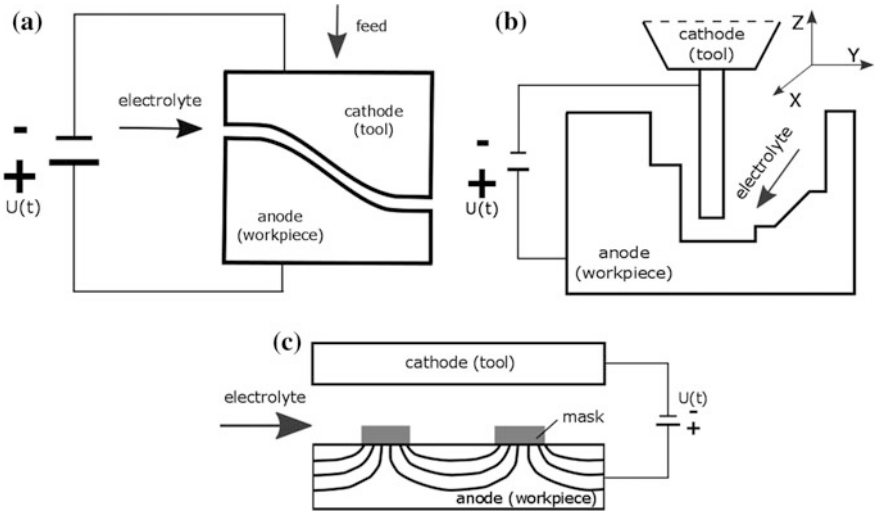

Fig. 1 Variants of electrochemical micromachining: **a** sinking, **b** machining with universal electrode tool, and **c** through-mask electrochemical micromachining

problem with effective gap flushing occurs; therefore, the range of dimensions is limited (machined area is in range of mm^2). Therefore, in micromachining dominate operations where simple electrode tool (i.e., cylindrical with spherical or flat or tip, wire) can be applied [3, 4]. In this case, the machined shape results from the electrode tool path (similar to milling, Fig. 1b). It is also worth to mention about through-mask electrochemical micromachining (TMEMM), which was developed especially to generate the microdimple array with controlled shape and density (Fig. 1b). This process also includes masking to produce insulation layer or protect selected areas of workpiece from dissolution [5].

Application of the ECMM is related to top-down machining philosophy. It means that in order to produce smaller parts, production system which is commonly used in macromanufacturing, is applied after suitable modifications. These modifications relate to machining resolution increase and machine tools and tooling precision improvement. Figure 2 presents various important factors responsible for making ECMM suitable for micromanufacturing. Machining resolution is closely related to unit removal, which can be defined as a part of the workpiece removed during one cycle of removal action. Unit removal gives information about the smallest adjustable dimensions of the part, so unit removal of sub-micrometer range is necessary when the micropart is machined or when high precision of the part is required. Theoretically, in ECMM, the smallest unit removal is ion; however, the anodic dissolution is always connected with disadvantageous effect of widening the machining area on the distance significantly higher than working electrode diameter and interelectrode gap (Fig. 3). This is called as a delocalization effect, and the

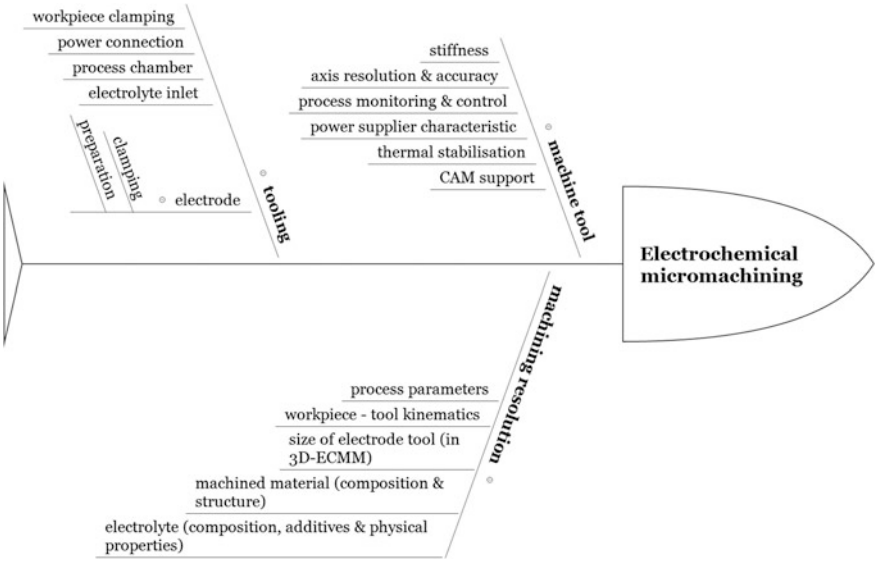

Fig. 2 Various factors of electrochemical micromachining responsible for its successful adoption to micromanufacturing

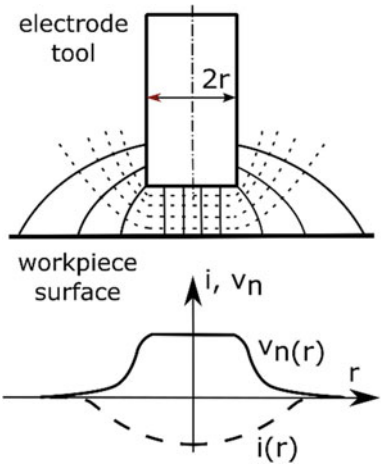

Fig. 3 Scheme of the machining area with electrical field distribution and corresponding distribution of current density i and dissolution velocity v_n

distribution of electric field in machining area is responsible for this phenomenon. Therefore, the dissolution should be controlled and limited only to specific workpiece areas. Minimization of unit removal is not enough to scale down the ECM process. It also requires adaptation of appropriate machine tools and tooling.

Recent research trends in the field of ECMM are focused around selection of optimal condition of dissolution under the small gap (<100 μm). These include especially [6]: (i) clarification of the phenomena during dissolution, (ii) modification of (resulting from primary electrical potential distribution) distribution of current density on workpiece surface, (iii) selection of proper electrolyte (composition, concentration, and additives), (iv) design of technological process (design of electrode tool shape or path, simulation of machining), (v) modification and development of machine tool (including also power supplier and technological tooling), (vi) control of the machining process (controlling the gap thickness and preventing the critical states), (vii) introduction of additional energy sources into area of dissolution to improve material machinability or machining conditions, (viii) integration with other technologies in sequential or complete machining process.

2 Localization of Electrochemical Dissolution

Dissolution localization can be defined as possibility to concentrate energy needed to remove material in relation to machined surface. The localization is narrower term than machining accuracy and can be identified with unit removal. High dissolution localization is prerequisite for high process resolution and accuracy; however, it is not sufficient. Localization is strictly connected with current density distribution over the machined surface. Taking into account simple case presented in Fig. 3, one can observe that there is some distance from the electrode tool edge

where dissolution occurs. Although current density decreases with distance from electrode, its value is large enough to dissolve distant material. To achieve high localized process, this effect has to be minimized.

Localization of electrochemical dissolution can be quantified by localization factor, which is calculated based on relation between dissolution velocity v_n and interelectrode gap thickness S. In good localized process, the curve $v_n(S)$ should be as steep as possible, so the material removal rate decreases sharply with gap thickness increase. For ideal process (curve 1 on Fig. 4), following relation takes place:

$$\frac{v_{n1}}{v_{n2}} = \frac{S_2}{S_1}$$

While high localized process should be characterized by steeper $v_n(S)$ relation (curve 2 on Fig. 4) which can be described by equation:

$$\frac{v_{n1}}{v_{n2}} = \left(\frac{S_2}{S_1}\right)^n$$

and n can be defined as localization factor. n = 1 for ideal process and to localize the dissolution, n should be as high as possible. Additionally in a good localized process, the gap thickness threshold S_L should occur (for $S > S_L$, there is no dissolution).

In recent years, several studies were carried out aimed to modify the primary current density distribution for increase in ECM localization and accuracy. The major ways include (Fig. 5):

- **decrease of interelectrode gap thickness**: accuracy is inversely proportional to interelectrode gap thickness; therefore, one of the main directions of development is to carry the process with as small as possible interelectrode gap with as high as possible technological reliability,

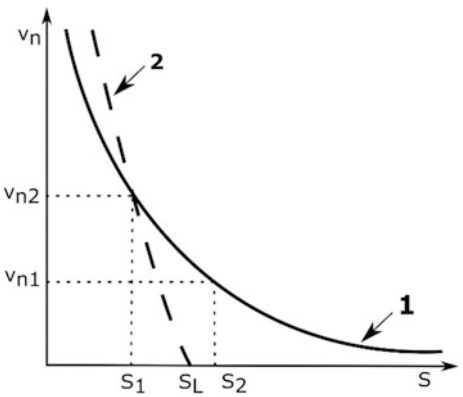

Fig. 4 Relation of dissolution velocity $v_n(S)$ from interelectrode gap thickness S; S_L limiting gap thickness

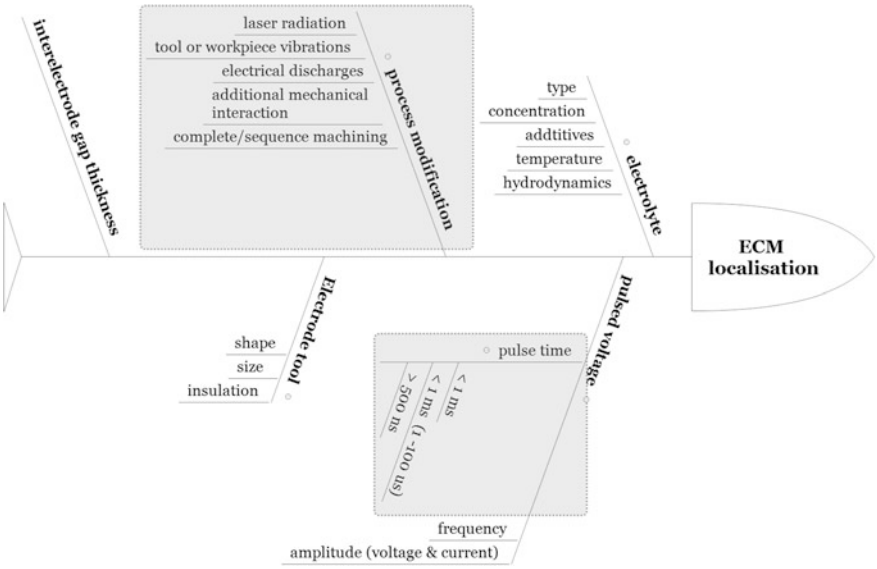

Fig. 5 Various factors responsible for improvement in anodic dissolution localization in the ECMM

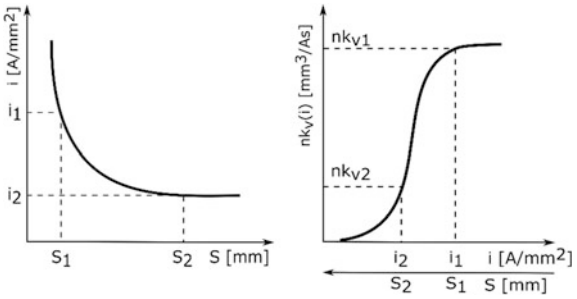

Fig. 6 Schematic relations between gap thickness S and current density i (left) and between current density i and electrochemical machinability ηk_v for passive electrolyte (right)

- **selection of proper electrolyte:** it gives possibility to obtain hyperbolic tangent-like relation between electrochemical machinability and current density (Fig. 6). This relation depends mainly on electrolyte properties (understood as its type and those resulting from the process). In ECMM application of passive electrolytes, for which lower limit of current density occurs (for $i < i_0$ no dissolution takes place) is preferred,
- **machining in electrolyte—gas mixture:** supply into the gap homogeneous mixture of electrolyte and gas (air, nitrogen, or carbon dioxide) allows to limit dissolution in areas where gap thickness is higher than assumed (in this area, gas expands to bubbles and electrolyte conductivity significantly decreases),
- **electrode tool insulation or special design:** in order to protect from dissolution distant areas of workpiece, which should not be machined, selected areas of the

electrode tool are coated with insulation layer (epoxy resin, ceramics, DLC or Teflon). In some cases, it is also possible to modify shape of electrode tool in order to concentrate dissolution in selected area (i.e., application of disk-like electrodes for hole drilling and groves machining or shaping of 3-D structures),
- **application of pulse voltage**: depending on pulse length, it gives possibility to: (i) increase process reliability (millisecond pulses), (ii) the use of electrolyte temperature increase (microsecond pulses), or (iii) use of transient phenomena (nanosecond pulses) to localize dissolution,
- **assistance of additional energy sources (hybrid machining)** or **integration with other technologies**: in complete or sequence machining.

From above-presented solutions, the most promising are application of voltage pulses and integration with other technologies/energy sources in complete or hybrid machining process. Sections 3 and 4 present the recent developments in this area.

3 Pulse Electrochemical Micromachining (PECMM)

Based on the duration of pulse time $t_{i,}$ the pulse electrochemical micromachining (PECMM) can be classified into three variants: (i) with pulse time 500 ms > t_i > *1* ms; (ii) with pulse time t_i < 1 ms (usually t_i in range 1–100 μs); (iii) with pulse time t_i < 500 ns. In the first two variants, the machining is carried out in a diffusion limited state, which generally means that the physical properties of the electrolyte in the gap determine distribution of electric current density *i*. In such case, *i* is mainly dependent on diffusion rate. While in PECMM with nanosecond voltage pulses, current density *i* is determined by activation overpotential.

3.1 Millisecond and Microsecond Pulse Electrochemical Micromachining

Accuracy of electrochemical machining increases with machining gap decrease. However, to carry out stable machining process with small gap thickness is difficult. In such case, increase of electrolyte temperature and contamination is significant; therefore, critical conditions (i.e., electrical discharges) can easily occur in the gap. Therefore, application of millisecond range voltage pulses (ms-PECMM) gives possibility to interrupt the dissolution process and refill the gap with fresh electrolyte. Additionally, in ms-PECMM: (i) reduction of the electrolyte properties that change along the gap reduces the impact of changes of electrolyte conductivity on shape errors; (ii) amount of hydrodynamics defects on workpiece surface decrease (smaller gap reduces electrolyte flow velocity). These give possibility to increase dissolution reliability under small gap condition; however, additional effect of dissolution localization does not take place. ms-PECMM enables precise machining

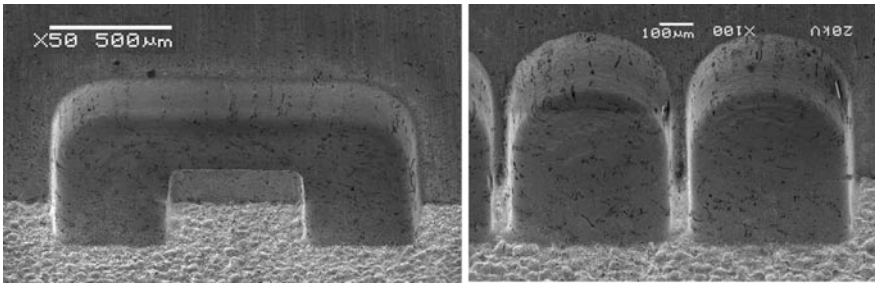

Fig. 7 Example of µs-PECM applications: microstructures machined in milling kinematics with following parameters: pulse time t_i = 1 µs, pause time t_p = 10 µs, pulse voltage U = 20 V, electrolyte 1% $NaNO_3$, electrode feed rate v_p = 50 µm/min, electrode rotation speed 500 1/min, electrode diameter D = 0.4 mm

with gap thickness of about 0.01–0.1 mm (in ECM, typical gap is in range of 0.1–1 mm).

A further reduction of the pulse time to the microsecond range (µs-PECMM) improves whole above-mentioned effects connected with dissolution homogeneity and reliability. However, in µs-PECMM, the gap thickness is smaller, and the electrolyte temperature increases more intensively. It is the reason of more intense electrolyte conductivity increase, and therefore, machining is carried out with higher current density *i*. Therefore, according to the relation between current density and electrochemical machinability in areas with smaller gaps, dissolution is more efficient (Fig. 6) and relation $v_n(S)$ is steeper. The key for µs-PECMM is avoiding electrolyte boiling in the gap; therefore, pulse length is limited by critical pulse time, which should be calculated based on thermal limitation in the gap [7]. µs-PECMM can be adopted for micropart and precision and manufacturing (see example in Fig. 7), and the limits of adaptation are defined by critical conditions in the gap. To ensure stable dissolution process, efficient gap flushing is necessary. It can be achieved electrically (by applying adequately long pulse pause) or mechanically (by applying pulse electrode tool vibration). When conditions of dissolution are optimal, the accuracy of µs-PECM can reach 5 µm.

3.2 Nanosecond Pulse Electrochemical Micromachining (Ns-PECMM)

The idea of nanosecond pulse electrochemical machining was developed in the end of the last century [8]. In ns-PECMM, the dissolution process is driven by the cyclic electric double layer (EDL) charging and discharging process. In workpiece areas where EDL charge reaches the activation overpotential, the dissolution starts. However, the time of EDL charging to the activation overpotential is a function of gap thickness; therefore, pulse time determines maximal distance between tool and

workpiece where dissolution occurs. When machining is carried out with a longer pulse time ($t_i > 0.5$ μs), the EDL is charged uniformly over the machining surface (dissolution is determined by diffusion); therefore, trainset effect connected with cyclic EDL charging and discharging is negligible. In ns-PECMM, due to extremely short pulse time, dissolution is carried out in accordance with Butler–Volmer equation, which exponentially relates current density i and overpotential. It means that large change of the current density is caused by a small change of the electrode potential. Due this effect, dissolution localization is also improved [9, 10].

The high capabilities of ns-PECMM have been identified in the research conducted. For example, 1.4301 steel can be machined with lateral gap ≈200 nm what gives possibility to obtain edge radius ≈1 μm [11]. The workpiece in ns-PECMM can be machined with many kinematic variants as hole drilling or sinking [12–14], with application of universal electrode tool [3, 15, 16], or in kinematic similar to wire cutting [4, 17]. However, it is worth to underline that majority of work presented in literature results of successive ns-PECMM application were obtained in laboratories, and this technology is not popular in the industry. The problems of commercialization are connected with difficulties in upscaling the process [18]. In ns-PECMM, the increase of electrode tool area is limited by reactance of the power supply circuit, what limits charging rate of EDL. In such case, achieving the activation overpotential requires increase of the pulse time $t_{i,}$ what results in change to diffusion limited process (and process characteristic like μs-PECMM). Machining of areas in range of 1 mm^2 by ns-PECMM needs application of high current pulse power suppliers and careful selection of type and doping of electrolyte. Therefore, ns-PECMM is most effective with application of universal electrode tool with pin, conical, cylindrical, or disk-like tip and diameter less than 100 μm. The area of ns-PECMM application small series or single production of prototypes and tools with 3-D shapes is suggested. However, machining results depends from tool size, workpiece material composition and heterogeneity of the structure. Therefore necessity to precise choice of the electrolyte composition and its additives for each machining material significantly limits flexibility of this method.

4 Electrochemical Machining Integration with Other Technologies

Integrated or hybrid machining technologies are latest research topics these days. Hybrid machine tools are based on the combination of different manufacturing technologies in single workstation to obtain high-quality product [19]. Hybridization results in decrease in machining time, reduction in machining cost, and part quality enhancement, while reasons for developing hybrid machining processes (HMP) are to exploit their advantages together and to avoid their limitations when they are applied individually [20].

4.1 Hybrid Electrochemical Micromachining Processes

4.1.1 Electrochemical and Mechanical Interaction

The idea of combining electrochemical and mechanical interaction for efficient material removal was developed in the 1960s in the form of the electrochemical grinding (AECG). In AECG, a metal bonded abrasive tool is used as a cathode, and thus, the simultaneous mechanical and electrochemical material removal takes place. Zhu et al. [21] present an example of successful application of grinding and electrochemical removal in the micromachining domain (precise machining of small holes). They applied abrasive coated metal rod as a cathode tool to remove the material in pre-machined pilot hole. Depending on the machining parameters (like machining voltage, cathode rotation speed, and feed rate), the way of material removal can be balanced between mechanical and electrochemical. In this process, small holes of diameter down to 0.6 mm with sharp edges and without burrs were drilled.

An example of effective combination of electrochemical and mechanical energy to remove material electrochemically assisted microturning process is mentioned [22]. In this case, electrochemical assistance changes the machinability while the microcutting directly removes the material (Fig. 8). Produced in electrochemical reaction oxide layer has different mechanical properties than machined metal and can be removed with reduced cutting force. Research presented in [22] shows that electrochemical assistance of microturning decreases the average cutting force from a few to tens percent. In addition, surface machined with electrochemical assistance indicates decrease of plowing effect what leads to surface quality improvement (Fig. 9). This method can be applied to machine only passivating materials such as stainless steel, aluminum or titanium alloys. It is also worth emphasizing that electrochemical assistance gives benefits when the depth-of-cut is ≤ 1 μm.

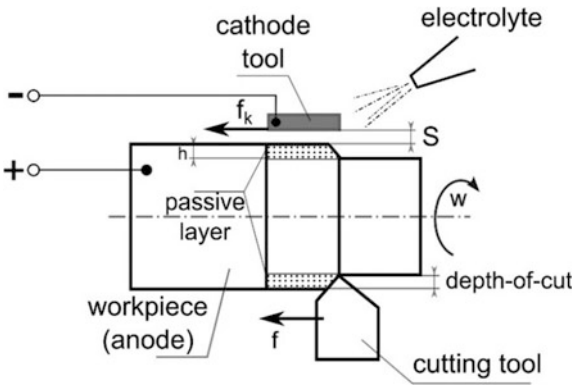

Fig. 8 Scheme of electrochemically assisted microturning process: *S*—interelectrode gap, *h*—passive layer thickness, *f*—cutting tool feed rate, f_k—cathode feed rate ($fk = f$), *w*—rotational speed [22]

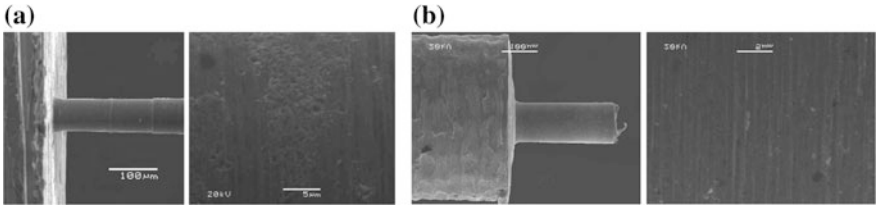

Fig. 9 SEM images of the shaft surface after microturning without (**a**) and with electrochemical assistance (**b**); machined material: 1.4301 steel, depth-of-cut 1 μm, $f = f_k$ = 0,02 μm/s, w = 60,000 1/min, U = 3 V, electrolyte 1% $NaNO_3$ [22]

4.1.2 Electrochemical Machining Supported by Electrode Vibrations

Application of the combination of synchronized low-frequency pulsed voltage and the oscillating electrode enables machining with reduced working gaps (in range 10–50 μm) and significantly higher current densities. When minimum gap thickness is achieved, voltage is switched on for period from 500 to 5000 μs (depends on application), which lead to removal process; however, due to small gap, only low amount of electrolyte is transported through machining area. While during pulse pauses, when the distance between anode and cathode is maximized, excellent supply of electrolyte takes place, and the waste electrolyte is replaced with the fresh one. Oscillation movement of electrode tool is superimposed by its forward movement. It is worth to underline that in this process, high amount of time is used for gap flushing; therefore, material removal rate is reduced in comparison to ECM. Due to high localization, vibration-assisted PECMM is applied for the manufacturing of complex microstructures or precise machining of cutting tools or structured metal parts (i.e., razor shave cabs).

In [23, 24], authors proposed application of low amplitude (5 μm or less) and low frequency (tens or hundreds Hz) of vibration of tool to improve the flow of electrolyte during machining of high-ratio microstructures. Research was carried with application of MHz range pulse voltage frequency with no synchronization between tool periodical movement and electrical signal. Obtained results prove that tool vibration gives possibility to increase mass transport in the gap, improve stability of micromachining due to improved flow of electrolyte, and lead to material removal rate increase. The same authors also proposed application of low amplitude tool vibration to improve shape accuracy of borehole [25]. Also in this case, current density increases and additional effect of borehole quality improvement occurs (more cylindrical, lesser overcut, and better surface finish). Authors conclude also that amplitude of vibrations can be used as parameters to adjust borehole taper angle.

The other proposition is to apply vibration in ultrasonic frequency range. According to [26], it can be mentioned that ultrasonic vibration (i) improves products removal from the gap, (ii) supports diffusion, (iii) decreases the rate of

passivation, (iv) changes electrochemical machinability, and (v) improves hydrodynamic condition. Whole this effects permits machining with high current density. Young et al. [27] applied ultrasonic vibrations with frequency of 40 kHz and an amplitude of 4 μm straight to the electrolyte volume. Such a solution is simpler to design and to control than to apply vibration to the workpiece or tool. They drilled microholes with diameter less than 100 μm and depth up to 300 μm with ns-PECMM setup, which was not available for machining without ultrasonic vibrations. Decrease of machining time leads also to decrease diameter at entrance, and thus, machining precision was also improved.

4.1.3 Electrochemical–Electrodischarge Machining

Discussing electrochemical–electrodischarge machining, it should be pointed that in the literature, this term is connected with two different hybrid machining methods. The first one is also referred as spark-assisted electrochemical machining (SAEM) [28, 29]. In SAEM, electrochemical reactions between electrode tool and auxiliary electrode cause the formation of hydrogen gas film around electrode tool, and it is a medium wherein arc discharges take place. It leads to remove material by combined mechanism of local heating and chemical etching. It is an emerging micromachining process especially preferred to fabricate microchannels, grooves, holes, and 3-D complex shapes on nonconductive materials like glass, ceramics, or quartz. It is worth to underline that in SAEM process, electrochemical reactions only create conditions for material removal; however, they are not used directly to remove material.

Electrochemical–electrodischarge machining (ECDM) involves combination of electrochemical reactions and electrical discharges to remove material. In this process, depending on the machining parameters (gap thickness, voltage, current density, and pulse on/off time), the material is removed by electrochemical dissolution or simultaneous electrochemical dissolution and electrical discharges. The share of discharges in the removal process is directly connected with the intensity of the electrochemical reactions. When the electrochemical process is carried out close to critical state, the electric current flow generates Joule heating, the electrolyte begins to boil and evaporate, and gas–vapor layer is created near in the gap. Finally, electric discharges occur, and the material is removed in a typical way for the EDM process. The electrical erosion is localized in areas of the workpiece where the current density is higher than the critical value (it depends on gap thickness) and for the rest of the surface, the metal dissolves electrochemically. The benefits of this process are a significant increase of the material removal rate in comparison to ECM and EDM, respectively, and decrease of tool wear in comparison to EDM. Electrochemical discharge machining can be used in different kinematic variants, although hole drilling and die sinking are preferred [30].

4.1.4 Jet-Assisted Electrochemical Machining

In Jet-ECM, the cathode tool is created by small nozzle which ejects electrolyte with high pressure (jet velocity in range of tens of m/s). The jet has well-defined geometrical shape (which can be treated as a tool), which hits the workpiece in perpendicular direction to its surface. In this process, the dissolution is restricted to limited area of the jet and high current densities, local material removal and high localization is achieved [31, 32]. In some application, to form closed electrolytic jet, this process is assisted by surrounding air [33], or to enhance material removal, electrolyte-guided laser beam is applied [34]. Due to excellent supply of fresh electrolyte and efficient removal of dissolution products in Jet-ECM, continuous voltage can be used. Jet-ECM allows to machine microstructured planar surfaces and complex three-dimensional shapes by changing position of nozzle and adjusting electric current.

4.1.5 Laser-Assisted Electrochemical Machining

The combination of the laser radiation and electrochemical impact on the machined material can be applied as combined process (see next paragraph) and as a hybrid machining process. The anodic dissolution begins, when the energy of the metal ions become higher than the desired reaction activation energy E_a. This energy is determined by the electrical potential and surface temperature. At a higher temperature, there is a greater proportion of electroactive ions with the energy $E \geq E_a$; therefore, changing the surface temperature leads to increase of current density on the workpiece–electrolyte interface. This effect is described by exponential Arrhenius equation, so increase of workpiece surface temperature results in several time current density increase (Fig. 10) [35]; therefore, the selective workpiece heating gives possibility to localize the dissolution. According to [36], the best choice for workpiece surface heating in ECM is green laser with wavelength in range 470–560 nm.

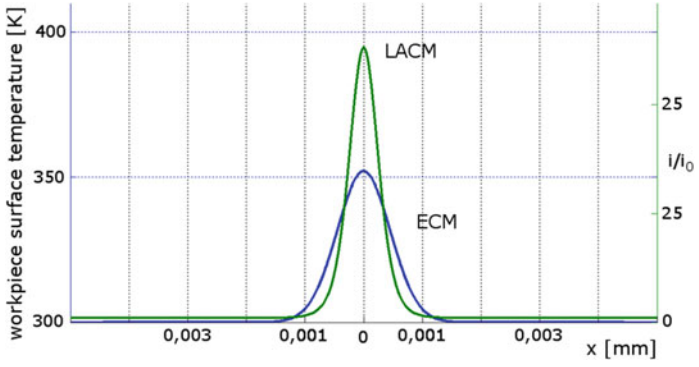

Fig. 10 Effect of workpiece surface temperature increases on current increase, ΔT = 60 K, laser beam waist w_0 = 1.8 mm (i_0—current density during electrochemical process without heating, i—current density during electrochemical process thermally enhanced)

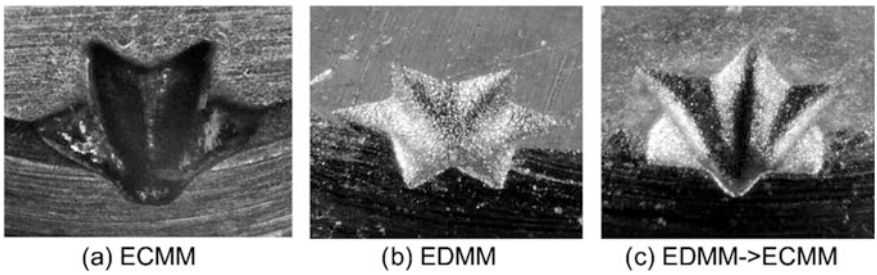

Fig. 11 Photographs of cavities machined during: **a** electrochemical sinking, **b** electrodischarge sinking, and **c** sinking when using the EC/EDMM sequence [42]

In case of material removal, the most effective solution is application of electrolyte jet-guided laser beam. After using effective solution, De Silva et al. [34] found higher material removal rate in axial rather than in lateral direction with improvement in dimensional precision. In addition to the localization effect, the laser beam favors surface depassivation, what improve machining of passivating materials like titanium, aluminum alloys, or stainless steel. Application of laser assistance improves material removal rate for these materials up to 50% and improves shape accuracy (noticeable reduction of overcut occurs).

Due to much higher activation energy, the most promising is introduction of the laser beam in the electrochemical deposition process. In this case, laser assistance results in almost a thousand times increase of deposition velocity. Typical example of such effective laser application is described in [37]. The copper anode is immersed in mixture of $CuSO_4$, H_2SO_4, and HCl with 5 mm distance from cathode surface. The interelectrode voltage value is set slightly below the copper deposition border, and then the workpiece surface has been selectively heated with application of DPSS green laser. In these areas, the copper deposition occurs (layer thickness about 10 μm).

The potential application of laser-enhanced electrochemical machining is workpiece surface structuring, especially for biomedical and bearing applications. With laser-enhanced ECM, fabricate series of micrometer-sized cavities of different size, shape, and separation distance is possible, that can be useful for the changes of such surfaces' functional properties.

4.2 Sequential Electrochemical Micromachining Processes

4.2.1 Laser and Electrochemical Processing Sequence

In sequential integration of laser and electrochemical machining, the laser is used for positive or negative workpiece surface masking. The process is carried out in similar way to the lithographic one, but instead of series of chemical treatments, the

laser radiation is applied. In positive masking, it takes place in four steps: anodizing, laser masking, electrochemical dissolution, and ultrasonic cleaning [37, 38]. In negative masking, as the result of the laser impact, thin layer of nonconductive oxides (Cr_2O_3, FeO, and Fe_2O_3) and some structural changes on the workpiece surface occur [40, 41]. These areas are characterized by significantly lower electrical conductivity, and therefore, ratio of electrochemical dissolution is smaller in comparison to native material. Thanks to fiber optics, and technological equipment positive laser masking and electrochemical dissolution can be carried out on the same machine tool. Over lithographic methods, this process has following advantages, i.e., relatively inexpensive way of mask registration (masking takes place in air, no major requirement for room cleanliness), environment-friendly processing (significantly less chemical agents), and greater process flexibility (the process is more effective in short and prototype series). But the main disadvantage compared to lithography is relative long time of mask registration (tens of minutes).

4.2.2 Sequential Electrochemical—Electro Discharge Processes

The characteristics of electrochemical and electrodischarge micromachining as presented in [42] indicate the number of essential complementary advantages and many similarities between both processes. Therefore, in the recent years, many ways of electrochemical and electrodischarge machining combinations in one sequence have been proposed. The presented research has been focused on applying electrochemical treatment to improve the surface layer quality of EDM-ed microparts [43–47]. These ideas include the realization of processes in sequence on the same machine tool and with the same electrode, although the differences concern power supply and the working fluids medium system. In [43], the milling kinematic sequence was carried out with the application of different working fluids and independent power suppliers for EDMM and ECMM. For such system, the removal of 13 μm allowance thickness during ECM finishing gives the possibility of decreasing EDM-shaped surface roughness from Ra = 0.707 μm to 0.143 μm. In addition, the recast layer, burrs, craters, and micropores are removed. The results as presented in [44] also show that correct drilling sequence design allows machining efficiency to be improved by 9.2 times with simultaneous improvement of hole precision and shape accuracy. The other approach is to apply the same machining liquid (partially deionized water) and the same power suppliers. In such case, nature of machining (ECMM or EDMM) results from the appropriate process control (change from EDMM to ECMM can be achieved by the decrease of power supply capacitance and electrode feed rate [46]). Such strategy gives the possibility to improve Ra from 1 to 0.6 μm in sinking and from 0.9 to 0.2 μm in ECMM followed by EDMM milling operation. In literature, EDMM and ECMM were also carried out with the same pulse voltage signal (voltage amplitude 60 V, frequency 500 kHz, and duty factor in range 0.25–0.4) [47]. The developed control strategy is based on an electrode tool feed rate which ranges from 50 to 10 μm/s. In the case of 50 μm/s, the electrical discharges dominate in material removal mechanism due to

small interelectrode gap, while reducing the feed rate to 10 μm/s promotes material dissolution and reduces the surface roughness to Ra = 0.022 μm. In sequence EDMM followed by ECMM, one disadvantage is a decrease in accuracy and edge rounding during the ECMM finishing in comparison to the part machined by EDMM. To minimize this effect, an application of 704-silica side-insulation electrode tool was proposed in milling operation [44]. This gave the possibility of minimizing hydrogen bubble generation on the electrode sidewall and allowed to obtain uniform side-machining gap.

Carrying out ECMM followed by EDMM on the same machine tool allows for an essential reduction of the disadvantages and enhances the advantages of both methods [42]. Application of the ECMM -> EDMM sequence allows for an almost double decrease in the machining time in comparison to EDMM (Fig. 12a). Additionally, the mean edge radius of cavities is significantly smaller than that in ECMM (Fig. 12b). It is also worth to underline that the thickness of allowance machined in EDMM phase is only 100 μm; therefore, the effect of tool wear on the cavity shape is negligible (Fig. 13).

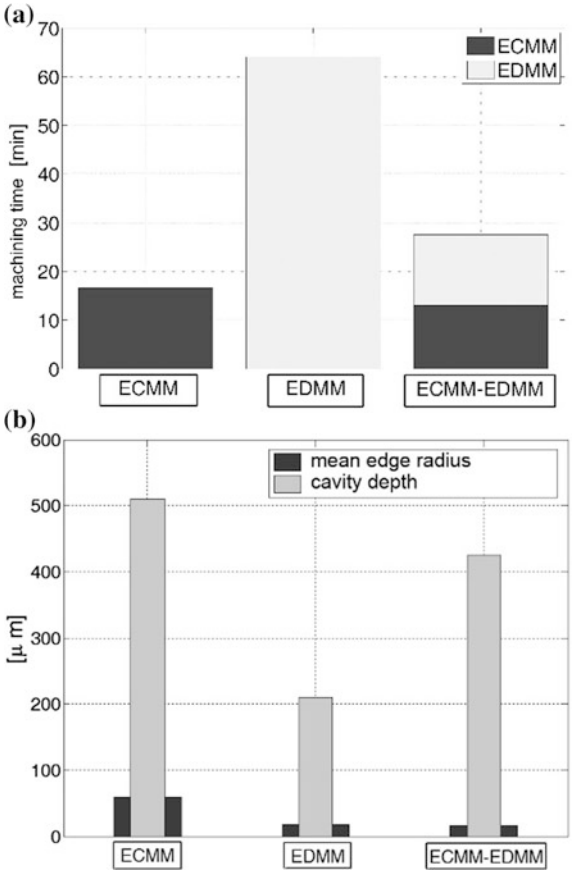

Fig. 12 Comparison of machining time (**a**) and mean edge radius and cavity depth (**b**) for the ECM, EDM, and ECMM followed by EDMM sequence (machining results presented in Fig. 11) [42]

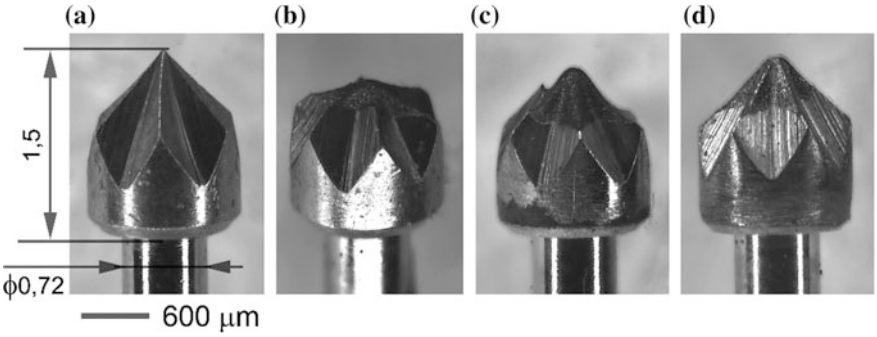

Fig. 13 Photographs of the electrode tool after: **a** ECMM, **b** EDMM, **c** an improperly designed EC/EDMM machining sequence, and **d** a properly designed EC/EDMM machining sequence of the cavity presented in Fig. 12 [42]

5 Summary

In this chapter, specificity of electrochemical micromachining and recent trends in this area are addressed. The special attention was paid to developments and limitations connected with shaping accuracy increase. In this area, the most promising are (i) application of voltage pulses (in range of milli-, micro-, and nanoseconds) and (ii) integration with other technologies/energy sources in complete or hybrid machining process. In both of these areas, significant progress in recent years has been observed that makes ECM a very attractive micromachining technology. The preferred application areas for electrochemical micromachining include: (i) machining of microholes with circular or polygonal cross section; (ii) surface structuring to improve structural and tribological properties of parts for medical applications, bearing, or tooling industry; (iii) manufacturing of 3-D structures, tools, (i.e., micromolds), parts of technological tooling, and prototypes of MEMS parts.

References

1. Davydov AD, Volgin VM, Lyubimov VV (2004) Electrochemical machining of metals: Fundamentals of electrochemical shaping. Russ J Electrochem 40(12):1230–1265
2. Wang W, Zhu D, Qu N, Huang S, Fang X (2009) Electrochemical drilling inclined holes using wedged electrodes. Int J Adv Manuf Technol 47(9–12):1129–1136. https://doi.org/10.1007/s00170-009-2247-9
3. Kim, BH, Ryu SH, Choi DK, Chu CN (2005) Micro electrochemical milling. J Micromech Microeng 15(1):124–129. https://doi.org/10.1088/0960-1317/15/1/019
4. Wang S, Zhu D, Zeng Y, Liu Y (2010) Micro wire electrode electrochemical cutting with low frequency and small amplitude tool vibration. Int J Adv Manuf Technol 53(5–8):535–544. https://doi.org/10.1007/s00170-010-2835-8

5. Chen X, Qu N, Li H, Xu Z (2016) Electrochemical micromachining of micro-dimple arrays using a polydimethylsiloxane (PDMS) mask. J Mater Process Technol 229:102–110. https://doi.org/10.1016/j.jmatprotec.2015.09.008
6. Rajurkar KP, Sundaram MM, Malshe AP (2013) Review of electrochemical and electrodischarge machining. Procedia CIRP 6:13–26. https://doi.org/10.1016/j.procir.2013.03.002
7. Kozak J (2004) Thermal models of pulse electrochemical machining. Bull Pol Acad Sci Tech Sci 52(4):313–320
8. Schuster R (2000) Electrochemical Micromachining. Sci 289(5476):98–101. https://doi.org/10.1126/science.289.5476.98
9. Kirchner V, Xia X, Schuster R (2001) Electrochemical nanostructuring with ultrashort voltage pulses. Acc Chem Res 34(5):371–377. Retrieved from http://www.ncbi.nlm.nih.gov/pubmed/21727446
10. Kock M, Kirchner V, Schuster R (2003) Electrochemical micromachining with ultrashort voltage pulses–a versatile method with lithographical precision. Electrochim Acta 48(20–22):3213–3219. https://doi.org/10.1016/S0013-4686(03)00374-8
11. Cagnon L, Kirchner V, Kock M, Schuster R, Ertl G, Gmelin WT, Kück H (2003) Electrochemical Micromachining of Stainless Steel by Ultrashort Voltage Pulses. Z Phys Chem 217(4–2003):299–314. https://doi.org/10.1524/zpch.217.4.299.20383
12. Fan Z, Hourng L (2011) Electrochemical micro-drilling of deep holes by rotational cathode tools. Int J 555–563. https://doi.org/10.1007/s00170-010-2744-x
13. Jo CH, Kim BH, Chu CN (2009) Micro electrochemical machining for complex internal micro features. CIRP Ann—Manuf Technol 58(1):181–184. https://doi.org/10.1016/j.cirp.2009.03.072
14. Maurer JJ, Mallett JJ, Hudson JL, Fick SE, Moffat TP, Shaw GA (2010) Electrochemical micromachining of Hastelloy B-2 with ultrashort voltage pulses. Electrochim Acta 55(3):952–958. https://doi.org/10.1016/j.electacta.2009.09.004
15. Liu Y, Zhu D, Zhu L (2012). Micro electrochemical milling of complex structures by using in situ fabricated cylindrical electrode. Int J, 977–984. https://doi.org/10.1007/s00170-011-3682-y
16. Yong L, Di Z, Yongbin Z, Shaofu H, Hongbing Y (2010) Experimental investigation on complex structures machining by electrochemical micromachining technology. Chin J Aeronaut 23(5):578–584. https://doi.org/10.1016/S1000-9361(09)60257-0
17. Zeng YB, Yu Q, Wang SH, Zhu D (2012) Enhancement of mass transport in micro wire electrochemical machining. CIRP Ann—Manuf Technol 61(1):195–198. https://doi.org/10.1016/j.cirp.2012.03.082
18. Skoczypiec S (2016) Discussion of ultrashort voltage pulses electrochemical micromachining : A review. Int J Adv Manuf Technol 87:177–187. https://doi.org/10.1007/s00170-016-8392-z
19. Lauwers B, Klocke F, Klink A, Tekkaya AE, Neugebauer R, Mcintosh D (2014) Hybrid processes in manufacturing. CIRP Ann—Manuf Technol. https://doi.org/10.1016/j.cirp.2014.05.003
20. Gupta et al (2016) Chapter-1 Overview of hybrid machining processes. In (eds.) Hybrid machining processes, Springer, pp 1–7
21. Zhu D, Zeng YB, Xu ZY, Zhang XY (2011) Precision machining of small holes by the hybrid process of electrochemical removal and grinding. CIRP Ann—Manuf Technol 60(1):247–250. https://doi.org/10.1016/j.cirp.2011.03.130
22. Skoczypiec S, Grabowski M, Ruszaj A (2016) The impact of electrochemical assistance on the microturning process. Int J Adv Manuf Technol 86:1873–1880. https://doi.org/10.1007/s00170-015-8320-7
23. Ghoshal B, Bhattacharyya B (2015) Vibration assisted electrochemical micromachining of high aspect ratio micro features. Precis Eng 42:231–241. https://doi.org/10.1016/j.precisioneng.2015.05.005
24. Ghoshal B, Bhattacharyya B (2015) Investigation on profile of microchannel generated by electrochemical micromachining. J Mater Process Technol 222:410–421. https://doi.org/10.1016/j.jmatprotec.2015.03.025

25. Ghoshal B, Bhattacharyya B (2014) Shape control in micro borehole generation by EMM with the assistance of vibration of tool. Precis Eng 38(1):127–137. https://doi.org/10.1016/j.precisioneng.2013.08.004
26. Skoczypiec S (2010) Research on ultrasonically assisted electrochemical machining process. Int J Adv Manuf Technol (2011) 52:565–574. https://doi.org/10.1007/s00170-010-2774-4
27. Yang I, Park MS, Chu CN (2009) Micro ECM with ultrasonic vibrations using a semi-cylindrical tool. Int J Precis Eng Manuf 10(2):5–10. https://doi.org/10.1007/s12541-009-0020-5
28. Krötz H, Wegener K (2015) Sparc assisted electrochemical machining: a novel possibility for microdrilling into electrical conductive materials using the electrochemical discharge phenomenon. Int J Adv Manuf Technol 79(9–12):1633–1643. https://doi.org/10.1007/s00170-015-6913-9
29. Singh T, Dvivedi A (2016) Developments in electrochemical discharge machining: A review on electrochemical discharge machining, process variants and their hybrid methods. Int J Mach Tools Manuf 105:1–13. https://doi.org/10.1016/j.ijmachtools.2016.03.004
30. Yin Q, Wang B, Zhang Y, Ji F, Liu G (2014) Research of lower tool electrode wear in simultaneous EDM and ECM. J Mater Process Technol 214(8):1759–1768. https://doi.org/10.1016/j.jmatprotec.2014.03.025
31. Kunieda M, Mizugai K, Watanabe S, Shibuya N, Iwamoto N (2011) Electrochemical micromachining using flat electrolyte jet. CIRP Ann—Manuf Technol 60(1):251–254. https://doi.org/10.1016/j.cirp.2011.03.022
32. Lipiec P, Wyszynski D, Skoczypiec S (2013) Primary research on jet ECM processing of difficult to cut materials. Key Eng Mater 554–557:1793–1799. https://doi.org/10.4028/www.scientific.net/KEM.554-557.1793
33. Hackert-Oschätzchen M, Meichsner G, Zinecker M, Martin A, Schubert A (2012) Micro machining with continuous electrolytic free jet. Precis Eng 36(4):612–619. https://doi.org/10.1016/j.precisioneng.2012.05.003
34. De Silva AKM, Pajak PT, McGeough JA, Harrison DK (2011) Thermal effects in laser assisted jet electrochemical machining. CIRP Ann—Manuf Technol 60(1):243–246. https://doi.org/10.1016/j.cirp.2011.03.132
35. Skoczypiec S (2015) Application of laser and electrochemical interaction in sequential and hybrid micromachining processes. Bull Pol Acad Sci Tech Sci 63(1):305–314. https://doi.org/10.1515/bpasts-2015-0035
36. Zhang H, Xu J, Wang J (2009) Investigation of a novel hybrid process of laser drilling assisted with jet electrochemical machining. Opt Lasers Eng 47(11):1242–1249. https://doi.org/10.1016/j.optlaseng.2009.05.009
37. Wee LM, Li L (2005) Multiple-layer laser direct writing metal deposition in electrolyte solution. Appl Surf Sci 247(1–4):285–293. https://doi.org/10.1016/j.apsusc.2005.01.142
38. Chauvy PF, Hoffmann P, Landolt D (2003) Electrochemical micromachining of titanium using laser oxide film lithography: Excimer laser irradiation of anodic oxide. Appl Surf Sci 211(1–4):113–127. https://doi.org/10.1016/S0169-4332(03)00256-3
39. Chauvy PF, Hoffmann P, Landolt D (2003) Applications of laser lithography on oxide film to titanium micromachining. Appl Surf Sci 208–209:165–170. https://doi.org/10.1016/S0169-4332(02)01361-2
40. Shin HS, Chung DK, Park MS, Chu CN (2011) Analysis of machining characteristics in electrochemical etching using laser masking. Appl Surf Sci 258(5):1689–1698. https://doi.org/10.1016/j.apsusc.2011.10.010
41. Shin HS, Park MS, Chu CN (2010) Electrochemical etching using laser masking for multilayered structures on stainless steel. CIRP Ann—Manuf Technol 59(1):585–588. https://doi.org/10.1016/j.cirp.2010.03.134
42. Skoczypiec S, Ruszaj A (2014) A sequential electrochemical-electrodischarge process for micropart manufacturing. Precis Eng 38 (2014):680–690. https://doi.org/10.1016/j.precisioneng.2014.03.007

43. Zeng Z, Wang Y, Wang Z, Shan D, He X (2012) A study of micro-EDM and micro-ECM combined milling for 3D metallic micro-structures. Precis Eng 36(3):500–509. https://doi.org/10.1016/j.precisioneng.2012.01.005
44. He XL, Wang YK, Wang ZL, Zeng ZQ (2011) Micro-hole drilled by EDM–ECM combined processing. Key Eng Mater 562–565:52–6
45. Hu MH, Li Y, Zhu XG, Tong H (2011) Influence of side-insulation film on hybrid process of micro EDM and ECM for 3D micro structures. Adv Mater Res 230–232:517–521
46. Kurita T, Hattori M (2006) A study of EDM and ECM / ECM-lapping complex machining technology. Int J 46:1804–1810. https://doi.org/10.1016/j.ijmachtools.2005.11.009
47. Nguyen MD, Rahman M, Wong YS (2012) Enhanced surface integrity and dimensional accuracy by simultaneous micro-ED/EC milling. CIRP Ann—Manuf Technol 61(1):191–194. https://doi.org/10.1016/j.cirp.2012.03.011

Precision Photochemical Machining

Atul R. Saraf, Shivam P. Yadav and M. Sadaiah

Abstract This chapter describes the role of photochemical machining (PCM) in micromanufacturing and discusses the critical issues in this process. The competitive market has witnessed a rapid increase in demand of low-cost microcomponents and microproducts in various industrial sectors including medical implants, optics, automotive, electronics and biotechnology. Photochemical machining is a low-cost process for the manufacturing of such miniature components and parts. Photochemical machining requires chemically stable resist mask with superior adhesion quality. The photoresist chemistry and image development technology plays an important role in precision manufacturing. This chapter has reviewed the development of photoresist chemistry and image development technology which improves the performance and yield. The chemistry of photoresists is very complex due to the different components and the component characteristics required for each photoresist. This chapter explains the role of oxygen, photoinitiator, free radical formation and exposure time in photoresist. Review of the various assisted processes of PCM such as magnetic field-assisted PCM and ultrasonic-assisted PCM is discussed.

A.R. Saraf (✉)
Mechanical Engineering Department, Chh. Shahu College of Engineering, Aurangabad, India
e-mail: atul.saraf001@gmail.com

S.P. Yadav · M. Sadaiah
Mechanical Engineering Department, Dr. B. A. Technological University, Lonere, India
e-mail: shivamdv96@gmail.com

M. Sadaiah
e-mail: msadaiah@dbatu.ac.in

K. Gupta (ed.), *Micro and Precision Manufacturing*, Engineering Materials,
https://doi.org/10.1007/978-3-319-68801-5_3

Keywords Etching · Image development · Microfluidics · Photochemical machining · Photoresist

1 Introduction

Photochemical machining is tightly controlled selective corrosion technique which produces burr-free and stress-free flat metal components through photochemical production mask. Ultra-precise, complex, stress-free and burr-free miniature components of biocompatible materials can be produced in a relatively short time. PCM industries working together with leading companies in the medical industry deliver high-quality and high-precision metal parts. It is applied in a broad range of industries and applications where high precision is needed. Critical shapes can be easily produced from imaginations to actual and from prototype to a large-scale production.

In the photochemical machining process, a phototool is used, which is a clear polyester sheet with black lines and therefore contains the master image pattern. The photochemical machining process is used for fabricating thin gauge metal and ceramic or glass parts. The thickness of the part ranges from 0.001 to 0.080 in. depending on the type of metal. This phototool allows transference of this image on the photoresist. After the development of the parts of the images, and washing away the uncured "resist", the metal about the part is dissolved using an etching chemistry [1]. With constant development of medical science, the medical industry and healthcare industry see tremendous growth opportunities as well as challenges. Traditional manufacturing processes such as stamping, EDM, waterjet cutting and laser cutting can no longer meet the demanding requirements the industry faces nowadays. Photochemical etching, on the other hand, turns out to be the perfect technology that enables continuous innovative development in medical and healthcare application. Applications of PCM products include microneedle, hearing aid, medical saw, medical blade, vascular stiffener, contact, grid, mesh and all kinds of electrical parts in medical devices.

2 Need of PCM

The resulting part from the photochemical process has no deformation or burr in the workpiece. PCM process provides an inexpensive, flexible and fast way to manufacture a wide variety of precision microcomponents. Phototool replaces conventional dies and tools. These phototools can be rapidly generated and inexpensively regenerated. Since the phototool operates like a stencil, there is no "tool wear" that needs to be monitored. Hence, PCM is an attractive alternative. PCM offers several advantages over conventional methods such as low-cost tooling, stress-free and burr-free, high accuracy and complexity, fast prototyping,

complexity without cost, unaffected material properties, easy processing of high strength materials and high flexibility [2].

3 Steps in PCM

The process of photochemical machining can be classified into four major stages: manufacturing of the phototool, coating of the cleaned metal part with the photoresist, processing of photoresist and the etching process. Figure 1 depicts the flow chart of PCM steps. It elaborates that the manufacturing of the phototool and the coating of the photoresist can be carried out simultaneously.

The following steps are used in the PCM.

3.1 Phototool Manufacturing

It starts with the generation of the artwork in a 2D CAD file after which artwork is downloaded on a laser imager which exposes the required image on the photographic film. This exposed film is then developed. Thus, film areas become opaque which are exposed by the laser imager to UV light, while the transparency is observed in unexposed areas. Basically, a phototool is a clear polyester sheet with black lines and therefore contains the master image pattern. This phototool allows transference of this image on the photoresist. In PCM, double-sided phototool is usually manufactured, as etching is usually carried out on both sides of the metal foil simultaneously in order to reduce undercutting phenomenon. Phototools allow

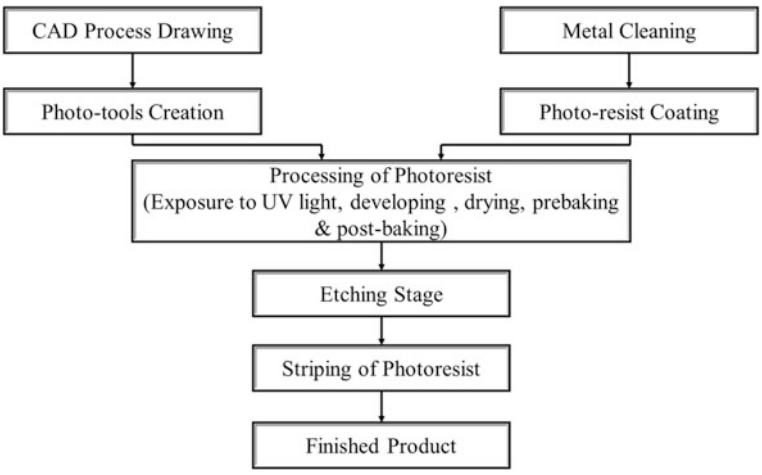

Fig. 1 Step-by-step photochemical machining process [3]

fine details to be obtained, and the shape of the part can be changed very easily. Thus, modifying some details of the part is not a problem because phototools are relatively inexpensive.

3.2 Photoresist Coating

The first part of this stage is to clean the metal surfaces prior to having the photoresist applied. The cleaning operation aims to remove any substance which is at the surface of the metal. Indeed, oil or grease could prevent good adhesion of the photoresist on the metallic surfaces. Two main methods are considered in industry. The first one is mechanical, in which slurry is sprayed on the sheet. Basically, the slurry is formed of a mixture of abrasives with water. The limitation of this method is the metal thickness because good results are not achieved with very thin gauge metal. The second one is chemical; the most common processing cycles involve: (i) alkaline or emulsifying soak cleaner to remove organic contamination metals; (ii) water rinse; (iii) acidic removal of inorganic contaminants; (iv) water rinse and drying.

It can be noticed that a good solution for checking whether or not the cleaning is efficient is to spray water on the "clean" metal surface and determine whether a uniform and continuous thin film of water forms over the surface. This phenomenon indicates an efficient cleaning. Once the metal cleaning is done, the photoresist can be applied to the dried metal. The photoresist is liquid photopolymers which have their chemical structures altered by exposure to UV light. Two kinds of photoresist exist, positive-working resists and negative-working resists. Basically, negative resists harden and strengthen during UV exposure, and positive resists degrade during UV exposure. Negative-working resists are most commonly used. Many photoresist coating processes exist in the PCM industry, but the most accurate method is roller coating using a grooved or structured roll.

3.3 Photoresist Processing

Before being exposed to the UV light, the substrate coating looks like a sandwich as shown in Fig. 2. It can be noticed that there is no polyester layer because Fig. 2 represents a liquid resist coating. In the case of a photoresist coating, a polyester layer would be between the negative-working photoresist and the phototool.

During exposure, misalignment occurs on double-sided exposures. Once the whole assembly is in contact, it is exposed to UV light. By considering a negative-working resist, the photoresist will harden where the phototool areas are transparent, whereas the unhardened photoresist (i.e. areas which were protected by the phototool) is then washed away by using an aqueous solution. Then, the protective film (polyethylene terephthalate) has to be removed if a dry photoresist is

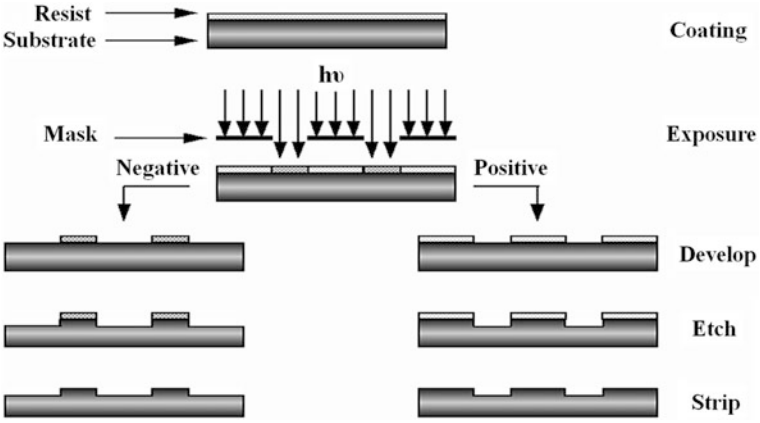

Fig. 2 Processing of photoresist in photochemical machining

used. The next step is to remove the unexposed photoresist from the material (development process). This consists in spraying the exposed material with sodium carbonate-based solution.

3.4 Workpiece Etching

Etching is the process where the metal is machined. It consists in using an etchant solution which dissolves the metal. Currently, ferric chloride is extensively used; it has a low toxicity and can be recycled tool. The etchant has to be inexpensive, environment-friendly and able to attack most of the metals. Several etchant solutions can be used such as nitric acid, Dutch mordant, and ferric chloride. An important characteristic of the etching process is the etch factor. It consists in dividing the depth of etch by the undercut as shown in Fig. 3.

This ratio is dependent on the depth of etch and process chemistry. This is used to achieve an accurate shape of the part. Moreover, it is more productive if the etchant is sprayed perpendicular to the workpiece, involving a chemical process only based on a diffusion phenomenon. It can be noticed that the etch rate slows as the edge profile becomes vertical. Once the workpiece has been etched, the last step is to remove the photoresist by using a chemical solution in which the stencil dissolves.

4 Fine Line Challenges (Precision) Requirement

PCM technique is used to produce thin metal sheet parts with complex features. Chemical industry utilizes the PCM technique for producing the microparts, shapes and features (shown in Fig. 4) which requires close control over the process parameters to get fine line over the substrate. The main parameters are image development, fine line etching and stripping, cleaning and lamination, materials and equipment for the development of fine lines.

In old days, companies such as Boeing, EchoStar, Rockwell, IBM, Delphi developed the technique for producing very small lines and spaces. Figure 5 shows the developed PCB with 38-µm line and 76-µm hole. Latest technologies have demanded the production of board with line and spaces as small as 10 µm for the mass production.

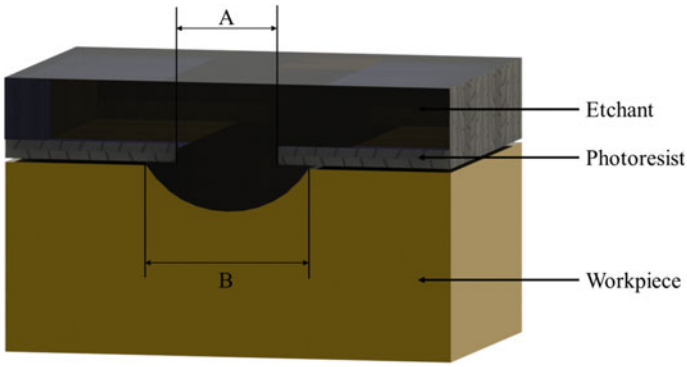

Fig. 3 Expression for the undercut (A–B)/2

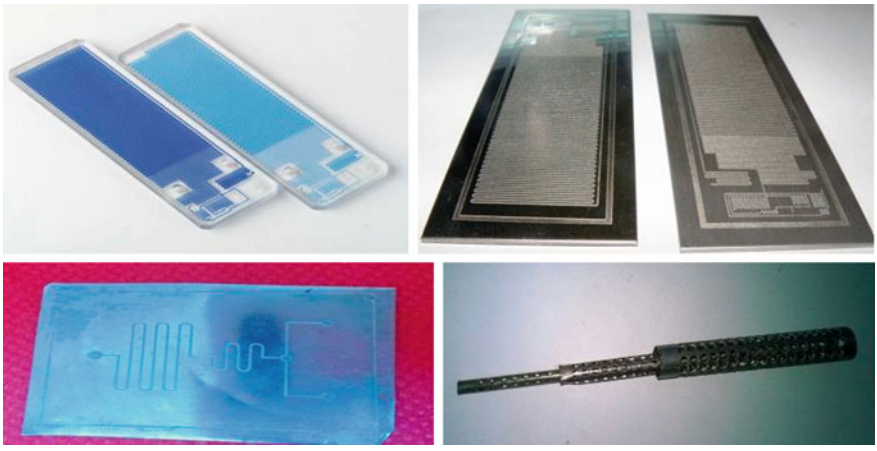

Fig. 4 Precision microfeatures made by PCM

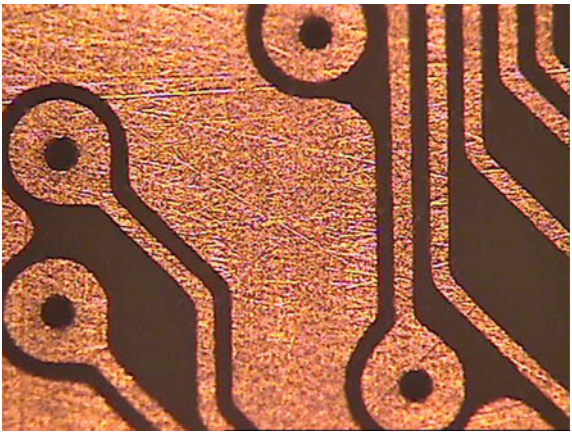

Fig. 5 PCM board with 38-µm line and 76-µm holes [3]

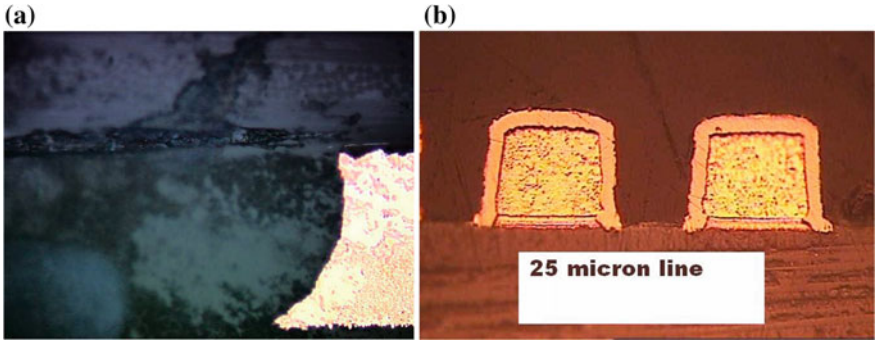

Fig. 6 **a** Side etching of normal copper substrate **b** very straight 25-µm line [3]

At the stage of image transfer, if the imperfections or burr are present over the tool surface, it will get transferred over the substrate, resulting in defected image transfer over the substrate. Also, the presence of dust particles and moisture influences at the stage of exposure or transfer of the image.

The undercut from etching distorts the shape of track as much as 50 µm. Etching takes place in both the direction results in sidewalls getting damaged as shown in Fig. 6.

5 Photoresist Adhesion for Fine Line

While manufacturing fine line or precise features involve an integrated approach to imaging, the PCM process requires better adhesion between photoresist and work surface. While photoresist coating, variables and their relative importance on adhesion are addressed, also the surface preparation of the work material goes through critical processes with the photoresist coating. Optimum photoresist adhesion requires special tools and processes on the work surface. There are several changes in surface preparation and substrate construction which are partially driven by cost and pressure required to establish the capacity to handle and clean thin cores [3]. Metal preparation is the initial step in photochemical machining. Clean surface is important to obtain the better adhesion with resists. Better adhesion depends upon the pre-etching step, conversion coating, physical cleaning and chemical cleaning.

Photochemical machining requires chemically stable resist mask with superior adhesion quality. The photoresist chemistry and image development technology plays an important role in photomask quality. The development of dry-film photoresist chemistry and image development technology improves the performance and yield. The chemistry of dry-film photoresists is very complex due to the different components and component characteristics required for each resist. The role of oxygen, photoinitiator, free radical formation and exposure time plays an important role in dry-film resist.

The photoresist chemistry and the patterning technique play a vital role in accuracy and geometrical features of microsystems and patterning. The basic steps of photoresist coating, exposing of photoresist and image development are same as that of photolithography. In addition to this, electrodeposition requires photoresist with high chemical stability and superior adhesion. Therefore, this investigation deals with the requirement of resists and photoresist chemistry.

6 Dry-Film Resist

The development of dry-film resist system may be divided into two groups: (1) processing performance, including physical characteristics of dry film such as colour, and processing chemicals and (2) product performance, e.g. resolution, used as a plating and/or etching resist.

The advancement of aqueous dry-film technology has always been led by the need for a cheaper and more environmentally safe process. In recent years, far more research time has been dedicated to aqueous dry-film technology than to solvent or semi-aqueous systems. This is partly because of great difficulties in trying to achieve the perfect aqueous product. So, why shouldn't an aqueous resist perform as good as a semi-aqueous or even a solvent resist?

To answer this question, it is worth considering the various tasks required of a resist: (1) it must first laminate onto a variety of work surfaces, cleaned with one of several types of surface preparation. (2) The product then must perform consistently on a variety of light sources for exposure. (3) The developing of the dry film must take place in a selection of equipment. (4) At this stage, the resist must withstand etching or plating solutions.

With aqueous resist systems, it is at present very difficult to produce a product which combines optimum performance in all characteristics, i.e. a universal resist. It is also very difficult to combine chemical properties with individual physical properties. For example, if gold plating performance is improved, it is likely that stripping speed and size will substantially increase.

6.1 Dry-Film Chemistry

The basic film chemistry consists of:

A binder which the rest of the system is built around. The polymeric binder provides the backbone of the structure. It also provides the physical strength and determines whether the photoresist will be aqueous, semi-aqueous or solvent process able.

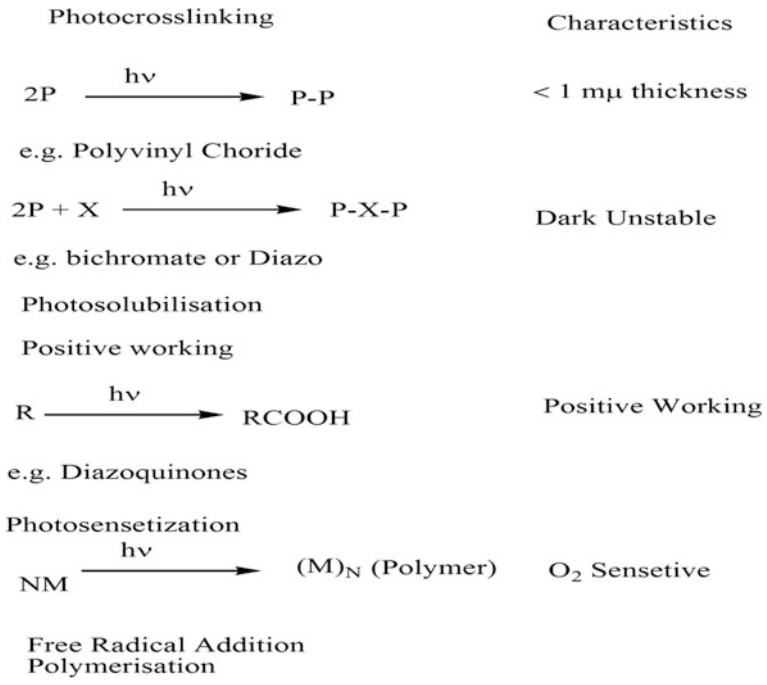

Fig. 7 Reaction mechanisms of photocross-linking, photosolubilization and photosensatization in photochemical machining

A monomer which takes part in the photopolymerization process and undergoes photopolymerization and/or cross-linking.
A photoinitiator which is activated by light to initiate the photopolymerization process.
Plasticizers *and* ***adhesion promoters*** which provide physical and performance characteristics to the dry film.
Dyes provide colour to the film at time of exposure [4].

Several different types of photopolymers are available for use in dry films. The most common type is the free radical addition polymerization. The primary characteristic of this type of system is that it is oxygen-sensitive. Another type of system that is available is photosolubilization, which results in a positive-working film. Characteristics of this system include long exposure times and a positive-working image. Figure 7 identifies types of photopolymers.

Table 1 Photographic imaging speeds

Process	Absolute speed Ergs/cm
Silver halide—high speed	2×10^6
Silver halide—medium speed	2×10
Electrophotography	1
Photopolymerization	10^{-2}–10^{-6}
Photochromism	10^{-5}–10^{-6}
Diazo and vesicular	10^{-6}–10^{-8}

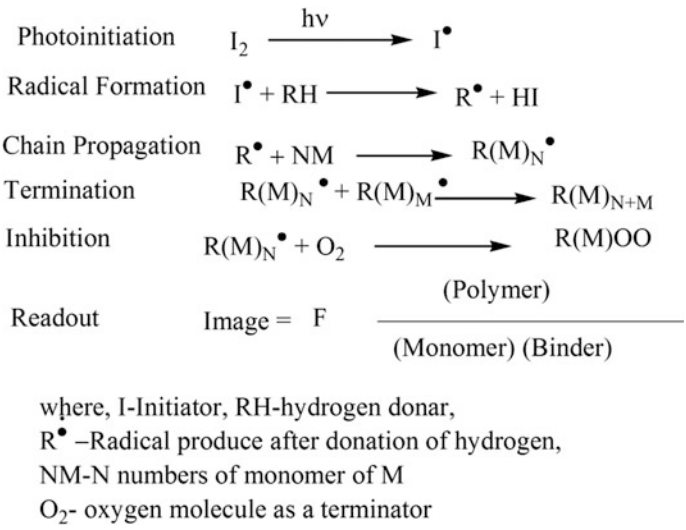

Fig. 8 Ultraviolet-initiated free radical photopolymerization chemistry

Fig. 9 Kinetic mechanism of photoinitiation in PCM

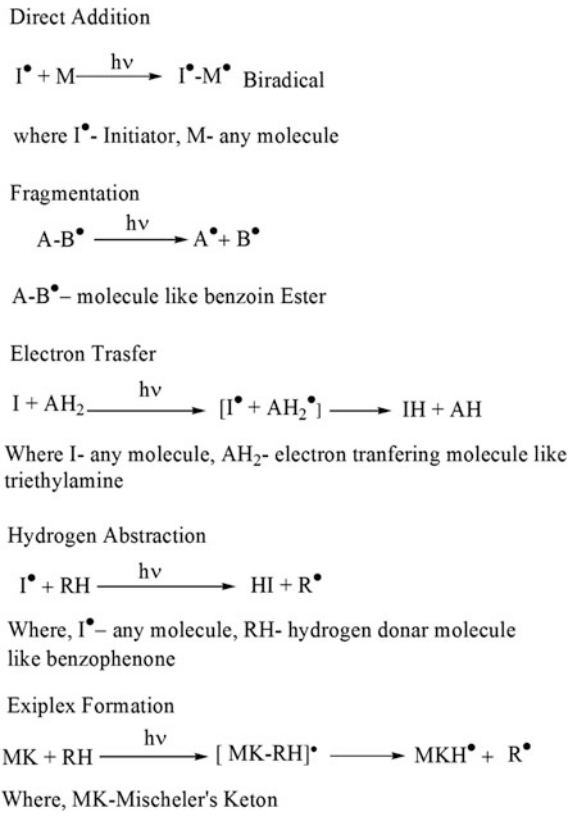

Table 2 List of photopolymerization initiator systems with sensitivity range

Class	Sensitivity range (nm)
Carbonyl compounds	360–420
Azo compounds	340–400
Organic sulphur compounds	280–400
Redox systems	300–450
Halogen compounds	300–400
Sensitizing dyes	400–700
Organometallic compounds	300–450
Metal carbonyls	360–440

The photopolymerization process is relatively slow compared to high-speed silver halide systems; however, it is much faster than diazo- and vesicular-type systems. Table 1 identifies relative photographic imaging speeds.

During the photopolymerization process, UV light is absorbed by the photoinitiator and a free radical formation is formed. Chain propagation due to reaction of the free radical with monomers and/or binders initiates and continues the chain formation. Termination can occur as free radicals are eliminated. Inhibition and

termination of the reaction can also occur due to the polymer/monomer/binder ratio. Figure 8 reviews photopolymerization chemistry and image formation.

Many different types of photoinitiators have been evaluated in dry films over the years. They include direct addition, fragmentation, hydrogen abstraction, electron transfer and exciplex formation [7]. Figure 9 provides examples of some of the type of photoinitiation systems that have been evaluated in dry films.

Photopolymerization initiator systems for dry films are usually selected to match the spectra output of the exposure units. Many initiator systems are available and must be carefully evaluated for compatibility with the photoresist chemistry and the dry-film process [5]. Table 2 identifies classes of chemicals which qualify as photopolymerization initiator systems.

The role of oxygen must be understood because it affects the polymerized resist. Oxygen must be consumed during the induction period of exposure. Once the oxygen is consumed, rapid polymerization occurs and polymerization decreases as the available monomer is consumed along with available initiator.

The polyester cover sheet functions as a protective barrier from oxygen during exposure. When the cover sheet is removed, exposure times usually increases if oxygen is present. Figure 10 shows the role of oxygen during photopolymerization, and how the effect may be reduced. The cover sheet serves two purposes by remaining

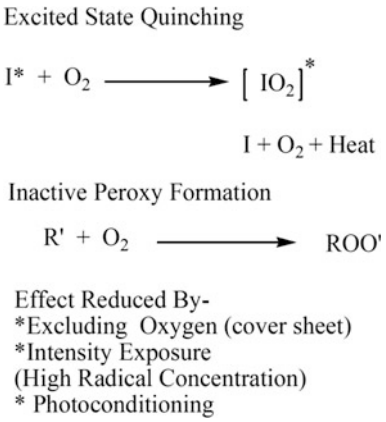

Fig. 10 Role of oxygen in photopolymerization

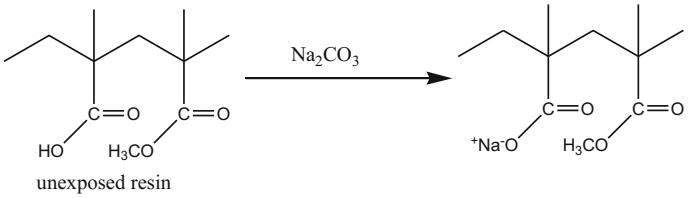

Fig. 11 Development of aqueous resist binder

Table 3 Estimated consumption of photoresists for PCM

Resist	Percentage of total use (%)
Dry-film photoresist	86
Screen ink	10
Liquid film photoresist	4

on the resist surface through exposure. It protects the resist from physical damage before exposure and eliminates oxygen from the surface of the resist during exposure.

The process by which the resist forms an image includes the following:

1. UV radiation
2. Photoinitiation and free radical formation.
3. Polymerization and cross-linking of the monomer from the exposed image.
4. During the development, the unexposed areas wash off, leaving behind the exposed developed image.

During the development process, the binder of aqueous photoresist in the unexposed areas converts to a sodium salt and washes off. The exposed image is insoluble to the developer solution and remains on the board to form the circuit pattern. Solubility of the photoresist increases with increased active sites on the binder in the unexposed resist areas. Figure 11 illustrates the development of the aqueous resist binder.

Sodium carbonate in a 1% concentration is the ideal developing chemistry for aqueous resist. This chemistry is inexpensive, easy to make up, controllable, relatively stable and compatible with the exposed image and has good loading capacity. Since the introduction of aqueous films in 1970, aqueous solutions have included trisodium phosphate and various concentrations of sodium carbonate. Today, the dry-film chemistries are optimized for the development in solutions with a 0.5–1.0% sodium carbonate concentration.

Aqueous dry-film chemistry has been optimized during the last 40 years so that aqueous resists can be used for pattern plating, print and etch, fine line resolution and tenting applications. Dry-film suppliers have fine-tuned aqueous dry-film chemistry to match industry needs. The estimated consumption of various types of photoresist in PCM industries is given in Table 3.

7 Exposure Techniques

Once the photoresist is applied over the surface of the substrate, the next step involved is transferring of the image from phototool over the substrate by using different exposing techniques.

Contact printing is the common method of imaging PCB. Contact printing involves the transfer of an image template (phototool), consisting of transparent and opaque areas, into a polymerized resist pattern by radiating UV light through the transparent areas of the phototool to initiate photopolymerization. Polymerization is reasonably well limited to the exposed resist areas, if two conditions are met:

inhibitor levels in the resist are sufficiently high to provide a threshold against unwanted polymerization in non-exposure areas due to scattered radiation, and polymerization kinetics are fast compared to the speed of inhibitor migration. This exposure process works well if the light is collimated (parallel), if it is perpendicular to the exposure plane (no declination angle) and if the light is not scattered. However, these conditions cannot be perfectly met, and some radiation reaches non-exposure areas where it causes some degree of polymerization. This unintended partial exposure can be minimized by bringing the phototool in very close contact with the resist and by eliminating sources of scatter along the light path [5].

7.1 Exposure System

The circuit densities continue to shrink, and this challenges the capability of PCB fabricators. Most manufactures of UV exposure equipment claim excellent fine line resolution on dry-film photoresist as used during primary image processes. Conventional UV exposure system makes use of vacuum evacuation to achieve hard contact between phototool and resist coated substrate. To get the fine line resolution, the equipment should have following features:

(a) A high capacity vacuum system for achieving the hard contact.
(b) Good uniformity of light intensity across the entire exposure plane.
(c) Filtering out unwanted infrared radiation.
(d) A cooling system to minimize heat build-up within the exposure system in order to minimize temperature rise and distortion of phototool.

Fine line resolution is mainly dependent on the UV light intensity and feature of light collimation. High declination angle ensures that phototools are opaque and clear areas will be accurately reproduced on photoresist. Collimated light eliminates trace nose and poor adhesion characteristics in developed photoresist lines.

7.2 Trends in Image Transfer

In case of conventional printing, some problems occur, such as working on fine line challenges, image development due to defects, dirt or any other unwanted part, radiation in unexposed areas. These problems are preventing by using laser direct imaging and projection imaging technique, but these techniques are not yet usually used.

7.2.1 Collimated Exposure Systems

The parallel sets of the rays of light which has the capability to spread slowly as the rays propagate are known as the collimated light. As the distance increases from the point source, flattening of the spherical wave fronts takes place leading it to become flat and approach it nearer to the plane waves that are collimated perfectly.

Collimated light is produced by using a point source lamp. In most cases, high-pressure xenon bulb is used. The collector is placed near to the lamp. The UV light is passed through light integrator and concentrated over the collimating mirror, where the divergence angle of beam is removed and parallel light rays are reflected to the work area [5].

Drawbacks while using collimating exposure system are as follows:

(a) Reflective surface that is used on highly collimated exposure system is very unstable. This will cause uniformity problem, which leads to under- or over-exposed areas on a circuit board.
(b) Collimated light provides point-to-point print on substrate/board; therefore, any dust particle or scratch on the phototool will be printed. Hence, the system is required to maintain at clean atmosphere.
(c) Highly collimated unit exposes a blue light which can only be used for primary imaging. This light cannot be used for solder mask.
(d) The use of high-pressure mercury xenon lamp is subjected to explosion.

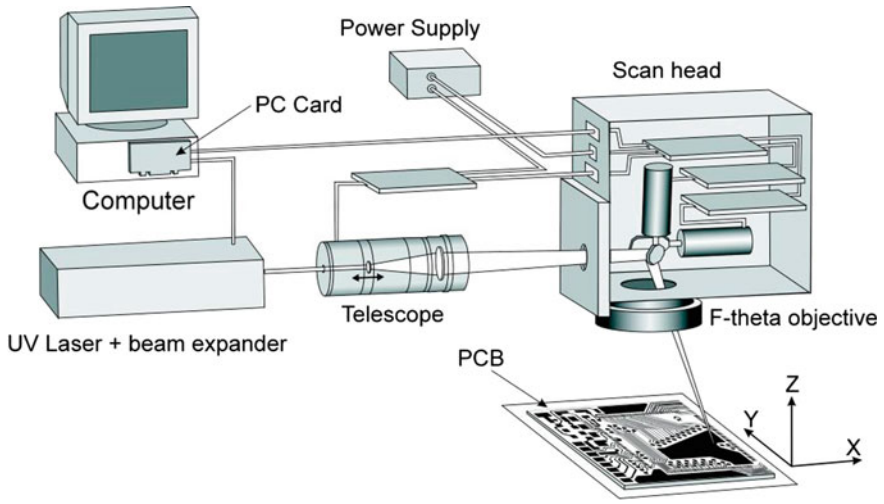

Fig. 12 Scheme of LDI system connections [7]

7.2.2 Laser Direct Imaging

The growing demand for better efficiency and miniaturization of electronic devices and components has a significant effect on the needs facing the PCB industry and the application which require precise dimensioning. PCB manufacturers are driving to produce high-density HDI boards while significantly reducing execution time and cost. Microimage development of MEMS and NEMS possesses a rapidly increasing challenge for photochemical machining manufacturers due to line width and space having tighter and smaller registration requirements. Present methods are unable to provide the perfect solution. Currently, LDI technology is widely using to face these problems. LDI is a method of developing image directly on the photoresist without use of phototool [6, 7].

In LDI, as per design of microcomponent, the scanning of the photoresist surface is carried out with help of computer-controlled system as shown in Fig. 12. The

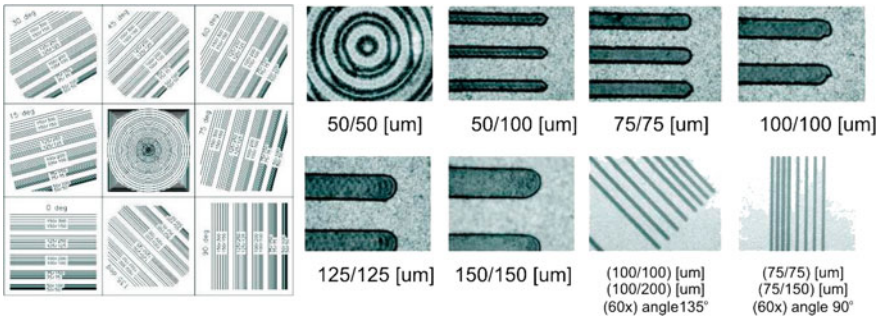

Fig. 13 Different submicron images developed by LDI [7]

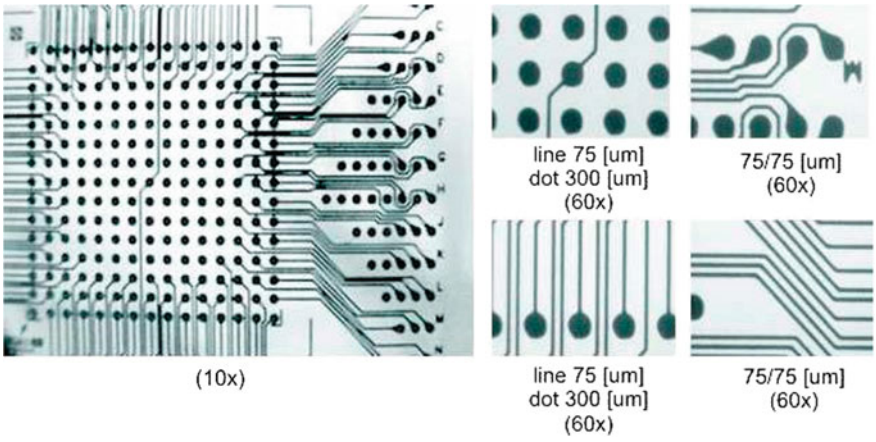

Fig. 14 Patterns on PCB [7]

laser scanning is used to create UV expose to the photosensitive resist. The LDI provides better alternative to contact printing, with image exposing time closer to the contact printing. Production rate of present LDI with combination of high-speed resist is 60 double-sided high-density panel per hour.

The significant benefits of LDI method are as follows:

- Elimination of the defects in printing and due to phototool.
- Possibility of eliminating or reducing effects of humidity and temperature on the image/parts and minimizing the ingress of dust due to the controlled environment within the laser imaging systems.
- Due to small size of laser beam, improved resolution of image developed.
- Submicron features are easily developed.
- Due to mask-less system, the steps are reduced in imaging conductive pattern on PCB.

Laser direct imaging method removes the use of phototool, which creates major problems in fine line imaging, especially as the phototool moves anisotropically with humidity and temperature changes. The different patterns developed by the LDI are shown in Figs. 13 and 14.

7.2.3 Projection Imaging

A projection imaging is the best-known method that has become the standard practice in integrated circuit imaging, and now, it is introducing to PCM. In projection-type exposure, one can distinguish between traditional photomasks that have a permanent image [5]. The schematic diagram of the projection imaging is shown in Fig. 15.

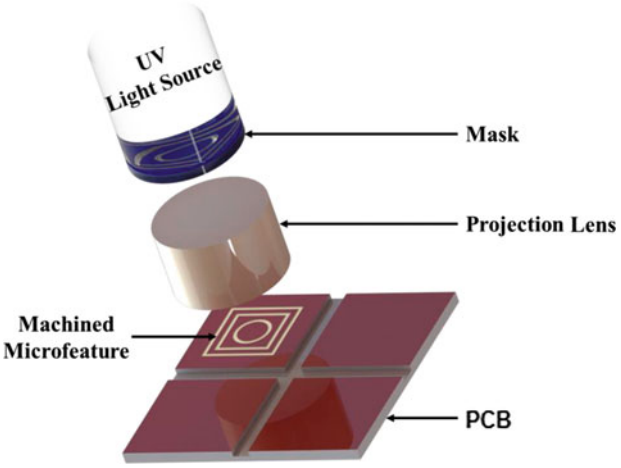

Fig. 15 Projection imaging step and repeat [3]

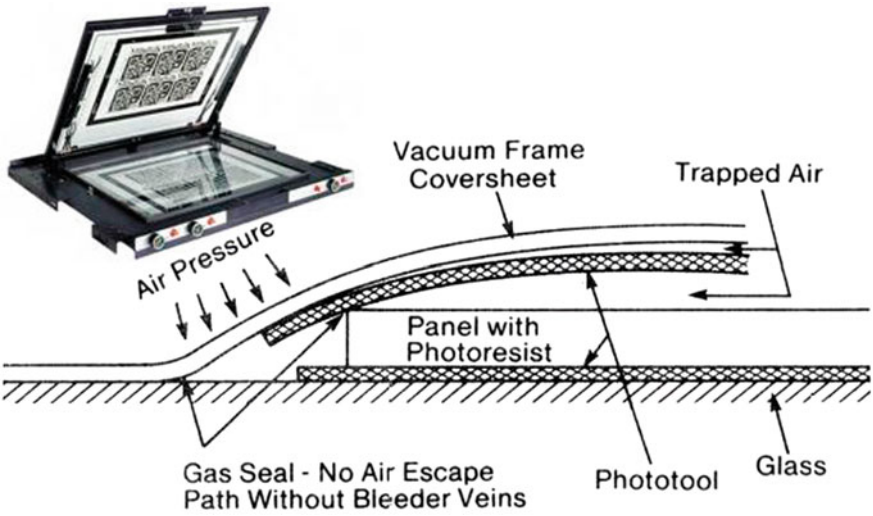

Fig. 16 Contact-type exposures with vacuum frame [3]

7.2.4 Contact Printing

Using the spacer or shims, bleeder strips, bleeder veins and channels are formed. Vacuum frames placed over glass-to-glass fixtures are shown in Fig. 16. In addition to making bleeder channels, spacer or shims in glass-to-glass fixtures are used to prevent the breaking of the glass in case of large difference between the panels on the glass size.

The refraction of light by textured pattern negatively affects the resolution, which is a disadvantage of textured cover sheets. The removal of dirt and the visibility of dirt from the cover are difficult in textured pattern. To provide an air path from the perimeter of the phototool/panel package to the vacuum port, the proper positioning of bleeder strips is necessary. In its absence, premature gas seal formation around the panel leaves air trapped between the phototool and the panel [3, 5]. In conventional UV exposure, the phototool is placed in direct contact with photoresist with the help of vacuum frames so that the off-contact exposure is avoided. The air is removed through vacuum ports for creating the vacuum. To prevent the entrapping of air, the air channels to these ports must be kept open.

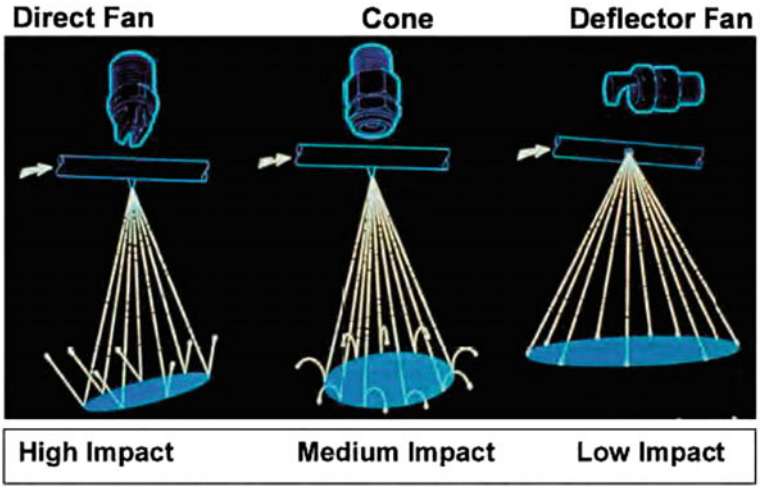

Fig. 17 Spray impacts of different types of spray nozzles

8 Developing

8.1 Developer Control Parameters

To achieve high yields, resolution, good circuit line definition (sidewall) and line uniformity, the control of photoresist aqueous development is extremely important. The process parameters and critical equipment features are interdependent and linked. Some of the features and process variables include the following: resist loading, quality of water, temperature, concentrations, spray pressure, pH, development time, break point, drying parameters, post-development rinsing and resist loading. These parameters are important, and some are relatively easy to control within the required limits (e.g. temperature and time).

8.2 Developer Sprays

The different spray actions are available—each with their own advantages and disadvantages. There are fixed spray nozzle arrays, spray bar arrays that oscillate back and forth transverse to the machine direction and stationary bars that pivot along a fixed axis, resulting in a spray pattern with oscillating angles shown in Fig. 17.

Achieving a uniform spray pattern across the entire surface of the substrate/board is one of the primary objectives. Additional, high-impact spray action helps to improve the developer chemistry with better mechanical erosion of the photoresist and replenishment fluid dynamics. For reducing the thickness of the

Table 4 Various etchants and their use [1, 8, 14]

Sr. No.	Etchant	Materials
1	Sodium hydroxide	Aluminium, anodized aluminium
2	Acidified cupric chloride	Copper and its alloys, brass and beryllium copper
3	Acidified ferric chloride	Stainless steel, nickel, Inconel 718, Nimonic, Monel 400, phosphor bronze, brass, copper and its alloys, invar, Kovarr
4	Alkaline potassium ferricyanide	Aluminium, Molybdenum and tungsten
5	Hydrofluoric acid	Glass, titanium, Hastey Alloy, beryllium, cobalt–chromium, and niobium

stationary liquid boundary layer, high surface velocity of the developer solution is required. This is largely determined by spray pressure and nozzle-type selection. The highest yield was achieved by direct fan nozzles, whereas cone nozzles give lower impact, and deflector fan nozzles provide the least impact. The direct fan nozzles are mostly used.

For randomizing the shadowing effect, guide wires are oscillated. The resist features that form during the development process can also shadow sprays and interfere with clean, complete development. Close attention to the developing chemistry and its control and process equipment design are critical to achieving clean blind holes and straight sidewalls of the through holes.

For improving the etch factor at very low free acid normality, controlling acid etchants is necessary. This is inline with the work that portrayed that instead of HCl, NaCl as a source of chloride ions in acid etchers results in an improved etch factor by complexing the copper salts and keeping them from precipitating. The etch factor is highly dependent on the etch chemistries. Acid etchants give more favourable etch factor than alkaline etchants. Some investigations show a less etch factor with cupric chloride than ferric chloride, but outcomes are not always conclusive [8–10].

9 Etching

In photochemical machining process, the etching stage is the major machining step. Careful attention is provided to achieve controlled etching of the complex geometries. The fabricator must ensure excellent adhesion of the resist to the surface of the substrate so that the action of the etching chemistry does not cause excessive undercut or lead to removal or lifting of the resist. In microcomponent manufacturing, various problems are linked with etching, few are independent, and few are interrelated [11]. Some of the common etching problems are undesirable

Table 5 Tolerances in photochemical machining

Materials thickness (T)	General tolerance achievable	Hole/slot size
0.025–0.050	±0.020–0.025	0.1000–0.1018
0.050–0.1000	±0.020–0.025	0.1000–0.1018
0.100–0.125	±0.020–0.025	120% T
0.125–0.150	±0.020–0.025	120% T
0.150–0.200	±0.030–0.0325	120% T
0.200–0.250	±0.030–0.0325	120% T
0.250–0.500	±12% T	120% T
0.500–1.000	±12% T	120% T
1.000–2.000	±12% T	120% T

All dimensions are in mm

lateral etching, top-to-bottom variation due to pudding effect, etch variation due to obstruction in the way, variation in etch rate due to phototool/image pattern.

It has been found that controlling acid etchants at very low free acid normality improves the etch factor. Some of the research findings also showed that by using NaCl instead of HCl as a source of chloride ions in acid etchers results in an improved etch factor by complexing copper salts and keeping them from precipitating.

Different etch chemistries result in slightly different etch factors. Alkaline etching typically yields a less favourable etch factor than acid etchant. Some studies show a better etch factor with ferric chloride than with cupric chloride, but results are not always conclusive [13].

In PCM, ferric chloride ($FeCl_3$) is most prominently used etchant. The primary role of the etchant is to attack and remove unwanted metal from selected area. Table 4 shows the various etchants and their use.

10 Tolerances in PCM Process

The summary of the range of tolerance for the different material thickness in photochemical machining is shown in Table 5 [8–15].

The width and length follow the same rules. In general, it is considered for dimensions 1.2× thickness and 12% of thickness for tolerance.

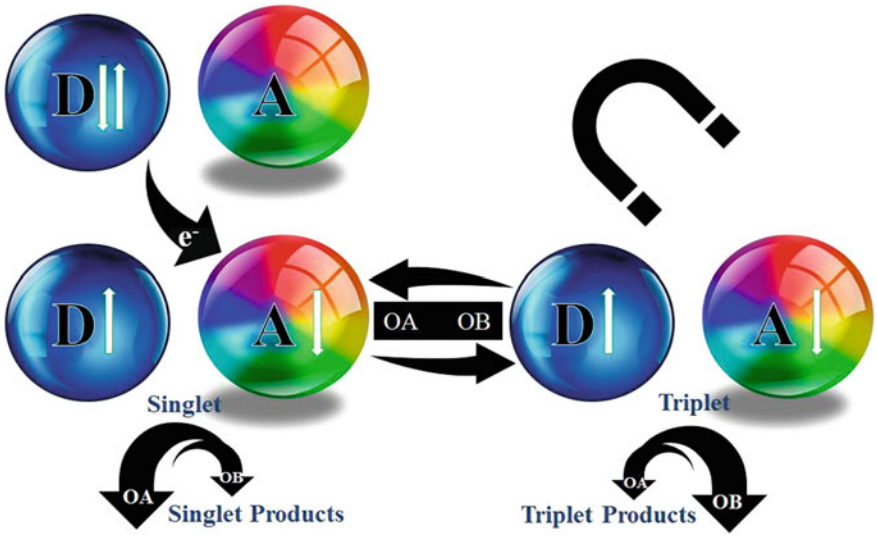

Fig. 18 Effect of magnetic field on the PCM process

11 Magnetic Field-Assisted Photochemical Machining

A chemical reaction performed in a controlled strategy by the association of the etchant with the metallic components is known as photochemical machining. Generally, the magnetic field influenced radical intermediates found as intermediate products in chemical reactions pave way to alter the product distribution, yield or rate of the reaction. The molecules having odd number of electrons, accordingly consists of an unpaired electron spin that may be found in one of 2 spin states: ↑ or ↓ which represents the involvement of radicals which play a decisive role in magnetically sensitive reactions. The low lifespan of a radical pair is considered as an intermediate in a reaction which comprises of 2 radicals designed in tandem with either parallel (↑↑, a triplet state, T) or antiparallel (↑↓, a singlet state, S) spins of the unpaired electrons. The external and internal magnetic fields are influenced by the magnetic moment associated with each electron spin which in turn is affected by the chemical fates and interconversion into the S and T states. The interpretation of these pairs can be performed by engaging the radical pair mechanism. Figure 18 shows the schematic of the effect of magnetic field in PCM process.

$FeCl_3$ is the most commonly used etchant. In the reaction of $FeCl_3$ with stainless steel, the reaction contains two types of ions, Fe(III) ions and Fe(II) ions, which are paramagnetic and diamagnetic in nature, respectively. The hypothesis is that the transportation of all ions in the solution takes place under the influence of a magnetic field. This transportation takes place owing to the difference in magnetic susceptibility. The direction of an applied magnetic driving force and velocity of ions in the chemical reagent is the same as that of the gradient of paramagnetic ions.

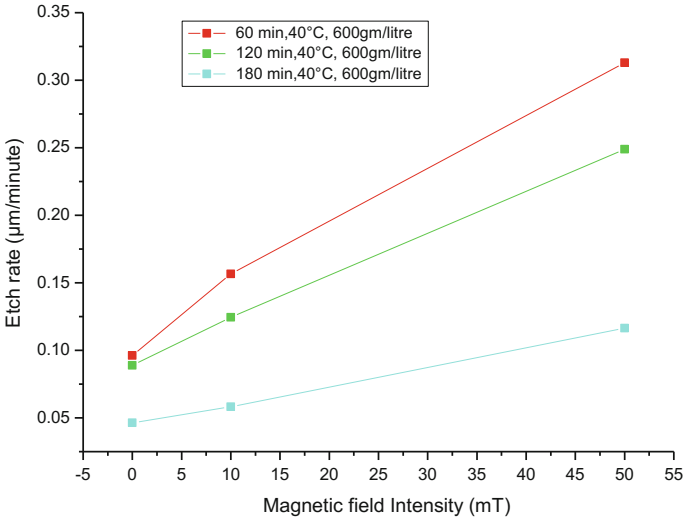

Fig. 19 Variation of etch rate with respect to magnetic field

It is clear that a magnetic field introduces two forces into the etchant—namely Lorentz force and field gradient force. Movement of the etchant is caused by the force acting on the moving charge carriers, which is known as the Lorentz force. This movement improves the mass transport. Due to the force generated by the field gradient, there is a tendency of accumulation of the paramagnetic particles near the solenoids.

The sensitivity of a radical pair to an external magnetic field is considered as bare minimum criteria in terms of chemical reactions. Sensitivity can be stated as the reaction of at least one of the S and T, while the other pair is not open which can be granted as the conservation of angular spin moment. The basic requirement at the formation of opposite spin free radicals is represented by the chemical reaction, which forms the basis of the construction of a magnetic compass. The step-by-step individual reactions are as follows (assuming that the radicals are completely immobile).

From Fig. 19, it is clear that due to magnetic field the etch rate increased as compared to the usual PCM process. This is due to the reaction between metal and etchant containing Fe(II) ions and Fe(III) ions that are in paramagnetic in nature. When magnetic field is applied to the solution, Fe(II) diamagnetic ions moved away from the coil and Fe(III) paramagnetic ions are attracted by the coil. As a result, Fe (III) concentration is more near the coil or workpiece (as it is placed near the coil). As Fe(III) concentration is more near workpiece, it reacts with workpiece. The formed Fe(II) ions are moved away from the workpiece due to applied magnetic field. Stirring action takes place automatically due to the presence of paramagnetic and newly created diamagnetic ions at the liquid and workpiece interface by

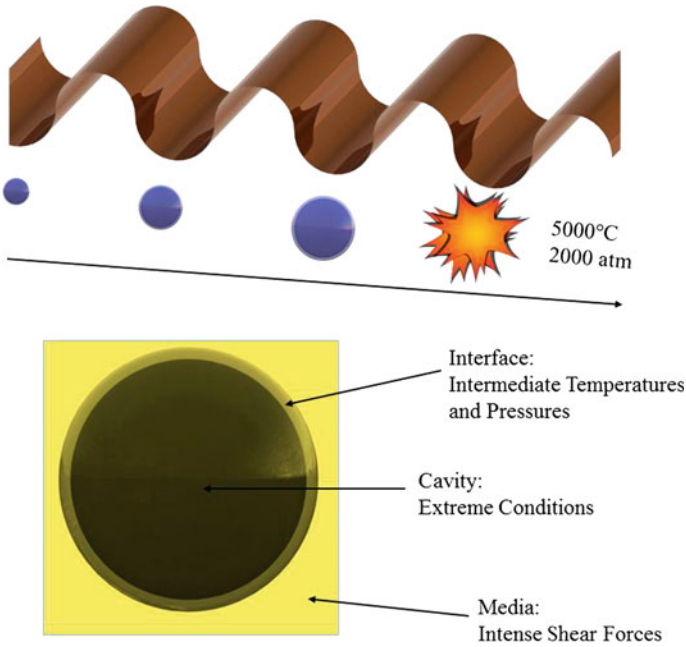

Fig. 20 Principle of Ultrasonic-assisted photochemical machining

replacing diamagnetic ions formed during the reaction between ferric chloride and workpiece. This transportation of ions also helps to increase the etch rate [6, 14].

12 Ultrasonic-Assisted Photochemical Machining

Assistance of ultrasounds towards photochemical machining leads to the chemical reaction caused due to high energy of the ultrasound. Figure 20 represents the complete lifespan of a bubble starting from its birth, growth and implosive collapse which is caused by acoustic cavitation in the etchants. There is excessive heating of the bubble during the course of the cavitational collapse leading to the formation of localized hot spots posing temperatures around 5000 °C and pressures measuring roughly to be 500 atm and having a lifespan of a few microseconds. Collision of the interparticle posing high velocities is caused due to the shock waves from the cavitation in a liquid–solid slurry, and the sufficiently, high energy of the collisions has the capability to melt most metals. Applications to chemical reactions exist in both homogeneous liquids and in liquid–solid systems. Metals are produced with a clean and highly reactive surface with the combination of ultrasound with PCM which has the special synthetic applications. It is also found that many of the

catalytic reactions can be both initiated and augmented with the assistance of ultrasound in homogeneous as well as heterogeneous mediums.

Acoustic streaming and/or cavitation bubble formation is caused by the effect of ultrasonic vibration in liquid which depends upon the parameters of ultrasonic frequency, power, characteristics of sonic source and solution phenomena such as volatility, viscosity and the presence of dissolved gases or other nucleation sites.

Acoustic cavitation incorporates ultrasound based on physical phenomenon for specific activation in chemical reactions. The attractive forces in the liquid phase of the molecule which is destroyed due to the mechanical activation process are called as cavitation. On application of the ultrasound, the liquid is compressed initially which is followed by rarefaction (expansion) where gaseous oscillating small bubbles are formed due to a sudden drop in pressure. Expansion of the bubbles formed occurs with each outgoing cycle of the ultrasonic energy, and later, they collide and violently collapse when an unstable size of the bubbles is reached.

It can be observed from Fig. 21 that the etch rate increases with increase in ultrasonic vibrations in PCM process. The major drawback in the conventional etching is the formation of oxide layer on the surface of the metal during the reaction between etchant and metal. As temperature increases, the etch rate increases but due to natural flow of the etchant, the etch rate is slow and oxide layer formed on the surface also reduces the etch rate. The oxide particles adhering to the surface are responsible for the formation of layer on the surface. Some of the oxide

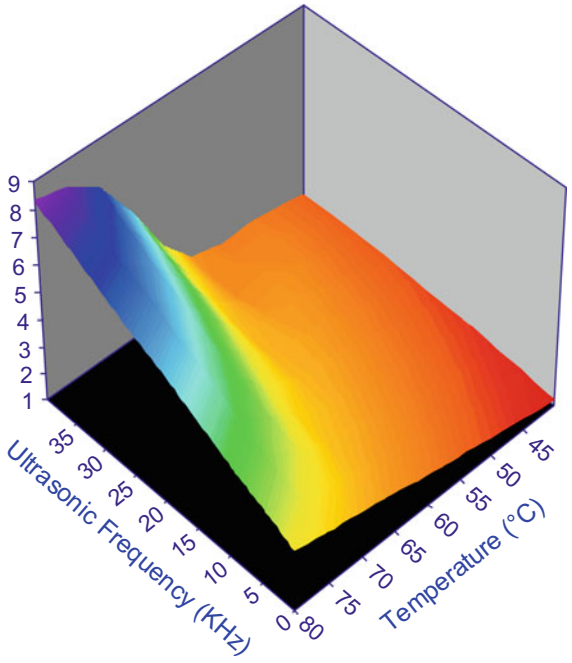

Fig. 21 Variation of etch rate with respect to ultrasonic frequency

particles are larger than others and consequently acts as a mask. During an ultrasonic-assisted chemical etching, due to the cavitation effect, microbubbles are formed which consists of tremendous amount of energy inside it due to the combination of pressure, temperature and velocity. Bubbles propagate through etchant and strut near the metal surface. Collapsing of such bubbles is a combination of erosion and corrosion due to the combination of cavitation and highly corrosive etchant. From Fig. 21, it is also observed that as the temperature of etchant increases etch rate also increases (in case of UAPCM). This is due to increase in the cavitation effect.

In comparison with ultrasonic-enhanced etching and conventional etching, the etch rate is much higher. As in case of ultrasonic-enhanced etching, the collapsing of bubble near metal surface is helping to remove or restrict the formation of oxide layer on the surface of metal and the metal removal is due to the combination of both erosion and corrosion. Also, ultrasonic gives best stirring to etchant which improves the etch rate or reaction rate.

In addition to above, with ultrasonic-enhanced stirring, the diffusion process is accelerated significantly and eliminates the stratification of etchant. The uniform depth is achieved during etching with the constant etch rate. It is shown in Fig. 21 that the etch rate of SS316L in ultrasonic stirring process is much greater than the same with no agitation used, keeping temperature and solution same. In many cases, if sufficiently high-density smut is formed on the surface, the etch rate can drop in great amount. This explains the decreasing of rate of reaction in addition to the reflects mentioned in the earlier paragraphs.

Comparing with electrochemical and chemical method, the ultrasonic method is a mechanical one and could be well adopted to many etchants with no adverse effects on the reagent and the process which is hugely advantageous to PCM. Hence, synchronising with chemical etching, it gives more satisfactory results [6–13].

13 Grey Photochemical Machining

There is wide range of growing importance to the microstructures in three-dimensional (3D) features with generative power in the miniaturization of fluidic or mechanical devices, elements of optics, tissue-engineering scaffolds and components with capability of self-assembling, in between them. The widely used technique for microdevice fabrication is the traditional PCM which is not suitable for the fabrication of 3D components as its principle of working lies on the concept of “photomask”-assisted illumination of the layer which is photosensitive (a plate which is transparent but contains solid-state, unalterable, opaque features) that results in unavoidable features of non-deviating height.

PCM considers the criticality of the size of fabrication which technically symbolizes huge mainstream of microdevices including microelectromechanical system (MEMS), microfluidic devices, microelectronic circuits and protein microarrays/nucleic acid. Illumination with the help of UV light of the thin photosensitive layer ("photoresist") providing a mask to the portions containing opaque features (e.g. ink emulsion or metal) on a transparent background (e.g. plastic or glass) is all the contents comprising of PCM. The two basic and fundamental limitations imposed by photomasks on the production of features are as follows: (i) the illumination process results in all—or—none exposure to non-deviating height features of the photoresist; hence, the microstructures of three-dimensional (3D) features for its fabrication by traditional PCM involve steps that require multiple exposure/alignment steps. (ii) Features of photomask are existing perpetually, and thus, alterations in the design demand the (slow and costly) fabrication of an entirely new photomask, however a foremost obstacle in the investigation settings consuming quick reversal of the microdevice prototyping.

The major task is to eliminate the use of multiple exposure/alignment steps. This developed novel technique of photochemical machining using colour phototool for the development of the three-dimensional (3D) microstructure. The realization of controlling the three-dimensional (3D) photoresist structures may be done by the transmitted UV light intensity in a process termed grey phototool-based photo-

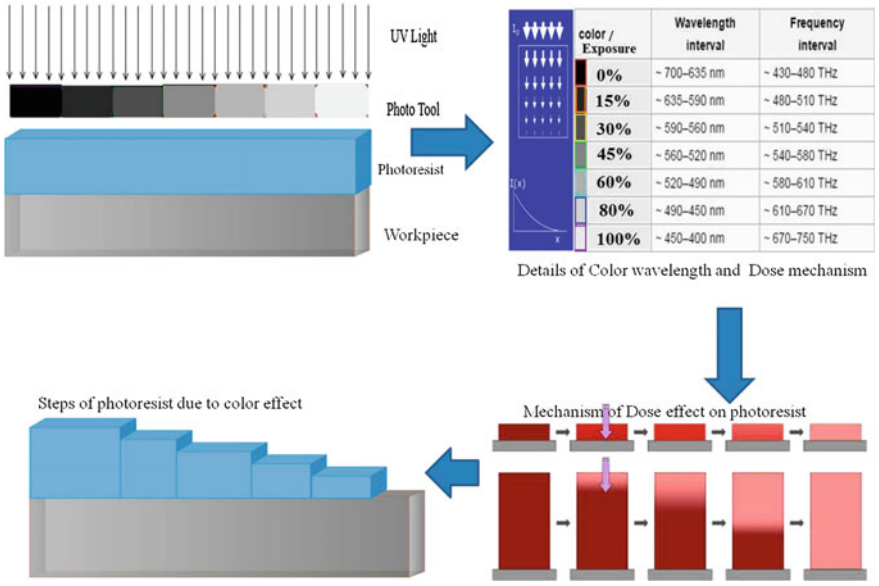

Fig. 22 Top-down schematic of grey photochemical machining

chemical machining.

Fig. 23 Grey phototool and 3D pattern developed by the grey PCM

Traditional phototool comprises of black and white colour, which implies the white colour is unable to absorb any UV radiations and black which absorbs all radiations incident on it. The two distinct phases are present on the workpiece surface, viz. the presence and absence photoresist due to traditional photochemical etching after the development. It clearly states that the development of photoresist is clearly based on the theory of absorbance. The absorbance is the ratio of incident radiation to transmitted radiation through a material. The older technique PCM requires only the presence or absence of photoresist for etching purpose which eradicates the use of other colours in photochemical machining appearing in fade light. The different combination of white and black is having different absorbance capacity. The wavelength and energy level of main colour are given in Fig. 22. The effect of various colours on the photoresist exposure reveals that the phototool comprises of main seven combinations as shown in Fig. 22. The photoresist is coated on the metal surface which is to be etched. For the development of an image on the coated surface, the grey phototool and UV rays are used as shown in Fig. 23. By using optical meter, the measurement of the wavelengths of UV light passing through different colours is quantified. It is clear that the colour of shorter wavelength absorbs more incident light as compared to colour of longer wavelength.

Currently, PCM on a greyscale can be developed using ultra-high-resolution "halftone" photomasks, micromirror projection display, scanning lasers, high-energy beam-sensitive glass photomasks or photomasks with metal-on-glass. The production of 3D structures collaborates to be enormously useful where the approach of these greyscales is either to (i) aggravate the costs/turnaround times of

PCM standardization or (ii) to permit limited levels on the greyscale. Figure 23 shows the 3D components and grey phototool developed for the PCM process.

14 Conclusions

PCM is extensively used for the manufacturing of components such as integrated circuit lead layouts, nameplates, printed circuit boards, encoder disc, jewelleries, microreactor and microfluidics for decorative, aerospace, precision and electronics industries. This process plays a key role in the manufacturing of micron-size machined parts. The manufacturing of parts with fine line features is the area of intense research activity these days. The growing demand of manufacturing circuit boards with lines and spacing below 1 millimetre is the requirements. The key issue is how to control the exposure energy and controlled etching in different directions. Fine line features can easily be achieved by making use of collimated light beams while exposing the image, controlling the intensity of light beams during exposing, avoiding the undercuts in etching by controlling etch rate, controlling the thickness of photoresist over the substrate, properly aligning the phototool with substrate, using ultrathin foils, etc. Various advanced versions of PCM technique are available now, such as ultrasonic-assisted PCM, magnetic field-assisted PCM, greyscale PCM to fulfil the special application requirements. Moreover, various techniques have been developed to make the processes safe, clean and efficient.

References

1. Allen DM (2004) Photochemical machining: from 'manufacturing's best kept secret' to a $6 billion per annum, rapid manufacturing process. CIRP Ann Manuf Technol 53(2):559–572
2. Wei W et al (2008) Non-traditional machining techniques for fabricating metal aerospace filters. Chin J Aeronaut 21(5):441–447
3. Farkate S (2015) Fine line challenges in photochemical machining. M.Tech. thesis, Dr. B.A. Technological University, Lonere
4. Saraf AR (2017) Some studies on the effect of processes parameters in photochemical machining of SS316L. Ph.D. thesis, Dr. B.A. Technological University, Lonere
5. Pimpin A, Srituravanich W (2011) Review on micro-and nanolithography techniques and their applications. Eng J 16(1):37–56
6. Nowak MR et al (2013) Laser prototyping of printed circuit boards. Opto-Electron Rev 21 (3):320–325
7. Barbucha R et al (2008) Laser direct imaging of tracks on PCB covered with laser photoresist. Tech Sci 56(1)
8. Cakir O (2006) Copper etching with cupric chloride and regeneration of waste etchant. J Mater Process Technol 175(1):63–68
9. Çakır O, Temel H, Kiyak M (2005) Chemical etching of Cu-ETP copper. J Mater Process Technol 162:275–279
10. Çakir O, Yardimeden A, Ozben T (2007) Chemical machining. Arch Mater Sci Eng 28 (8):499–502

11. Saraf AR, Sadaiah M (2016) Photochemical machining of a novel cardiovascular stent. Mater Manuf Process 1–7
12. Saraf AR, Sadaiah M (2013) Application of artificial intelligence for the prediction of undercut in photochemical machining. Int J Mechatron Manuf Syst 6(2):183–194
13. Saraf AR, Sadaiah M (2017) Magnetic field-assisted photochemical machining (MFAPCM) of SS316L. Mater Manuf Processes 32(3):327–332
14. Allen DM, Ler LT (1999) Increasing utilisation efficiency of ferric chloride etchant in industrial photochemical machining. J Environ Monit 1(1):103–108
15. Keskitalo T, Tanskanen J, Kuokkanen T (2007) Analysis of key patents of the regeneration of acidic cupric chloride etchant waste and tin stripping waste. Resour Conserv Recycl 49 (3):217–243

Nano-Machining, Nano-Joining, and Nano-Welding

Kush Mehta, Munish Gupta and Priyaranjan Sharma

Abstract This chapter sheds light on the role and use of nanotechnology in manufacturing. The theme of this chapter is basically focused on nano-machining, nano-joining and welding, and nano-EDM technologies exploited for the production of precision engineered parts and components to cater the need of increasing global trend of miniaturization. Major nano-techniques in the aforementioned manufacturing areas, their development, current trend, salient features, and applications are exclusively discussed in this chapter.

Keywords Nano-machining · Nano-welding · Nano-EDM · Precision

Nanotechnology is a specific area of science which involves the art of manipulating the materials between 1 and 100 nm. The word nanotechnology was first coined by the Tokyo Science University Professor Norio Taniguchi in 1974 to describe the precision manufacture of materials with nanometer tolerances [1]. The particular field of technology has huge significance because when we consider any material in nanometer scale it assumes properties that are much different from those when it is considered in bulk form. The unique importance of this area can provide numerous applications in all fields of science and engineering [2]. The use of nanoparticles in

The original version of this chapter was revised: Incorrect author name has been corrected. The erratum to this chapter is available at https://doi.org/10.1007/978-3-319-68801-5_9

K. Mehta (✉)
Mechanical Engineering Department, School of Technology,
Pandit Deendayal Petroleum University, Raisan, Gandhinagar, India
e-mail: kush_2312@yahoo.com

M. Gupta
Discipline of Mechanical Engineering, National Institute of Technology Hamirpur,
Hamirpur, India

P. Sharma
Mechanical Engineering Department, Institute of Engineering and Technology,
JK Lakshmipat University, Jaipur, India

K. Gupta (ed.), *Micro and Precision Manufacturing*, Engineering Materials,
https://doi.org/10.1007/978-3-319-68801-5_4

cutting fluids for environment-friendly machining [3, 4], manufacturing of nano-composites [5], and fabrication of nano-devices to be used in some important energy and electronic-based applications has demonstrated the importance of nanotechnology in manufacturing [6]. The manufacturing sector has also been complemented by nanotechnology. Various avenues have been explored where the nanotechnology could assist to achieve the objectives as regards to produce/manufacture nano-size engineered parts or components. It includes the nanotechnology interventions in machining, welding, and joining.

1 Nano-Machining

The demand for nano-featured components is rapidly increasing in electronics, optical, medical, automotive, communication, and aerospace industries [7–12]. The machining of nanoscale components with high precision has become one of the essential requirements of modern manufacturing industries. Due to the increased demand of nanometer size machined components, new cutting edge technology needs to be introduced [8, 9]. Manufacturing of devices at nanoscale needs some reliable, repeatable, precise, accurate, and detailed process design fabrication methods. Therefore, the process of nano-machining process has been established as the major prerequisite, which further meets the above requirements namely, highly precision and flexibility. Fundamentally, nano-machining is defined as a material removal process in which dimensional accuracy of the component can be achieved <100 nm [7]. The examples of nano-machining processes (see Fig. 1) with details are presented in the subsequent sections.

Nano-indentation is a nanotechnology based technique used to measure the mechanical properties of any material at nanoscale. These materials could be of single-crystal type, polycrystalline type, and amorphous type. In the case of single

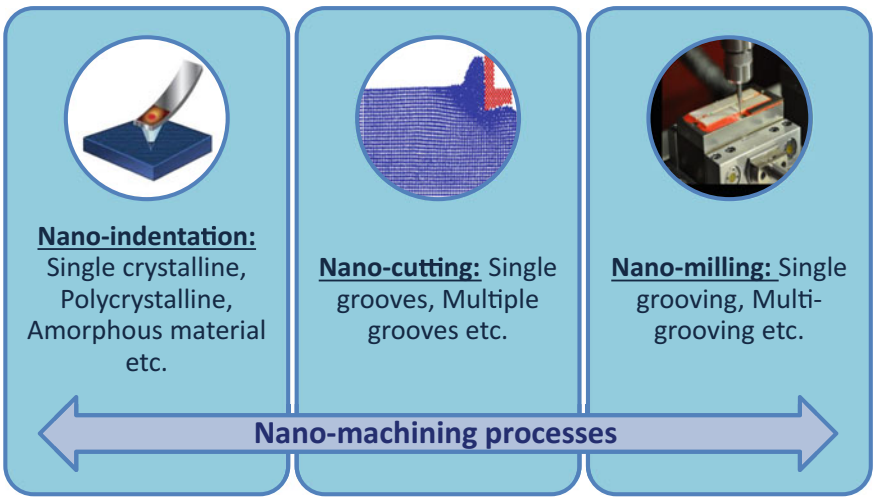

Fig. 1 Nano-machining processes

crystalline material, a number of basic problems such as determination of stresses, calculation of atomic scale contact area, and temperature conversion are produced. Similarly, dislocations of material, repulsive forces, and shear stresses are the major issues in the case of polycrystalline materials which limit its applications [13]. The amorphous materials such as silicon carbide show a series of load dropped associated with the local rearrangements of atoms, similar to that of crystalline 3C–SiC [13]. Considering the aforementioned challenges, nano-indentation technology is being developed day by day to perform the material testing task efficiently.

There have been many difficulties and/or challenges faced while scaling down the size of any component from micro to nano. Many fruitful results have been obtained based on the research conducted by various researchers on nano-cutting processes. For example, Cheong et al. [14], and Zhang and Cheong [15] impressively made the detailed study on molecular dynamics (MD) simulations for nano-cutting operations, with respect to the control volume determination, potential function selection, boundary condition setup, and time step justification. In another work of Cheong and Zhang [16], the investigations were made on damage mechanisms of multiple cutting tips during the nano-cutting operation. Likewise, Zhang et al. [17] investigated the prospect of achieving the hypothetical shear strength at work-tool interface in the case of small depth of cut. From these current documented work, it has been clearly found that the performance of nano-cutting process in terms of subsurface damage is merely depends upon some important factors such as tool, workpiece material, and cutting parameters. For example, in the case of tool material, the various types of tool materials namely diamond, tungsten, chromium, and iron are used in nano-cutting operations. The plastic deformation of these tool materials at nanoscale is very little as compared to other scales. The tool life is increased with the decrease in workpiece hardness, as the tool hardness is more than the workpiece hardness. Similarly, the rake angle is also the prominent factor, which affects the performance of nano-cutting operations. Depending upon the workpiece materials properties, the different rake angles in the range of $-75°$ to $75°$ have been used in the nano-cutting operations. For example, in the case of ductile material like copper, the negative rake angle is used because the chip length is decreased with the negative rake, which results in plowing ahead of the tool and subsurface deformation underneath the machined surface. On the other hand, the positive rake is used in brittle material. Thus, choosing the optimal parameters settings is necessary for the success of the nano-cutting process [13]. The subclassification of these factors is presented in Fig. 2.

Nano-milling is well-known flexible process used to generate accurate 3D surfaces in die/mold, milling tools, and micro-electro-mechanical systems (MEMS) applications. The complex design, high cost involvement, and complicated fabrications of components are the major limitations of the nano-milling process. The single-grooving and multi-grooving are the basic operations of nano-milling process, whereas milling forces, groove profiles, etc., are their perspective responses. Many studies or scientific work has been performed on these nano-milling processes. For example, single-groove nano-end-milling operation on single crystal copper material using diamond cutting tool has also been attempted [18].

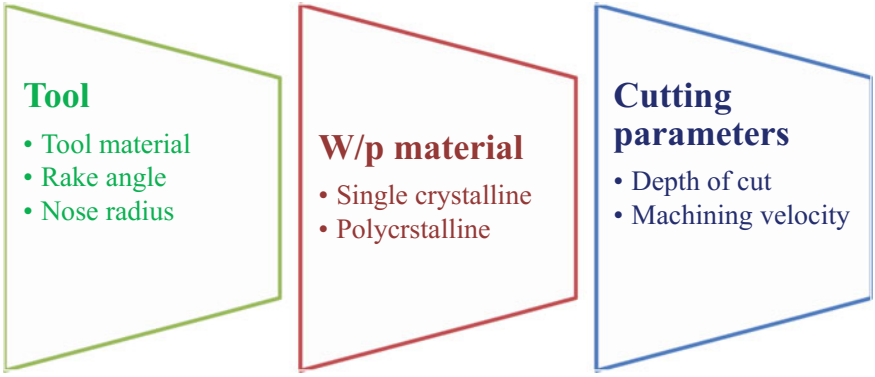

Fig. 2 Factors affecting nano-cutting processes

The milling force includes two basic force components such as feed force and transverse force, which follows the sinusoidal path and semi-sinusoidal path, respectively. The analytical force models were used to evaluate the forces in nano-milling operation. Equation (1) describes the use of such model:

$$F_t = K_m A_c \tag{1}$$

Where F_t is the tangential force, K_m is the material constant, and A_c is the atomic contact area, respectively. Similarly, there were three basic criterion used to evaluate groove profiles in nano-milling such as (i) top edges distorted (ii) the groove profiled at the outlet side of the tool rotation aligned more closely with the designed geometry, and (iii) increasing depth of cut improved groove quality. To explain the observed phenomena, the key physics parameters, i.e., surface energy, strain rate, and residual stress were investigated [18].

The piezoelectric Nano-Grinding process has also been developed for machining geometric features such as channels in lab-on-chip devices for micro- and nano-fluidic applications [19, 20]. The laser-dressed vitrified alumina grinding wheels were identified the best option to produce finer finish than the wheels made of other materials and dressed by other techniques.

2 Nano-EDM and ECM

It is well known that the processing of materials at nano-level is quite challenging and limited by spacing between atoms of solid material (about 0.3 nm). The atomic-level processing of materials requires energy density higher than atomic bonding energy which is too high for conventional machining processes. Therefore, to process the material at the nano-level, it requires non-conventional processing

techniques which use energy particles such as electrons, photons, ions, and chemically reactive atoms for removal of material at micro- and nano-level. A past study carried out by Rajurkar et al. [21], Zhang et al. [22], and Benilov et al. [23] revealed that Electrical Discharge Machining (EDM) and Electrochemical Machining (ECM) techniques exhibit the great capability to machine nanoscale components and can be explored further to fulfil the precision nano-machining requirements.

2.1 Nano-EDM Process Details

With the demand of more precise nanoscale components for modern industries, the technology as regards to the conventional EDM process needs to be developed and extended to achieve nanometric level machining accuracy. Nano-EDM is a non-contact electrothermal machining method in which material is removed by a series of ultra-fine discharge pulse, and most suited for the machining of nanometric components because of its high machining accuracy and precision. The mechanism of nano-EDM is almost similar to the conventional EDM with the basic difference between the two is the size of the crater formed on the machined surface. If the size of the crater formed on the machined surface is >1 μm, then it is called as conventional EDM, however, nano-EDM offers the crater size <100 nm due to its modified pulse generator technology.

Generally, conventional EDM uses relaxation-type pulse generator, where discharge energy of spark can be reduced by reducing the capacitance of the pulse generator. According to Han et al. [24], the diameter of discharge crater can't be reduced <0.2 μm using conventional pulse generator technology because of its inability to remove the stray capacitance. The stray capacitance can be found easily in a conventional EDM between the electrode gaps which helps in machining even if the capacitor is disconnected. According to Kawakami and Kunieda [25], stray capacitance has a great role to control the discharge energy per spark. Further, Egashira et al. [26] have attempted to reduce the stray capacitance by shortening the electric feeders in order to achieve the desired miniaturization. Thereafter, Kunieda et al. [27] have proposed the new generator technology to achieve nano-EDM. They obtained a nanometric discharge crater of 570 nm by coupling the pulse generator to the tool electrode. To overcome the issue of conventional pulse generator of the EDM process, a novel pulse generator technology based on electrostatic induction feeding (ESIF) was used by Yang et al. [28] which then utilized to achieve miniaturization in EDM and its variants. The principle of ESIF-based pulse generator is shown in Fig. 3 where pulse voltage (*V)* is applied for the fixed pulse duration. C_1 represents the capacitance between feeding electrode and tool electrode, whereas C_2 represents the capacitance between tool electrode and workpiece. C_1 was assumed to be 10 times larger than C_2. When the voltage of pulse generator reaches to *V,* then C_1 and C_2 become charge (a). Within the working gap, workpiece and tool electrode are charged with negative polarity which creates a strong electric

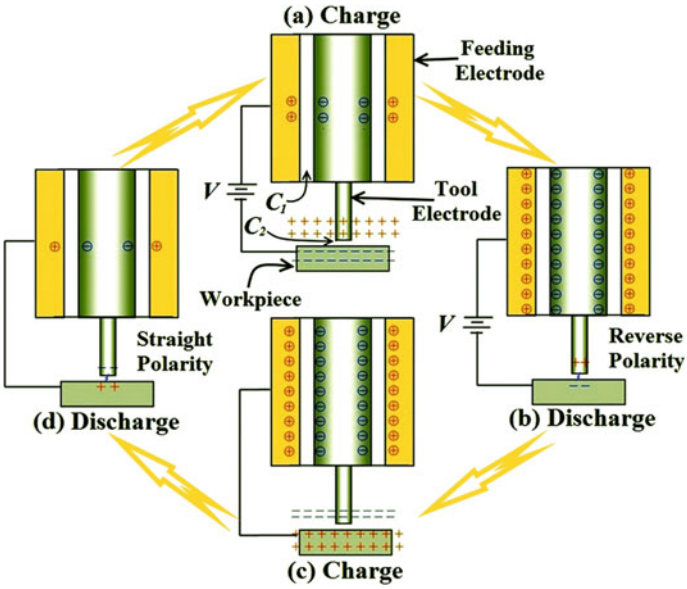

Fig. 3 Principle of electrostatic induction feeding-based pulse generator [29], with kind permission from Elsevier

field. Consequently, discharge occurs, then, electrons are conducted from workpiece to a tool electrode (b). After discharge, the working gap voltage becomes equal to the discharge voltage due to the absence of current conduction in the circuit. Further, discharge won't occur until pulse supply voltage reaches to zero (c). In earlier discharge, tool electrode has accepted electrons; therefore, it was charged negative, whereas workpiece is charged positive. Accordingly, discharge occurs with straight polarity. After discharge, the working gap voltage won't increase till next cycle (d). With the use of ESIF method, it became possible to reduce the effect of stray capacitance in the generator circuit because electric feeding was achieved without any contact between the electrodes. Therefore, allowing single discharge for each cycle of pulse voltage and helps in maintaining the constant discharge energy per pulse.

Further, Yang et al. [29] have applied the ESIF method to wire electrical discharge machining (WEDM) process in order to achieve the miniaturization. They have observed the better machining stability and lower discharge energy compared to relaxation-type pulse generator. Likewise, Koyano et al. [30] also obtained the high accuracy and machining speed using ESIF method.

In order to achieve an accurate gap of nanometers between the electrodes of nano-EDM, scanning tunneling microscopy (STM) and atomic force microscopy (AFM) type scanning probe techniques were employed. It resulted in the discharge crater size <100 nm [31]. Malshe et al. [8] presented the new technology of nanofabrication called as nano-electrical machining (nano-EM). They have

achieved consistent machined features of 10 nm diameter on atomically flat gold using scanning probe platinum-iridium tool electrode.

The use of ultra-small diameter tool is another technique to obtain success in nano-EDM. Cheng et al. [9] have developed the ultra-precise novel tool fabrication system to achieve nano-machining using an EDM process. With the help of fabricated tool, they have achieved average surface roughness less than 10 nm. More recently, Zhang et al. [22] have constructed a computational simulation model by combining the two-temperature model and MD simulation model for single discharge process in nano-EDM. The developed model is found to be useful to understand the machining mechanism of nano-EDM from a thermal point of view. Currently, nano-EDM is gaining more and more interest of researchers because of its capability to manufacture the components with nanoscale dimension along with high precision. Moreover, it is potentially applicable to manufacture the prototypes and masterpiece because it is quite flexible, cost-efficient, and fully automatic. Even though, nano-EDM is an efficient process to manufacture the components with nanoscale precision, it is not yet fully industrialized due to the robustness of EDM theory which hindered the advantage of nano-EDM technology. Still, nano-EDM is on developing stage and requires a constructive effort of researchers to establish it at industrial level.

2.2 *Introduction to Nano-ECM*

Nano-ECM is also an effective process to manufacture the components with features <100 nm as it uses ultra-short pulse of nanosecond duration for material removal and allow electrochemical reactions down to the nanometer level for high precision and accuracy [21]. Moreover, nano-ECM offers improved control strategy compared to traditional ECM in terms of lower pulse duration, variable voltage pulse, and optimized duty factor. With the use of ultra-short voltage pulse of 500 ps, the machining accuracy below 100 nm can easily be achieved [32] and it is possible to achieve complex nano-features [33]. In order to substitute the expensive ultra-short pulse generator, Koyano and Kunieda [34] have developed an ultra-short pulse electrochemical system using ESIF method and obtained the ultra-short current pulse of 6 ns. Even though, nano-ECM is an emerging machining process to obtain nanoscale components, further research is also required to industrialize it.

2.3 *Nano-Machining Prospects of Other Advanced Processes*

The nano-level advancements in other advanced processes such as laser beam machining (LBM), electron beam machining (EBM), and ion beam machining (IBM) processes are extremely difficult due to some technological constraints.

Basically, LBM process uses photon as energy particle to ablate and machine a wide range of materials. But, the dimensional accuracy of the machined components mainly depends upon the laser beam diameter. The laser beam can be focused to a diameter close to the laser wavelength which is in the range of 100 nm–10 μm but not <100 nm [35]. Although laser has been used frequently to assist other processes for nanofabrication [36, 37] but further advancements as nano-LBM still requires extensive research and development in the technology. In addition, EBM based on thermal evaporation also can't be implemented for nano-machining. That's because, nano-EBM requires an electron beam of a diameter of few nanometers but it is not effective for machining as most of the electrons are absorbed by the surface layer of the workpiece. However, there is scope of EBM in lithography techniques where fine focused beam of reactive electrons can be used to produce sub-nanometer accuracy on polymer-based components. Wong et al. [38] have worked on the new concept of nanoscale machining where a laser beam was used to heat a workpiece to a threshold temperature within a microscopic region out of which nanoscopic region was subjected to a focused electron beam. The approach is found to be useful for nanoscale machining of thin metallic film deposited on a transparent substrate. Focused ion beam process is mostly suitable for ion implantation rather than nano-machining and is used to patch or modify existing semiconductor devices.

3 Nano-Joining and Welding

3.1 Introduction

Nano-joining and welding is employed to fabricate nano-components or nano-structures that are having dimensions of the order of nanoscale such as 100 nm [39, 40]. Advances in nano-joining/welding technologies provide an extension to the applications of miniaturization at the different sectors of industries [40]. Nano-joining has been found promising for applications of nano-electronics, nano-medicine, nano-photonics, and nano-electromechanical systems (NEMS), wherein joining of nanotubes, nanowires, nano-sensors, nano-structures, and bonding of nanoparticles for semiconductors are reported in the recent literatures [39–42]. Most of these applications require heterogeneous structure at the interface of joint that is challenging. Additionally, nano-contact setup, fixturing, nano-joint defect detection, testing and characterization of nano-joints, and joining repeatability are challenges that one has to take into consideration for nano-joining and welding [40]. Conventional joining processes are not applicable to nano-components due to small size scale. Different joining processes such as nano-soldering, nano-welding and mechanical bonding, and nano-fastening are being progressed in order to fabricate nanoscale components [39, 40]. Classification of nano-joining methods under four major categories are presented in Fig. 4, based on state of art hitherto.

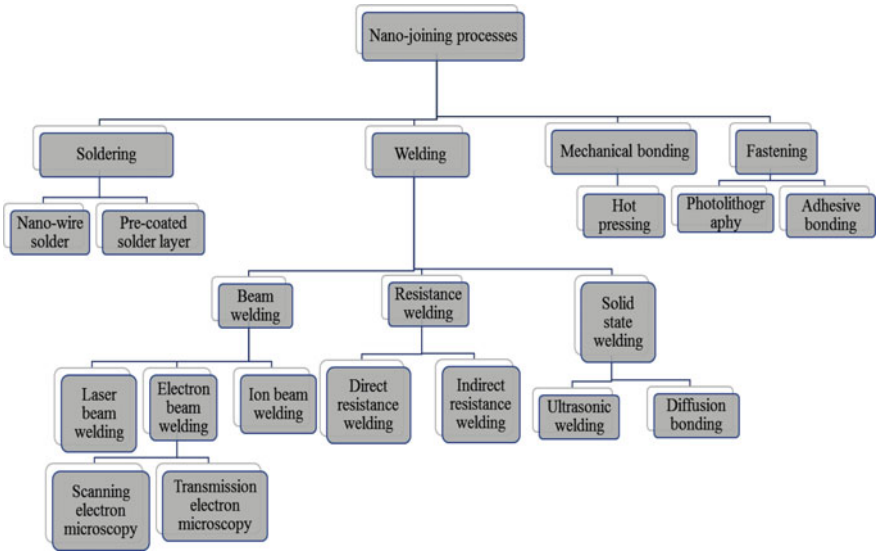

Fig. 4 Classification of nano-joining processes

3.2 Nano-Soldering

Nano-soldering is a process where nano-components (such as nano-wires) are joined together with the help of external nano-solder [42–44]. Nano-solder wire is also known as sacrificial nano-wire. The melting point of this nano-solder wire is relatively lower than the nano-base materials that is melted and subjected to the joint area in order to form a permanent connection. Various nano-solder materials such as indium, tin, indium-tin, tin-lead alloy, and tin-lead-copper alloy are reported in the literatures by which different nano-wires of gold, silver, and copper can be joined [42–44]. Nano-manipulators such as scanning electron microscopy manipulators are used to position the nano-wires that consequently form the joint configuration. The sacrificial nano-solder is heated by the means of electrical current that means appropriate current and voltage is applied [42, 44]. Nano-solders such as tin, tin-silver, and tin-silver-copper are developed with low melting point and generally applied to the end of nano-wires through electrodeposition process. These coated end of nano-wires are connected with each other to obtain unique nano-structure, wherein coated area only melts and forms the joint. This technique allows nano-soldering easy to perform for multi-nano-wires in order to assemble nano-structure [42]. Figure 5 shows 'NANO' word assembly of gold nano-wires prepared by nano-soldering [44].

Another nano-soldering approach is reported polymer adhesive coating [42]. Nano-wires that are to be joined are processed through hydrophobic thiol solution (for gold segment) or hydrophilic solution (for nickel segment). This solution is act

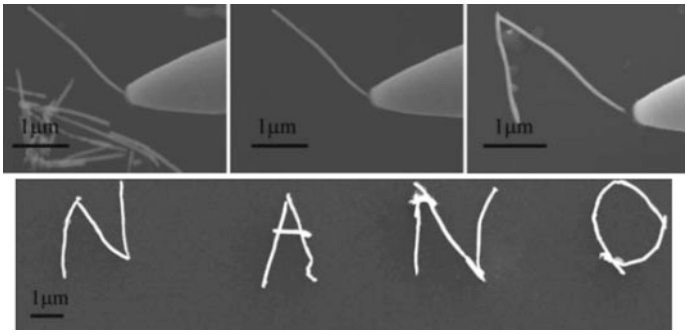

Fig. 5 Assembly procedure of NANO word from individual gold nano wires, Reprinted with permission from [44]. Copyright 2009 American Chemical Society

like adhesive when subjected to heat, which is normally applied through ultraviolet light. Au–Ni–Au type of nano-wires can be successfully joined by this method [42].

3.3 Nano-Welding

Nano-welding is reported for joining of carbon nanotube (CNT), NEMS components and nano-wires through various welding techniques such as beam welding, resistance welding, cold welding, ultrasonic welding, and diffusion welding [40–43]. Different beam welding techniques such as laser beam welding, ion beam welding, scanning electron microscopy and transmission electron microscopy techniques are utilized for nano-welding and joining [39].

Transmission electron microscopy (TEM) is a technique, in which the nano-joining is performed at a high accelerating voltage such as 1.25 MV under 800 °C temperature of specimen [39]. Nano-component such as single-walled nanotube (SWNT) is required to be dispersed in the ethanol in order to have TEM observations and subsequent procedures. The joining is obtained with the help of electron irradiation and annealing effect (higher than 300 °C) at the contact region of nanotube [39]. However, the main mechanism of joint formation depends on the target material and characteristics of nanoparticles [39, 45]. It is reported that, the kinetic energy transfer electronic excitations, ionization are the mechanisms observed for nano-joining by irradiation and annealing effect [39, 45]. The knock-on atom displacements caused by kinetic energy transfer are main mechanism observed for carbon nanotube atomic bonding. It is reported that, different junctions of SWNT such as X, T, and Y, can be structured through controlled electron irradiation of TEM [45]. Examples of these junction configurations are shown in graphitic Fig. 6.

Electron beam of scanning electron microscope (SEM) is also utilized to generate nanoscale welds in which energy of beam to workpiece interactions is used to

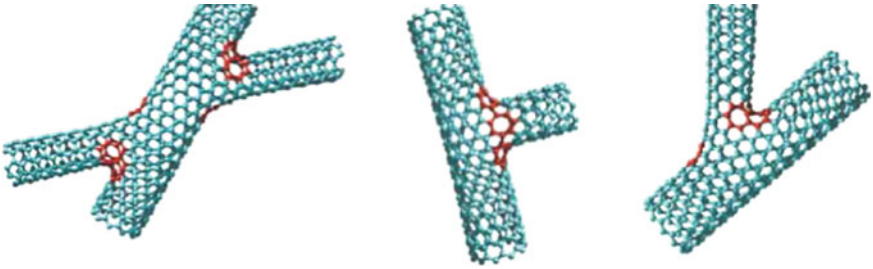

Fig. 6 Single-walled nanotube junctions prepared by TEM nano-joining [45], with kind permission from American physical society

melt the small scale material [39]. It is reported that, SEM electron beam is focused to a spot size in the range of 50–125 nm approximately that can melt area of 100 nm consequently [45]. Nanoscale weld by SEM is advantageous as for its reliability and an unparalleled control. Defect-free sound nano-welds on nickel, alumel, polysilicon, chromel, and tophet can be produced by high-magnification SEM along with control of beam deflection lens current and defined amplitude of scan area [39, 45]. TEM and SEM techniques have proved its capability as promising technologies for nano-welding.

In case of laser welding technology, picosecond laser pulses are recruited to adjoin, hold, and weld nano-gold particles on TEM carbon-coated copper grid [39]. It is reported that the gold nanoparticles (of 9.3 nm) with an average diameter of 13 nm are dispersed in the water that are processed for absorption of Surface-Plasmon absorption of resonances at 520 nm prepared through $HAuCl_4$. This gold nanoparticles are dropper on carbon-coated TEM grid using micro-pipet. After that, Nd:YAG laser is irradiated as second harmonic pulses of 532 nm at duration of 30 ps at 10 Hz frequency and 4-mm spot diameter in order to adjoin, hold, and weld closely the gold nanoparticles with TEM grid [39]. Laser irradiation helps to make association of nanoparticles on a wet TEM grid. The control of irradiation power is reported as important parameter for optimum nano-welding [39].

Another nano-welding method is resistance-type nano-welding in which ohmic controlled heating is responsible mechanism to obtain welds at nanoscale [42]. Direct resistance welding can be applied to nano-components such as nanotubes and substrate through small current and threshold voltage by means of sharp tungsten tips that works as electrodes [39, 42]. Direct resistance nano-welding is obtained at current in the order of 1×10^{-5} A and voltage of 1–5 V [39, 42]. Resistance heating can be applied differently such as copper particles are filled into carbon nanotube that acts as nano-spot welder. This nano-spot welder is nothing but nano-robotic manipulator that is subjected to a joint area. Afterward, small voltage such as 1.5 V is applied at the nano-carbon tube which is filled with copper material. This copper gets melted due to resistance heating and subjected to the nano-empty space of joint configuration, which consequently leads to the formation of joint [39, 42].

Ultrasonic nano-welding is developed to join SWNT to metallic electrode, which is also known as ultrasonic wire bonder [39]. A pressing surface was made up of 50 μm^2 single crystal and welding head of 0.2 nm rms roughness is mounted on it. It is reported that, a clamping force of 78.4 mN is required to press the welding head, at an ultrasonic frequency of 60 kHz through ultrasonic transducer, in order to weld 1.6 nm diameter SWNT to Ti electrodes [39]. An average ultrasonic power of 0.07 W is reported. At the time of ultrasonic nano-welding, the high-frequency ultrasonic energy is applied to soften the material, and consequently, it leads to the plastic deformation of the material under the effect of clamping stresses due to the acoustic softening [39]. This process is also successful for welding of multiple SWNT to metallic electrode.

Nano-diffusion bonding comes under the category of solid state nano-welding as the joining occurs below the melting temperature of the materials such as 25% of the melting temperature [42]. Acidic solvents and heat are applied to have diffusion of Au nano-wires and subsequently that leads to the bonding of it. Diffusion bonding can be utilized to form 3D network structure of the nano-wires for the surface-related applications [42].

Recent advancement in nano-joining is capillary force-induced cold welding, wherein silver nano-wire–wire joint is obtained by capillary force applied through moisture [46]. Figure 7 shows the procedure if capillary force-induced cold welding. The moisture is applied through humidifier for 1–3 s. This liquid provides bridging action between two nano-wires of Ag. Now, gentle fanning action is applied (for 30–40 s) in order to have drying action [46]. As soon as the water evaporates, the meniscus-shaped bridge of capillary forms at the gap between two nano-wires as shown in Fig. 7b. This consequently leads to produce attractive force that ultimately results into formation of joint [46].

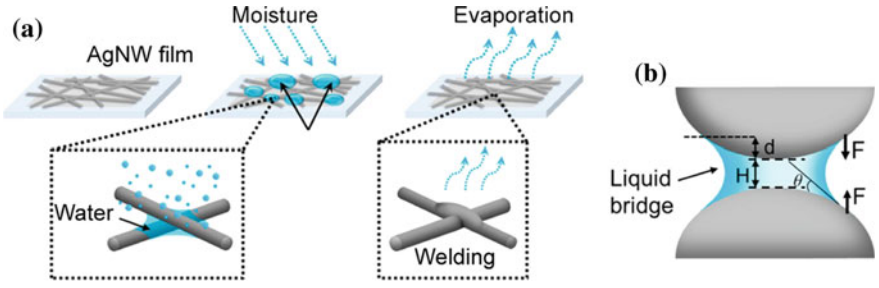

Fig. 7 Schematic of moisture treatment for capillary-force-induced cold welding of silver nano-wires. **b** The mechanism of capillary interaction between two particles connected with a liquid bridge, Reprinted with permission from [46]. Copyright 2009 American Chemical Society

3.4 Mechanical Bonding

Hot pressing technique is reported as mechanical bonding nano-joining technique. Hot embossing device is used for the hot pressing of nano-components, wherein sandwich-type nano-wire-electrode structure can be obtained at 180 °C temperature and suitable pressure is applied [42]. The joining mechanism is nothing but the deformation of the material due to applied temperature and pressure. The electrodes are used to position the nano-wires at the setup of the hot embossing [42]. Suitable tool is used to press the nano-wires to the respective electrode. The contact surface of tool is coated with the specific material such as silicon wafer is coated with carbon like diamond film, in order to avoid adherence of nano-wires to the tool [42].

The recent developments suggest that, nano-joining by mechanical pressing can be obtained at the room temperature [47]. Ag nano-wire is joined on to Au substrate with the help of nano-indenter whose tip is made up of diamond. The bonding force of 200–500 μn is applied at a loading speed of 20 μN s^{-1} [47]. These parameters have produced a defect free nano-joint through mechanical plastic deformation obtained through pressure of room temperature.

3.5 Fastening

Photolithography and electrodeposition techniques are types of nano-fastening classification [42]. Different processes such as photoresist (PR) coating, exposure, development, metallization, and liftoff are required to be performed in order to complete photolithography technique. Photolithography can be applicable to small number of nano-wires or single nano-wire. Photolithography is not preferred for joining of multiple nano-wires/structures [42]. In case of electrodeposition, the extra material is pasted on to a nano-wire and bonding is achieved between extra pasted material and external material [42]. The pasting of extra material can be obtained by electrolytic plating that requires suitable external current and voltage [42, 43].

4 Summary

This chapter discusses the fundamentals and basic knowledge used to understand the nanotechnology interventions in machining, joining, and welding arena. The nano-machining processes which have mainly been focused are; nano-indentation, nano-cutting, and nano-milling. The various important aspects such as tool geometry, work material, stresses, forces have been discussed with the relevant examples. The recent development in the field of nano-EDM and nano-ECM has

also been reported. Further, other advanced/non-conventional processes are also discussed in respective of their capabilities in the field of nanoscale machining. Although nano-EDM and nano-ECM are under development stage, however, exhibits a great potential to obtain the nanoscale dimension on the machined components. Lastly, the nano-joining and welding techniques are discussed considering their applications and parameters. Nano-soldering, nano-beam welding, nano-resistance welding, nano-ultrasonic welding, nano-diffusion bonding, nano-mechanical bonding, and nano-fastening are covered. Single- and multi-walled carbon nanotubes and nano-wires of gold, silver, lead, tin, and copper are main applications for nano-components. In future, the nano-joining and welding processes will be developed stable and reliable joints and scalability for assembly. Additionally, several important problems of cost reduction, efficiency enhancement, and massive integration of nano-wires can be considered as future prospects of nano-welding and joining. This chapter hopes further efforts of researchers involved in academia as well as in industries for research and development in nano-machining, nano-joining, and welding of modern materials.

References

1. Pokropivny V, Lohmus R, Hussainova I, Pokropivny A, Vlassov S (2007) Introduction to nanomaterials and nanotechnology, University of Tartu, p 225 (Special lecture course for bachelors, MSc, post-graduates and specialists in nanotechnology), ISBN: 978–9949–11–741–3, Tartu University Press
2. http://www.fi.tartu.ee/~rynno/raamat/Introduction%20in%20nanomaterials-sisu.pdf
3. Gupta MK, Sood PK, Sharma VS (2016) Optimization of machining parameters and cutting fluids during nano-fluid based minimum quantity lubrication turning of titanium alloy by using evolutionary techniques. J Cleaner Prod 135:1276–1288
4. Gupta MK, Sood PK (2017) Surface roughness measurements in NFMQL assisted turning of titanium alloys: an optimization approach. Friction. doi:10.1007/s40544-017-0141-2
5. Priyadarshi D, Sharma RK (2016) Effect of type and percentage of reinforcement for optimization of the cutting force in turning of Aluminium matrix nano-composites using response surface methodologies. J Mech Sci Technol 30(3):1095–1101
6. Davim JP, Jackson MJ (2008) Nano and Micro Machining wiley-ISTE
7. Jackson MJ (2007) Micro and Nanomanufacturing, Springer, USA, pp 591–634
8. Malshe AP, Virwani K, Rajurkar KP, Deshpande D (2005) Investigation of nanoscale electro machining (nano-EM) in dielectric oil. CIRP Ann Manuf Technol 54(1):175–178
9. Cheng X, Nakamoto K, Sugai M, Matsumoto S, Wang ZG, Yamazaki K (2008) Development of ultra-precision machining system with unique wire EDM tool fabrication system for micro/nano-machining. CIRP Ann Manuf Technol 57(1):415–420
10. Chae J, Park S, Freiheit T (2006) Investigation of micro-cutting operations. Int J Mach Tools Manuf 46:313–332
11. Grzesik Wit (2008) Advanced machining processes of metallic materials. Elsevier, Oxford
12. Malekian M, Park SS, Jun MB (2009) Tool wear monitoring of micro-milling operations. J Mater Process Technol 209:4903–4914
13. Cui DD, Zhang LC (2016) Nano-machining of materials: understanding the process through molecular dynamics simulation. Adv. Manuf. doi:10.1007/s40436-016-0155-4

14. Cheong WCD, Zhang LC, Tanaka H (2001) Some essentials of simulating nano-surfacing processes using the molecular dynamics method. In: Key engineering materials, Trans Tech Publ, pp 31–42
15. Zhang LC, Cheong WCD (2003) Molecular dynamics simulation of phase transformations in mono-crystalline silicon. High Press Surf Sci Eng 57:285
16. Cheong WCD, Zhang LC (2003) Mono-crystalline silicon subjected to multi-asperity sliding: nano-wear mechanisms, subsurface damage and effect of asperity interaction. Int J Mater Prod Technol 18:398–407
17. Zhang LC, Johnson K, Cheong WCD (2001) A molecular dynamics study of scale effects on the friction of single-asperity contacts. Tribol Lett 10:23–28
18. Cui DD, Zhang LC, Mylvaganam K et al (2015) Nano-milling on mono-crystalline copper: a molecular dynamics simulation. Mach Sci Technol
19. Ahmed W, Jackson MJ (2015) Emerging nanotechnologies for manufacturing. In: Micro and nanotechnology series, 2nd edn. Elsevier, London, ISBN 978-0-323-28990-0
20. Jackson MJ, Robinson GM, Whitfield MD, Hyde LJ, Underdown FJ, Sein H, Ahmed W (2015) Nanogrinding with Abrasives. In: Jackson and Morrell (eds) Machining with nanomaterials, Springer, Berlin
21. Rajurkar KP, Levy G, Malshe A, Sundaram MM, McGeough J, Hu X, DeSilva A (2006) Micro and nano machining by electro-physical and chemical processes. CIRP Ann Manuf Technol 55(2):643–666
22. Zhang G, Guo J, Ming W, Huang Y, Shao X, Zhang Z (2014) Study of the machining process of nano-electrical discharge machining based on combined atomistic-continuum modeling method. Appl Surf Sci 290:359–367
23. Benilov A, Skryshevsky V, Robach Y, Cabrera M (2008) Micro and nano electrical discharge machining in micro-fluidics and micro nanotechnology. Int J Mater Form 1(1):1315–1318
24. Han F, Yamada Y, Kawakami T, Kunieda M (2003) Investigation on feasibility of sub-micrometer order manufacturing using micro-EDM. In: ASPE 2003 Annual Meeting 30: 551–554
25. Kawakami T, Kunieda M (2005) Study on factors determining limits of minimum machinable size in micro EDM. CIRP Ann Manuf Technol 54(1):167–170
26. Egashira K, Mizutani K (2005) EDM at low open-circuit voltage. Int J Electr Mach 10:21–26
27. Kunieda M, Hayasaka A, Yang XD, Sano S, Araie I (2007) Study on nano EDM using capacity coupled pulse generator. CIRP Ann Manuf Technol 56(1):213–216
28. Yang XD, Wan Y, Hu FQ (2010) Study on influence of stray inductance in micro EDM using electrostatic induction feeding method. Key Eng Mater 447:263–267
29. Yang X, Xu C, Kunieda M (2010) Miniaturization of WEDM using electrostatic induction feeding method. Precis Eng 34(2):279–285
30. Koyano T, Kunieda M (2010) Achieving high accuracy and high removal rate in micro-EDM by electrostatic induction feeding method. CIRP Ann Manuf Technol 59(1):219–222
31. Virwani KR, Malshe AP, Rajurkar KP (2007) Understanding dielectric breakdown and related tool wear characteristics in nanoscale electro-machining process. CIRP Ann Manuf Technol 56(1):217–220
32. Kock M, Kirchner V, Schuster R (2003) Electrochemical micromachining with ultrashort voltage pulses–a versatile method with lithographical precision. Electrochim Acta 48 (20):3213–3219
33. Trimmer AL, Hudson JL, Kock M, Schuster R (2003) Single-step electrochemical machining of complex nanostructures with ultrashort voltage pulses. Appl Phys Lett 82(19):3327–3329
34. Koyano T, Kunieda M (2013) Ultra-short pulse ECM using electrostatic induction feeding method. Procedia CIRP 6:390–394
35. Samad RE, Machado LM, Junior NDV, Rossi W (2012) Ultrashort laser pulses machining. In: Laser Pulses—Theory, Technology, and Applications. InTech, pp 143–174
36. Kabashin AV, Meunier M (2003) Laser-induced treatment of silicon in air and formation of Si/SiOx photoluminescent nanostructured layers. Mat. Sci Eng. B 101:60–64

37. Kabashin AV, Meunier M, Kingston C, Luong JHT (2003) Fabrication and characterization of gold nanoparticles by femtosecond laser ablation in aqueous solution of Cyclodextrins. J Phys Chem B 107:4527–4531
38. Wong BT, Mengüç MP, Vallance RR (2004) Nano-scale machining via electron beam and laser processing. J Heat Transfer 126(4):566–576
39. Zhou YN (ed) (2008) Microjoining and nanojoining. Elsevier, Amsterdam, pp 545–579
40. Mehta K (2017) Advanced joining and welding techniques: an overview. In: Advanced manufacturing technologies Gupta K (ed), (pp 101–136). Springer International Publishing. doi:10.1007/978-3-319-56099-1_5
41. Guo KW (2009) A review of micro/nano welding and its future developments. Recent Pat Nanotechnol 3(1):53–60
42. Li X, Gao F, Gu Z (2011) Nanowire joining methods. Open Surf Sci J 3:91–104
43. Moszner F, Cancellieri C, Becker C, Chiodi M, Janczak-Rusch J. Nano-structured Cu/W brazing fillers for advanced joining applications
44. Peng Y, Cullis T, Inkson B (2008) Bottom-up nanoconstruction by the welding of individual metallic nanoobjects using nanoscale solder. Nano Lett 9(1):91–96
45. Terrones M, Banhart F, Grobert N, Charlier JC, Terrones H, Ajayan PM (2002) Molecular junctions by joining single-walled carbon nanotubes. Phys Rev Lett 89(7):075505
46. Liu Y, Zhang J, Gao H, Wang Y, Liu Q, Huang S, Ren Z (2017) Capillary-force-induced cold welding in silver-nanowire-based flexible transparent electrodes. Nano Lett 17(2):1090–1096
47. Peng P, Guo W, Zhu Y, Liu L, Zou G, Zhou YN (2017) Nanoscale wire bonding of individual Ag nanowires on Au substrate at room temperature. Nano-Micro Lett 9(3):9–26

Fabrication of Optical Components by Ultraprecision Finishing Processes

Gourhari Ghosh, Ajay Sidpara and P.P. Bandyopadhyay

Abstract The demand of ultraprecision optical components is increasing extensively with the rapid development of the modern optics. The optical components used in X-ray microscopy and extreme ultraviolet lithography (EUVL) demand surface roughness of about 0.1 nm rms, a figure accuracy about 1 nm peak-to-valley (p–v) and no induced subsurface crystallographic damage. Furthermore, an aspherical surface is gaining more interest over the past few years for its favourable properties, and many new optical materials are also being developed. Fabrication of ultraprecision optical components became a great challenge to the optical fabrication industry. Aspheric optical components are generally fabricated by shaping methods followed by precision finishing processes. Near net shape of the component can be accomplished by the shaping methods (e.g. single-point diamond turning, deterministic micro-grinding, etc.). The application of optical components fabricated by this method is limited to the infrared (IR) optics owing to the presence of high-spatial-frequency surface irregularities which lead to the possibility of scattering for shorter wavelength applications. Desired surface finish, figure accuracy and surface integrity can be attained by precision finishing techniques to make it suitable for shorter wavelength applications. In the recent years, ion beam figuring, elastic emission machining, nanoparticle colloid jet machining and magnetorheological finishing are extensively used for fabrication of ultraprecision optics. In this chapter, principle mechanism of material removal and applicability of aforementioned ultraprecision finishing processes to different materials are discussed.

Keywords Optical fabrication · Figure accuracy · Surface roughness · Subsurface damage · Ultraprecision finishing

G. Ghosh · A. Sidpara (✉) · P.P. Bandyopadhyay
Mechanical Engineering Department, Indian Institute of Technology Kharagpur, Kharagpur, India
e-mail: ajaymsidpara@mech.iitkgp.ernet.in

K. Gupta (ed.), *Micro and Precision Manufacturing*, Engineering Materials,
https://doi.org/10.1007/978-3-319-68801-5_5

1 Introduction

Recently, ultraprecision optical components are in high demand in various industrial and scientific applications. Ultra-smooth optical components are extensively used in the integrated circuit, synchrotron beam line, a micro-electromechanical system (MEMS), astronomical telescopes, cameras, high-power laser systems, low-scatter windows, luminescence, semiconductor industry, optical communication, defence equipment, etc. [1–3]. Ultraprecise mirrors with nanometre-order figure accuracy and atomic-order surface finish are the major requirement of the prime technologies such as generation synchrotron radiation sources and next-generation extreme ultraviolet lithography systems (EUVL) in the field [4, 5]. Hence, fabrications of the ultra-smooth surface become the prime concern of optical system manufacturers.

Optical components (e.g. mirrors and lenses), are the heart of any optical system, and are engaged to control the propagation and modulation of the light beam. The direction of propagation, the intensity and the polarization state of light rays largely rely on the characteristics of optical components [6]. The characteristics of optical components and its influence on performance are shown in Table 1. In order to maintain ultra-high reflectivity and better performance of optical components, suitable fabrication techniques have to be applied to generate high surface finish, high shape accuracy and minimum subsurface damage (SSD) [6, 7]. SSD have detrimental effect on the stability of the optical system, image quality, anti-laser damage threshold, and it may also accelerate the chance of system failure [1].

Besides the optical material properties, imaging quality of optical components is significantly affected by geometrical aberrations (spherical aberration, coma, etc., and diffraction effects). The aspherical optical component has the ability to avoid geometrical aberrations [6]. Therefore, the demands of aspherical optical components are increasing rapidly. Apart from that, the good quality image can be obtained by employing less number of optical components in a system. As a result, the size and mass of the optical system can be reduced [9]. Hence, fabrication technique is selected based on its ability to finish the aspherical surface.

Characteristics of the optical components greatly depend on its structure and chemical composition. Optical materials can be subdivided into following groups [10, 11]:

- Glasses (fused silica, BK7, etc.)
- Advanced ceramics (ALON, Cordierite, Silicon carbide, Spinel, Zinc selenide and Zinc sulphide)
- Low-thermal expansion materials (ULE, Zerodur and Clearceram)
- Metals (Al, Cu or GlidCop with electroless nickel coating)
- Crystalline materials (Calcium fluoride, Germanium, Sapphire and Silicon)

In extreme ultraviolet lithography (EUV) system, near about 30% of the incident light on the optical component is not reflected and it is converted into heat energy. Hence, low-thermal expansion material like ULE glass and Zerodur is suitable for

Table 1 Characteristics of optical components [8]

Characteristics of optical components	Influence to its optical performance
Surface shape	Spherical surfaces cause geometrical aberrations
Shape accuracy	Inaccurate shape causes geometrical aberrations
Surface roughness	Causes scatter and is responsible for the loss of imaging contrast
SSD that was generated during the fabrication (micro-cracks, stress, physical and chemical changes of the material, etc.)	Causes light loss; limits lifetime and increases absorption by the optical component
Absorption	Can cause unwanted light loss in the optical system
Reflection	Can cause unwanted light loss in the optical system and produce ghost images
Transmission	Changes the intensity of the light ray
Dispersion	Causes chromatic aberrations
Refractive index	Inhomogeneities of the refractive index cause distortion to the phase of the light ray
Sensitivity to environmental influences (temperature, mechanical vibrations, pressure, radiation, humidity, contamination (e.g. dust))	Limits lifetime of the optical component; changes amount of SSD, roughness and shape accuracy
Strength	It is responsible for the deformability and crack initiation of the optical surface
Density of the material	Inhomogeneities cause unwanted changes to absorption and refractive index and change the phase and intensity of the light ray
Chemical and physical inhomogeneity of the material	Inhomogeneities cause changes in refractive index, reflection, the phase of the light ray, etc.

this application [12]. Higher brilliance beam of third-generation synchrotrons generates high demands on reflection optics. To retain the reflection geometries and properties under severe heat load density, the optical components should be cooled significantly. Single-crystal silicon became the suitable material for front-end optics owing to its high heat conductivity, low-thermal expansion coefficient and low degradation quality. Fused silica and Zerodur are occasionally used for downstream optical components where beam exposure is not much intensive. Furthermore, when the heat load is not so much high, a metal mirror made of mostly aluminium, copper or GlidCop (alumina dispersion strengthened OFHC copper alloy) with a thin (i.e. 100 μm) electroless Ni-coating is used [13, 14]. Recently, beryllium is gaining interest for the space optics for its light weight and high strength. Owing to very low X-ray absorption property, beryllium may be selected as a substrate material for fourth-generation synchrotron X-ray mirrors [13]. Chemical-vapour-deposited (CVD) silicon carbide mirrors are widely used for astronomical applications. Only

small-sized CVD silicon carbide mirrors may be used at synchrotron facilities [13]. Optical materials for manufacturing optical components and its application are given in Table 2.

The effort to develop the precision finishing technologies has been initiated in 1980s to meet the requirement of ultra-high-quality optical components [17]. The evolution of the computer numerically controlled (CNC) machining has incorporated the determinism in optics fabrication [18]. It is more difficult to achieve

Table 2 Optical materials and its application [15, 16]

Optical components	Material	Application
Precision lenses	Zinc Selenide (ZnSe), Zinc Sulphide (ZnS), Germanium (Ge), Silicon (Si), Chalcogenides	Dental imaging, dermatology, endoscopy, hyperspectral imaging, lasers, machine vision inspection, metrology, optometry, projection, range finding, surveillance, target identification, targeting and designating, thermal imaging
Synchrotron mirror	Single-crystal silicon, Zerodur, Astrositall, Fused silica, Ultra-low expansion glass (ULE), silicon carbide, Cu and Al with electroless Ni layer	Synchrotron beamline, X-ray free electron laser (XFEL)
EUV mirror	ULE, Zerodur	EUV lithography, high-order harmonics applications
Optical windows and flats	ZnSe, ZnS, Ge, common glasses, fused silica, glass-ceramics	Biomedical instrumentation, corrosive chemistry, directed energy applications, industrial instrumentation, IR imaging, laser cavities, machine vision, multiphoton imaging
Waveplates	Crystal quartz, Magnesium fluoride (MgF_2)	Aerospace, astronomy, biomedical, laser power control and attenuation, military, optical isolation, polarimetry, remote sensing, semiconductor metrology, spectroscopy, surveillance
Ring laser gyroscope components	Fused silica, Zerodur	GPS, hyperspectral imaging, infrared microscopy, laser scanning microscopy, metrology, optical failure analysis for semiconductor processing, range finding, reconnaissance, surveillance, target identification, targeting and designating
Infrared optics	ZnSe, ZnS, Ge, Calcium fluoride (CaF_2), MgF_2, chalcogenides, silicon, sapphire	Hyperspectral imaging, infrared microscopy, laser scanning microscopy, metrology, optical failure analysis for semiconductor processing, range finding, reconnaissance, surveillance, target identification, targeting and designating, thermal imaging
Optical domes	ZnSe, ZnS, Ge	Seeker head optics, submersibles, underwater cameras
Precision mirrors	Metallic coating: Au, Pt, Al others	Laser cavities, laser range finders, target designators

ultra-smooth surface in case of the aspherical surface compared to spherical one. Fabrication of aspheric optical components consists of shaping mode followed by precision finishing mode [6]. In the shaping mode, the aspheric surface is produced by removing material at a higher rate. In this mode, brittle fracture and plastic deformation are considered as the material removal mechanisms [19]. Therefore, subsurface damage (dislocations, stress, micro-cracks, etc.) is induced in the surface. Single-point diamond turning (SPDT) [20, 21] and deterministic micro-grinding [22, 23] have been extensively used for the shaping of aspherical components. Presence of turning marks on the surface is the main limitation of SPDT and which restricts its application in the fabrication of infrared (IR) optics owing to the possibility of scattering for shorter wavelength application [9]. Deterministic micro-grinding has the ability to fabricate optical components with 10–20 nm (rms) surface roughness, λ/2 p–v figure accuracy (λ = 633 nm) and SSD of 2 μm [24]. In the finishing mode, SSD which is generated in shaping mode has to be removed and surface finish and figure accuracy must be improved to make it suitable for shorter wavelength application. Ultraprecision finishing processes, like ion beam figuring (IBF) [25, 26], chemo mechanical polishing [27, 28], plasma chemical vaporization machining (PCVM) [29], elastic emission machining (EEM) [30, 31], nanoparticle colloid jet machining (NCJM) [32], bonnet polishing [33, 34] and magnetorheological finishing (MRF) [35, 36] are extensively used for the fabrication of high-quality optical components. In this chapter, mechanism of material removal, surface integrity and applicability of ion beam figuring, elastic emission machining, nanoparticle colloid jet machining and magnetorheological finishing to different materials are discussed.

2 Precision Finishing Techniques Used for Fabrication of Optical Components

In recent years, the demand for micro-sized aspherical glass lenses has been increased rapidly. These were traditionally produced by grinding using small rigid tools. Presence of high-spatial-frequency surface irregularities or ripples is the inherent problem of those finishing techniques [37]. Hence, the development of new precision finishing processes to solve the problems is greatly needed. In order to fabricate the ultraprecision optical components, finishing techniques must be precisely controlled and external disturbances (like vibration deformation and thermal deformation) should be minimized. Furthermore, it should be deterministic and capable of producing sub-nanometre figure accuracy and surface roughness without incorporating SSD [24]. Figure 1 shows the classification of the precision finishing processes in terms of shaping and finishing of optical materials. Near net shape of optical components can be achieved by the shaping methods and desired figure accuracy and surface finish to make it suitable for a particular application can be achieved by the finishing methods.

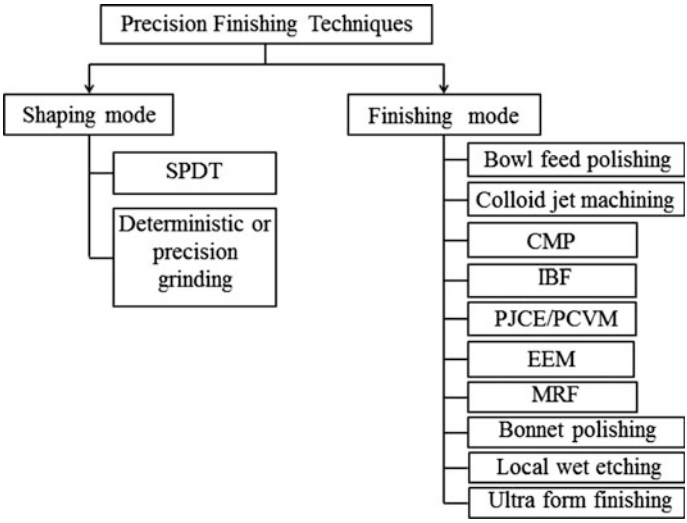

Fig. 1 Classification of precision finishing techniques used for optical components fabrication

2.1 Single-Point Diamond Turning (SPDT)

Single-point diamond turning (SPDT) of optics was started in 1960s, but it became an important fabrication technique for optical components after 1970s [38]. SPDT is a precision machining technique has the ability to produce aspherical or freeform surface with deterministic form accuracy. It is performed by engaging a single-point diamond tool in high-precision lathe under controlled environment [39]. The efficiency of this process depends on the stiffness of the machine, accuracy of feedback control system with a laser metrology and reliability of single-crystal diamond tool [40]. Diamond turning machine must be stiff enough to avoid the effect of vibration or other external disturbances on the cutting tool movement. To produce high-quality optical components, the cutting tool should move precisely and it should be sharp enough without any defects [41]. Lower cutting force is expected as the feed and depth of cut are much lower compared to the conventional machining. It has the ability to finish metal like Cu and Al to achieve nanometre range surface roughness and figure accuracy. Furthermore, high stiffness, accuracy and lower cutting force associated with the diamond turning machine make it suitable for precision finishing of brittle materials. Figure 2 shows the fishbone diagram of SPDT parameters that have a significant effect on surface roughness and form accuracy.

2.2 Grinding

Grinding is a widely accepted finishing process for machining of brittle materials. It is recognized as a pre-finishing or shaping method in the optical fabrication. During

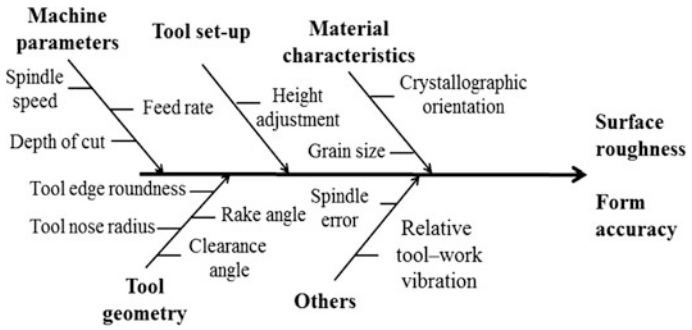

Fig. 2 Fishbone diagram of process parameters affecting SPDT operation

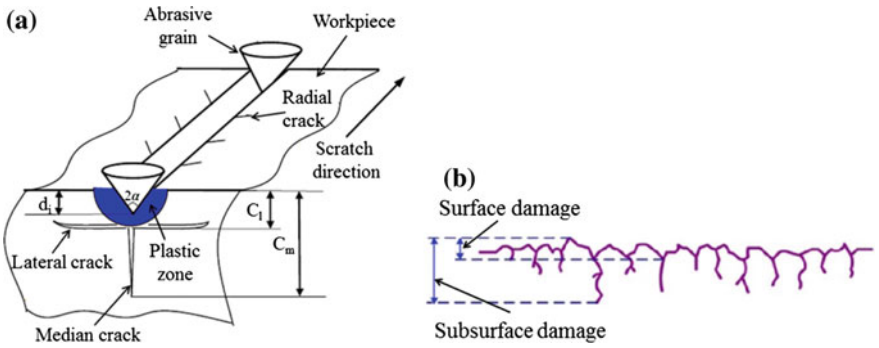

Fig. 3 **a** Brittle mode material removal during conventional grinding (d_i = depth of penetration of abrasive grit, C_m = median crack length, C_l = depth of lateral crack, α = half-apex angle of abrasive grit) [42], **b** surface of fused silica which is grounded by brittle mode [43]

the conventional grinding of optical components, material is removed through the crack propagation beneath the sharp cutting edge [42]. When the load on sharp abrasive grit exceeds the critical value, median cracks and lateral cracks are generated beneath the abrasive grit as shown in Fig. 3a. The lateral cracks are propagated to the top surface of the workpiece, and the material is removed as chips due to the brittle fracture [42, 43]. The median cracks appear as micro-cracks below the ground surface, which is responsible for the generation of subsurface damage. Figure 3b shows the fused silica surface which is grounded by brittle mode having a surface as well as subsurface damage.

Hence, the crack-prone surface which is generated by brittle mode in conventional grinding does not meet the requirements of the optical components. Post finishing of the ground sample using lapping followed by polishing became an essential step of optical fabrication to reduce the scattering and absorption loss and finally to get an optical quality surface [44]. Hence, the conventional technique of optical fabrication became a time-consuming and uneconomical process.

In the recent years, ductile mode grinding was getting significant importance in optical fabrication as it has the ability to eliminate lapping and sometimes a part of polishing. It is perceived that the possibility of ductile mode of grinding may be independent of material characteristics (hard or soft, brittle or ductile), and optical brittle materials also can be machined by ductile mode of grinding [45]. If the energy required for crack propagation is higher than the energy employed for material removal in grinding, material removal is taken place through the plastic deformation. Plastic deformation energy (E_p) is proportional to the volume of deformation ($\propto d_i^3$) while energy required for propagation of brittle fracture (E_f) is proportional to the area generated by the crack propagation ($\propto d_i^2$).

The ratio of material removal energies can be written as follows [45]:

$$\frac{E_p}{E_f} \propto d_i \tag{1}$$

where d_i is the depth of indentation. Hence, when the depth of penetration is sufficiently small, plastic flow becomes the predominant mode of machining than a brittle fracture. Therefore, there must have a critical depth of cut to accomplish shear (ductile) mode grinding. The critical depth of penetration for brittle–ductile transition for grinding is modelled by Bifano, and it is written as follows [45]:

$$d_c = 0.15 \frac{E}{H} \left(\frac{K_c}{H} \right)^2 \tag{2}$$

where E is the elastic modulus, H is the hardness, and K_c is the fracture toughness of the material which all are material properties.

Therefore, to perform ductile mode grinding for achieving crack-free surface, maximum undeformed chip thickness should be less than the critical chip thickness. In ductile mode grinding, the subsurface damage can be reduced but it cannot be eliminated completely. Hence, further polishing is required to obtain optical quality surface.

It has been already discussed in the previous section that single-point diamond turning (SPDT) has the capability to perform ductile mode machining of optical materials. However, rapid tool wear becomes a problem in SPDT [46]. Therefore, multipoint ductile cutting (grinding) for optical material become more economical [47].

In recent days, deterministic micro/ultraprecision grinding is extensively used to execute ductile regime grinding of optical components. The material removal rate of different abrasive machining processes is shown in Fig. 4, and it is perceived that there is a substantial gap between conventional grinding and polishing. This gap is related to brittle–ductile transition and micro-grinding falls in this region.

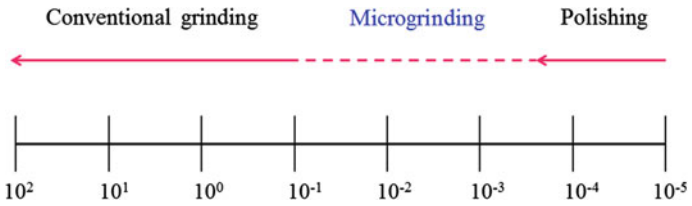

Fig. 4 Material removal rate in abrasive machining processes (mm^3/mm s) [48]

2.2.1 Deterministic Micro/ Ultraprecision Grinding

Deterministic micro/ultraprecision grinding is extensively used as a pre-finish machining step for the fabrication of optical components [49]. Generally, resin or metallic-bonded diamond grinding tool is precisely moved using a rigid machining centre for fabrication of spherical, aspherical and freeform surfaces as shown in Fig. 5. The deterministic micro-grinding machine has following characteristics [48–51]:

- The main spindle is made of glass-ceramics having zero thermal expansion, and spindle error motions should be less than 50 nm
- Hydrostatic oil bearings to impart vibration absorptivity, high rigidity and rotational accuracy of the spindle.
- Highly precise and vibration-free set-up
- High loop stiffness between the tool and workpiece
- High-resolution motion control and smooth feedback control (resolution less than 10 nm)
- High thermal stability
- Ability to achieve small depth of cut

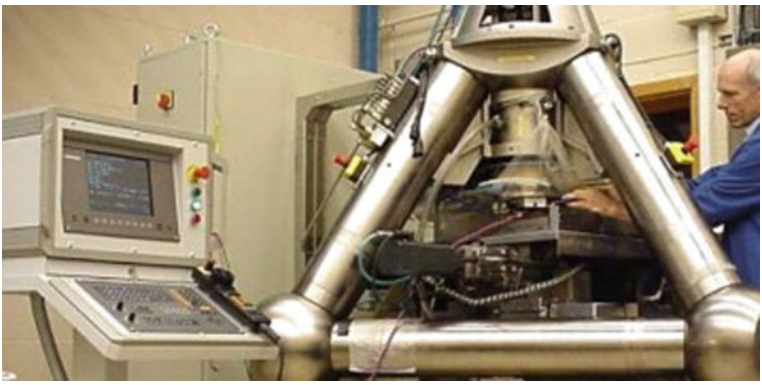

Fig. 5 Ultraprecision grinding machine [48]

As the very small depth of cut around 0.1 μm can be employed, ductile mode grinding can be executed successfully to obtain good surface finish (less than 10 nm Ra), better form accuracy (0.5 μm p–v) and to minimize subsurface damage (less than 1 μm) [52].

For optical glasses fabrication, the range of grinding tool rotation may be 5000–30,000 rpm and workpiece rotation may be 50–300 rpm. A fine-grained bounded diamond tool with a reducing grain size 100–2 μm is generally used and damaged layer created by one tool is removed by the succeeding more fine-grained diamond tool [52, 53].

A fine-grained diamond tool which is used in micro-grinding to obtain good quality surface, suffer high wear rate [54]. Therefore, the tool must be dressed periodically to maintain the sharpness of grains and the profile of the tool [55]. Self-sharpening of grinding does not take place because the very small depth of cut is employed [49]. Besides, periodic conventional dressing processes are laborious and time-consuming techniques. Hence, in-process dressing technique must be coupled with ultraprecision grinding to maintain the efficiency and effectiveness of grinding during the batch production of precision optical components.

2.2.2 Nanogrinding

Nanogrinding is comparatively an advanced process, that is gaining substantial importance in the optical fabrication industries nowadays. It is executed in an ultraprecision machine having high stiffness and high-resolution motion control [56]. It has the ability to employ depth of cut in nanometre scale [57]. The very fine-grained diamond grinding tool is used for this process. Hence, ductile regime grinding of brittle optical material can be performed perfectly to obtain better quality surface. Figure 6 shows the ultraprecision machine set-up for nanogrinding. The workpiece is fixed on the rotary table, and cup-type grinding wheel is used for machining. Rotary table spindle and grinding wheel spindle both are surrounded by air bearing with 50 nm motion error [58].

Earlier, the soft metal plate (tin) was conditioned and then diamond particles are embedded on the plate to make nanogrinding tool [59]. These days, vitrified diamond wheel is used for the same. Nanogrinding can be employed for machining of brittle material like Si, SiC and germanium for making lens and mirrors with high precision.

2.2.3 Piezoelectric Nanogrinding

In piezoelectric nanogrinding, the piezoelectric material is coated with submicron size diamond particle to make the nanogrinding tool. This can be also made by bonding porous diamond tool to the piezoelectric crystal. The workpiece is held

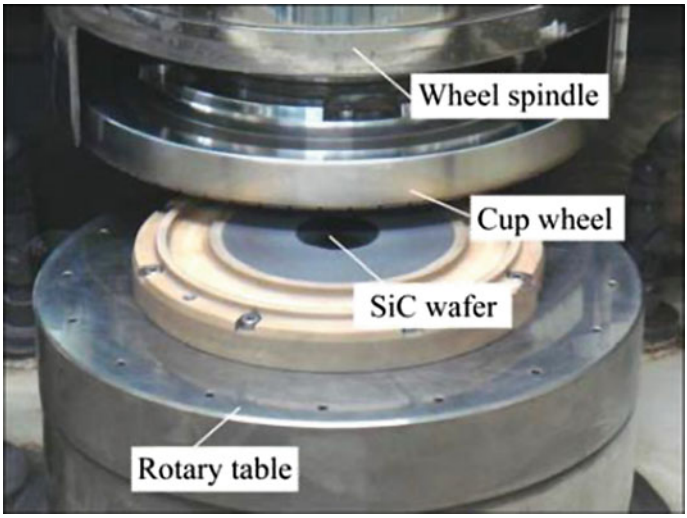

Fig. 6 Ultraprecision machine set-up for Nanogrinding [58]

tightly in a vice after that the tool and workpiece are aligned, and depth of cut is employed in the step of 10 nm. Thereafter, electric current is applied to the coated piezoelectric material and it causes straining of the material just beneath the sharp abrasive grits. The nanoscale fragments of the materials will be removed, consequently. Material removal rate can be controlled by the magnitude of the applied current. The experiments should be performed on the precision and vibration-free set-up to make the process more efficient and effective [60]. Processing of different materials by deterministic grinding and major finding of the reported works are mentioned in Table 3.

Although ultraprecision grinding and nanogrinding are performed on a very stiff, rigid and precise machine, optical quality surface cannot be produced by grinding alone. As the bonded abrasive tool comes in contact with the workpiece, generation of the subsurface crack becomes an inevitable part of deterministic grinding. But, it is far smaller than cracks created by conventional grinding. Namba et al. [67] have reported 0.3 µm subsurface damage during ultraprecision grinding of CaF_2. Huo et al. [70] observed that during nanogrinding of Si, around 60 nm subsurface damage consists of amorphous layer followed by dislocation layer is introduced. The subsurface damage generated by nanogrinding is far lower than the deterministic micro-grinding, but it is not totally eliminated. Hence, deterministic grinding is recognized as a pre-finish machining step or shaping method in optical fabrication industries. To make the optical components suitable for shorter wavelength application, the ground sample should be further processed by some ultraprecision finishing techniques like IBF, NCJM, PCVM, EEM, MRF.

Table 3 Literature survey of processing of different materials by deterministic grinding

Authors	Materials	Major findings
Deterministic micro/ultraprecision grinding		
Namba et al. [61]	Glasses	• The mode of grinding (fracture, ductile and fracture and ductile mode) is influenced by grain size of the diamond wheel • Surface finish relies on the feed per revolution, grain size and material properties. The depth of cut has very small effect • Optical quality surface with 0.2 nm rms, 2 nm Rmax was achieved by ductile mode grinding
Bifano et al. [62]	CVD SiC	• Ductile regime grinding is more economically viable than polishing owing to the comparatively small Preston coefficient and large critical depth • Reflectivity of the ground surface is sufficient for IR application
Lambropoulos et al. [22]	Different types of glasses	• Glass properties like elastic modulus, hardness and fracture toughness have a significant effect on surface quality
Namba [63]	CVD SiC	• Feed, cutting edge wear and average diamond grain size have a significant effect on surface quality. Surface finish of 0.4 nm (rms) was reported • Reflectivity is found 88.7% of the ground surface when tested using 0.834 nm X-ray
Burns et al. [64]	AlON	• Grain highlighting was observed owing to the polycrystalline material and having high hardness and bigger grain size (100–200 μm) • Small surface pits were reported during grinding with finer grain (2–4 μm) tool • Low feed rate is desirable to achieve good surface finish
Yin et al. [65]	Polycrystalline SiC	• Spherical surface with surface roughness 9.92–17.22 nm (Ra) and form accuracy 0.13–0.37 μm were achieved • During process, the diamond tools are self-sharpened because SiC can be conducted as a dresser
Yang et al. [66]	K9	• The form accuracy of 4–5 μm and 3–4 μm (P–V) for spherical and flat surface was achieved, respectively
Namba et al. [67]	CaF_2	• Small diamond grain size of grinding wheel and low feed rate can generate crack-free surface • Surface roughness relies on the grinding direction, diamond grain size, crystalline plane and feed rate • The surface is finished to 1 nm Ra. Subsurface damage of 0.3 μm is observed on a ⟨111⟩ plane

(continued)

Table 3 (continued)

Authors	Materials	Major findings
Yin et al. [68]	Polycrystalline zirconia, WC composite, Si, SiC	• Except for zirconia, the surface roughness of materials increases with brittleness in ultraprecision grinding • In ultraprecision grinding of zirconia, the stress-induced phase transformation does not allow a fine finish
Yao et al. [69]	BK7	• Feed rate and wheel speed have adequate effect on subsurface crack and surface roughness • The ratio of subsurface damage and surface roughness relies on the half-apex angle of abrasive grain
Zhao et al. [55]	BK7 and Zerodur	• Coarse-grained diamond wheel can perform precision grinding in ductile mode with better wheel profile consistency and wear rate • Micro-cracks, subsurface cracks, micro-pits were observed owing to its multiphase structure
Nanogrinding		
Huo et al. [70]	Si	• 2 nm (Ra) surface roughness and 15 nm (p–v) were found using vitrified bond (CeO_2 and SiC) #10000 diamond wheel and 7 μm/min feed rate • Subsurface damage of 60 nm was reported
Zhang et al. [71]	Si	• 0.6 nm (Ra) and 6.4 nm (p–v) were found using vitrified bond (SiC, NaCl, SiO_2 and Al_2O_3) # 12000 diamond grinding wheel and 6 μm/min feed rate • A subsurface damage layer of 40–60 nm was found
Huo et al. [58]	SiC wafers	• High-quality surface with 0.42 nm (Ra) and less than 1 μm flatness is reported • Lower subsurface damage is observed during grinding with #600 diamond wheel

2.3 Ion Beam Figuring (IBF)

Ion beam figuring (IBF) is a deterministic ultraprecision finishing technique, and it is widely used as a final step fabrication technique for precision finishing and figuring of the optical components [72, 73]. The stringent requirements of the optical components which are used in EUV lithography, synchrotron beam line and astronomical application have been processed by IBF in the recent days [74]. It has the ability to remove the material in atomic scale by the interaction of ion beam with the molecules or atoms of the workpiece surface [75]. Prior to the IBF, the ground-turned surface and diamond-turned surface are polished to attain surface finish and figure accuracy up to a certain minimum level [76]. The residual fine surface errors or polishing errors are removed by IBF for further improving the contour accuracy and to meet the desired specification.

In 1965, at first Meinel et al. [77] employed IBF for polishing of glass but it was damaged owing to the high energy of ion beam. After developing low energy ion beam by Kaufman [78], known as Kaufman ion source, Gale [79] started working again in 1978. Wilson et al. [80] have successfully applied this technique for improving contour accuracy and surface finish of Zerodur, fused silica and copper using Kaufman ion source in 1987. Thereafter, IBF became an integral part of optical fabrication industries.

Generally, Kaufman ion source is used for generation of ions and the generated ions are accelerated and directed by the charged grid to form a beam. Thereafter, the ion beam is neutralized by supplying electrons from a neutralizer to eliminate the chance of workpiece charging and to prevent the deflection of ion beam in the presence of electromagnetic fields [75]. When the ion beam strikes the surface atoms of the workpiece, a collision cascade is generated within the workpiece. After the ending of the cascade, the surface atoms acquire sufficient energy to overcome the surface binding energy and finally removed from the surface [81]. The distance of ion source from the workpiece, the beam energy, incident angle of the beam and the material properties of workpiece have a significant effect on the amount and distribution of material removal owing to the sputtering [81]. High vacuum environment is required for avoiding beam collision during travelling from the source towards the workpiece. For accomplishing constant sputtering rate, the fixed beam energy is maintained. The ion beam raster scan is employed for improving figure accuracy of the whole surface [75] as shown in Fig. 7b. The spatially and temporally stable ion beam is positioned perpendicularly at a fixed distance from the workpiece, and its motion is controlled by a 5-axis CNC system as shown in Fig. 7a.

Figure 8 shows the basic steps of IBF process. In the first stage, the contour of the optical surface to be processed is measured by optical interferometry. Thereafter, the measured contour is compared with the desired surface contour to finalize the removal map which gives the idea about the amount and distribution of material to be removed. Next important step of IBF is the determination of material removal function (influence function). It shows the variation of material removal

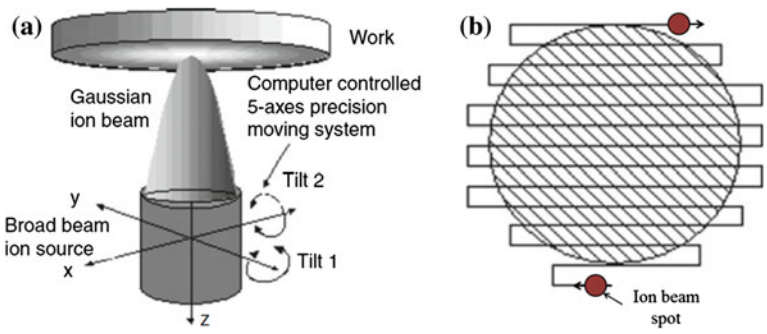

Fig. 7 **a** Schematic of IBF process, **b** ion beam raster scan [75]

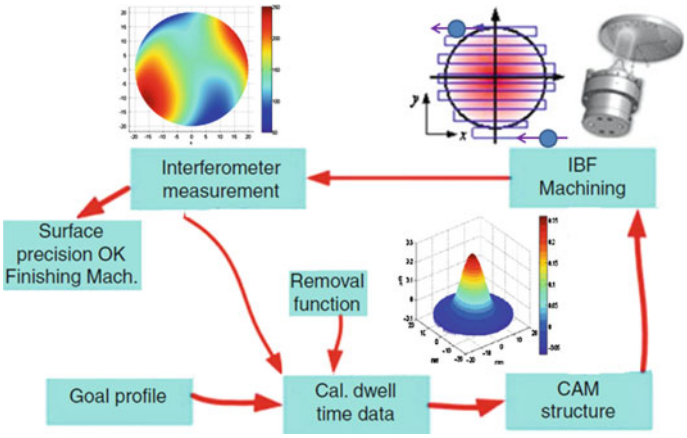

Fig. 8 Flow of IBF process [75]

depth with radial length from the centre of the ion beam. Thereafter, dwell time is calculated based on the removal map and material removal function. Using CAM system, velocity and moving routine of the ion beam are finalized. Afterwards, the ion beam raster scan is employed over the surface based on moving routine and dwell time. It is assumed that the material removal function is time invariant. Material which is going to be removed (R(x, y)) can be expressed as a function of beam removal function (B(x, y)) and dwell time (T(x, y)) [75].

$$R(x, y) = B(x, y) * T(x, y) \tag{3}$$

IBF has the following advantages [75, 82, 83]:

- Ultraprecision surface with sub-nanometre or nanometre scale figure accuracy can be achieved as the material removal is taken place at the atomic scale. Fine finishing error having small wavelength can be successfully removed using narrower tool size even less than 0.5 mm. Long spatial wavelength errors can also be removed efficiently.
- The highly deterministic material removal process can be accomplished by maintaining constant beam parameters. As a result, the desired specification can be attained easily and processing time requirement can also be reduced.
- The tool wear, loading force on the surface and edge roll-off effect which are more prominent in case of mechanical machining and polishing are not associated with IBF, as it is a non-contact finishing technique. Consequently, the possibility of surface or subsurface damage generation is immensely reduced.
- It has the capability to figure any types of surface like spherical, aspherical or freeform. The hard polycrystalline material also can be processed.

It also has following disadvantages [75, 82, 83]:

- It needs vacuum environment for processing the optical component.
- During the processing, the ions having several thousand eV strike the optical surface, which makes too much heating of the surface.
- Owing to the ion "sandblasting" effect occurred at the atomic level, surface finish is degraded for some optical materials.
- Material removal rate is very low (hundreds of nanometre per minute)

Materials which can take a thermal load of around a few of 10 W can be successfully processed by IBF. Very hard materials (e.g. Si, Sic and WC, etc.) and crystalline materials (e.g. ZnSe, CaF_2 and MgF_2, etc.) can also be figured to the desired accuracy [26]. For processing of the high thermal expansion materials (e.g. BK9, BK7, etc.), special care must be taken to control the excessive heating of workpiece by maintaining the beam parameters [75].

The variation of surface roughness evolution with the material removed depth is reported for different optical materials. Material removal depth has less effect on the evolution of roughness for processing of some materials (e.g. glass, CVD SiC, etc.). However, the roughness increases rapidly during processing of electroplated metals. During processing of polycrystalline materials, the surface roughness may increase owing to the different material removal rate at different grain orientations [83]. Ion beam parameters (e.g. gas, energy) have a significant influence on the surface roughness evolution. Some unfavourable materials (polycrystalline material like Zerodur, etc.) can also be processed by maintaining very small material removal depth or by making a coating of suitable material on the substrate [83]. Processing of different materials by IBF and major finding of the reported works are mentioned in Table 4.

2.4 Nanoparticle Colloid Jet Machining (NCJM)

Nanoparticle colloid jet polishing is a newly developed deterministic polishing process for ultraprecision optical component [91]. Optical quality surface without introducing any crystallographic damage can be obtained by removing material in atomic scale by utilizing the chemical reaction between the atoms of the optical component and nanoparticle [92]. The components are shaped and pre-finished by some shaping methods (SPDT, deterministic micro-grinding) before processing using NCJM. The material removal rate is low as few nanometre per min owing to the atomic scale removal [93]. The nozzle along with the colloid injection system is generally mounted on a multi-axis computer numerical control machine having 3 linear and 3 rational motion axes. Schematic of polishing concave surface in nanoparticle colloid jet machining is shown in Fig. 9.

The heart of this process is polishing colloid (PH value 10) which contains nanoparticles (SiO_2 or CeO_2, 30% by volume), pure water, additive and surfactant

Table 4 Literature survey of processing of different materials by IBF

Authors	Materials	Major findings
Wilson et al. [84]	Fused silica	• No appreciable variation of surface roughness with the etching depth is observed • Fused silica was finished from 1.8 waves (p–v) and 0.41 waves (rms) to 0.27 waves (p–v) and 0.042 waves (rms), respectively
Allen et al. [85]	Zerodur	• Surface roughness and figure accuracy were improved from 0.726 µm (rms) and 3.23 µm (p–v) to 0.09 µm (rms) and 0.51 µm (p–v), respectively • Warping of the surface due to extreme heating of surface is observed. Very fine surface irregularities perpendicular to the beam scanning direction is perceived
Drueding et al. [86]	Fused silica and CVD SiC	• The surface finish of both the components was improved using precision ion machining system (PIMS) at NASA. Severe surface defect is observed • Fine surface errors are successfully eliminated by small apertures ion beam, but its removal rate is very less
Flamm et al. [87]	CaF_2	• Low beam energy and gases having high atomic masses lead to good surface finish • CaF_2 is decomposed into metallic calcium and calcium oxide near surface owing to the sputtering • Self-arranged nanoscale structures like ripple, hole, meandering and dot are observed on the surface
Gailly et al. [88]	CVD silicon carbide, electroplated nickel, PVD gold	• Rapid increase of roughness for electroplated nickel (> 5 nm/µm) and a small decrease of roughness for PVD gold (0.3 nm after 0.2 µm) were reported • A roughing rate of 1 nm per µm etching depth was observed for CVD silicon carbide • Ion beam energy and operating gas have significant effect on the roughness evolution rate of CVD SiC
Weiser [89]	Fused silica, ULE, Zerodur	• Capable to meet the requirements of lithographical optics • Surface roughness is reduced to 0.13 nm (rms) and 0.19 nm (rms) for spherical and aspherical lenses, respectively.
Demmler et al. [90]	Si	• Figure accuracy was reduced from 513 nm (p–v) to 65 nm (p–v), and surface roughness was decreased from 120 nm (rms) to 7 nm (rms) • No surface or subsurface defects were observed

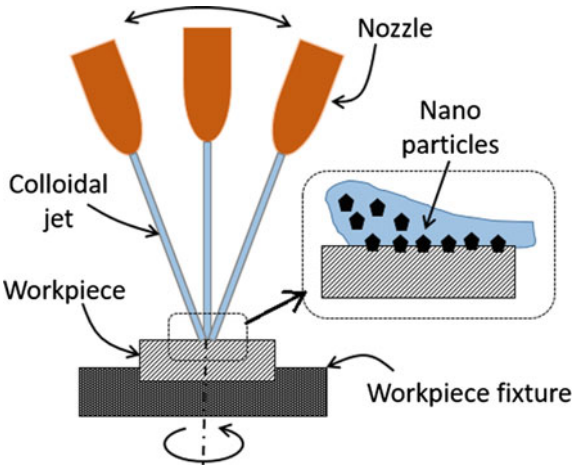

Fig. 9 Schematic of polishing concave surface in nanoparticle colloid jet machining

[94]. Nanoparticles have large surface area, high chemical activity and unsaturated chemical bonds [95]. Nanoparticles are hydroxylated completely owing to the presence of hydroxide radical (OH) in the colloid [96]. The surface, which is previously pre-finished mechanically, has some defects (dislocation, vacancies and lattice defects). The atoms which are belonging to the defect side are highly unsaturated [96]. The binding energy of the atoms at the defective side (also known as a reactive side) is lesser compared to others place [97]. The OH groups are easily adsorbed by the reactive side atoms, and complete hydroxylation is occurred. After hydroxylation, binding energy of surface atoms (E_B) is reduced and it can be expressed as follows [94]:

$$E_B = E_A - \frac{1}{2}kT \times n_{OH} \tag{4}$$

where E_A is the binding energy of the atoms of defect side before hydroxylation, k is the Boltzmann constant, T is the temperature (in K) and n_{OH} is the number of the hydroxyl group adsorbed.

Presence of OH group in both the nanoparticles as well as work surface leads to the chemical reaction between them where the binding energy of atom is lesser than reaction activation energy. The chemical reaction is a reversible polymerization, and decomposition reaction which will generate an oxo bond (N–O–W) and a H_2O molecule as follows [94]:

$$N - OH + OH - W \leftrightarrow N - O - W + H_2O \tag{5}$$

where N and W denote the nanoparticle surface atom and the work surface atom, respectively.

Thereafter, the nanoparticles along with the surface atoms are removed by the drag force of colloid jet [95]. The schematic diagram of the mechanism of material

Table 5 Literature survey of processing of different materials by NCJP

Authors	Material	Major finding
Song et al. [98]	K9 glass	• The roughness is reduced to less than 1 nm (rms) from 30 nm (rms) within 10 h • The atoms of uppermost side have more probability to be detached due to the less binding energy
Zhang et al. [93]	K9 glass	• The surface roughness is reduced to 0.519 nm (Ra) • Material removal rates of 1 nm level per minute can be obtained
Song et al. [92]	Quartz glass	• The surface roughness is achieved 0.540 nm from 3.16 nm • It has the ability to improve surface finish and microstructure
Peng et al. [96]	Silica glass	• The MRF marks are removed completely • Surface roughness is reduced to 0.41 nm from 0.72 nm • The surface figure accuracy is well maintained

removal is shown in Fig. 11 in the section of elastic emission machining (EEM). Nozzle diameters, the velocity of the jet, incident angle, pressure and impact distance are the typical process parameters.

It has the following advantages [96]:

- The very complex shape can be processed successfully, as very fine jet has the capability to reach and process each part of complex geometry.
- No tool wear as it is a non-contact process.
- Precipitation is not needed as the nanoparticles can suspend easily.

Besides, it has very low material removal rate (few nm per minute) and also the impregnation mechanism of nanoparticle and material removal mechanism is very complex. Processing of different materials by NCJM and major finding of the reported works are mentioned in Table 5.

2.5 Elastic Emission Machining (EEM)

Elastic emission machining is widely used for the fabrication of the optical component used in EUVL and synchrotron radiation system. It is an essential ultraprecision finishing process to obtain sub-nanometre scale surface roughness, figure accuracy and crystallographically perfect surface [99, 100]. In EEM, atomic scale material removal takes place by utilizing the chemical reaction between surface atoms and abrasive particles atoms. When two different solid materials come in contact with each other, the binding force between the two interacting surface develops owing to the releasing of surface energy [101]. Furthermore, the interface region of the surfaces may be electrically polarized owing to the local charge up induced by the presence of different types of atoms electron states. As a consequence, the top work surface atoms are in a different situation than the atoms of the underlying layer (bulk material). Hence, surface atoms can be removed easily by some external means (abrasive particles) [102].

In EEM, ultrafine abrasive particle (SiO_2, ZrO_2, etc., with a diameter less than 1 μm) which is chemically active to the work surface is mixed with ultrapure water uniformly. The mixture is transported to the work surface. Generally, two methods are used for generating the slurry flow: one is rotating sphere [102] and other is nozzle jet [103]. Figure 10a shows the schematic diagram of numerically controlled EEM machine with rotating the spherical head. A polyurethane sphere is coupled with a variable-speed motor to achieve a different rotational speed of the sphere. Polyurethane is selected as the sphere material due to its elasticity and stability to water. The close-up view of finishing zone is shown in Fig. 10b where ultrafine abrasive particles are dragged to flow over the surface by rotating the polyurethane sphere with a little normal load [101]. Thereafter, the abrasive particles interact with the surface to remove the material at atomic level [104] and the same can be postulated using molecular dynamic simulation as shown in Fig. 10c.

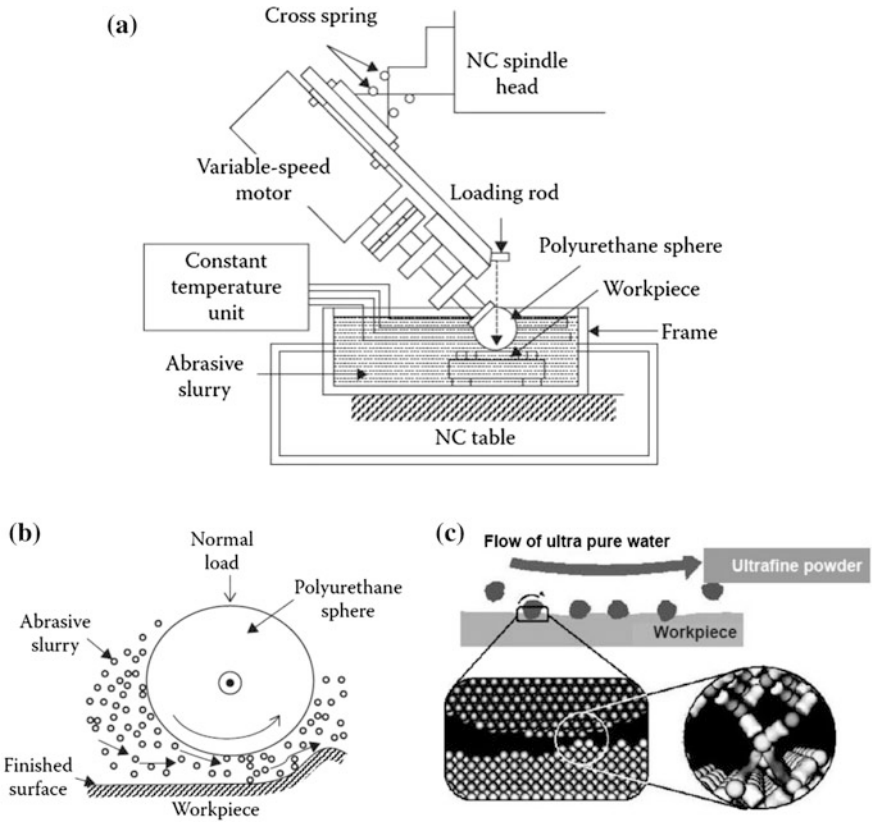

Fig. 10 **a** Schematic diagram of EEM machine with rotating spherical head [101], **b** schematic of close-up view of finishing zone [101], **c** atomic interaction between the abrasive particle and workpiece surface [19]

The probable steps of atomic removal mechanism in EEM are shown in Fig. 11. The atoms of both workpiece and powder particle are hydroxylated in the presence of water (Fig. 11a). Thereafter, both the hydroxylated atoms (workpiece and abrasive particles) come closer and bonded by the hydrogen (Fig. 11b). An interface structure is formed between workpiece atom and abrasive particle atom by polymerization and dehydration as shown in Fig. 11c. Owing to the high electronegativity of the oxygen atom of the interface structure, binding energy between the surface atoms and the atoms of the underlying layer (bulk material) decreases [105, 106]. Consequently, the surface atom can be easily removed by the flow of abrasive laden fluid. In this way, material removal takes place through the atom by atom [107]. The working area is restricted to less than 1 nm^2 [101].

Although the ultrafine abrasive particles interact with the surface with some kinetic energies, the shock of the impingement on the work surface is not aggressive as the mass of the particles is very less. Therefore, the possibility of surface defects generation due to the impact brittle fracture and scratching can be neglected [102]. The thickness of the fluid film in the working gap should be retained greater than the diameter of powder particle to avoid the possibility of surface damage (scratches and deep indentation). The film thickness varies with the concentration of powder particles, load and the rotational speed of the sphere [104].

The material removal rate is immensely low as removal takes place atom by atom. By controlling the abrasive particle characteristics like morphology, concentration, size and shape, removal rate can be improved. Agglomerated particles may be used to enhance the removal rate, as it has notable surface irregularities which increase the contact area with surface and removal rate increases, consequently [108]. The removal rate is inversely proportional to the rotational speed of the sphere, and it increases with the particle concentration up to 15% (by volume) after that rapidly decreases [104].

Figure 12 shows a nozzle-type head which is used in EEM to supply ultrafine abrasive particles to the work surface using a jet flow. It has an ability to generate a high-shear flow rate of fine abrasive particles. The size of influence function can be controlled by changing the aperture size of the nozzle. Spatial wavelength greater than 0.3 mm can be successfully figured with 1 nm (p–v) figure accuracy. Influence function is measured several times in 100 h and compared for the changes.

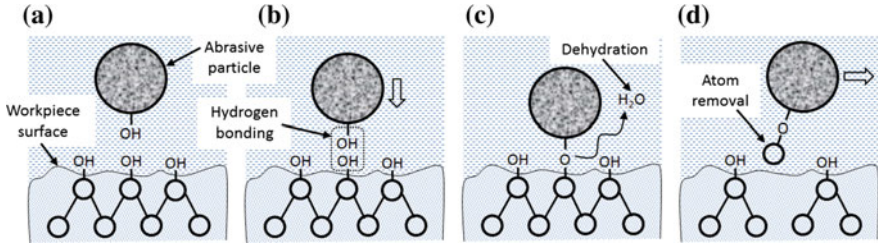

Fig. 11 Schematic explanation of the interaction between abrasive particles and workpiece surface: (**a**) before interaction, (**b**) hydrogen bonding, (**c**) dehydration and (**d**) atom removal [105]

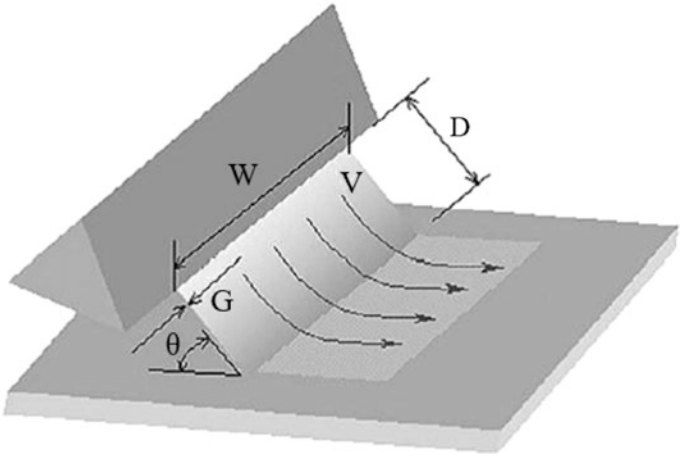

Fig. 12 Schematic of EEM process using Nozzle-type head (W = width of the slit, D = facing distance, θ = incident angle, gap of the slit, V = inlet velocity of fluid) [109]

Table 6 Literature survey of processing of different materials by EEM

Authors	Materials	Major findings
Inagaki et al. [105]	Si	• SiO_2 and ZrO_2 powders are used separately for processing the surface. The binding energy of the ZrO_2 particle is less than the SiO_2 particle. Removal rate with ZrO_2 particles is higher, consequently
Kubota et al. [109]	SiC	• Scratches on the pre-machined surface are removed completely, and 0.1 nm (rms) surface roughness is obtained • Crystallographically perfect surface with atomic level flatness can be obtained
Arima et al. [107]	Si	• 0.1 nm (rms) surface roughness is achieved • Atomic level flatness of the processed surface is observed
Kanaoka et al. [4]	ULE, Zerodur	• Surface roughness decreases with the increase of removal depth, and 0.1 nm surface roughness is accomplished after a certain removal depth • Rotating sphere head has a high temporal stability, and no degradation of surface finish is observed after 12 h of continuous processing
Kubota et al. [110]	SiC	• Surface protrusion is selectively removed with the advancement of removal depth • It is perceived that surface can be figured in the range of 0.07–10 μm spatial wavelength

However, the negligible difference is observed which proves the stability of the process over a long time usage [103]. But, the machining efficiency of nozzle head EEM is not sufficient to fabricate EUV optics. The finishing rate of rotating sphere head is 1000 times greater than the nozzle head [4]. Processing of different materials by EEM and major finding of the reported works are mentioned in Table 6.

2.6 Magnetorheological Finishing (MRF)

Magnetorheological finishing (MRF) is a deterministic ultraprecision polishing process. It becomes an integral part of optics manufacturing industries for its ability to improve the figure and surface finish of complex shape optics (spherical, aspherical and freeform lenses and mirrors) successfully without introducing any surface or subsurface damage [111]. Many different types of optical materials have been processed by MRF to the desired level of surface finish and figure for different industrial applications [19, 112]. The magnetorheological (MR) fluid used in MRF process consists of nonmagnetic abrasive particles, magnetic carbonyl iron particles (CIPs), carrier liquid and some additives or stabilizers. Figure 13 is a schematic presentation of finishing of small optics by MRF process. MR fluid is deposited over the rotating carrier wheel by a nozzle and pump arrangement [113]. When magnetic field is applied in the working gap using electromagnet or permanent magnet, MR fluid gets stiffened as its viscosity and yield stress increases substantially and behaves like a visco-plastic fluid [114]. Stiffened MR fluid ribbon proceeds towards the finishing zone by rotating carrier wheel, and it abrades the workpiece. The zone of contact is restricted to a spot due to the continuous forming of the compliant sub-aperture polishing lap which makes it suitable for finishing of a complex surface.

When MR fluid ribbon comes in contact with the workpiece, then abrasive particles get penetrated in the workpiece due to the action of the normal force (Fn) and peaks are sheared off with the help of tangential force (Ft) [115].

Figure 14 shows a schematic diagram of the general shape of influence function for the wheel type configuration of MRF set-up. The shape of influence function varies with the different configurations of the machine set-up. It is perceived that

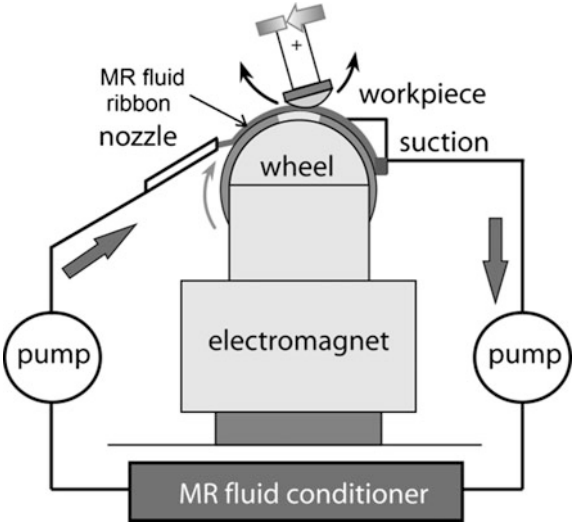

Fig. 13 Schematic representation of magnetorheological finishing

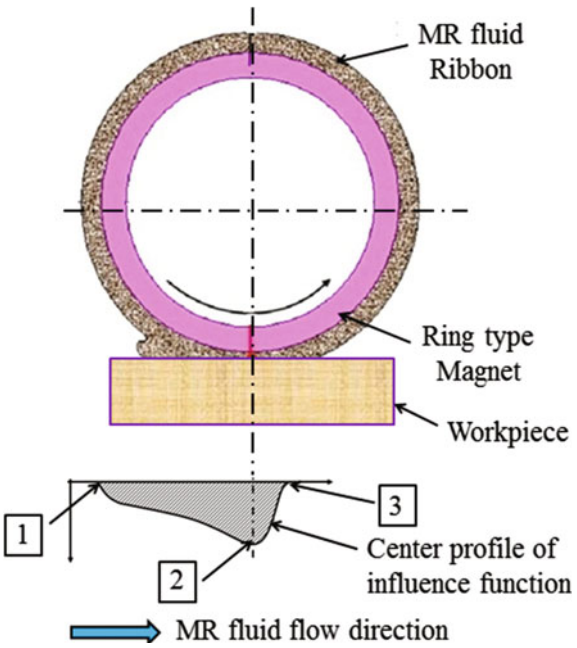

Fig. 14 Schematic diagram of centre profile of influence function for wheel type MRF set-up, **a** spot leading edge, **b** depth of deepest penetration and **c** spot trailing edge

depth of deepest penetration (ddp) is situated at the minimum working gap between the workpiece and carrier wheel, as the MR fluid is compressed utmost here (Fig. 14c). Influence function contains the information of material removal characteristics like the depth of deepest penetration, finishing area and volume of material removed [116]. High consistency of the influence function indicates lower residual surface profile-error and better quality of the finished surface. Influence function of wheel based MRF configuration depends on many parameters such as magnetic field strength, MR fluid volume on the wheel, wheel speed, workpiece penetration depth in MR fluid, duration of contact, MR fluid properties (viscosity, age, constituents, etc.) workpiece material (hardness, curvature, initial surface roughness, etc.) [117].

2.6.1 Experimentation

Figure 15 shows vertical and horizontal tool configuration of MRF process. The vertical set-up is mostly used for finishing of flat surfaces. In case of vertical set-up, permanent magnet (NdFeB, N48 grade) is used for magnetization of MR fluid. MR fluid gets stiffened and forms a flexible magnetic brush under the effect of magnetic field as shown in Fig. 15. A circular blank of single-crystal silicon (50 mm diameter and 6 mm thickness) is chosen as a workpiece material. MR fluid consists of CIPs of average particle size 1.1 μm (HQ grade from BASF, Germany), cerium oxide (CeO_2) as abrasive of particle size 1.1–1.8 μm (Universal Photonics Inc.,

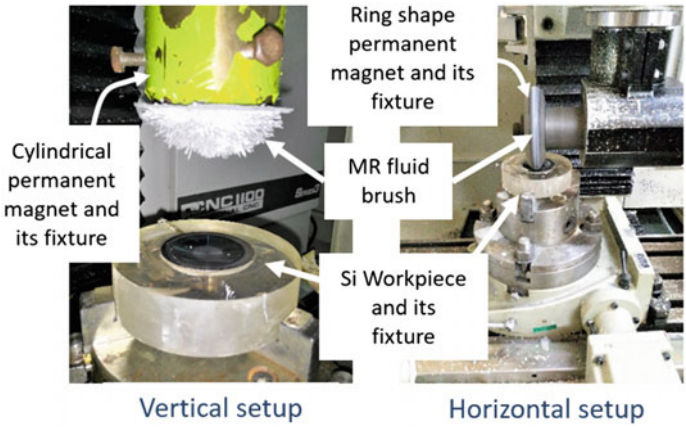

Fig. 15 Vertical and horizontal finishing tool configurations of MRF set-up

USA), glycerol as a stabilizer, sodium carbonate as a buffer (Na_2CO_3) and deionized water. Na_2CO_3 (PH near about 11) retards the corrosion of CIPs in the alkaline environment and impede the particles agglomeration by making particles charged and mutually repulsive [118].

The rotary motion to the MR polishing brush is provided by the vertical spindle. In the first stage of the experiment, to-and-fro tool motion has been employed and that motion system controls the feed rate in the x-direction shown in Fig. 16. In the second stage of the experiment, the motion of the tool used is zigzag. In to-and-fro motion, straight distance traversed by the MR finishing tool is 80 mm. The same straight distance is travelled by the tool in case of zigzag path. However, due to the zigzag tool path, total distance travel by tool is more as compared to to-and-fro tool path. The MR finishing tool diameter (60 mm) is larger than the work piece diameter (50 mm), during finishing MR finishing tool comes in contact with the workpiece surface.

The surface topography of the workpiece before and after finishing is analysed by 3D non-contact profilometer (CCI MP, Taylor Hobson, UK). The surface roughness (Sa) of silicon is reduced to 10.5 nm from 1.8 µm within 160 min using to-and-fro tool motion. Using zigzag tool motion, 4.84 nm (Sa) is achieved from initial Sa of 2.26 µm within 248 min. Using 3D, 2D surface profiles and actual photographs of unfinished and finished by zigzag path are shown in Fig. 17. Low surface roughness is achieved in case of the zigzig path due to more interaction time between the tool and the work piece.

Horizontal configuration of the tool can be used for flat as well as concave, convex and freeform surfaces depending on the diameter of the carrier wheel. Carrier wheel consists of a ring-shaped permanent magnet, and magnet fixture is mounted on the in-house designed horizontal head of the machine as shown in Fig. 15. Sintered Nd–Fe–B ring-shaped permanent magnet (N42 grade, outer diameter = 100 mm, thickness = 8 mm) is used for magnetization of the MR fluid,

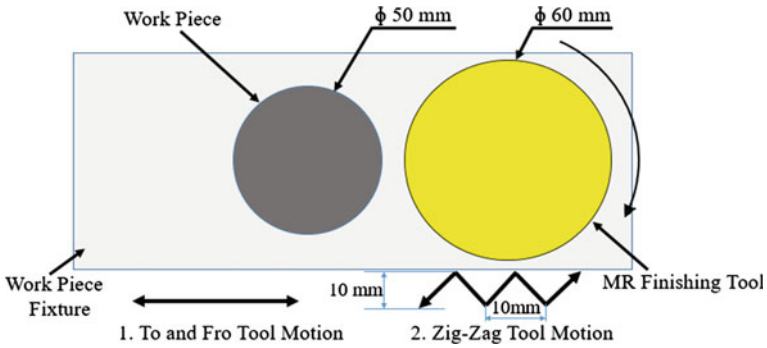

Fig. 16 Schematic diagram of the MRF vertical process set-up (top view) showing different tool paths

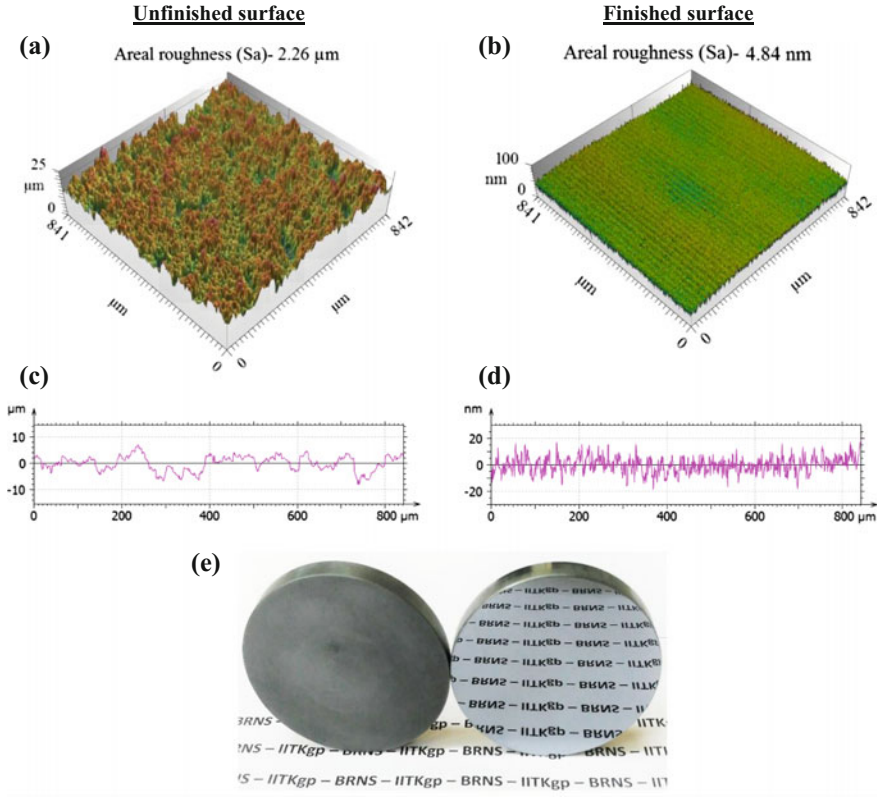

Fig. 17 Comparison of unfinished and finished surface of silicon by (**a**–**b**) 3D and (**c**–**d**) 2D topography and (**e**) actual photograph

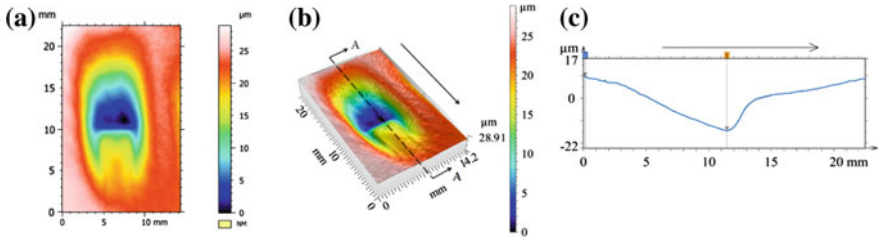

Fig. 18 (**a**) 2D topography, (**b**) 3D topography of the influence function, (**c**) 2D surface profiles through the deepest penetration (along the cross section A–A), arrow (**b**) indicates the direction of MR fluid ribbon motion

which has maximum energy product (BHmax) of 40–43 MGOe. MR fluid is deposited on the rotating carrier wheel, and it forms a ribbon-like compliant finishing tool as shown in Fig. 15. The width and height of the ribbon are 8.5 and 2 mm, respectively. The MR fluid ribbon is dragged into the finishing zone by the rotating carrier wheel, and it interacts with the workpiece and material removal takes place. It is observed by the previous researchers [36] that the quality of MR fluid (in terms of yield stress and viscosity) deteriorates with time. Hence, MR fluid is removed from the carrier wheel after each cycle and fresh MR fluid is loaded (approximately 35–40 gm) for the next experiment. A circular blank of single-crystal silicon (Ø50.8 × 6 mm) is chosen as a workpiece material. No feed is given to the tool or workpiece for influence function experiments, and dwell time is fixed as 10 min.

The surface profile of the influence functions is analysed for calculating the material removal rate and depth of deepest penetration using 3D non-contact profilometer. Figure 18a, b shows the 2D and 3D topography of influence function. The direction of MR fluid ribbon motion is indicated by the direction of the arrow. To find the depth of deepest penetration for each influence function, the 2D profile is extracted along the cross section A–A as shown in Fig. 18c. The information obtained by the influence function is important to calculate dwell time and subsequently material removal for finishing of the whole workpiece precisely.

3 Summary

Some of the well-known processes for optical fabrication such as ion beam figuring, elastic emission machining, nanoparticle colloid jet machining and magnetorheological finishing have been described in this chapter. Superfine surface finish and high figure accuracy are the prime requirements for the commercial applications of optical materials. Therefore, aforementioned processes which do not apply very aggressive force during finishing are more acceptable for optical fabrication. These processes are comparatively slower than the conventional finishing processes like

grinding and lapping but produce much better finish and figuring accuracy than them. It is also observed that more than one process are mostly required to achieve the desired surface roughness and figure accuracy, as the single process is not capable to match the required specifications. An experimental study based on finishing of the silicon surface by MRF process where an areal roughness of 4.84 nm is achieved and has been reported. This chapter hopes to facilitate researchers and engineers working in the field of optical fabrication and encourages further research and development in the field.

Acknowledgements The funding support from IIT Kharagpur under ISIRD grant and Board of Research in Nuclear Sciences (BRNS), Bombay is acknowledged.

References

1. Peng W, Guan C, Li S (2013) Ultrasmooth surface polishing based on the hydrodynamic effect. Appl Opt 52(25):6411–6416
2. Zhang SJ, To S, Zhu ZW, Zhang GQ (2015) A review of surface roughness generation in ultra-precision machining. Int J Mach Tools Manuf 91:76–95
3. Li Y, Wu Y, Wang J, Yang W, Guo Y, Xu Q (2012) Tentative investigation towards precision polishing of optical components with ultrasonically vibrating bound-abrasive pellets. Opt Express 20:568–575
4. Dinger U, Seitz G, Schulte S, Eisert F, Muenster C, Burkart S, Stacklies S, Bustaus C, Hoefer H, Mayer M, Fellner B (2004) Fabrication and metrology of diffraction limited soft x-ray optics for the EUV microlithography. In: Optical science and technology, SPIE's 48th annual meeting. International Society for Optics and Photonics, pp 18–28
5. Schindler A, Haensel T, Nickel A, Thomas HJ, Lammert H, Siewert F (2004) Finishing procedure for high-performance synchrotron optics. In: Optical science and technology, SPIE's 48th annual meeting. International Society for Optics and Photonics, pp 64–72
6. Faehnle OW, Brug HH (1999) Novel approaches to generate aspherical optical surfaces. Optical manufacturing and testing III. Proc SPIE 3782: 170–180
7. Shi F, Shu Y, Dai Y, Peng X, Li S (2013) Magnetorheological elastic super-smooth finishing for high-efficiency manufacturing of ultraviolet laser resistant optics. Opt Eng 52: 075104-075104
8. Sanger GM (1987) The precision machining of optics. In: Shannon RR, Wyant JC (eds) Applied optics and optical engineering. Academic Press, Cambridge
9. Dumas P, Golini D, Tricard M (2005) Improvement of figure and finish of diamond turned surfaces with magneto-rheological finishing (MRF). Proc SPIE 5786:296–304
10. https://www.zygo.com/?/opt/opticalmaterials/
11. http://seso.com/portfolio/polishing/
12. Kanaoka M, Liu C, Nomura K, Ando M, Takino H, Fukuda Y (2007) Figuring and smoothing capabilities of elastic emission machining for low-thermal-expansion glass optics. J Vac Sci Technol, B 25:2110–2113
13. Khounsary A, Fernandez P, Assoufid L, Mills D, Walters D, Schwartz J, Robichaud J (2002) Design, fabrication, and evaluation of an internally cooled silicon carbide mirror. Rev Sci Instrum 73(3):1537–1540
14. https://www.zeiss.com/content/dam/smt/downloads/products_and_solutions/optic_systems/ENsynchrotron.pdf
15. https://goochandhousego.com/product-categories/precision-optics

16. http://www.standaphotonics.com/off-axis-mirrors/synchrotron-radiation-and-extra-uv-mirrors.php
17. Zimmerman J (1990) Computer-controlled optical surfacing for off-axis aspheric mirrors. In: Astronomy'90, Tucson AZ, 11–16 Feb 90 1990 Jul 1, International Society for Optics and Photonics, pp 663–668
18. Pollicove H, Golini D (2002) Computer numerically controlled optics fabrication. In: Guenther AH (ed) SPIE PM119: International trends in applied optics
19. Mori Y, Yamamura K, Endo K, Yamauchi K, Yasutake K, Gotob H, Kakiuchi H, Sano Y, Mimur H (2005) Creation of perfect surfaces. J Cryst Growth 275:39–50
20. Baker PC, Brown NJ (1978) Polishing single-point diamond-turned metal reflective optics. Opt Eng 17:595–601
21. Brehm R, van Dun K, Teunissen JCG, Haisma J (1979) Transparent single-point turning of optical glass. 1(4): 207–213
22. Lambropoulos JC, Fang T, Funkenbusch PD, Jacobs SD, Cumbo MJ, Golini D (1996) Surface microroughness of optical glasses under deterministic microgrinding. Appl Opt 35:4448–4462
23. Lee ES, Baek SY (2007) A study on optimum grinding factors for aspheric convex surface micro-lens using design of experiments. Int J Mach Tools Manuf 47:509–520
24. Golini D, Kordonski WI, Dumas P, Hogan S (1999) Magnetorheological finishing (MRF) in commercial precision optics manufacturing. Proc SPIE 3782:80–91
25. Gailly P, Collette JP, Renson LF, Tock JP (1999) Ion beam figuring of small BK7 and Zerodur optics: thermal effects. Proc SPIE 3739:124–131
26. Demmler M, Zeuner M, Allenstein F, Dunger T, Nestler M, Kiontke S (2010) Ion beam figuring (IBF) for high precision optics. Proc SPIE 7591:75910Y
27. Zhou L, Audurier V, Pirouz P, Powell JA (1994) Chemomechanical polishing of silicon carbide. J Electron Soc 144:L161–L163
28. Aida H, Doi T, Takeda H, Katakura H, Kim SW, Koyama K, Yamazaki T, Uneda M (2011) Ultraprecision CMP for sapphire, GaN, and SiC for advanced optoelectronics materials. Curr Appl Phys 12:S41–S46
29. Mori Y, Yamauchi Y, Yamamura K, Mimura H, Saito A, Kishimoto H, Sekito Y, Kanaoka M, Souvorov A, Yabashi M, Tamasaku K, Ishikawa T (2001) Development of plasma chemical vaporization machining and elastic emission machining systems for coherent x-ray optics. Proc SPIE 4501
30. Su YT, Wang SY, Chao PY, Hwang YD, Hsiau JS (1995) Investigation of elastic emission machining process: lubrication effects. Precis Eng 17(3):164–172
31. Kim JD (2002) Motion analysis of powder particles in EEM using cylindrical polyurethane wheel. Int J Mach Tools Manuf 42(1):21–28
32. Song XZ, Zhang Y, Zhang FH (2012) Ultra-precision shaping and ultra-smooth polishing investigation of high-purity quartz glass in nanoparticle colloid jet machining. Adv Mater Res 426:396–399
33. Xie DG, Gao B, Yao YX, Yuan ZJ (2006) Study of local material removal model of bonnet tool polishing. Key Eng Mater 304–305:335–339
34. Beaucamp A, Namba Y (2013) Super-smooth finishing of diamond turned hard X-ray molding dies by combined fluid jet and bonnet polishing. CIRP Ann Manuf Technol 62:315–318
35. Shorey AB, Kordonski W, Tricard M (2004) Magnetorheological finishing of large and lightweight optics. Proc SPIE 5533:99–107
36. Sidpara A, Jain VK (2012) Nano–level finishing of single crystal silicon blank using magnetorheological finishing process. Tribol Int 47:159–166
37. Tuell MT, Burge JH, Anderson B (2002) Aspheric optics: smoothing the ripples with semi-flexible tools. Opt Eng 41(7):1473–1474
38. Balasubramaniam R, Suri VK (2010) Diamond turn machining. In: Jain VK (ed) Introduction to micromachining. Narosa publishing, pp 3.1–3.29
39. Saito TT (1976) Diamond turning of optics. Opt Eng 15(5):431–434

40. Nakasuji T, Kodera S, Hara S, Ikawa N (1990) Diamond turning of brittle materials for optical components. CIRP Ann Manuf Technol 39:89–92
41. Rhorer RL, Evans CJ (2010) Fabrication of optics by diamond turning. Handbook of Optics. Mcgraw Hill, New York
42. Wang C, Fang Q, Chen J, Liu Y, Jin T (2016) Subsurface damage in high-speed grinding of brittle materials considering kinematic characteristics of the grinding process. Int J Adv Manuf Technol 83:937–948
43. Wang H, Chen H, Fu G, Xiao H (2016) Relationship between grinding process and the parameters of subsurface damage based on the image processing. Int J Adv Manuf Technol 83:1707–1715
44. Namba Y, Yoshida K, Yoshida H, Nakai S (1997) Ultraprecision grinding of optical materials for high-power lasers. Laser-induced damage in optical materials. Proc SPIE 3244:320–330
45. Scattergood RO, Blake N (1990) Ductile-regime machining of germanium and silicon. J Am Ceram Soc 73(4):949–957
46. Fang FZ, Liu XD, Lee LC (2003) Micro-machining of optical glasses—a review of diamond cutting glasses. Sadhana 28(5):945–955
47. Ikawa N, Donaldson RR, Komanduri R, Konig W, Aachen TH, McKeown PA, Moriwaki T, Stowers IF (1991) Ultraprecision metal cutting—the past, the present, the future. Ann CIRP 40(2):587–594
48. Brinksmeier E, Mutlugünes Y, Klocke F, Aurich JC, Shore P, Ohmori H (2010) Ultra-precision grinding. CIRP Ann Manuf Technol 59(2):652–671
49. Pollicove HM, Moore DT (1992) COM: working to move the optics industry into the 21st century. Photonics Spectra 26(5):127–134
50. Namba Y, Wada R, Unno K, Tsuboi A (1989) Ultra-precision surface grinder having a glass-ceramics spindle of zero-thermal expansion. Ann CIRP 38(1):331–334
51. Ahearne E, Byrne G (2004) Ultraprecision grinding technologies in silicon semiconductor processing. Proc Inst Mech Eng Part B J Eng Manuf 218:253–267
52. Tong S, Gracewski SM, Funkenbusch PD (2006) Measurement of the Preston coefficient of resin and bronze bond tools for deterministic microgrinding of glass. Precis Eng 30:115–122
53. Brinksmeier E, Preuss W (2012) Micro-machining. Phil Trans R Soc A 370:3973–3992
54. Zhao Q, Guo B (2015) Ultra-precision grinding of optical glasses using mono-layer nickel electroplated coarse-grained diamond wheels. Part 2: ELID assisted precision conditioning of grinding wheels. Precis Eng 39:67–78
55. Klocke F (2009) Manufacturing processes, 2nd edn. Springer, Heidelberg
56. Jackson MJ, Davim JP (2011) Machining with abrasives. Springer, New York, pp 303–343
57. Joshi SS (2012) Ultraprecision Machining (UPM). In: Encyclopedia of nanotechnology. Springer, Netherlands, pp 2789–2795
58. Huo FW, Guo DM, Kang RK, Guang FE (2012) Nanogrinding of SiC wafers with high flatness and low subsurface damage. Trans Nonferrous Met Soc China 22(12):3027–3033
59. Gatzen HH, Maetzig JC (1997) Nanogrinding. Precis Eng 21(2–3):134–139
60. Lim HS, Fathima K, Kumar AS, Rahman M (2002) A fundamental study on the mechanism of electrolytic in-process dressing (ELID) grinding. Int J Mach Tools Manuf 42(8):935–943
61. Namba Y, Abe M, Kobayashi A (1993) Ultraprecision grinding of optical glasses to produce super-smooth surfaces. CIRP Ann Manuf Technol 42:417–420
62. Bifano T, Yi Y, Kahl K (1994) Fixed abrasive grinding of CVD SiC mirrors. Precis Eng 16:109–116
63. Namba Y (1996) Ultra-precision grinding of chemically vapor deposited silicon carbide mirrors for synchrotron radiation. Proc SPIE—Int Soc Opt Eng 2856 BT:323–330
64. Burns SJ, Funkenbusch PD, Gracewski SM, Lambropoulos JC, Ruckman J (2001) Surface features and residual strains in AlON grinding. Proc SPIE 4451:165–173
65. Yin L, Vancoille EYJ, Lee LC, Huang H, Ramesh K, Liu XD (2004) High-quality grinding of polycrystalline silicon carbide spherical surfaces. Wear 256:197–207

66. Yang LX, Wang JXQ, Zhou GZ (2006) Research on deterministic precision grinding on large-scale K9 optics. In: 2nd International symposium on advanced optical manufacturing and testing technologies. International Society for Optics and Photonics, 61492G-61492G
67. Namba Y, Yoshida T, Yoshida S, Yoshida K (2007) Surfaces of calcium fluoride single crystals ground with an ultra-precision surface grinder. CIRP Ann Manuf Technol 54:503–506
68. Yin L, Huang H (2008) Brittle materials in nano-abrasive fabrication of optical mirror-surfaces. Precis Eng 32:336–341
69. Yao Z, Gu W, Li K (2012) Relationship between surface roughness and subsurface crack depth during grinding of optical glass BK7. J Mater Process Technol 212:969–976
70. Huo F, Zhao H, Zhao D (2011) Nanogrinding of silicon wafer using a novel vitrified diamond wheel. Mater Manuf Process 26:977–981
71. Zhang Z, Huo F, Wu Y, Huang H (2011) Grinding of silicon wafers using an ultrafine diamond wheel of a hybrid bond material. Int J Mach Tools Manuf 51(1):18–24
72. Dai Y, Liao W, Zhou L, Chen S, Xie X (2010) Ion beam figuring of high-slope surfaces based on figure error compensation algorithm. Appl Opt 49(34):6630–6636
73. Egert CM (1992) Roughness evolution of optical materials induced by ion-beam milling. In: San Diego'92. International Society for Optics and Photonics, pp 63–72
74. Arnold T, Böhm G, Fechner R, Meister J, Nickel A, Frost F, Hänsel T, Schindler A (2010) Ultra-precision surface finishing by ion beam and plasma jet techniques—status and outlook. Nucl Instrum Methods Phys Res Sect A 616(2): 147–156
75. Xie X, Li S (2015) Ion beam figuring technology. Handbook of manufacturing engineering and technology. Springer, London, pp 1343–1390
76. Allen LN (1995) Progress in ion figuring large optics. In: Laser-induced damage in optical materials. International Society for Optics and Photonics, pp 237–247
77. Meinel AB, Bushkin S, Loomis DA (1965) Controlled figuring of optical surfaces by energetic ionic beams. Appl Opt 4:1674
78. Kaufman HR, Reader PD, Isaacson GC (1977) Ion sources for ion machining applications. AIAA J 15(6):843–847
79. Gale AJ (1978) Ion machining of optical components. In: Optical society of America annual meeting conference proceedings
80. Wilson SR, McNeil JR (1987) Neutral ion beam figuring of large optical surface. Proc SPIE 818:320–324
81. Sigmund P (1973) A mechanism of surface micro-roughening by ion bombardment. J Mater Sci 8:1545–1553
82. Zeuner M, Kiontke S (2012) Ion beam figuring technology in optics manufacturing. Optik & Photonik 7(2):56–58
83. Gailly P, Fleury-Frenette K, Lecat JH, Collette JP, Defise JM (2008) Ion beam figuring for precision optics. SPIE Newsroom ID x2364
84. Wilson SR, Reicher DW, McNeil JR (1989) Surface figuring using neutral ion beams. In: 32nd annual technical symposium. International Society for Optics and Photonics, pp 74–81
85. Allen LN, Keim RE, Lewis TS, Ullom JR (1992) Surface error correction of a Keck 10-m telescope primary mirror segment by ion figuring. In: 8th International symposium on gas flow and chemical lasers. International Society for Optics and Photonics, pp 195–204
86. Drueding TW, Fawcett SC, Wilson SR, Bifano TG (1995) Ion beam figuring of small optical components. Opt Eng 34(12):3565–3571
87. Flamm D, Schindler A, Berger M (2003) Ion beam milling of optically polished CaF2 surfaces. Proc SPIE 5180:81–88
88. Gailly P, Collette JP, Jamar C, Fleury-Frenette K, Médart P, Stockman Y (2004) Roughness evolution of some X-UV reflective materials induced by low energy (< 1 keV) ion beam milling. Nucl Instrum Methods Phys Res Sect B: Beam Interact Mater Atoms 216:206–212
89. Weiser M (2009) Ion beam figuring for lithography optics. Nucl Instr Methods Phys Res Sect B Beam Interact Mater Atoms 267(8):1390–1393

90. Demmler M, Zeuner M, Luca A, Dunger T, Rost D, Kiontke S, Krüger M (2011) Ion beam figuring of silicon aspheres. In: SPIE OPTO. International Society for Optics and Photonics, pp 793416–793421
91. Zhang FH, Song XZ, Zhang Y, Luan DR (2009) Polishing of ultra smooth surface with nanoparticle colloid jet. Key Eng Mater 404:143–148 (Trans Tech Publications)
92. Song XZ, Zhang Y, Zhang FH (2011) Ultra-precision shaping and polishing experiments in nanoparticle colloid jet machining. Adv Mater Res 291:1759–1763 (Trans Tech Publications)
93. Zhang F, Song X, Zhang Y, Luan D (2009) Figuring of an ultra-smooth surface in nanoparticle colloid jet machining. J Micromech Microeng 19(5):054009
94. Song XZ, Zhang Y, Zhang FH (2008) Study on removal mechanism of nanoparticle colloid jet machining. Adv Mater Res 53:363–368 (Trans Tech Publications)
95. Ranjbar Z, Rastegar S (2009) The influence of surface chemistry of nano-silica on microstructure, optical and mechanical properties of the nano-silica containing clear-coats. Prog Org Coat 65(1):125–130
96. Peng W, Li S, Guan C, Shen X, Dai Y, Wang Z (2013) Improvement of magnetorheological finishing surface quality by nanoparticle jet polishing. Opt Eng 52(4):043401
97. Harrison WA (1980) Electronic structure and the properties of solids. W.H. Freeman and Company
98. Song X, Zhang Y, Zhang F, Luan D (2009) Experimental investigation on polishing of ultrasmooth surface in nanoparticle colloid jet machining. In: 4th International symposium on advanced optical manufacturing and testing technologies: advanced optical manufacturing technologies. International Society for Optics and Photonics, 72820E-72820E
99. Takei Y, Mimura H (2013) Effect of focusing flow on stationary spot machining properties in elastic emission machining. Nanoscale Res Lett 8(1):237–242
100. Sidpara A (2017) Elastic emission machining. Nanofinishing science and technology: basic and advanced finishing and polishing processes. CRC Press, Boca Raton, pp 111–132
101. Mori Y, Yamauchi K, Endo K (1987) Elastic emission machining. Precis Eng 9(3):123–128
102. Mori Y, Yamauchi K, Endo K (1988) Mechanism of atomic removal in elastic emission machining. Precis Eng 10(1): 24–28
103. Yamauchi K, Mimura H, Inagaki K, Mori Y (2002) Figuring with subnanometer-level accuracy by numerically controlled elastic emission machining. Rev Sci Instrum 73 (11):4028–4033
104. Kanaoka M, Takino H, Nomura K, Mimura H, Yamauchi K, Mori Y (2008) Factors affecting changes in removal rate of elastic emission machining. In: Proceedings of ASPE 2008 annual meeting and the twelfth ICPE. Portland, Oregon, pp 615–618
105. Inagaki K, Yamauchi K, Mimura H, Sugiyama K, Hirose K, Mori Y (2001) First-principles evaluations of machinability dependency on powder material in elastic emission machining. Mater Trans 42(11):2290–2294
106. Yamauchi K, Hirose K, Goto H, Sugiyama K, Inagaki K, Yamamura K, Sano Y, Mori Y (1999) First-principles simulations of removal process in EEM (elastic emission machining). Comput Mater Sci 14(1):232–235
107. Arima K, Kubota A, Mimura H, Inagaki K, Endo K, Mori Y, Yamauchi K (2006) Highly resolved scanning tunneling microscopy study of Si (001) surfaces flattened in aqueous environment. Surf Sci 600(15):185–188
108. Kubota A, Mimura H, Inagaki K, Mori Y, Yamauchi K (2006) Effect of particle morphology on removal rate and surface topography in elastic emission machining. J Electrochem Soc 153(9):G874–G878
109. Kubota A, Mimura H, Inagaki K, Arima K, Mori Y, Yamauchi K (2005) Preparation of ultrasmooth and defect-free 4H-SiC (0001) surfaces by elastic emission machining. J Electron Mater 34(4):439–443
110. Kubota A, Shinbayashi Y, Mimura H, Sano Y, Inagaki K, Mori Y, Yamauchi K (2007) Investigation of the surface removal process of silicon carbide in elastic emission machining. J Electron Mater 36(1):92–97

111. Jacobs SD, Arrasmith S (1999) Overview of magnetorheological finishing (MRF) for precision optics manufacturing. Ceram Trans 102:185–199
112. Tricard M, Dumas PR, Golini D (2004) New industrial applications of magnetorheological finishing (MRF). In: Optical fabrication and testing. Optical Society of America
113. https://qedmrf.com/en/mrfpolishing/mrf-technology/how-it-works
114. Arrasmith SR, Kozhinova IA, Gregg LL, Shorey AB, Romanofsky HJ, Jacobs SD, Golini D, Kordonski WI, Hogan SJ, Dumas P (1999) Details of the polishing spot in magnetorheological finishing (MRF). Proc SPIE, 3782, Optical Manufacturing and Testing III
115. Sidpara A, Jain VK (2011) Experimental investigations into forces during magnetorheological fluid based finishing process. Int J Mach Tools Manuf 51:358–362
116. Schinhaerl M, Smith G, Geiss A, Smith L, Rascher R, Sperber P, Pitschke E, Stamp R (2007) Calculation of MRF influence functions. In: Optical Engineering + Applications, International Society for Optics and Photonics, 66710Y
117. Sidpara A, Jain VK (2017) Magnetorheological finishing. In: Jain VK (ed) Nanofinishing science and technology: basic and advanced finishing and polishing process. CRC Press, USA
118. Jacobs SD, Kordonski W, Prokhorov IV, Golini D, Gorodkin GR, Strafford DT (1998) Magnetorheological fluid composition. U.S. Patent 5,804,095

Condition Monitoring in Micro-Injection Moulding

C.A. Griffiths

Abstract This chapter looks at the condition monitoring of the micro-injection moulding process (μ-IM). This manufacturing process has been applied successfully to a wide range of products in the micro-scale and is also an appropriate technology for manufacturing meso-parts with both micro- and nano-features. Improvement in the quality and the accuracy of parts made from polymers can be successfully achieved by determining the optimum conditions for replication. Process control in manufacturing is critical, and condition monitoring of μ-IM is a control method for improved understanding of the effects of selected parameter settings. This chapter reports on the condition monitoring methods used to improve the factors that affect part's quality. For each of the examples, the Taguchi design of experiments (DOE) method is used together with demonstrations of various experimental set-ups and the acquisition of data. The chapter advises on the obtainment of information regarding the behaviour of the μ-IM and the significant factors affecting the process. The selected case studies demonstrate the condition monitoring of the cavity pressure, forces, temperature distribution and air evacuation. For each, the research findings are discussed and conclusions are made.

Keywords Micro-injection moulding · Design of experiments · Microfluidics · Cavity · Polymer

Nomenclature

ABS	Acrylonitrile Butadiene Styrene
ANOVA	Analysis of variance
D	Diameter of the runner
d	Diameter of measuring
DOE	Design of experiments
E_a	Air evacuation

C.A. Griffiths (✉)
College of Engineering, Swansea University, Swansea SA2 8PP, UK
e-mail: c.a.griffiths@swansea.ac.uk

K. Gupta (ed.), *Micro and Precision Manufacturing*, Engineering Materials,
https://doi.org/10.1007/978-3-319-68801-5_6

E_p	Pressure sensitivity
F^e_{max}	Maximum ejection force
P	Pressure
PC	Polycarbonate
P_c	Cavity pressure
P_i	Injection pressure
P_{max}	Maximum pressure
PP	Polypropylene
P_{rate}	Pressure rate
PVT	Pressure–volume–temperature
P_{work}	Pressure work
Q	Airflow rate
Q_{max}	Maximum air flow rate
SVR	Surface to volume ratio
T_b	Melt temperature
T_m	Mould temperature
t	Time
t_{max}	Maximum time
t_h	Holding pressure time
V_i	Injection speed
μ-IM	Micro-injection moulding process
η	Viscosity

1 Introduction

The trend for broadening existing part functionality with micro-features and the downscaling of existing designs has led to new micro-products entering the industrial market place. With size decreases, cost reductions can be achieved through the use of less material, energy, storage space and transport. To capitalise on this economic potential of new products, it is paramount that production systems are created to allow for the translation of micro-engineering ideas into commercial opportunities. However, downscaling requires that traditional design concepts may need to be reconsidered. The physical properties of micro-parts may be influenced by forces, pressures, speed, temperature and time in an unexpected way, and the behaviour of the parts is less understood when compared to meso-scale parts. Product miniaturisation requires the development of key technologies for producing the parts in high volumes. In particular, mass production requires the capabilities of replication techniques such as micro-injection moulding (μ-IM). μ-IM is a complex process with many control factors such as temperature, pressure and injection speed for producing quality parts. To further understand and recognise the importance of individual or combinations of process factors, an investigative analysis is required.

This chapter highlights novel condition monitoring methods for measuring the demoulding forces and cavity pressure, temperature and airflow. The understanding of the phenomena being monitored is presented, along with an experimental case study. Finally, validation and verification of the results are shown in order to demonstrate to engineers and designers the opportunities that condition monitoring provides for further understanding the behaviour of the replication process.

2 Condition Monitoring of Cavity Pressure

2.1 Understanding Cavity Pressure

During the cooling stage of the IM process, the polymers experience volume change. These variations are due to the pressure–volume–temperature (PVT) behaviour. Importantly, part shrinkage can be known using the PVT data and there is an increasing recognition that cavity pressure can be used to experimentally validate the PVT behaviour and theoretical shrinkage.

Condition monitoring of pressure in moulding is important to compensate the effects of shrinkage and confirm that pressure (P) in the cavity is maintained. The monitoring of cavity P is particularly important for thin wall parts where the high P can cause tool deformation by flexuration or compression from the polymer material. This section will investigate a cavity pressure condition monitoring system and highlight proven experiments for identifying pressure control for improved part quality. The link between part quality and cavity P has been investigated by researchers [1–7]. Condition monitoring of P in μ-IM can be used to understand the process better and by incorporating a piezoelectric transducer into the injection pin the following conditions can be identified:

- The start of injection.
- Filling of the cavity volume.
- The second stage pressure.
- P reduction during solidification.
- A drop to atmospheric pressure after part demoulding.

Condition monitoring is used in μ-IM to quantify relationships between part quality and process factors. In this case study, Dynisco PCI piezoelectric force transducer with the data acquisition unit and Labview 8 software was used to investigate the P in the cavity area. The mould and the Battenfeld Microsystem 50 moulding machine had been adapted to allow for a transducer behind the measuring pin (d) (see Fig. 1). When the transducer experiences a mechanical load, there is an electrical signal which is converted into a measurable voltage using a Kistler charge amplifier. The specifications of the transducer and charge amplifier are:

- *transducer*: 0 to 10,000 N range and force sensitivity (E_f) of 4.2 pC/N;
- *amplifier*: 5000 pC measuring range and 0–10 V output.

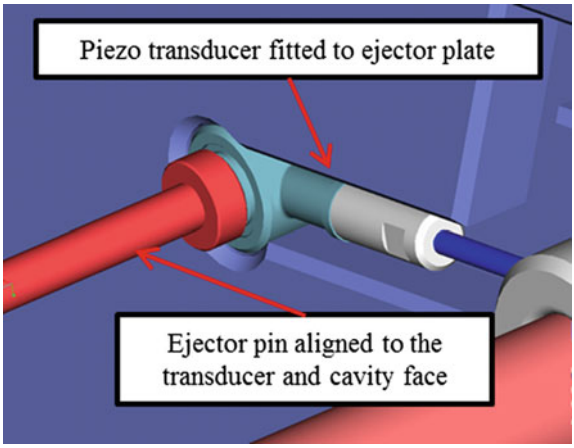

Fig. 1 Piezo sensor assembled to the mould

The output is monitored with a 16-bit module instrument. The pressure sensitivity (E_p) is expressed as follows:

$$E_p = \frac{d^2 \cdot \pi \cdot 0.1}{4} E_f. \tag{1}$$

P in MPa is calculated as follows:

$$P = \frac{\text{Output}(v) \times 500(\text{pC})}{E_p} \div 10. \tag{2}$$

In the following example, the influence of process parameters on maximum pressure (P_{max}), pressure work (P_{work}) and rate of pressure change (P_{rate}) is analysed using a condition monitoring set-up [8]. This investigation focuses on the filling during μ-IM (Fig. 2). With a large amount of recorded condition monitoring data pre-processing is required. In this way, it is possible to construct the data for further analysis. A MATLAB software tool is used to identify the key values, and a t series function provides key variables to determine the P conditions. P_{max} is measured to find the highest P value that the tool experiences. This is a maximum P that the cavity reaches at t_{max}.

$$P_{max} = P_{cavity}(t_{max}) = \max\left(P_{cavity}(t)\right). \tag{3}$$

P_{work} is calculated using P over t. This is defined as the integral value of the filling stage pressure P_{start} and ending with P_{max}. P_{work} is a P sum starting at time (t_{start}) and ending at the time of P_{max}, t_{max}. This is multiplied with a time step of Δt (0.01 s) based on the data acquisition sampling rate. Thus, P_{work} is calculated with

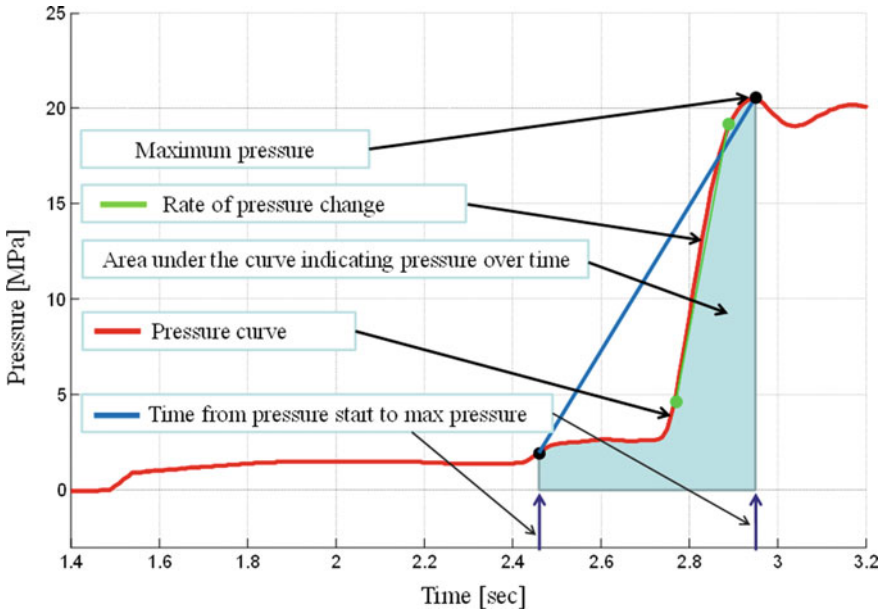

Fig. 2 Pressure during filling curve

the following equation:

$$P_{\text{work}} = \left(\sum_{t=t_{\text{start}}}^{t_{\max}} P_{\text{cavity}}(t) \right) \cdot \Delta t. \tag{4}$$

The rate of pressure change (P_{rate}) represents a gradient of the cavity pressure curve during the compression stage of the process. It starts when the cavity pressure reaches 10% above the compression threshold and the end point is determined to be at 10% below $P_{\max}$ of the pressure curve.

$$P_{\text{rate}} = \frac{0.9 \cdot P_{\max} - 1.1 \cdot P_{\text{start}}}{t_{\text{Slope\_end}} - t_{\text{Slope\_start}}}, \tag{5}$$

where 1.1 and 0.9 are constants to reduce the gradient error for P_{start}, $1.1 \cdot P_{\text{start}} = P_{\text{cavity}}(t_{\text{slope\_start}})$, and $P_{\max}$, $0.9 \cdot P_{\max} = P_{\text{cavity}}(t_{\text{slope\_end}})$, respectively.

2.2 An Experimental Case Study for Pressure Monitoring

In this study, the design of a 15 mm × 20 mm × 1 mm microfluidics part was used to analyse P in the cavity during the production of micro-parts (Fig. 3a). The

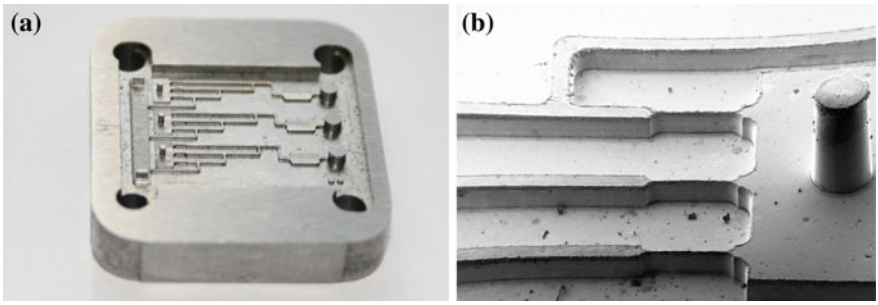

Fig. 3 **a** Mould design and **b** its microfluidics features

design has commonly microfluidics features such as reservoirs and channels. The pins are 500 μm diameter and 600 μm height, and the main channels cross section is 50–200 μm. The tool is made of brass machined by conventional and micro-milling techniques (Fig. 3b). Three commonly used moulding materials, Polypropylene (PP), Acrylonitrile Butadiene Styrene (ABS) and Polycarbonate (PC), are used for the experiments. The make of moulding machine used is Battenfeld Microsystem 50. To investigate the process influence on P, the following four factors T_b, T_m, P_h and V_i were considered, each was set at two different settings and a DOE was used to plan the experiments. The assessment would be based on the results obtained for the 50 μm channel width features and the part weight is also considered.

2.3 Validation, Verification and Results Using Pressure Monitoring

Using a Taguchi design of experiments approach and employing a L_{16} Orthogonal array, the effects on P_{max}, P_{work} and P_{rate} were studied. The average P_{max} result showed the highest P_{max} was 48 MPa when processing PC material and ABS was the lowest at 7.29 MPa. For all three materials, there was a wide distribution of results. The P_{max} normal distribution identified PC with an average pressure of 29.24 MPa, PP had 16.78 MPa and ABS was the lowest with 13.01 MPa. The distribution result also shows that process factors have more of an influence on PC compared to ABS and PP. The normal distribution for P_{work} also shows that the highest result was for PC (1267.8 MPa.s) and the lowest was for ABS (15.6 MPa.s). There is also a wide variation in the results, with the highest average recorded for PC (633.7 MPa.s) then PP (200.1 MPa.s) and ABS, (130.3 MPa.s). The results also show that the chosen control factors influence PC the most, this indicates that the choosing the correct settings for P_{work} control this material is critical. For P_{rate}, the results show that the highest and lowest recorded measurements were for PC at

1.88 MPa/s and 0.05 MPa/s, respectively. The highest average change in pressure was for PP (0.54 MPa/s) then ABS (0.50 MPa/s), and PC (0.37 MPa/s).

The results were used to identify the process effects on pressure using analysis of variance (ANOVA), in this way the influence of each parameter on P_{max}, P_{work} and P_{rate} can be known. For P_{max}, the results show that there is no specific selection of settings that is optimum for controlling the pressure for the three polymers chosen. Temperature is shown to be the most important factor, with T_m ranking high for PP and T_b being high for ABS and PC. A T_b increase results in a P_{max} decrease for ABS (32%) and PC (41%). The viscosity curves for ABS and PC show that melt temperature has an influence on the polymers so the condition monitoring results confirm this relationship. For optimisation of P_{work}, there is also no specific selection of settings for the three polymers. V_i was identified as the important factor for ABS and PC and ranked second for PP, for all three materials an increase in V_i reduces P_{work}. An increase in T_m results in an increase in P_{work} for the three materials. The influence of the parameter setting on P_{rate} was similar for each of the polymers, where an increase of T_B and V_i increase the P_{rate}. The control factors of T_m and P_h, when increased, decrease the P_{rate}. Overall T_m had the highest influence where an increase in the temperature setting reduced P_{rate}, this shows that through temperature control viscosity is maintained causing an increased rate of filling.

This case study reports on the effects of four process factors: T_b, T_m, P_h and V_i on pressure conditions in micro-cavities when replicating parts in three different polymers and employs a design of experiment approach. Three cavity pressure related factors (P_{max}, P_{work}, P_{rate}) were investigated and the research showed the following:

- It is possible to assess cavity pressure conditions during part filling by employing a specially designed condition monitoring set-up. It was shown that P_{max}, P_{work} and P_{rate} were dependent on both materials and processing conditions.
- The mean value of P_{max}, P_{work} and P_{rate} was analysed, and the results identify a clear relationship between P_{max} and P_{work}. It was shown that the mean values for each material were similar in terms of their distribution over the considered pressure range. PC had the broadest P_{max} and P_{work} distributions while PP the narrowest, thus indicating that PC is affected more by the process factors (Fig. 4). The P_{rate} distributions showed that the process factors led to a similar rate of pressure change.
- The process parameters' effects on P suggest that in context of P_{max}, P_{work} and P_{rate} there are no specific parameter levels considered to be optimum for the selected polymers. Temperature can be considered the most influential parameter for P_{max}, while V_i for P_{work}. Increasing both decreases the P.
- T_m dominates as the most influential parameter for P_{rate}. Also, it can be concluded that the parameters influence is similar for all materials, furthermore for all materials, it is shown that increasing the T_B and V_i increases the P_{rate}, and an increase of T_m and P_h decreases P_{rate}.

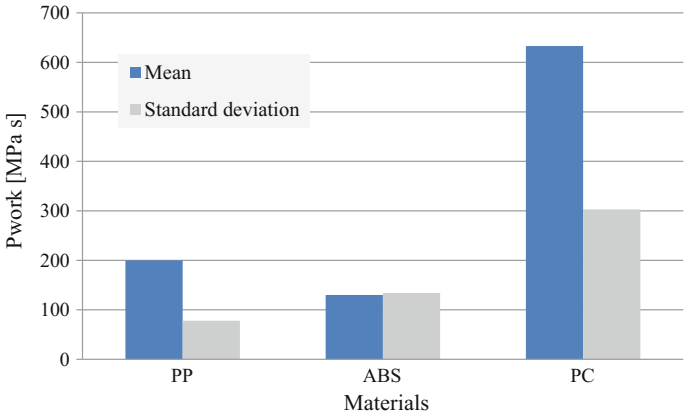

Fig. 4 Normal distribution of P_{work} results

3 Condition Monitoring of Forces

3.1 Understanding Demoulding Forces

In this section, the effect of the process on the forces in the demoulding of micro-parts is discussed and an experimental study is reported. Micro-parts have a high surface to volume ratio (SVR), and this causes fast cooling times that can result in high residual stresses in the parts [9]. After cooling the parts need to be removed from the cavity and the applied force should not be higher than the polymer material tensile yield stress [10]. The part-mould forces are due to contact pressure that is increased because of the inherent shrinkage of the polymer onto the surface and the coefficients of friction at the surface [11]. Ejecting parts and the associated demoulding force (F_e) can cause part damage such as cracks and stress to the design features [12]. The higher SVR of micro-parts increases the risk of damage during demoulding, and studies on F_e have shown that surface friction, the amount of surface area and the contact pressure in this area play an important part [11]. P is known to influence part warpage [13], but it can also increase the demoulding stress [14]. The influence of temperature at ejection is also important; experimental results show that surface T influenced F_e and a decrease can be observed with an increase in T, so increasing the control factor T_m can be used to reduce F_e [15]. A critical temperature range (Tcr) has been identified as important when considering F_e for micro-structures [16]. The tool design also has an influence of force where the deformation experienced by the part is influenced by the positions and the number of pins in the mould cavity [17]. Monitoring the factors in the IM process is a method for identifying quality of the moulded parts. Therefore, it is critical to research the influence of different factors on Fe and identify processing optimisation routes to reduce the forces.

Forces experienced during moulding can cause elastic deformation of part features and this can influence part quality. To acquire the necessary information about these forces, a condition monitoring experimental set-up is demonstrated (Sect. 6.3.2). The recorded force curves are of special interest for process optimisation, and in this section, a solution for extracting the force data will be shown. This case study demonstrates a condition monitoring set-up to investigate both injection pressure (P^{i}) and cavity pressure (P^{c}) influences on the demoulding. It has been shown in the previous section that P can be measured by integrating a piezoelectric transducer behind the injection pin. This study also used a second transducer integrated behind the ejector pin where P^{i}_{max} and P^{c}_{max} are used to obtain the highest P value that the tool experiences. The pressure work (P^{i}_{work} and P^{c}_{work}) is calculated using P over t during filling. The P curve is defined with values, corresponding to the data acquisition sample rate, where P_{work} starting with P at t_{start} and ending with the mould opening time ($t_{mould\_opening}$), multiplied with the time step of Δt (0.001 s) based on the sample rate of the data acquisition. Thus, the P^{i}_{work} is calculated as follows:

$$P^{i}_{work} = \left(\sum_{t=t_{start}}^{t_{mould\_opening}} P^{i}(t) \right) \cdot \Delta t. \tag{6}$$

P during demoulding, (Fig. 5), is used to calculate F^{e} (Fig. 6). Here, the focus is on maximum ejection force (F^{e}_{max}) that parts can experience calculated using the following equation:

$$F^{e}_{max} = F^{e}(t^{e}_{max}) = \max(F^{e}(t)). \tag{7}$$

P^{i} is indirectly measured using a piezoelectric transducer behind the injection pin, and P^{c} was measured using different transducer behind the ejector pin (Fig. 1). The mould tool was modified to allow the measuring ejector pin at the centre of the insert, and the transducer is positioned on the ejector assembly. When the ejector pushes the part from the cavity, the transducer is subjected to a load that generates an electric power. The power is then converted by a ICAM Type 5073A Industrial Charge Amplifier. The sensor signals are then downloaded to a data acquisition unit and ready for accessed using Labview 8 software.

3.2 An Experimental Case Study for Force Monitoring

A microfluidics part used for smart diagnostic chips is used for this study [18]. The system design has a microfluidics channel system and sections for the application of biosensors for disease detection. The dimensions of the chip are 10 mm in diameter and 1 mm thickness, and the main channels are 50 μm in width with a depth of 80 μm. The mould insert shown in Fig. 7 is made of steel and the polymer material

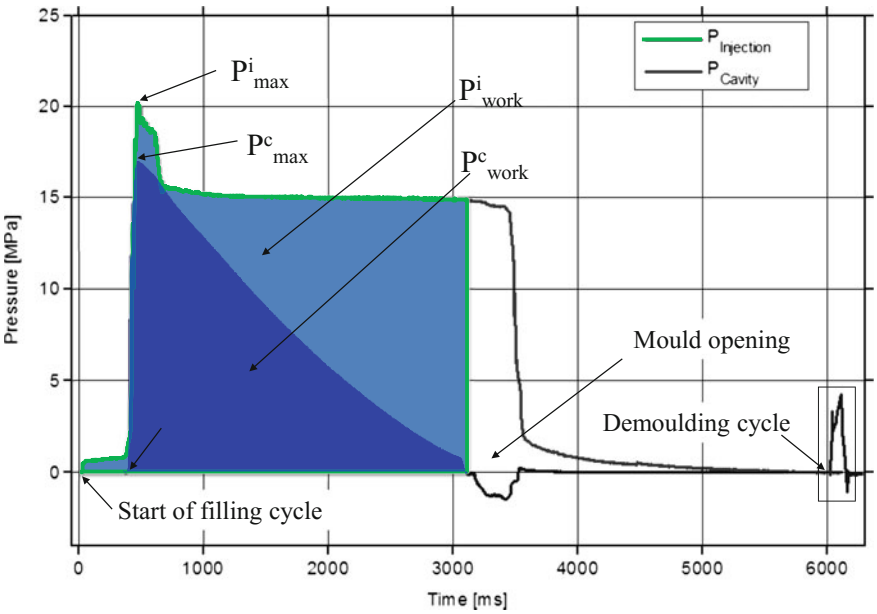

Fig. 5 Injection pressure, cavity pressure and demoulding curves

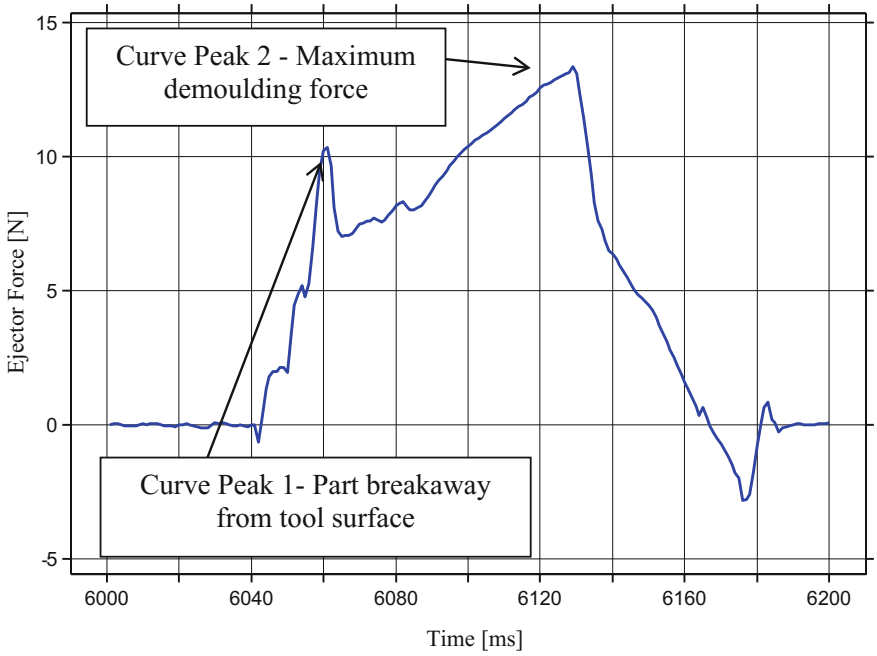

Fig. 6 Enlarged force curve from the demoulding cycle in Fig. 5

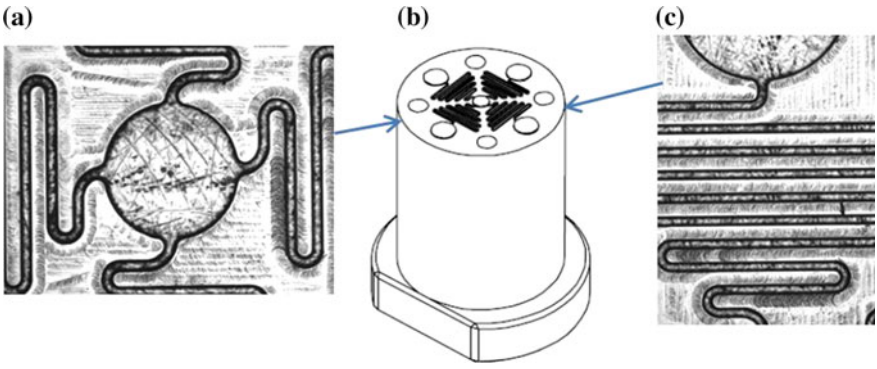

Fig. 7 **a** Microfluidics central inlet **b** Mould insert **c** microfluidics rib features

used is Topas cyclic olefin copolymers (COC) 5013. A L_{16} Taguchi DOE is used to plan experiments where the effects of T_b, T_m, P_h and V_i were investigated at two levels and the response variables measured were F^e_{max}, P^i_{max}, P^i_{work} P^c_{max} and P^c_{work}.

3.3 Validation, Verification and Results Using Force Monitoring

In this case study also a Taguchi design of experiments approach was adopted. For each trial, the effects of the four selected process factors on F^e were investigated. For the 160 experiments, the mean F^e_{max} was 21.5 N, and the highest and lowest recorded F^e_{max} were 26.3 and 8.7 N, respectively. The results for the control factors and their selected levels show that they have a varying influence on F^e_{max} and pressure. This is identified by the difference in the results for experiments 1–16, with some experiments showing significant variations. The variation in F^e_{max} can be explained with changes in process conditions especially those due to P_h and V_i. For these two factors, the high settings cause a high F^e_{max}. It is also observed that a high V_i with high P^h leads to high F^e_{max} measurements. The high V_i and P_h settings result in the highest peaks for both F^e_{max} and pressure. A correlation between the pressure and F^e_{max} results is observed through measurement and this result from condition monitoring shows the dynamics nature of the process and the differing state of the polymer during processing.

In order to analyse the significance of the process parameters affecting F^e, an ANOVA was performed based on the results of the study. The P_h was found to be most significantly contributed (20.9%) and increase in its value causes in an increase of F^e_{max}. V_i settings provide the lowest effect (2.7%) meaning that a high or low setting has little influence compared to P_h. The main effects of the parameters on F^e_{max} show that force is influenced mainly by P_h but also that F^e_{max} increases as

T_m is increased. The packing pressure factor associated with P_h compresses the polymer in the cavity and this pressure is only released after ejection making demoulding increasingly difficult. A further interaction analysis was used to look at the relationships between one or more control factors. It was shown that P_h and V_i interactions had a high influence F^e_{max}, and that interactions between T_m and V_i had a low influence F^e_{max}. For optimum parameters levels, it was possible to identify the best settings in respect to controlling F^e using the selected μ-IM parameters. In this case, the best condition for part quality is when F^e_{max} is at its lowest. It is observed that the lowest F^e_{max} values can be obtained by the low settings of the process parameters. The only factor that did not follow this observation was V_i where the high settings caused lower force values.

This case study reports on the effects of injection and cavity pressures on demoulding conditions that influence the ejection of the parts from the mould. The following conclusion can be drawn:

- It was identified that P_{max}, P_{work} and F^e_{max} were dependent on the processing conditions and the demoulding force behaviour can be analysed easily by monitoring P.
- The study showed a direct correlation exists between the P and the demoulding force (Fig. 8). The F^e_{max}, P_{max} and P_{work} interval plots showed significant variations between the experiments. These variations are due to the two different P_h and V_i settings, with the high levels providing an increase of P and F^e_{max}. The P^i_{work} response is closest to the F^e_{max} response.
- A correlation between the process and the force experienced during demoulding is observed and it is possible to identify factors with a significant (Table 1). P^i_{max} variations are attributed to P_h with high settings providing a high P.
- Process setting influence on P and F^e_{max} show that T_b was the most important factor for P^c_{max} and P^c_{work}, P_h was important for F^e_{max} and P^i_{work} and V_i was for P^i_{max}. For each factor increased settings resulted in a P increase.
- The high influence of P_h shows that the holding phase is critical for filling. A trade-off between P_h and demoulding is thus important when considering part damage.

4 Condition Monitoring of Temperature

4.1 Understanding Cavity Temperature

In injection moulding, it is critical to completely fill the parts if a multi-impression cavity is used, and to do this a high melt temperature (T_b) and mould temperature (T_m) needs to be maintained [19]. For moulding of micro-components, it has been found that filling was influenced mostly by T_m and injection speed (V_i) [20]. During filling a frozen layer forms at the walls of the mould and this affects the polymer

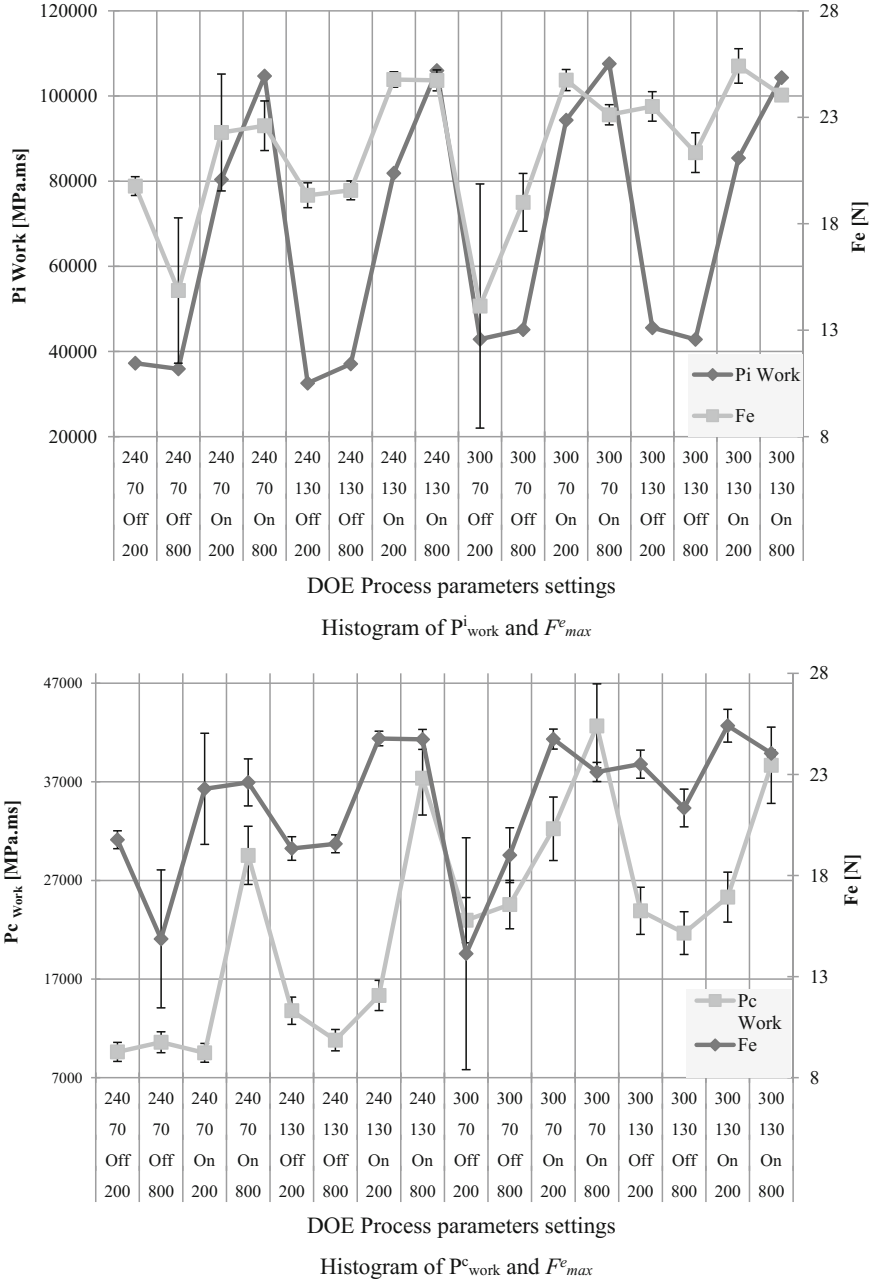

Fig. 8 Histogram of P_{work} and F^{e}_{max} results

Table 1 Response table for F^{e}_{max}, P_{max} and P_{work}

F^{e}_{max} results				
Factor	T_b (°C)	T_m (°C)	P_h (±)	V_i (mm/s)
DOE level 1 [N]	20.99	20.07	18.94	21.75
DOE level 2 [N]	21.91	22.84	23.97	21.16
Importance	3	2	1	4
Influence [%]	4.1	12.1	20.9	2.7

flow. Subsequently, a thicker frozen layer reduces the flow of polymer melt and heat loss increases and further adding to the frozen layer volume. The flow resistance during filling can then cause pressure increases when filling multiple cavities [21]. Runners are generally required to fill multiple cavities and it is important to study the effects of different runner designs on the frozen layer thickness. One solution is to use condition monitoring to measure the maximum cavity pressure (P_{max}) during filling [22, 23]. Runner systems for meso-scale components consider the relationship between the part size and weight. The main runner diameter is an important variable for controlling the heat loss [24] and several cross-sectional shapes can also be considered. Some designs have increased heat loss at the walls and use more material volume when compared to circular cross-sectional designs, and for this reason circular geometry is the most efficient [11, 25]. Another option for avoiding runner heat loss is to increase the temperature. However, high temperature settings also mean additional time is required to cool down the polymer to a sufficient ejection temperature [26].

In multi-cavity mould tools, simultaneous filling is essential in order to replicate all features. The mould and polymer temperatures in the cavity are often unknown. Therefore, to ensure the selected temperatures are optimum for filling and cooling cycles, a condition monitoring system can be applied. In this section, a state-of-the-art of cavity condition monitoring for identifying temperature variation during the moulding filling cycle is shown. The case study investigation will provide an experimental procedure for recording temperature readings directly from the runner area of a mould tool. The temperature readings are taken at the entry and end of the runner, where the difference signifies thermal efficiency. The purpose of the runner systems is to fill all of the cavities simultaneously at the same pressure and temperature without a drop in the melt temperature (T_b) [27]. Other than cyclic iso-thermal temperature changes the runner temperature is the same as T_m. When designing runner systems the selected polymer viscosity (η) change due to heat loss is critical. The heat loss in the material starts at the runner walls where a vitrified layer of polymer becomes an insulator to the polymer at the flow core. The chosen T_b must be maintained for the cavity to be filled completely. For micro-moulding, the SV_R of the runner should be a consideration and this is due to the high SV_R of micro-parts having an effect on the filling behaviour [28]. As a circular geometry is the most efficient cross section, only this runner type is looked at in this case study. To monitor temperature variation, thermocouples at the tool–polymer interface have

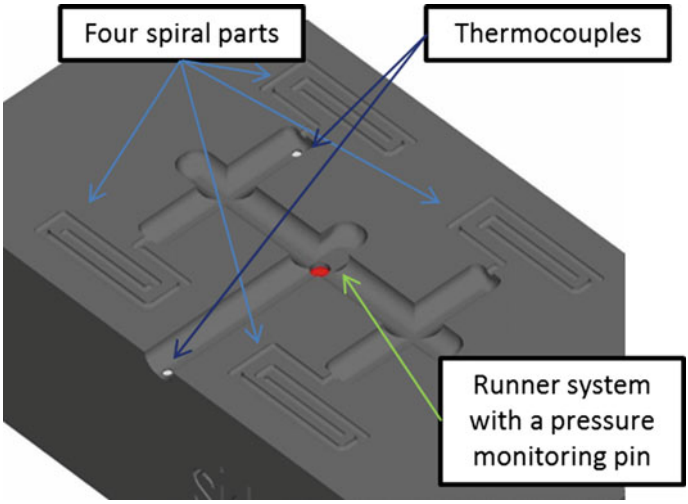

Fig. 9 Condition monitoring mould insert with a runner and 4 × spiral parts

been used in previous studies [29]. The temperature measurements were taken directly from the runner. *K* type thermocouples with 500 μm diameter were accommodated to assess the thermal efficiency of the runners (Fig. 9). Temperature measurements were taken at the entry and exit of the runners; the difference between the two identifies the efficiency of the runner. The readings are measured with a 24-bit module instrument.

4.2 An Experimental Case Study for Temperature Monitoring

A spiral with a total length of 29 mm and a cross section of 500 × 250 μm was used to investigate the runner size influence on the filling (Fig. 9) [30]. Three tools were made with four identical spiral cavities that are symmetrical in position, and the runner cross section is round with a melt overflow (Fig. 10). The diameter of the runner is in the range of 1–3 mm for the three tools. Two materials PP and ABS are chosen for the experiments and Battenfeld Microsystem 50 was used. The speed and temperature control determine the filling of micro-cavities; therefore, the effects of T_b, T_m, V_i and holding pressure time (t_h) are also considered. For each runner size and material, a Taguchi L_9 DOE is used. With three runners and two materials selected, six L_9 arrays are used and there are ten trials for each combination. For each, the temperature difference in the runner was measured.

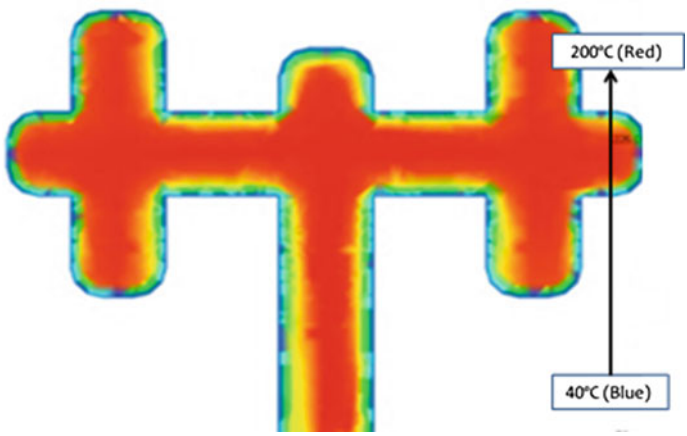

Fig. 10 3 mm runner test part cross section (40–200 °C scale)

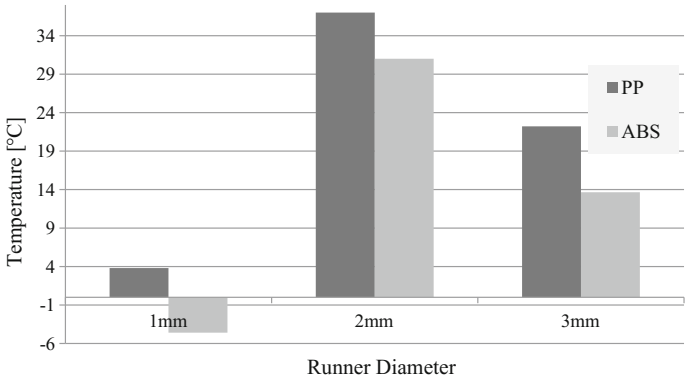

Fig. 11 The temperature changes in the runner system

4.3 Validation, Verification and Results Using Temperature Monitoring

The case study demonstrates a condition monitoring system for monitoring the change in the temperature of micro-parts in micro-cavities with a focus on the filling of parts and runner size. The following findings are derived from this research [30].

A temperature rise of the T_b was shown for each of the materials and the runner sizes, except for ABS with the 1 mm runner system (Fig. 11). The use of the 2 mm runner resulted in the highest increase of the average temperature while the 1 mm runner was the least subjected to temperature variations. For PP, the temperature variations in the runner system do not seem to affect the filling performance. Markedly, the micro-cavities were completely filled when using the 1 and 2 mm

runners yet not with the 3 mm one in spite of the significant increase of temperature compared with the 1 mm runner system. This suggests that PP is not sensitive to temperature fluctuations due to its low viscosity characteristics. On the contrary, the results for ABS suggest that the flow temperature affects the filling performance. Notably, the highest flow length was obtained when the highest temperature increase was recorded using the 2 mm runner system. In contrast, for the 1 mm runner the decrease in temperature led to the lowest flow length.

5 Condition Monitoring of Airflow

5.1 Understanding Cavity Air Evacuation

In this section, the focus will be on the factors that influence the air evacuation from the cavity during the filling stage. One condition for consistent replication results is the evacuation of air or gas from the cavity. Inadequate venting can result in air pockets trapped against the cavity walls and/or between converging flow fronts. A novel condition monitoring of airflow in the micro-cavity will be identified for the purpose of improved part quality and also the prevention of tool damage. The case study will focus on the factors that influence the air evacuation (E_a) from the cavity during filling. In μ-IM, the T settings can exceed those used in conventional IM. Distinctly, high T_b can improve the polymer flow while high T_m leads to a more uniform distribution of residual stresses in moulded parts [31]. However, high T and V_i settings can also result in uneven melt fronts, gas traps and burning of the moulded polymers [32]. Increasing T_b, T_m and V_i improves cavity filling, though in some cases the part edge definition can be compromised. One explanation is that the expanding residual air is not completely vented and therefore hinders the melt flow [19]. Liou and Chen observed residual cavities of air in sub-micron structures with high-aspect ratios [33]. Yuan et al. [28] identified that during injection when trapped air was compressed, T could increase and resulting in thermal degradation of the polymer. Ruprecht et al. [34] used E_a to prevent the burning of plastic caused by the diesel effect. In this study, $\dot{Q}$ variations in the cavity area were investigated using an airflow transducer, Omron D6F-01A1-110, as shown in Fig. 12 [35]. This gas flow sensor uses MEMS technology to accurately measure low $\dot{Q}$ over a range of T. Inside each sensor there is a MEMS flow chip that has two thermopiles on a heater element for measuring deviations in heat symmetry from passing airflow. With no $\dot{Q}$ present, the T distribution at the heater is uniform and the differential voltage of the two thermopiles is zero volts. With a $\dot{Q}$ presence, the sensor facing the source of the airflow cools and the opposite side warms thus disturbing the T equilibrium. The T difference results in a differential voltage between the thermopiles which allows $\dot{Q}$ to be calculated. A National Instruments cDAQ-9172 USB data acquisition records the signal. When the gas sensor is subjected to $\dot{Q}$, this results in an electrical output that is monitored by a National Instruments NI 9205

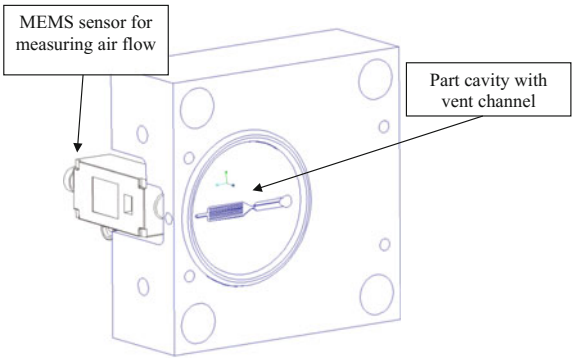

Fig. 12 Mould moving half

16-bit module. In this study, the effects of the process are analysed using a condition monitoring experimental set-up which is capable to measure the maximum flow rate, $\dot{Q}_{\max}$ [ml/s], and calculate the integral of Q [ml]. $\dot{Q}_{\max}$ is monitored in order to determine the peak $\dot{Q}$ value that the gas sensor has experienced. This value is the maximum of $\dot{Q}$ over t where $t_{\max}$ represents the time when $\dot{Q}$ in the cavity reaches its maximum.

$$\dot{Q}_{\max} = \dot{Q}(t_{\max}) = \max\left(\dot{Q}(t)\right). \tag{8}$$

The total airflow over time, Q, determines $\dot{Q}$ over the whole duration of the filling stage and is the integral of $\dot{Q}$. Resulting from the fact that the $\dot{Q}$ curve (Fig. 13) is defined by the measured discrete values, Q is the sum of $\dot{Q}$ from the start of the filing stage, t_{start}, until its completion, t_{end}, multiplied by a time step (Δt). The chosen Δt is 1 ms is determined by the sampling rate of the measuring system. Thus, Q is calculated employing the following equation:

$$Q = \left(\sum_{t=t_{\text{start}}}^{t_{\text{end}}} \dot{Q}(t) \right) \cdot \Delta t. \tag{9}$$

5.2 An Experimental Case Study for Cavity Airflow Monitoring

The test design used to analyse E_a is a 5 mm × 21 mm × 250 µm microfluidics part (Fig. 14). The part includes seven micro-channels with cross sections of 100 × 100 µm^2 and 14 mm in length. The part surface area is 226.5 mm^2, and the volume is 18.7 mm^3. ABS polymer is chosen for experiments and the machine used was a Battenfeld Microsystem 50. The mould tool uses Hasco K-standard modular system parts. To control the amount of E_a from the cavity through such a primary

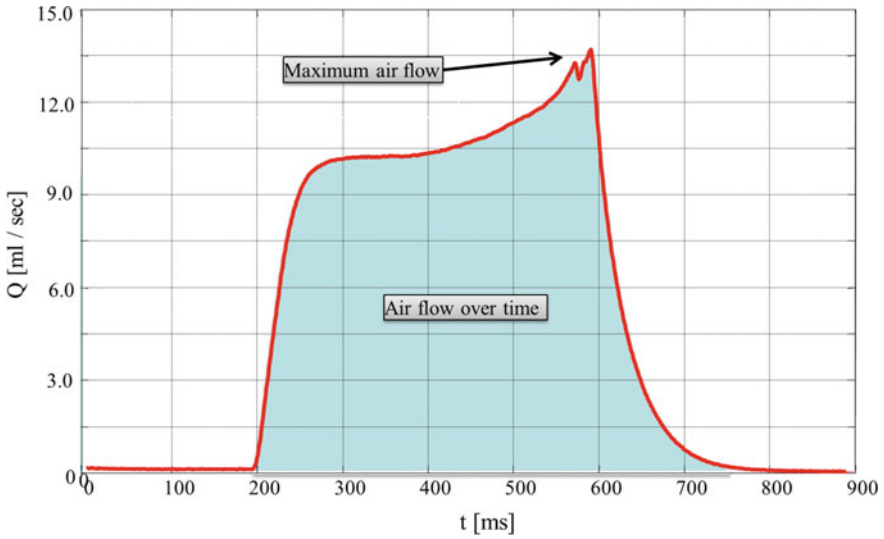

Fig. 13 Airflow over time

Fig. 14 Part design

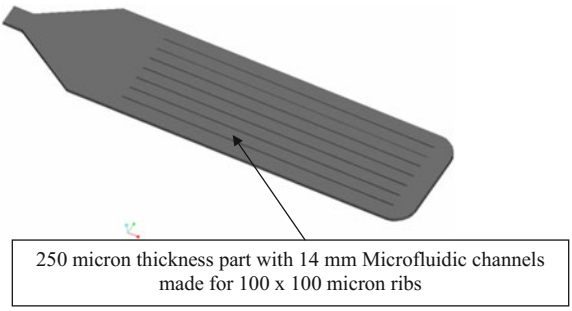

vent, a circular channel is machined to accommodate a 4 mm diameter O-ring (46 mm inside diameter). The O-ring surrounds the cavity, seals the shut off faces and restricts E_a through the primary vent. The 3 mm diameter half round runner, gate and micro-part cavity, as shown in Fig. 12, are machined on the moving half of the mould by micro-milling. At the flow path end and as far as possible from the gate, a secondary vent, 1 mm × 5 mm × 200 µm, is machined on the cavity face. This vent leads to a 1 mm diameter air relief orifice, through which E_a from the cavity is channelled to a sealed airflow transducer. This experimental set-up uses a Taguchi L_{16} orthogonal array (OA) and the response variables considered are $\dot{Q}_{max}$, Q and part flow length.

5.3 Validation, Verification and Results Using Monitoring

This case study reports on the effects of air evacuation conditions in micro-cavities when moulding. To analyse the airflow during filling, a condition monitoring system is designed and integrated into the mould cavity. The main conclusions from the research are:

- It is possible to assess air evacuation (E_a) conditions during part filling by employing a specially designed condition monitoring set-up. It was shown that maximum airflow ($\dot{Q}_{max}$) and airflow over time (Q) were dependent on the processing conditions.
- The data recorded for $\dot{Q}_{max}$ and Q shows a normal distribution of the experimental results. This indicates that the process factors significantly influence $\dot{Q}_{max}$ and Q. Regarding the flow length results, it was observed that the part length was not uniform (Fig. 16).
- The recorded $\dot{Q}_{max}$ and Q data have identified the influence of the selected factors for process control. The parameters' effects on E_a suggest that V_i can be considered as the most influential parameter (Fig. 15). In particular, an increase of V_i led to an increase of $\dot{Q}_{max}$. This suggests that the increase in the speed of the polymer entering the cavity contributes to an increase in the rate of E_a.
- The part flow length data has identified that an increased resistance to air evacuation (E_a^R) results in a lower overall flow length (Fig. 16).

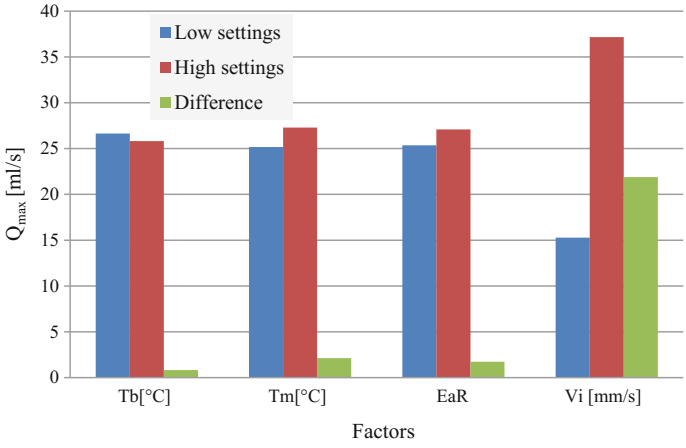

Fig. 15 Experiment results for $\dot{Q}_{max}$ showing the high influence of V_i

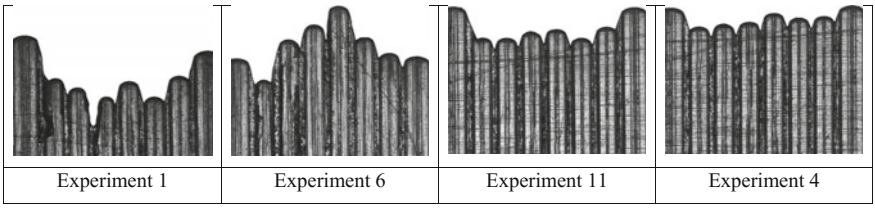

Fig. 16 Variation in the part flow length

6 Conclusions

The characteristics of manufacturing systems are mainly responsible for the development of miniaturised products. Micro-injection moulding is a cost-effective method to develop precision micro-parts in high volume. The engineering challenge tackled in this chapter is to broadening understanding of the moulding process using condition monitoring. To validate this method, four experimental condition monitoring set-ups were designed and implemented, together with a design of experiments approach. The main conclusions from the case studies are as follows:

- For monitoring of pressure conditions, it is possible to assess cavity pressure conditions during part filling by employing a specially designed condition monitoring set-up. It was shown that results were dependent on both materials and processing conditions. The similar process behaviour for all three polymers has been investigated. The significant reduction in filling has been observed with increase in injection speed and decrease in mould temperature.
- The study on the effects of injection and cavity pressures on demoulding conditions identified that pressure and force were also dependent on the processing conditions. The findings showed a direct correlation exists between the pressure and force and that by monitoring the pressure behaviour it is possible to analyse the demoulding force. In terms of the chosen settings, it is possible to identify factors with a significant influence on part quality.
- Temperature condition monitoring was used for the investigation of runner size effects together with other process factors. The results showed that polymer temperature and injection speed settings have a direct influence on the runner filling performance. A chosen runner size can affect the pressure and temperature of the polymer flow and an optimum runner surface to volume ratio can aid filling performance. Importantly, it is shown that runner selection is very important when designing micro-moulds.
- Filling of mould cavities can be improved by understanding the effects of airflow. The study showed that high process settings and poor venting significantly impact on the filling behaviour. An inability of the cavity air to vent can result in air traps that are bad for the mould and part quality, so there is a design necessity for vents and vacuum for air evacuation in μ-IM.

Condition monitoring as a means of gathering empirical data using a systematic experimental approach is invaluable to engineers who need to identify processing conditions that are difficult to predict. The chapter shows that it is possible to gather and assess complex process behaviour by developing specially designed systems for condition monitoring. In order for engineers to determine the best production routes for less well-known manufacturing processes they consider a wide range of condition monitoring approaches. It is also important for practitioners to investigate new sensor technologies and to find innovative ways of applying those to novel micro-manufacture systems for improved productivity and high precision of micro-parts.

References

1. Orzechowski S, Paris A, Dobin CJB (1998) A process monitoring and control system for injection molding using nozzle-based pressure and temperature sensors. In: Proceedings of the 1998 56th ANTEC, pp 424–428
2. Hellmeyer HO, Lixfield HD, Menges G (1977) Control of maximum pressure in the injection mould. Kunstst Ger Plast 67(4):4–6
3. Homes W, Kabus R (2001) Controlling injection moulding processes in real time. Kunstst Plast Eur 91(1):29–30
4. Kuek SC, Angstadt DC (2007) Process monitoring in micro-injection molding. In: Proceedings of the ASME international manufacturing science and engineering conference 2007, MSEC2007, Atlanta, GA
5. Michaeli W, Schreiber A (2009) Advanced process control for injection molding based on cavity pressure. In: ANTEC 2009—Proceedings of the 67th annual technical conference and exhibition, Chicago, IL, 22–24 June
6. Michaeli W, Hopmann C, Gruber J (2004) Process control in injection moulding. Kunstst Plast Eur 94(1):20–24
7. Schnerr O, Kudlik N, Michaeli W (1998) Self-adaptive closed-loop cavity pressure control for injection moulding. In: Society of plastic engineers, Proceedings of the annual technical conference—ANTEC, Atlanta, GA, vol 1, pp 410–413
8. Griffiths CA, Dimov SS, Scholz S, Tosello G (2011) Process factors influence on cavity pressure behaviour in micro-injection moulding. ASME Trans, J Manufact Sci Eng 133 (3):031007 (10 pages). doi: 10.1115/1.4003953
9. Haberstroh E, Brandt M (2002) Determination of mechanical properties of thermoplastics suitable for micro systems. Macromol Mater Eng 287(12):881–888
10. Navabpour P, Teer DG, Hitt DJ, Gilbert M (2006) Evaluation of non-stick properties of magnetron-sputtered coatings for moulds used for the processing of polymers. Surf Coat Technol 201(6):3802–3809
11. Menges G (1993) How to make injection molds. In: Menges G, Mohren P (eds) Hanser Publisher, Munich, Vienna, New York
12. Heyderman LJ, Schift H, David C, Gobrecht J, Schweizer T (2000) Flow behaviour of thin polymer films used for hot embossing lithography. Microelectron Eng 54(3–4):229–245
13. Gui DY, Ernst LJ, Jansen KMB, Yang DG, Goumans L, Bressers HJL, Janssen JHJ (2008) Effects of molding pressure on the warpage and the viscoelasticities of HVQFN packages. J Appl Polym Sci 109(3):2016–2022
14. An C-C, Chen R-H (2007) Experimental study of demolding properties on stereolithography tooling. J Manuf Sci Eng 129(4):843–848

15. Pontes AJ, Pouzada AS (2004) Ejection force in tubular injection moldings. Part I: effect of processing conditions. Polym Eng Sci 44(5):891–897
16. Fu G, Tor SB, Loh NH, Tay BY, Hardt DE (2008) The demolding of powder injection molded micro-structures: analysis, simulation and experiment. J Micromech Microeng 18 (7):075024 (12 pp)
17. Kwak S,Kim T, Park S, Lee K (2003) Layout and sizing of ejector pins for injection mould design using the wavelet transform. Proc Inst Mech Eng, Part B: J Eng Manufact 217(4):463–473
18. Griffiths CA, Dimov SS, Scholz S, Tosello G (2014) Influence of injection and cavity pressure on the demoulding force in micro-injection moulding. ASME Trans, J Manufact Sci Eng 136 (3):(10 pages). Paper No: MANU-11-1170. doi:10.1115/1.4026983
19. Sha B, Dimov S, Griffiths C, Packianather MS (2007) Investigation of micro-injection moulding: factors affecting the replication quality. J Mater Process Technol 183(2–3):284–296
20. Sha B, Dimov S, Griffiths C, Packianather MS (2007) Micro-injectionmoulding: factors affecting the achievable aspect ratios. Int J Adv Manufact Technol 33(1):147–156
21. Spina R (2004) Injection moulding of automotive components: comparison between hot runner systems for a case study. J Mater Process Technol 155–156:1497–1504
22. Coates PD, Whiteside BR, Martyn MT, Spares R, Gough T (2006) Micromoulding—precision processing for controlled products. In: Proceedings of the second international conference on multi-material micro manufacture (4 M), pp 13–15
23. Min BH (2003) A study on quality monitoring of injection molded parts. J Mater Process Technol 136(1–3):1–6
24. Yen C, Lin JC, Li W, Huang MF (2006) An abductive neural network approach to the design of runner dimensions for the minimization of warpage in injection mouldings. J Mater Process Technol 174(1–3):22–28
25. Tang SH, Kong YM, Sapuan SM, Samin R, Sulaiman S (2006) Design and thermal analysis of plastic injection mould. J Mater Process Technol 171(2):259–267
26. Zhao J, Lu X, Chen Y, Chow LK, Chen G, Zhao W, Samper V (2005) A new liquid crystalline polymer based processing aid and its effects on micro-molding process. J Mater Process Technol 168(2):308–315
27. Yen C, Lin JC, Li W, Huang MF (2006) An abductive neural network approach to the design of runner dimensions for the minimization of warpage in injection mouldings. J Mater Process Technol 174(1–3):22–28
28. Yuan S, Hung NP, Ngoi BKA, Ali MY (2003) Development of microreplication process—micromoulding. Mater Manufact Process 18(5):731–751
29. Bendada A, Derdouri A, Lamontagne M, Simard Y (2004) Analysis of thermal contact resistance between polymer and mold in injection molding. Appl Thermal Eng 24(14–15):2029–2040
30. Griffiths CA, Dimov SS, Brousseau EB (2008) Micro injection moulding: the influence of runner systems on flow behaviour and melt fill of multiple micro cavities. Proc Inst Mech Eng Part B, J Eng Manufact 222(B9):1119–1130. ISSN 0954-4054. doi:10.1243/09544054JEM1084
31. Young WB (2005) Effect of process parameters on injection compression molding of pickup lens. Appl Math Model 29(10):955–971
32. Griffiths CA, Dimov SS, Brousseau EB, Hoyle RT (2007) The effects of tool surface quality in micro-injection moulding. J Mater Process Technol 189(1–3):418–427
33. Liou AC, Chen RH (2006) Injection molding of polymer micro- and sub-micron structures with high-aspect ratios. Int J Adv Manufact Technol 28(11–12):1097–1103
34. Ruprecht R, Gietzelt T, Müller K, Piotter V, Haußelt J (2008) Injection molding of microstructured components from plastics, metals and ceramics. Microsyst Technol 8(4–5):351–358
35. Griffiths CA, Dimov SS, Scholz S, Tosello G (2011) Cavity air flow behaviour during filling in microinjection moulding. ASME Trans, J Manufact Sci Eng 133(1):011006 (10 pages). doi:10.1115/1.4003339

Surface Finish Improvement of Additive Manufactured Metal Parts

Hany Hassanin, Amr Elshaer, Redha Benhadj-Djilali, Francesco Modica and Irene Fassi

Abstract Unlike materials subtractive technologies, additive manufacturing (AM) works on producing near-net-shape components according to a specific design at which the synthesis is achieved layer by layer. Additive manufacturing allows design freedom, making design-driven manufacturing a reality. However, its poor surface quality is considered as one of the key challenges that are worth to overcome. The main objective of this chapter is to report a comprehensive overview of the techniques used to improve the surface finish and their advancements of products made by metal additive manufacturing (AM) technologies and to highlight experimental processes and data. Powder bed fusion (PBF) and direct laser deposition (DLD) are the main processes covered in this review. The chapter starts with the literature review and introduction to the main metal AM processes and their surface roughness limitations, the effect of their parameters and the effect of the laser re-melting on the surface quality. Next, it is followed by a number of surface finishing techniques such as laser polishing, chemical and electropolishing. Experimental results of post-surface finishing of AM parts by microelectrical discharge machining are also presented.

Keywords Additive manufacturing · EDM · 3D printing · Laser · Surface finish

H. Hassanin (✉) · R. Benhadj-Djilali
School of Mechanical and Automotive Engineering, Kingston University, Roehampton Vale, London SW15 3DW, UK
e-mail: h.hassanin@kingston.ac.uk

A. Elshaer
Drug Discovery, Delivery and Patient Care (DDDPC), School of Life Sciences, Pharmacy and Chemistry, Kingston University London, Penrhyn Road, Kingston upon Thames, Surrey KT1 2EE, UK

F. Modica · I. Fassi
ITIA-CNR, Institute of Industrial Technologies and Automation, Bari, Italy

K. Gupta (ed.), *Micro and Precision Manufacturing*, Engineering Materials,
https://doi.org/10.1007/978-3-319-68801-5_7

1 Introduction

Additive manufacturing (AM) is looked at as the third industrial revolution [1–3]. Unlike conventional subtractive technologies, which cut or subtract from a solid block of the material to fabricate a final part, additive manufacturing builds parts or features on a part layer by layer according to a sliced 3D CAD model. Compared to conventional manufacturing techniques, additive manufacturing offers a wide range of advantages. It allows more freedom for the computer-aided design (CAD) designers to enable design and optimise topology, hence enabling the production of near-net-shape metal parts with intricate details and eliminating the need of expensive moulds. It also offers reduced lead time to market, minimise materials waste and lower the cost. The UK technology strategy board emphasised the strategic role of AM as a game-changer for future manufacturing. It has been anticipated that it will be possible to print buildings, constructions and complete body organs in the next 25 years [4].

Recently, industries such as aerospace, biomedical and automotive have implemented additive manufacturing in their research and production plans [5–8]. The global market of additive manufacturing was about $3.7 billion by 2015, and it is estimated to continue its rapid growth to reach over $6.5 billion by 2019 [9]. Wide range of materials can be printed using additive manufacturing including metal, ceramics and polymers. Polymers are currently the most popular material for 3D printing owning to their availability and their low cost. However, AM of metals holds a great potential in both the design and the choice of materials. Several metals and alloys are particularly attractive for AM such as steels, titanium, nickel superalloys and tungsten where subtractive machining is expensive and time-consuming. However, since its development in the 1980s, AM is held back by several technical challenges including processed materials, manufacturing speed, CAD software and reliability. The poor quality of the AM surfaces is another key issue that restricts the applications of AM products. Surface finish is considered as one of the standard quality properties for mechanical products. Typically, the fatigue strength is highly affected by the surface finish due to the initiation of cracks on surfaces with poor quality. On the other hand, material strength and corrosion resistance were proved sensitive to the surface quality. The quality of products with rough surfaces can be improved by selecting a proper AM facility, together with optimising the AM process parameters and raw material, and finally applying adequate post-processing operations.

2 Metal Additive Manufacturing Techniques

Metal additive manufacturing can be classified into two main groups: powder bed fusion (PBF) and direct laser deposition (DLD). PBF is an important category of AM processes with the highest economic impact. As a result, many research works

are available for PBF than DLD metal AM processes. PBF includes selective laser melting (SLM), selective laser sintering (SLS) and electron beam melting (EBM), while DLD includes blown powder (BP) and wire feed (WF) systems. The main metal additive techniques are summarised in Fig. 1.

AM techniques require a heat source to melt or sinter the processed material that could be in a powder or a wire form. In general, the heat source melts the selected areas using the absorbed power and the velocity of the energy source, and upon cooling the melted pool, it solidifies creating a layer of the part. PBF typically uses fine powder, and therefore, the power consumption of PBF is less compared to DLD processes. The microstructural, mechanical and physical properties of the AM parts produced by either PBF or DLD are affected by many factors including the used process (SLM, EDM, BP, WF), process parameters (power, speed, rate, substrate-heating, etc.) and materials' characteristics (particle, size, morphology, etc.). Figure 2 shows the AM regimes with respect to the beam power and speed [10].

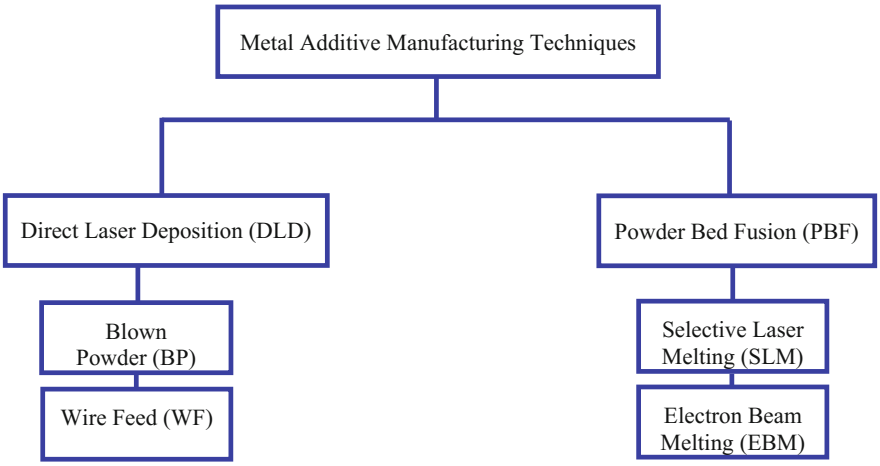

Fig. 1 Metal additive manufacturing techniques

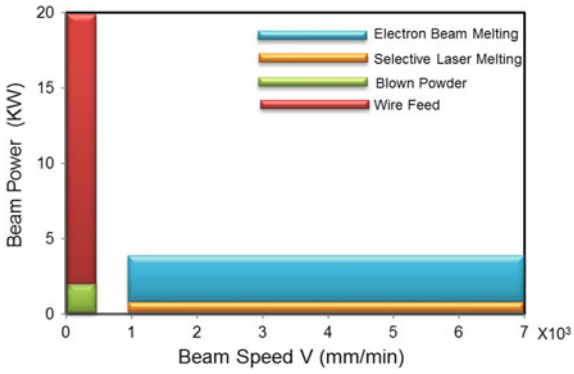

Fig. 2 Metal additive manufacturing techniques with respect to the beam power and speed [10]

PBF techniques were among the early metal AM techniques, first developed at the University of Texas. These techniques include all AM techniques that use focused energy from either a laser or electron beam to sinter or to melt a slice of metal material. In these techniques, a layer of powder is spread on to a build substrate while the electron and/or the laser beam is implemented to selectively consolidate the metal powder according to a digitalised CAD model. Then, another layer of powder is spread on to the previous layer and the process is repeated until the desired geometry is achieved [11, 12].

Selective laser melting (SLM) is one of the important PBF techniques to build near-net-shape components with complex geometries. These systems utilise laser beam as an energy source to build metal components by selectively melting layers of metal powder according to the CAD design. SLM technology offers numerous merits over the other AM techniques; besides, it can build complex-shaped components with a high degree of accuracy and resolution [13]. Electron beam melting (EBM) is another powder bed AM fusion technology. Compared to the SLM, EBM substitutes the laser beam with an electron beam as the energy source. In EBM, an electron beam can reach a velocity of up to 8000 m/s while the laser beam in SLM can achieve up to 10 m/s. In addition, vacuum conditions and a preheated substrate are required for EBM. As such, dense components can be achieved using EBM, but the process is restricted to conductive materials only [14]. Schematic diagrams of SLM and EBM processes are illustrated in Fig. 3.

Direct laser deposition (DLD) techniques allow the manufacturing of parts by deposition of the molten metals according to the CAD design. On the contrary, PBF creates selectively melted powder via laser or electron beams. DLD is achieved by simultaneously feeding a metal wire or powder into a focal point of high-energy laser. DLD is used as an AM of metal and functionally graded parts. In DLD, there is not a pre-deposited layer of powder and that is why it can be used as a method to coat or repair parts by cladding. Blown powder and wire feed systems are the two common processes for DLD [15]. In blown powder, the powder is sprayed through a nozzle under inert atmosphere gas such as argon. The powder is then melted on a focal point to create dense 3D structures or to coat the surface and/or specific feature of a part (see Fig. 4a). Blown powder is a precise process as it uses an automated robotic arm for the deposition of the metal materials with a thickness ranging from 0.1 mm to few millimetres [16, 17]. This offers the freedom in design in the production of complex structures. Moreover, the focused laser energy of blown powder process reduces the effect of the thermal effects when compared to other welding procedures. On the other hand, wire feed systems replace metal powder used in blown powder with a metal wire. The metal wire is extruded through a nozzle and melts using an energy source, typically a laser beam (see Fig. 4b). In a similar way to blown powder systems, an inert gas shielding is utilised either in an enclosed chamber or in an open environment. This process offers superior deposition rate in comparison with other AM techniques. Moreover, wire feed systems are cost-effective as they use metal wires that are cheap and more easily available than metal powders [18].

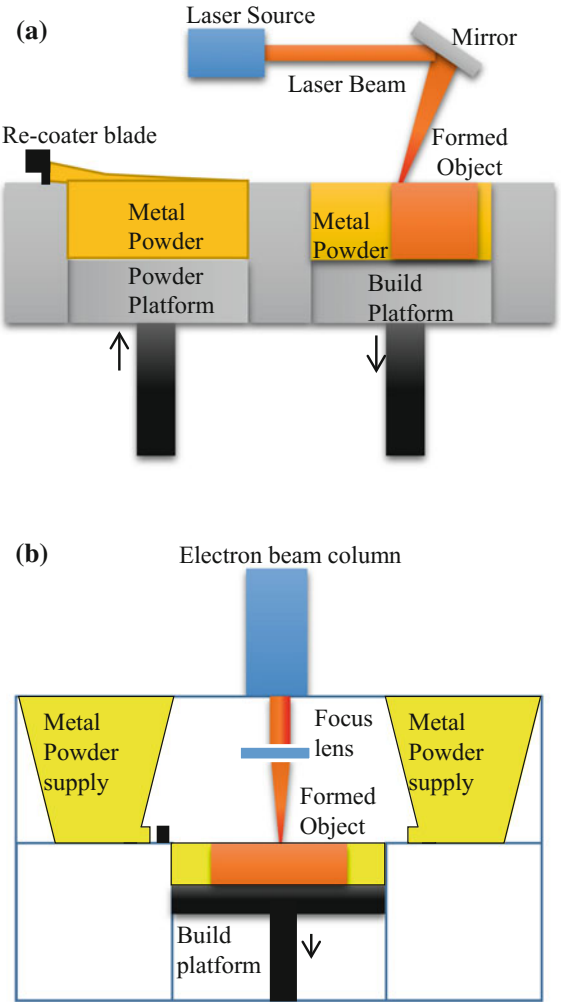

Fig. 3 Schematic of powder bed fusion systems **a** SLM system, **b** EBM system

The AM techniques as explained above can process wide range of metals, their number continues to expand as improved technologies, and optimised operation parameters emerge to cover new applications. The most popular metallic materials used for AM are titanium and titanium alloys, aluminium alloys, steels, nickel-based superalloys, steels and others. As a result of the explained AM sequences, AM parts are characterised with a directional and chaotic surface texture. The directional texture is caused by the layer-by-layer process, while the chaotic texture is caused by the partially melted powder. The directional texture is highly affected by the "stair step" or which is the layered approximation of geometries. Minimising slices' thickness can enhance the surface quality of AM metal parts. However, in most cases threshold layer thickness due to the minimum

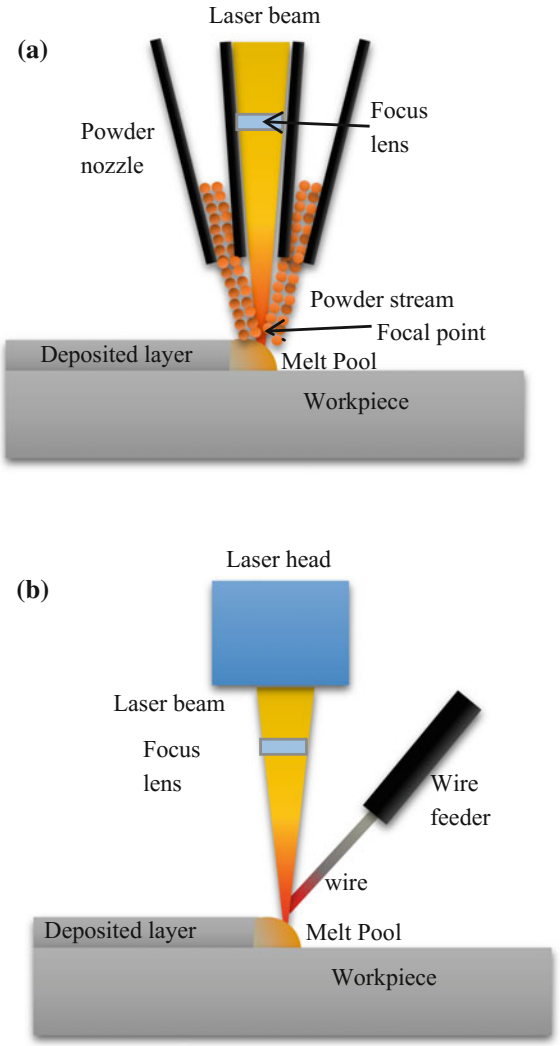

Fig. 4 Schematic of direct deposition **a** blown powder system, **b** wire feed system

Table 1 Surface roughness and materials of metal AM processes

Process	Energy/material form	Surface roughness (R_a) (μm)	Materials	References
SLM	Laser/powder	10–20	Ti, Al, Ni, Steel, W	[13, 19–30]
EBM	Electron beam/powder	10–50	Ti, Ni, Steel	[14, 31–34]
BP	Laser/powder	20–54	Ti, Ni, Steel, W	[16, 35–38]
WF	Laser/wire	200	Ti, Ni, Steel	[18, 39–41]

powder size or a technical barrier limits this approach. Therefore, various AM techniques result in different surface characteristics. The ranges of typical surface roughness generated by different metal AM processes are listed in Table 1.

3 Surface Finish Improvement Techniques for AM Parts

3.1 AM Process Optimisation

SLM process is considered the best process to give a smooth surface finish of 5–20 μm. Manufacturing on optimised SLM parameters has been implemented in order to improve surface quality. Ghanekar et al. investigated the influence of the powder layer thickness on the surface finish of SLM parts. The results showed that the stair stepping effect was minimised significantly upon using less thick powder layer [42]. Similar approach was carried out by Calignano et al. who used Taguchi statistical approach to optimise the surface roughness of AlSi10Mg parts. It was concluded that the scan speed has the dominant effect on the surface roughness. They were able to optimise the process parameters, and a significant improvement in the surface topography was obtained (see Fig. 5).

Several statistical approaches were implemented in order to evaluate the effect of the process parameters on the surface roughness of SLM parts and hence optimise the process parameters. Bacchewar studied the effect of five independent variables: speed, parts orientation, layer thickness and hatching space using central rotatable composite design (CCD) to plan the experimental work while the analysis of variance (ANOVA) and response surface were implemented to investigate the effect of AM variables on surface roughness. The authors also used the MATLAB optimisation tool box to carry out the optimisation process for minimum surface roughness. They found that build direction and the thickness of layers have the major influence on the up-facing surface characteristics. On the other hand, layer thickness, build orientation and laser power were proved to have major effect on down-facing surface roughness [44]. Moreover, Kaddar et al. studied the effect of the parts orientation on the surface roughness. It was found that SLM parts built with inclined angle range between 5° and 30° was susceptible to poor surface finish [45].

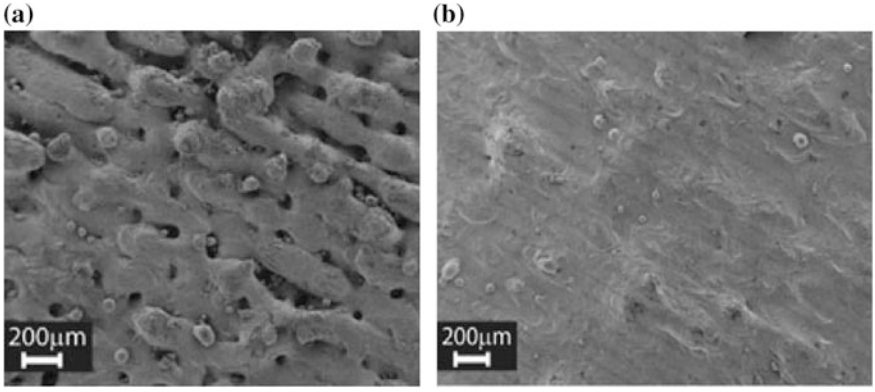

Fig. 5 SEM images of surface roughness of AlSi10Mg built **a** default parameters, **b** optimised parameters [43]

Electron beam melting (EBM) has the ability to fabricate parts with a surface roughness R_a of 10–50 μm (Table 1). Similar to SLM, researchers attempted to improve the surface roughness of EBM manufactured parts by optimising the EBM process parameters such as number of contours, contour offset, line offset and spacing between contours. In EBM, the energy of the electron beam increases as the current increases and speed decreases. Klingvall et al. investigated the effect of the EBM process parameters on the surface roughness. The authors found that contour offset and spacing between offsets significantly affect surface quality. However, the study could not conclude optimised process parameters, because of the large variation in the surface roughness R_a from build to build [46]. Later on, improved results were obtained by Safdar and co-workers [47]. The study found that the EBM process parameters and layer thickness have major effects on the average roughness R_a. It was revealed that the surface roughness reduces with increasing the scan speed and the offset focus, while it increases with increasing beam current and layer thickness. Similar to SLM, *Kleszczynski* et al. confirmed the dependency of surface roughness and the parts orientation. They found that samples with 45° inclined angle had high roughness [48]. Apart from the process parameters, the arrangement of parts in the building platform was proven to have a significant effect on the surface quality. For instance, more heat was generated when parts fabricated with a small spacing distance which increased the possibility to form partially melted powder and hence degrades the surface quality [49].

Table 1 shows that metal parts with surface roughness R_a of 10–50 μm can be achieved using BP direct laser deposition. The main process parameters of BP are the power and powder feed rate. The influence of BP process parameters on surface roughness was studied by *Vinod* et al. [50]. It was found that surface roughness increases as the laser power, scanning speed and feed rate increase. Side surface roughness of R_a = 4 μm and top surface roughness of R_a = 8 μm were achieved using the optimum process parameters. Another correlation between surface roughness and melt pools was also introduced by Gharbi et al. [51] who believed that the use of thin layer thickness and large melt pools enhances surface quality. Wire feed (WF) direct laser deposition is characterised by the largest layer thickness among the other additive manufacturing techniques. Therefore, the process is associated with poor accuracy and surface quality. The typical surface roughness R_a of WF products is about 200 μm (see Table 1). The main process parameters of WF manufacturing are wire feed, welding speed and laser power. The focus of optimising the WF process parameters is to enable continuous melt pool. By optimising WF process parameters, minimum surface roughness of R_Z = 63 μm can be achieved using laser powder of 3.0 kW, welding speed of 2.0 m/min and wire feed rate of 100 cm^3/h [18, 52]. As reviewed, it can be clearly seen that the surface roughness of AM metal parts is affected by the process, equipment, build direction and process parameters. It can be also noted that the SLM process produces the smoothest surfaces compared to other metal AM techniques. Process optimisation is particularly important for metal components with complex geometries where post-processing may be difficult to achieve.

3.2 *Laser Re-melting and Laser Polishing*

Laser re-melting (LR) is an approach to improve surface texture of SLM components. LR works by duplicating the laser melting of a layer so that the second scan enhances the part density and the surface topography. On the other hand, laser polishing (LP) is a potential post-processing technique to reduce surface roughness of AM metal products. It is based on melting the surface of manufactured parts using laser energy. A schematic diagram of the LP is shown in Fig. 6. When a laser beam hits a rough surface, it locally creates a melt pool. The liquid melt pool levels itself by the effect of surface tension and gravity. The temperature drops rapidly as the laser beam leaves the scanned area, and the melt pool solidifies with a reduced surface roughness. Alrbaey et al. [53] found that LR has the ability to reduce the surface roughness of SLM parts. They used statistical approaches to optimise the LR process parameters to largely eliminate the balling effect and improve the microstructure, shrinkage and agglomeration. They were able to obtain samples with almost 100% density and significantly improve the average R_a of up to 80% when compared to the original SLM part.

Originally, LP has been introduced to improve surface characteristics of metal materials fabricated using conventional methods, especially for materials which are difficult to machine. However, the process has gained much interest with the rise of metal additive manufacturing technologies. To date, the ability of LP in improving the surface finishing of AM metallic parts was applied successfully on a range of metallic materials including nickel alloys, titanium alloys, steels and aluminium alloy [54–57]. Ma et al. investigated the polishing of AM titanium alloys such as Ti-6Al-4V and TC11 using fibre laser. They studied the surface roughness of AM surface and laser-polished surfaces and investigated the effect of the laser polishing

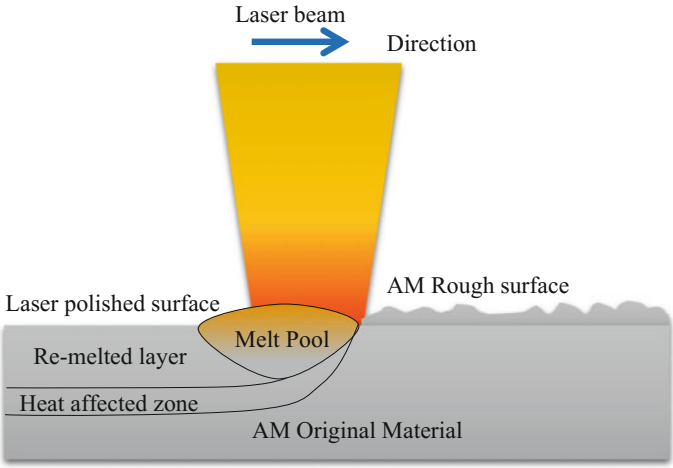

Fig. 6 Schematic of laser polishing

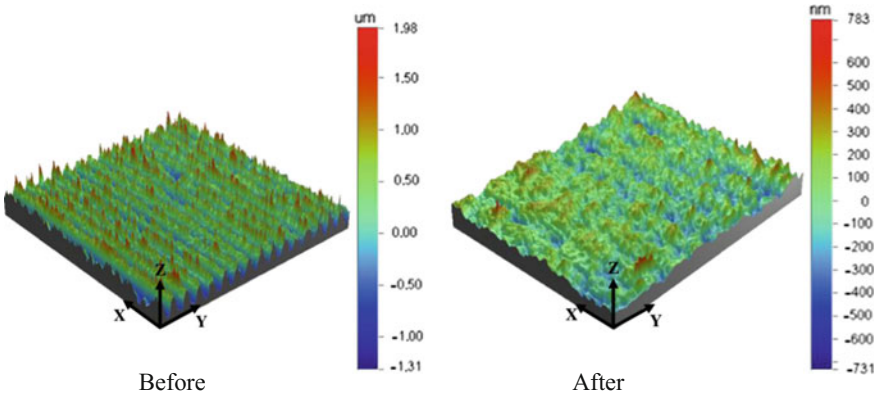

Fig. 7 Surface topography before and after LP [64]

microhardness, microstructure and wear resistance of the samples. It was revealed that laser polishing was able to reduce the surface roughness of the AM samples from more than 5 μm to about 1 μm without compromising the mechanical and microstructural properties [56].

Due to the novelty and potential capabilities of LP process, many research studies were devoted to investigate experimental uses of LP aiming to optimise process parameters to enhance surface quality of AM components. Process parameters of a typical LP are similar to those laser AM processes, and they include laser power (P), feed rate (V_f), overlap (O_v) and strategy of LP. Rosa et al. investigated the surface texture of AM thin parts. They were able to optimise the LP strategy and managed to achieve a surface roughness R_a = 0.79 μm from original R_a of 21 μm [58]. Similar results were obtained from literatures [59–63]. In general, LP has proven to lower the surface roughness significantly by optimising the LP process parameters (see Fig. 7) [64].

3.3 Chemical and Electropolishing

Chemical polishing is a process where chemicals are used to remove a layer of AM surface, thus polishing it and making it smoother. The process has been used not only for additive manufactured components but also for traditionally manufactured parts during which a wetted layer is created on a surface of metal part so that the peaks on the metal surface is faster dissolved than the shallower peaks. The process of chemical polishing titanium alloys can employ baths containing hydrofluoric acid and nitric acid [5]. The process was investigated by a number of researchers aiming to reduce the surface roughness of AM parts. Łyczkowska et al. and Pyka et al. chemically treated the surface of Ti–6Al–7Nb SLM components with complex geometry. Two different chemical baths such as hydrofluoric acid and nitric acid

were employed. They found a relationship between the chemical process parameters such as composition of the bath and polishing time on the mass loss, partially melted particles and struts diameter of AM samples. It was concluded that longer treatment time with more diluted bath under magnetic stirrer allows better control of the process and hence having better-polished samples [65, 66]. The process is promising especially for complex and open porous AM structures.

Electropolishing (also known as electrochemical) is a polishing technique that removes a layer from a metal component; it is the reverse of electroplating process. In this process, the part (anode) being polishing is placed in an electrolyte solution and subjected to an electrical current while the metal conductor is a cathode. Alrbaey et al. studied the effects of electropolishing on the surface morphology of 316L stainless steel parts fabricated by SLM and optimise the process parameters using statistical approaches. They found that the electropolishing of AM samples can improve surface roughness (R_a) to 0.5 µm (about 60% of the re-melted samples) by targeting the surface peaks via preferential dissolution, hence considered an attractive approach to decrease roughness of AM samples (see Fig. 8). Uniform dissolution can be achieved through optimising process parameters. Electropolishing can also remove oxide layer created during AM [67]. Electropolishing is not limited to stainless steel only, but it can polish other additive manufactured materials such as aluminium alloys, cobalt chrome and titanium alloys.

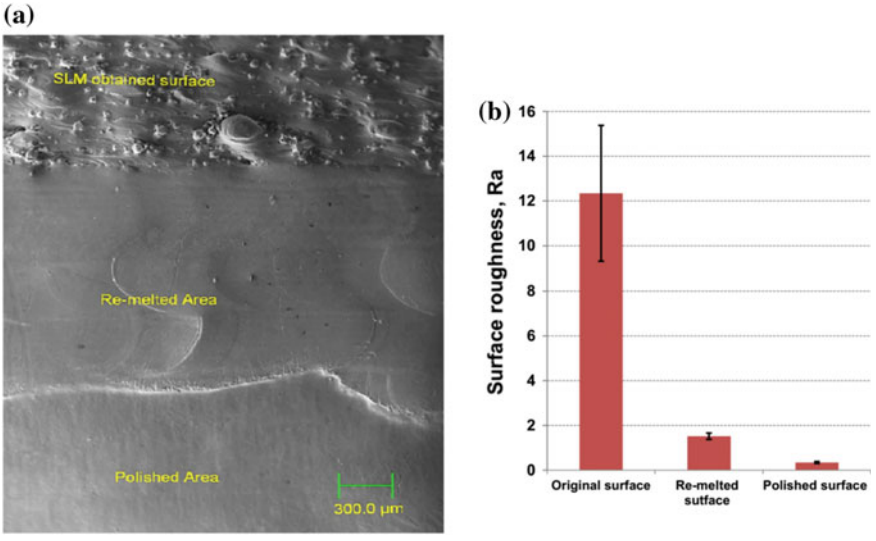

Fig. 8 **a** SEM micrograph of the SLM, re-melted, and electropolished areas, **b** comparison of surface roughness (R_a) [67]

3.4 Microelectrical Discharge Machining

Microelectrical discharge machining (μEDM) is a thermo-electric and contactless method that utilises discrete discharges for machining electroconductive material regardless their hardness or strength. It is denominated as "micro" since in this version of the process the energy used to machine the workpiece is very fine. This feature makes this technology suitable for micromanufacturing and high-precision machining, especially when difficult-to-machine materials (i.e. electroconductive ceramics) are processed [68]. The surface machined via μEDM process is characterised by overlapping craters derived by a series of discharges. Due to the low discharge energy, the crater dimensions can be few microns wide and, consequently, the surface roughness may range in fractions of micrometres [69, 70]. For all these reasons, μEDM can be a good candidate to play the role in the finishing process aimed at improving the surface roughness and enhance the quality of the SLM parts. Four different μEDM approaches are available; their choice depends mainly on the type of tool electrode adopted for machining. Drilling-EDM can produce microhole with high aspect ratio (up to 40), wire-EDM is usually adopted in case of 2D and half features because of its high material removal rate, whereas milling-EDM and sinking-EDM are usually adopted for complex 3D shapes.

Among the μEDM approaches, wire-EDM is the fastest and less sensitive to the initial rough surface of the workpiece. Due to the very fine energy employed, μEDM process is not suitable when a very rough surface is machined. The problem is related to the electrode wear phenomenon that changes the shape of the tool when very rough surface is polished. As a result, the machining conditions changed which causes machining error. Depending on the μEDM approach, several compensation methods can be implemented (Uniform Wear Method [71] in case of milling or multiple shaped tool electrodes for the sinking approach). On the contrary, the wire-EDM does not suffer from the tool wear phenomenon since the tool is a wire that is continuously renewed during machining. For these reasons, wire-EDM is less sensitive to rough surface produced by SLM process. Therefore, it was selected for the application presented in this chapter. In order to obtain the highest flexibility from μEDM, it recommended to combine multiple μEDM approaches sequentially [72]. A μEDM machine with one rotational axis, three linear axes (Sarix SX-200) set with a wire-μEDM is used for the present study. The tool electrode is a brass wire with a diameter of 0.2 mm. Two sets of technological parameters, reported in Table 2, have been tested on SLM samples in order to assess the μEDM process in finishing and roughing regimes. Hydrocarbon oil has been used as dielectric, and polarity of the workpiece has been set to positive. Three components were clamped on the machine, as shown in Fig. 9, and machined on the square and lateral faces using both roughing and finishing regimes.

The "Energy" level (E) is an index (used by Sarix micro-EDM machines) that determines the pulse shapes (long pulses, short pulses) and the maximum discharge energy achievable for a single spark. Hence, the erosion process regime, i.e. finishing or roughing, is chosen by the energy level parameter. The higher this index,

Table 2 Technological parameters (Sarix version) adopted in wire-EDM machining for roughing and finishing regimes

Regime		Roughing	Finishing
Energy	[index]	365	105
Polarity (workpiece)	±	+	+
Frequency	[kHz]	110	180
Width	[μs]	5	4.5
Current	[index]	70	80
Voltage	[V]	110	130
Gap	[index]	65	75
Gain	[index]	10/20	10
Feed rate[a]	[mm/min]	1.044/2.088	0.702
Wire Diameter	[mm]	0.2	0.2
Working Diameter	[mm]	0.22	0.21

[a]obtained by the other parameters

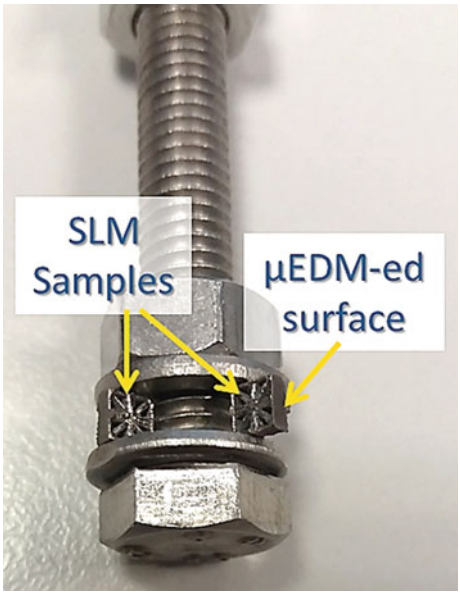

Fig. 9 Microcomponents clamped for μ-wire-EDM machining

the higher the energy released during the discharge. The "Frequency" (measured in kHz) and the "Width" (the time interval the generator is supplying the tool and the workpiece, often called t-on, and measured in μs) govern the number of discharged pulses. The "Current" parameter is also an index and used to limit the maximum current during a discharge when long pulses are considered, and it is strictly related to the "Energy" parameter. The "Voltage" parameter refers to the open voltage value (electric potential difference applied between electrodes, wire and workpiece) and measured in V. The "Gap" parameter refers to the distance between the workpiece and the tool favourable to start sparking, while the "Gain" parameter is

the control loop for the quick response of the system and for the process stability: these last two parameters act directly on the feed rate and process speed. Finally, the "Working Diameter" is the sum of wire diameter and the sparking gap, and it is measured in preliminary tests since it depends on materials and other technological parameters.

Before wire-EDM machining, the average surface roughness of the SLM components was estimated by confocal microscope (Zeiss CSM700) which gave back a value of 14.7 μm. Some technological parameters and performance results of the wire-EDM processes are summarised in Table 3. Two values of gain parameter have been used during the roughing regime. Also, different layer thicknesses for both regimes and different stripe widths have been considered for finishing one. The last two parameters determine the section area of the stripe removed during the erosion. The performance of the EDM process has been evaluated by measuring the average speed and the resulting surface roughness R_a.

It is evident that the layer thickness and the gain parameter affect the average speed and consequently the machining time. When the roughing regime is adopted, thanks to the high energy level, it is possible to engage 100% of the wire diameter. Thus, this regime is often used in cutting, contouring or shaping the workpiece. On the contrary, for finishing regime, it is necessary to reduce drastically the layer thickness down to few per cent of the wire diameter in order to proceed with comparable average speed. The surface roughness is only related to the energy level adopted for machining, and as such, its dramatic improvement is evident after the finishing regime.

Figure 10 displays a comparison of the lateral surface of a SLM sample before and after μ-EDM machining: the surface roughness has been largely enhanced from R_a = 14.7 μm to R_a = 4.6 μm after the first μEDM process using roughing regime. A further improvement of surface roughness has been accomplished after finishing, resulting in R_a = 0.8 μm. The irregular surfaces of the square face presenting microstructure are illustrated in Fig. 11a, b (opposite face), while Fig. 11c shows a face after μ-wire-EDM finishing. It is clearly visible that the machined surface has experienced a dramatic improvement in both R_a and flatness. Nonetheless, μ-wire-EDM process proves its insensitiveness to the geometric complexity of the face.

Table 3 Wire-EDM: technological settings and process performance

Machining regime	Layer thickness/percentage of the wire diameter	Stripe width (mm)	Max stripe section area (mm^2)	Gain	Average speed (mm/min)	R_a (μm)
Original	–	–	–	–	–	14.7
Roughing	0.1 mm/50%	3	0.3	10	0.68	4.6
	0.2 mm/100%	3	0.6	20	1.029	
Finishing	0.025 mm/12.5%	3	0.075	10	0.463	0.8
	0.01 mm/5%	3	0.03	10	0.796	
	0.01 mm/5%	1.5	0.015	10	1.682	

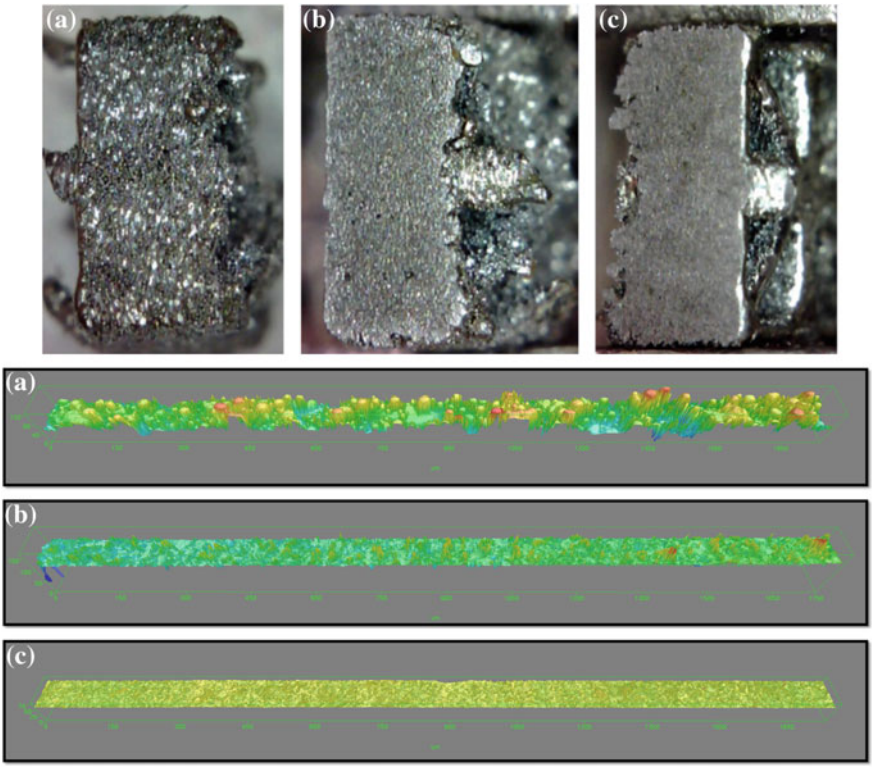

Fig. 10 **a** Part realised by SLM R_a = 14.7 μm, **b** surface after the EDM machining, roughing regime: R_a = 4.6 μm, **c** surface after EDM machining, finishing regime: R_a = 0.8 μm

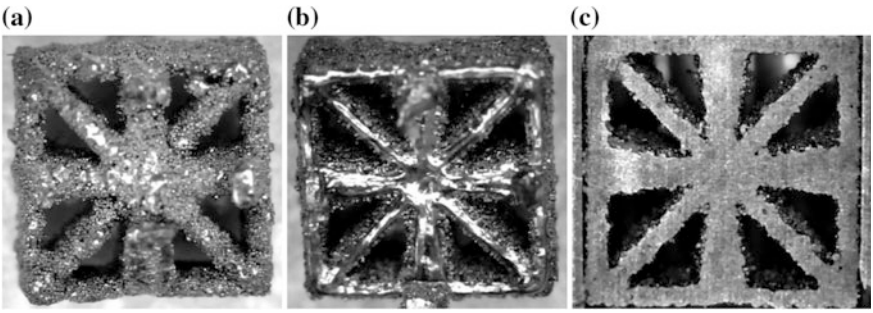

Fig. 11 SLM sample surfaces **a** before, **b** roughing, **c** polishing

It must be underlined that the proper implementation of the finishing phase via μEDM process does require that two machining steps (roughing and finishing) should be adopted in order to improve both surface quality (roughness and flatness) and machining time. Consequently, an adequate stock allowance on the nominal dimension should be taken into account before the sample is realised in SLM. Expected surface porosity and flatness of the SLM sample determine the stock allowance thickness.

4 Conclusion

The review and experimental work reported in this chapter indicate that research of polishing or surface modification of AM products is still in its early stages and many efforts are required to be done to fulfil the specific application requirements. Each of the metal AM techniques has its own surface quality and deposition rate characteristics that are inversely related, which makes it unfavourable trade-off to manufacturers. The review showed that surface roughness of SLM products is the lowest while WF deposition products are the highest. Two approaches for surface finish of metal AM exist: (1) Improve surface quality of as-fabricated products and (2) AM surface characteristics are not significant as many applications require post-processing to obtain surface quality requirements. These two approaches are valid, and research work will continue to investigate the current AM process and/or post-processing polishing. Several researchers tried to enhance surface finish through optimisation of AM process parameters. This trend has been implemented to all AM techniques, and success has been achieved in improving the surface characteristics. However, the results indicate that the obtained surface roughness does not fulfil the surface requirements of many niche applications such as aerospace and biomedical applications. Hence, end-user products have to be post-processed by polishing techniques.

As reported in this chapter, post-processing polishing techniques are promising to qualify AM products for specific applications. Laser polishing and EDM have shown their ability to improve the AM quality of flat surfaces. The preliminary conclusions led to the fact that laser polishing is well implemented to AM products of large simple components that are not complex. On the contrary, chemical and electropolishing were successfully adopted to complex geometries. The two processes showed a great potential in this field. However, a few research exists to claim this trend. In addition, unfavourable chemicals and contaminations are expected by using chemical and electropolishing. In summary, the future of AM surface improvement technology is bright and will enable manufacturing of high-quality AM metal components for various engineering applications.

References

1. Bhattacharjee N, Urrios A, Kang S, Folch A (2016) The upcoming 3D-printing revolution in microfluidics. Lab Chip Miniaturisation Chem Biol 16:1720–1742
2. Daly A (2016) Socio-legal aspects of the 3D printing revolution
3. Wirth M, Thiesse F (2014) Shapeways and the 3D printing revolution. In: ECIS 2014 Proceedings—22nd European Conference on Information Systems
4. UK Government Office for Science and Department for Business Innovationand Skills, The future of manufacturing: a new era of opportunity and challenge for the UK., 2013
5. Cox SC, Jamshidi P, Eisenstein NM, Webber MA, Hassanin H, Attallah MM et al (2016) Adding functionality with additive manufacturing: fabrication of titanium-based antibiotic eluting implants. Mater Sci Eng, C 64:407–415
6. Li S, Hassanin H, Attallah MM, Adkins NJE, Essa K (2016) The development of TiNi-based negative Poisson's ratio structure using selective laser melting. Acta Mater 105:75–83
7. Qiu C, Adkins NJE, Hassanin H, Attallah MM, Essa K (2015) In-situ shelling via selective laser melting: modelling and microstructural characterisation. Mater Des 87:845–853
8. Qiu C, Yue S, Adkins NJE, Ward M, Hassanin H, Lee PD et al (2015) Influence of processing conditions on strut structure and compressive properties of cellular lattice structures fabricated by selective laser melting. Mater Sci Eng, A 628:188–197
9. Yeh CC (2014) Trend analysis for the market and application development of 3D printing. Int J Autom Smart Technol 4:1–3
10. Seifi M, Salem A, Beuth J, Harrysson O, Lewandowski JJ (2016) Overview of materials qualification needs for metal additive manufacturing. JOM 68:747–764
11. Frazier WE (2014) Metal additive manufacturing: a review. J Mater Eng Perform 23:1917–1928
12. Murr LE, Gaytan SM, Ramirez DA, Martinez E, Hernandez J, Amato KN et al (2012) Metal fabrication by additive manufacturing using laser and electron beam melting technologies. J Mater Sci Technol 28:1–14
13. Yap CY, Chua CK, Dong ZL, Liu ZH, Zhang DQ, Loh LE et al (2015) Review of selective laser melting: Materials and applications. Appl Phys Rev 2
14. Körner C (2016) Additive manufacturing of metallic components by selective electron beam melting—a review. Int Mater Rev 61:361–377
15. Shamsaei N, Yadollahi A, Bian L, Thompson SM (2015) An overview of direct laser deposition for additive manufacturing; Part II: mechanical behavior, process parameter optimization and control. Add Manuf 8:12–35
16. Jones J, Whittaker M, Buckingham R, Johnston R, Bache M, Clark D (2017) Microstructural characterisation of a nickel alloy processed via blown powder direct laser deposition (DLD). Mater Des 117:47–57
17. Isanaka SP, Karnati S, Liou F (2016) Blown powder deposition of 4047 aluminum on 2024 aluminum substrates. Manuf Lett 7:11–14
18. Ding D, Pan Z, Cuiuri D, Li H (2015) Wire-feed additive manufacturing of metal components: technologies, developments and future interests. Int J Adv Manuf Technol 81:465–481
19. Lancea C, Chicos LA, Zaharia SM, Pop MA (2017) Microstructure and micro-hardness analyses of titanium alloy Ti-6Al-4V parts manufactured by selective laser melting. In: MATEC Web of Conferences
20. Agapovichev AV, Kokareva VV, Smelov VG, Sotov AV (2016) Selective laser melting of titanium alloy: investigation of mechanical properties and microstructure. In: IOP Conference Series: Materials Science and Engineering
21. Bassani P, Biffi CA, Casati R, Alarcon AZ, Tuissi A, Vedani M (2016) Properties of aluminium alloys produced by selective laser melting. In: Key Engineering Materials, vol 710, pp 83–88

22. Olakanmi EO, Cochrane RF, Dalgarno KW (2015) A review on selective laser sintering/melting (SLS/SLM) of aluminium alloy powders: Processing, microstructure, and properties. Prog Mater Sci 74:401–477
23. Lykov PA, Baitimerov RM, Vaulin SD (2016) Influence of SLM process parameters on porosity of nickel base heat resistance alloy EP648. In: Materials Science Forum, vol 843, pp 253–258
24. Carter LN, Martin C, Withers PJ, Attallah MM (2014) The influence of the laser scan strategy on grain structure and cracking behaviour in SLM powder-bed fabricated nickel superalloy. J Alloy Compd 615:338–347
25. Sander J, Hufenbach J, Bleckmann M, Giebeler L, Wendrock H, Oswald S et al (2017) Selective laser melting of ultra-high-strength TRIP steel: processing, microstructure, and properties. J Mater Sci 52:4944–4956
26. Yusuf SM, Chen Y, Boardman R, Yang S, Gao N (2017) Investigation on porosity and microhardness of 316L stainless steel fabricated by selective laser melting. Metals 7
27. Song B, Dong SJ, Liao HL, Coddet C (2012) Morphology evolution mechanism of single tracks of FeAl intermetallics in selective laser melting. Mater Res Innovations 16:321–325
28. Kotoban DV, Nazarov AP, Shishkovsky IV (2015) Comparative study of selective laser melting and direct laser metal deposition of Ni<inf>3</inf>Al intermetallic alloy. In: Materials Science Forum, vol 834, pp 103–111
29. Gu D, Dai D, Chen W, Chen H (2016) Selective laser melting additive manufacturing of hard-to-process tungsten-based alloy parts with novel crystalline growth morphology and enhanced performance. J Manuf Sci Eng Trans ASME 138
30. Delgado J, Ciurana J, Rodríguez CA (2012) Influence of process parameters on part quality and mechanical properties for DMLS and SLM with iron-based materials. Int J Adv Manuf Technol 60:601–610
31. Hrabe N, Gnäupel-Herold T, Quinn T (2017) Fatigue properties of a titanium alloy (Ti–6Al–4V) fabricated via electron beam melting (EBM): effects of internal defects and residual stress. Int J Fatigue 94:202–210
32. Algardh JK, Horn T, West H, Aman R, Snis A, Engqvist H et al (2016) Thickness dependency of mechanical properties for thin-walled titanium parts manufactured by Electron Beam Melting (EBM)®. Additive Manufacturing 12:45–50
33. Ramsperger M, Singer RF, Körner C (2016) Microstructure of the nickel-base superalloy CMSX-4 fabricated by selective electron beam melting. Metall Mater Trans A 47:1469–1480
34. Zhong Y, Rännar LE, Liu L, Koptyug A, Wikman S, Olsen J et al (2017) Additive manufacturing of 316L stainless steel by electron beam melting for nuclear fusion applications. J Nucl Mater 486:234–245
35. Mazumder J, Dutta D, Kikuchi N, Ghosh A (2000) Closed loop direct metal deposition: art to part. Opt Lasers Eng 34:397–414
36. Miller S, Heath M, Woods B, Costello A, Dolan D, Sears J (2005) Fabrication of titanium automotive parts with Laser Powder Deposition. In: MPMD sixth global innovations proceedings—trends in materials and manufacturing technologies for transportation industries and powder metall. Research and development in the transportation industry, pp 293–301
37. Riza SH, Masood SH, Wen C, Ruan D, Xu S (2014) Dynamic behaviour of high strength steel parts developed through laser assisted direct metal deposition. Mater Des 64:650–659
38. Yan A, Yang T, Wang Y, Ma Z, Du Y, Wang Z (2016) Effect of tungsten powder particle size and shape on consolidation and microstructure of W-xCu composites by selective laser melting. Zhongguo Jiguang/Chin J Lasers 43
39. Wendt U, Settegast S, Grodrian IU (2003) Laser alloying of aluminum with titanium wire. J Mater Sci Lett 22:1319–1322
40. Zhang YN, Cao X, Wanjara P (2015) Fiber laser deposition of nickel-based superalloys using filler wire feed. In: Proceedings of the ASME turbo expo
41. Nie Z, Wang G, McGuffin-Cawley JD, Narayanan B, Zhang S, Schwam D et al (2016) Experimental study and modeling of H13 steel deposition using laser hot-wire additive manufacturing. J Mater Process Technol 235:171–186

42. Ghanekar A, Crawford R (2003) Optimization of SLS process parameters using D-optimality. 4th international solid freeform fabrication symposium. Austin, Texas, USA, p 348
43. Calignano F, Manfredi D, Ambrosio EP, Iuliano L, Fino P (2013) Influence of process parameters on surface roughness of aluminum parts produced by DMLS. Int J Adv Manuf Technol 67:2743–2751
44. Bacchewar PB, Singhal SK, Pandey PM (2007) Statistical modelling and optimization of surface roughness in the selective laser sintering process. Proc Inst Mech Eng, Part B: J Eng Manuf 221:35–52
45. Kaddar W (2010) "Die generative Fertigung mittels Laser Sintern," Ph.D., Abteilung Maschinenbau und Verfahrenstechnik Universität Duisburg-Essen
46. Ek RK, Rännar L-E, Bäckstöm M, Carlsson P (2016) The effect of EBM process parameters upon surface roughness. Rapid Prototyping J 22:495–503
47. Safdar A, He HZ, Wei LY, Snis A, de Paz LEC (2012) Effect of process parameters settings and thickness on surface roughness of EBM produced Ti-6Al-4V. Rapid Prototyping J 18:401–408
48. Kleszczynski S, Ladewig A, Friedberger K, zur Jacobsmühlen J, Merhof D, Witt G (2015) Position dependency of surface roughness in parts from laser beam melting systems. In: 26th International Solid Free Form Fabrication (SFF) Symposium, USA, pp 360–370
49. Mahdi J, Radovan K (2015) The influence of heat accumulation on the surface roughness in powder-bed additive manufacturing. Surf Topogr: Metrol Prop 3:014003
50. Vinod AR, Srinivasa CK, Keshavamurthy R, Shashikumar PV (2016) A novel technique for reducing lead-time and energy consumption in fabrication of Inconel-625 parts by laser-based metal deposition process. Rapid Prototyping J 22:269–280
51. Gharbi M, Peyre P, Gorny C, Carin M, Morville S, Le Masson P et al (2013) Influence of various process conditions on surface finishes induced by the direct metal deposition laser technique on a Ti–6Al–4V alloy. J Mater Process Technol 213:791–800
52. Nowotny S, Thieme S, Albert D, Kubisch F, Kager R, Leyens C (2013) Generative manufacturing and repair of metal parts through direct laser deposition using wire material. In: Kovács GL, Kochan D (eds) Digital product and process development systems: IFIP TC 5 international conference, NEW PROLAMAT 2013, Dresden, Germany, 10–11 Oct 2013. Springer, Berlin, pp 185–189
53. Alrbaey K, Wimpenny D, Tosi R, Manning W, Moroz A (2014) On optimization of surface roughness of selective laser melted stainless steel parts: a statistical study. J Mater Eng Perform 23:2139–2148
54. Smith BH, See T, Hiersemenzel F, Kaja K, Antar M (2016) Laser polishing of additive manufactured steel and titanium components. In: Proceedings—ASPE/euspen 2016 summer topical meeting: dimensional accuracy and surface finish in additive manufacturing, pp 22–27
55. Ross I, Kumstel J, Bremen S, Willenborg E (2015) Laser polishing of laser additive manufactured surfaces made from Inconel 718 and ASTM F75. In: Proceedings—ASPE 2015 spring topical meeting: achieving precision tolerances in additive manufacturing, pp 136–140
56. Ma CP, Guan YC, Zhou W (2017) Laser polishing of additive manufactured Ti alloys. Opt Lasers Eng 93:171–177
57. Schanz J, Hofele M, Hitzler L, Merkel M, Riegel H (2016) Laser polishing of additive manufactured AlSi10Mg parts with an oscillating laser beam. In: Advanced Structured Materials, vol 61, pp 159–169
58. Rosa B, Mognol P, Hascoët J-Y (2015) Laser polishing of additive laser manufacturing surfaces. J Laser Appl 27:S29102
59. Dadbakhsh S, Hao L, Kong CY (2010) Surface finish improvement of LMD samples using laser polishing. Virtual Phys Prototyping 5:215–221
60. Marimuthu S, Triantaphyllou A, Antar M, Wimpenny D, Morton H, Beard M (2015) Laser polishing of selective laser melted components. Int J Mach Tools Manuf 95:97–104
61. Burzic B, Hofele M, Mürdter S, Riegel H (2017) Laser polishing of ground aluminum surfaces with high continuous wave laser. J Laser Appl 29

62. Bhaduri D, Penchev P, Batal A, Dimov S, Soo SL, Sten S et al (2017) Laser polishing of 3D printed mesoscale components. Appl Surf Sci 405:29–46
63. Chang CS, Chen TH, Li TC, Lin SL, Liu SH, Lin JF (2016) Influence of laser beam fluence on surface quality, microstructure, mechanical properties, and tribological results for laser polishing of SKD61 tool steel. J Mater Process Technol 229:22–35
64. Bordatchev EV, Hafiz AMK, Tutunea-Fatan OR (2014) Performance of laser polishing in finishing of metallic surfaces. Int J Adv Manuf Technol 73:35–52
65. Łyczkowska E, Szymczyk P, Dybała B, Chlebus E (2014) Chemical polishing of scaffolds made of Ti–6Al–7Nb alloy by additive manufacturing. Arch Civil Mech Eng 14:586–594
66. Pyka G, Burakowski A, Kerckhofs G, Moesen M, Van Bael S, Schrooten J et al (2012) Surface modification of Ti6Al4V open porous structures produced by additive manufacturing. Adv Eng Mater 14:363–370
67. Alrbaey K, Wimpenny DI, Al-Barzinjy AA, Moroz A (2016) Electropolishing of Re-melted SLM Stainless Steel 316L Parts Using Deep Eutectic Solvents: 3 × 3 Full Factorial Design. J Mater Eng Perform 25:2836–2846
68. Modica F, Marrocco V, Fassi I (2012) Machining of ceramic Si3N4-TiN scaffolds using micro-EDM. In: proceeding of 1st International Conference on Design and PROcesses for MEdical Device, pp 139–142
69. Tiwary AP, Pradhan BB, Bhattacharyya B (2015) Study on the influence of micro-EDM process parameters during machining of Ti–6Al–4V superalloy. Int J Adv Manuf Technol 76:151–160
70. Maradia U, Scuderi M, Knaak R, Boccadoro M, Beltrami I, Stirnimann J et al (2013) Super-finished Surfaces using Meso-micro EDM. Procedia CIRP 6:157–162
71. Yu ZY, Masuzawa T, Fujino M (1998) Micro-EDM for three-dimensional cavities—development of uniform wear method. CIRP Ann Manuf Technol 47:169–172
72. Modica F, Basile V, Marrocco V, Fassi I (2016) A new process combining micro-electro-discharge-machining milling and sinking for fast fabrication of microchannels with draft angle. J Micro Nano-Manuf 4:024501

Precision Coatings

Zoltan-Iosif Korka

Abstract Precision coatings are used to fulfil various surface engineering requirements such as to provide necessary protection to the surface of an engineered part, to impart necessary strength or hardness, or to increase its aesthetics. This chapter introduces various important surface coating technologies. It starts with presenting the concepts of universal underlying considerations—functions of coatings and then moves to addressing the different types of coatings. The method(s) and area of application, and the performance properties are presented for each coating category. Furthermore, this chapter aims to provide an effectiveness comparison of different coating types, enabling the reader to find the proper coating system for a particular application. In addition, some quality and precision aspects are presented. In this regard, the chapter discusses the main issues regarding the quality control of coatings, verification means, inspection equipment, as well as the applicable standards. Finally, the chapter is concluded with some practical examples of precision coatings applied on gear teeth for increasing their wear resistance and for improving their dynamic behaviour (vibration) and reducing the acoustic emission (sound level).

Keywords Gear · Deposition · Noise · Precision · Surface engineering · Tribology · Wear

1 Introduction

The terms "coating" and "painting" are often used interchangeably. "Painting" is traditionally used to describe the application of thin film pigmented materials as distinct from clear films such as varnishes or lacquers, while "coating" is a more general description for the process of applying a thin continuous layer to a surface. Therefore, the term "surface coating" may be considered by purists as tautological

Z.-I. Korka (✉)
University "Eftimie Murgu" of Reşiţa, Traian Vuia Square No. 1-4,
320085 Reşiţa, Romania
e-mail: z.korka@uem.ro

K. Gupta (ed.), *Micro and Precision Manufacturing*, Engineering Materials,
https://doi.org/10.1007/978-3-319-68801-5_8

[1]. However, in the UK and North America, there is a wide contrast between painting and other surface treatment, such as anodizing, electroplating or the lamination of a polymer film onto a surface. In the context of this chapter, the author will be most concerned with the term “coating”.

Given the distinction mentioned above, the term coating is defined by most experts in the field as the process of covering the surfaces of an object, usually referred to as the substrate, or applying a layer for functional or decorative reasons. The coating itself may cover only parts of the substrate, or may completely cover the substrate, being an all-over coating. Jewellers are using coatings such as metal plating only for decorative reasons, but in industrial applications, coating is used for improving functionality or for preventing corrosion.

Corrosion is frequently causing material and structural damage, side effects that are associated with extremely high-operating and repair costs can appear, as a consequence. These expenses have an impact over both economical and environmental aspects.

In some of the studies of the World Corrosion Organization (WCO), it is highlighted that the corrosion jeopardizes public safety, decreases the quality of life and causes damage to the environment. Recent studies by independent agencies have assessed the cost of corrosion worldwide at up to 2.2 billion US $/year, respectively, greater than 3% of world gross domestic product (GDP) [2]. This value includes, first, the direct costs of corrosion, such as the replacement of corroded materials and damaged components, and, second, the indirect costs of corrosion, for example, costs associated with production-related drops, environmental impact, effects on traffic and fatalities. The experts [2, 3] estimate that up to 25% of these costs can be saved through proper application of technologies and knowledge currently available on precision coating.

Recently, due to the development of new applications in the field of medical technology, electronics, optics, sensors and energy, where the requirements regarding precision, uniformity, stability, as well as high deposition rate of coatings have grown, even in case of big surfaces, the term **precision coatings** is used.

2 Functions of Coatings

Traditionally, the main functions of coatings are to protect and to decorate substrates [4]. More recently, a growth in the research and development, as well as in the commercialization of coatings with novel functions, has been observed, in addition to the initial protective and decorative properties. Coatings such as thermochromic, antireflective coatings for eyeglasses, or energy-efficient coatings for buildings are commercially available for more than twenty years. These classes of

coatings, often referred to as functional ones, are providing a significant added value. Generally, the function of coatings is provided in three distinct zones:

- at the interface between coating and substrate;
- in the bulk of the coating;
- at the interface between coating and the environment.

While the list is long, Table 1 highlights the main functions of coatings for industrial applications and some typical examples of use.

Table 1 Functions of coatings and examples of use

Functions	Examples of use
Protection of substrate	- Coatings for sealing and waterproofing of wood - Coatings for sealing the surface of concrete - Coatings for preserving machineries, equipments and structures from degradation (anticorrosion) - Coatings for passive fire protection
Improving the wear resistance	- Hard coating with titanium nitride (TiN) and/or titanium carbide (TiC) of cutting tools - Diamond-like carbon (DLC) coating of gears - Fluoropolymer coating of telescoping booms, ball reversers, rocker arms or ball joints
Improving the friction	- PTFE and moly-type coatings of air-cylinder pistons, hinges or slide bearings
Sealing	- Fluoropolymer coatings are ensuring a good thread-to-thread seal on fittings, pressure plugs, valve stems and other threaded fluid-power components
Changing adhesion properties	- Non-stick PTFE coating for demountable assemblies in offshore applications - Fluoropolymer coating of the throttle shaft and butterfly from a carburettor for eliminating ice build-up
Vibration and noise reduction	- Fluoropolymer coating of gears - Fluoropolymer coating of the rotors of a supercharger
Thermal insulation (Work on extreme temperatures)	- Fluoropolymer coatings applied on rubbing parts of temperature sensitive materials for preventing damaging “hot spots”
Optical properties	- Reflective coatings for mirrors - Antireflective coatings for eyeglasses - UV-absorbent coatings for increasing the life of substrate
Magnetic characteristics	- Coating with magnetic media such as cassette tapes or floppy disks
Electrical properties	- Conductive coatings for manufacturing some resistors - Insulating coatings of magnet wires used in electrical transformers

3 Classification of Coatings

As previously mentioned, the coating process involves the application of a thin film of functional material to the substrate. Classification of coatings may be based on various different criteria, such as:

(a) *Depending on the substrate on which the coating is applied*

From this point of view, coatings can be applied over:

- Metallic substrates;
- Non-metallic substrates (i.e. plastic, wood, paper, glass, ceramics, composite materials, cement-based products).

(b) *Depending on the material applied on the substrate*

In this respect, coatings can be:

- Non-metallic coatings;
- Metallic coatings.

Plastic coating and rubber coating are the most common non-metallic coatings, involving the application of a layer of the given material onto the substrate. A few examples of such coatings are:

Wire and cable coating where the whole length of an electrical cable or conducting wire is coated with a polymer or plastic, in order to ensure electrical or thermal insulation;
Planer coating which involves the deposition of a layer over a flat surface;
Counter plating applied over a 3-D object and accomplished by spraying or dipping.
Organic coatings are also a type of non-metallic coatings applied on different substrates in order to provide a barrier between the substrate and the environment. The application of an organic coating improves the appearance of the substrate surface without having an appreciable influence on its mechanical properties. Examples of organic coatings are listed below:

- Lacquering;
- Enamelling;
- Varnishing;
- Rubber-based coatings;
- Teflon coatings;
- Bituminous coatings.

Metallic coatings can be applied over non-metallic substrates (to give plastic, for example, a metallic appearance) as well as over metallic surfaces. A few examples of metallic coatings are electroplating, electroforming, galvanizing or anodizing.

(c) *Depending on the chemical composition of the applied metallic material on the substrate*

Metallic materials may be plated with various metals for multiple purposes, among which can be mentioned: increase of corrosion resistance, decorative scopes or increasing wear resistance. The deposition is made by an electrochemical process, called electroplating, and the most common procedures being listed in the following:

Cadmium plating (or cad plating) offers a long list of technical benefits like very good corrosion resistance in salt atmospheres, even at low thickness, malleability and softness, good galvanic compatibility with aluminium, freedom from sticky and bulky products, good ability to lubricate and can be dyed to various colours.

Chrome plating (less frequently chromium plating) is a finishing treatment applied to metallic surfaces using the electroplating technique. Applying a thin layer of chromium (often referred to simply as chrome) may have one of the following purposes: to provide corrosion resistance, for decorative and aesthetic reasons, as simple cleaning procedure, or as an increase of surface hardness and wear resistance. As the process involves the use of very toxic chemicals, their disposal is regulated in most of the countries. Working well either as paint base or as final finish, chrome plating is used in military, aviation and aerospace applications. For environmental concerns, the chrome plating process has to be done under very strict controlled conditions, because of the high toxicity of chromium metal.

Gold plating is a method of depositing a thin layer of gold onto the surface of another metallic material, the most often substrates being copper and silver. The procedure improves the corrosion resistance, respectively the electrical conductivity, and is mostly used in the modern electronics industry. A major problem which appears at gold plating of copper is the fact that the copper atoms have the tendency to diffuse through the gold layer, causing tarnishing of its surface and forming a sulphide and/or oxide layer. Therefore, a barrier metal layer of nickel is applied on the copper substrate, before gold plating, as nickel atoms do not diffuse to gold. Gold plating may be also applied to some metals for ornamental purposes, in order to improve their aesthetics.

Nickel plating is the electroplating process of depositing a thin nickel layer on metallic parts. The procedure may be decorative or may provide wear resistance and corrosion resistance. It can be also used for salvage purposes in case of overuse-related problems or to build up the undersized respective worn parts. Substrate materials may be steel, brass or zinc die castings. Main applications can be found in the automotive industry for bumpers, rims and exhaust pipes.

Zinc plating serves to prevent oxidation of small parts such as springs, fasteners, crank handles and other hardware items other than sheet metal. The protection is ensured by the zinc oxide which acts, if undisturbed, as a barrier against oxidation, similar to the anti-oxidation mechanism of aluminium or stainless steel.

Alloy plating is the co-deposition process achieved by electroplating, of two or more metals, forming an alloy deposit, in order to improve the physical and chemical properties of the metallic substrate. Nickel–Cobalt is the commonly used alloy for this process. Depending on the alloy system, the mechanism can be a solid solution strengthened one, or a precipitation hardening one, achieved by heat treating process.

(d) *Depending on the technological process used for covering the substrate*

Various functions of the coatings, of which the most important were listed above, may be achieved by using different coating materials and numerous coating technologies. In order to obtain the best results, these technologies have to be regarded as a system consisting the following three components: substrate material, coating material and coating process (Fig. 1). This system, which exists in any industrial application and needs to be coated, has to be defined and optimized.

The various choices of coating technologies leading to compound constructions are made possible due to a great number of coating techniques and variants, resulted from various specific needs and economic reasons. Therefore, coating technologies are available in a very wide range, the following section aiming to exemplify some of the most important processes used in precision coatings.

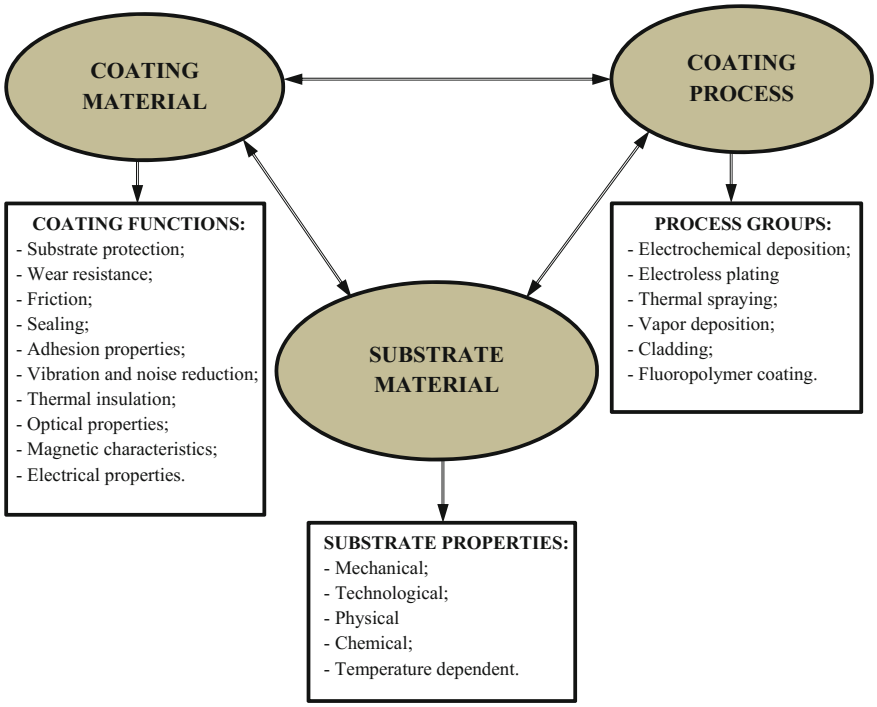

Fig. 1 System of coating technology

4 Precision Coating Technologies

4.1 Electrochemical Deposition

Electrochemical deposition, or electrodepositing for short, is also known as electroplating and consists of first, immersing the part to be coated in an electrolyte solution of the metal to be plated, and second, passing direct current between the respective part, and another electrode. Usually, in the electrolytic process, the cathode is placed to the workpiece, while the anode is made of metal to be plated onto the substrate. The electrolyte is an aqueous conducting solution containing metal ions.

The process is based on two laws from Faraday, which state that:

(a) The mass of substance set free in electrolysis is proportional to current flowing through the cell, and
(b) The mass of the material set free is proportional to its electrochemical equivalent (the mass in grams of that element transported by 1 coulomb of electricity).

As such, the process can be described by the expression [5]:

$$V = k \cdot I \cdot t, \tag{1}$$

where:

V (m^3) the volume of plated metal;
k $\left(\frac{m^3}{A \cdot s}\right)$ a constant depending on density and electrochemical equivalent of electrolyte;
t (s) the time for which the current is passing through.

Consequently, the character of the deposition depends on factors such as time, temperature and composition of the electrolytic bath. These variables can be adjusted to produce different coating thicknesses, or different mechanical properties (soft or hard, dull or bright, respective ductile or brittle), respectively.

Figure 2 exemplifies copper plating on a metal substrate. For such an application, the electrolytic bath is made of copper sulphate ($CuSO_4$), mixed with water. A Cu plate acts as anode while the metallic piece (Me), on which we want to plate copper, acts as cathode.

Electrochemical process occurs as follows:

– Copper is oxidized at the anode to Cu^{2+} by losing two electrons;
– The cathode Cu^{2+} is reduced to metallic copper by gaining two electrons;
– As a result, copper transfers from the anode, depositing on the cathode (the metallic piece).

Electroplating can be done with a single metal, multiple layers of different metals or even alloys (e.g. brass). For example, in automotive, a bumper is usually plated with three different layers: first, a layer of copper for a good adhesion; then, an

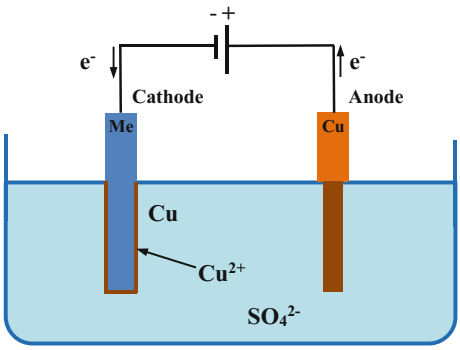

Fig. 2 Copper plating

intermediate layer of nickel for corrosion protection; and finally, a thin layer of chromium for aesthetic (appearance) reasons.

Most metals can be used for electrochemical deposition. In this regard, the largest quantities of metals plated by electrochemical deposition are (in order) nickel, tin, and cadmium, while gold, silver and platinum represent the most common plates.

4.2 Electroless Plating

Electroless plating, as indicated by its name, is an autocatalytic method used to deposit a metal layer onto a solid workpiece, such as plastic or metal. This chemical deposition process occurs in a liquid solution containing ions of the metal to be deposited, in the presence of a reducing agent, which reacts with the metal ions. Unlike electroplating, the process does not require an electric current to pass through the solution to form the deposit. In case of nickel electroless plating, the reducing agent is a hydrated sodium hypophosphite (H_2O + $NaPO_2H_2$), while the liquid solution containing nickel ions is nickel sulphate ($NiSO_4$). The chemical reaction which occurs in this case is:

$$NiSO_4 + H_2O + NaPO_2H_2 \xrightarrow[\text{[catalyst]}]{\text{heat}} \text{Ni} \quad \text{Plating} + NaHPO_3 + H_2SO_4, \qquad (2)$$

Copper (Cu), nickel (Ni) or nickel alloys are the most common metals used for this plating technique. The method is applied to prevent corrosion and wear of the substrate, providing an even deposit, regardless of the geometry of the workpiece. The coating thicknesses range from 2.5 to 150 μm, and the typical components used for industrial purposes having a thickness in the range 50–100 μm.

Compared to electroplating, the electroless plating has the following advantages:

- The method is suitable both on metallic as well as on non-metallic substrates.
- The process does not require a DC power source.

- Parts with a complex geometry can be coated with an uniform thickness.

From the disadvantages of the method, we list:

- limited lifespan of the chemicals;
- high cost of waste treatment due to speedy chemical renewal;
- porous nature of the plating, leading to inferior material structure.

4.3 Thermal Spraying

Thermal spraying is the coating process made possible by special devices, through which melted or heated materials are sprayed at a high speed onto a cleaned and prepared surface [6, 7]. Figure 3 shows the principle of thermal spraying.

The coating feedstock material is initially heated by chemical (combustion flame) or electrical (plasma arc) means, after which it is driven by process gases and, is finally sprayed on the substrate, where it crystallize onto a solid layer. As the liquid or molten particles of the feedstock material are impacting the surface with a high speed, the coating particles are deformed and spread in flattened form on the substrate. After the impact, the heat from the hot particles is transmitted to the base material, which is colder. Thereby, the particles shrink and solidify, thus creating porosities [8]. Obviously, in the coating layer, oxide and unmelted particles may also appear (Fig. 4).

Because the adhesion of the coating onto the base material principally consists of mechanical bonding, special attention has to be paid to careful cleaning and preparation of the substrate. After removing the surface impurities by mechanical or chemical procedures, the surface is roughened by grit blasting, usually with dry corundum. Depending on the application, alternative blasting media can be steel grit, chilled iron or silicon carbide (SiC). Besides the grit type, other important factors of the blasting process are particle size and shape, pressure, blast angle and purity of the grit media.

Regarding the coating material, for thermal spraying, any material that does not decompose during melting can be used, usually in form of powder, wire or rod.

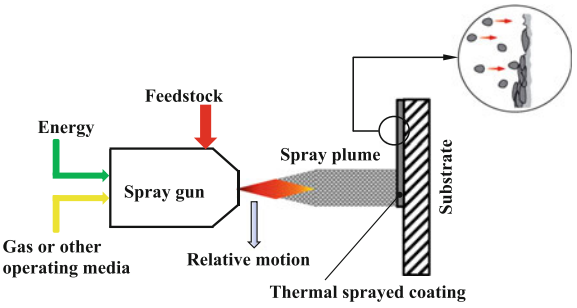

Fig. 3 Principle of thermal spraying

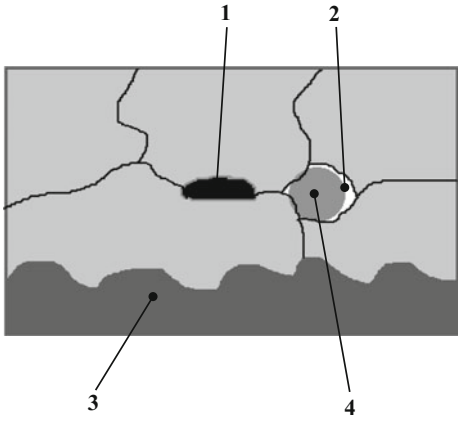

Fig. 4 Diagram of thermal sprayed coating (1 oxide particle; 2 porosity; 3 substrate 4 unmelted particle)

Commonly used materials are pure metals (Zn, Al, Cu, Ni), oxides (Al_2O_3, Cr_2O_3), self-fluxing alloys (FeNiBSi), carbides (Cr_2C_2, $WC_{12}Co$), ceramics or plastic.

Various technologies are utilized to apply a coating by thermal spraying, among which the following can be mentioned:

- Conventional flame spray;
- Electric arc wire spray;
- Plasma spray;
- High velocity oxy-fuel spray (HVOF).

(a) *Conventional flame spray* coating uses combustible gases, such as acetylene, propane, natural gas or hydrogen, to melt the coating material. Based on the form of the feedstock material, the process is divided into three subcategories: powder-, wire- or rod-flame spray. The schematic diagrams of the conventional flame spray using wire/rod and powder are presented in Fig. 5.

As it can be observed, in the case of wire and rod-flame spray, the coating material (wire or rod) is fed concentrically into the flame, where it is melt and atomized by adding the compressed air, that also drives the melted material against the workpiece surface. In powder flame spray, the coating material is a spray powder, which has the advantage of being available in a larger selection of spray materials, as compared to the wire and rod materials.

(b) *Electric arc wire spray* uses a low power electric arc formed between two oppositely charged metallic wires, usually having the same composition, leading to melting at the tip of the wires (Fig. 6). The compressed air atomizes the melted coating material, accelerating it against the substrate. The rate of spray is adaptable by proper adjustment of wire feed, as it is melted, so a constant arc can be managed.

A major advantage of the electric arc spray coating is that it produces the fastest coating rate of any thermal spray process. This technology is also the most

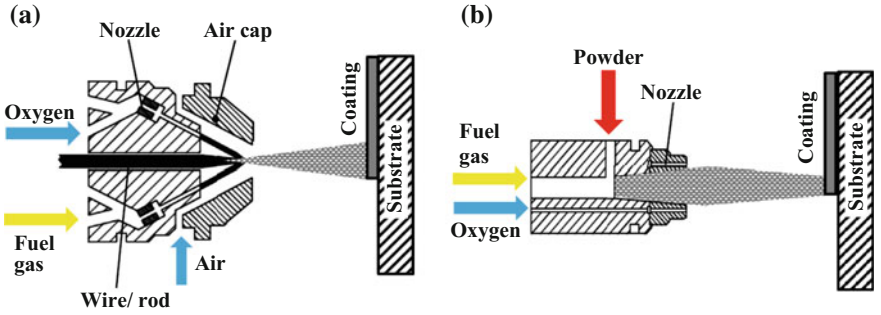

Fig. 5 Schematic diagrams of conventional flame spray process. **a** wire/rod-flame spray; **b** powder flame spray

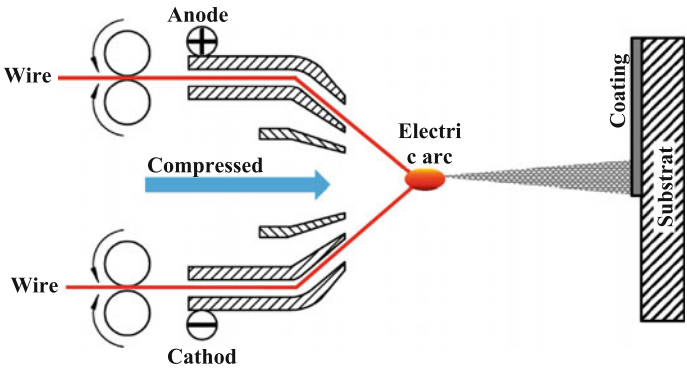

Fig. 6 Schematic diagram of electric arc wire spray process

thermally efficient, because there is no flame or plasma and, consequentially, an insignificant part of the associated heat is transferred to the substrate. The disadvantage of the method lies in the fact that it is limited to materials which are electrically conductive and can be produced into wires. Nevertheless, this inconvenience can be eliminated by incorporating the non-electrically conductive materials into the core of hollow conductive wires. Thus, materials such as carbides can be sprayed by electric arc using cored wires.

(c) *Plasma spray* is the most versatile of the thermal spray processes, being capable to deposit any material considered sprayable. The principle of the method is shown in Fig. 7.

As shown in the figure above, in the device, a high-frequency arc is formed between two electrodes (an anode and a tungsten cathode) in a plasma gas (mixture argon/hydrogen or argon/helium). The gas passing through the electrodes is ionized, creating a plasma plume with a length of several centimetres. Inside the plum, the temperature can reach about 16,000 K. As the gas mixture is heated by the

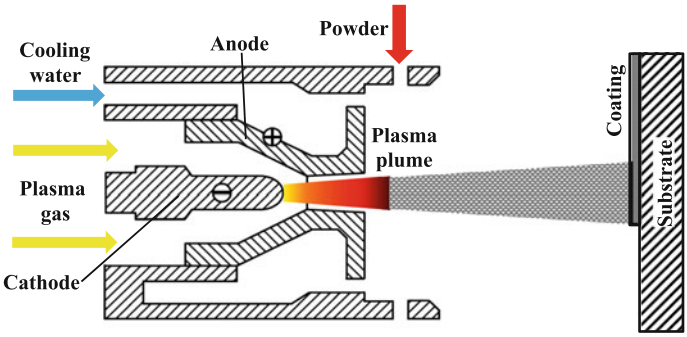

Fig. 7 Schematic diagram of the plasma spray technology

formed arc, it expands, being accelerated through a nozzle, creating velocities up to Mach 2. The coating material is added as powder from outside of the nozzle into the plasma plume, where it melts and it is then sprayed onto the workpiece surface.

Different nozzle designs and powder injection schemes, together with the ability to reach very high plasma temperatures, provide plasma spraying the possibility to use a very large range of coating materials. The options vary from materials with low melting temperatures, such as nylon, to materials with very high melting points, such as tantalum, tungsten, ceramic oxides or refractory materials. Being the most versatile of the thermal spray processes, plasma spraying is commonly used in a wide range of applications in industries such as agriculture, aerospace, automotive, medical devices.

(d) *High velocity oxy-fuel spray (HVOF)* is a relative new process among the thermal spray technologies. The procedure differs from conventional flame spray in that it uses confined combustion and an extended nozzle for heating and accelerating the powder coating material. Most of HVOF devices move the gas at velocities greater than Mach 5 (hypersonic speed). This high kinetic energy enables this technology to obtain very dense coatings (typically less than 0.5%), with a good adhesion. The principle of the method is shown in Fig. 8.

HVOF uses different types of gases, as propane, acetylene, propylene, natural gas and hydrogen, but also liquid fuels such as kerosene and diverse coating materials such as ceramics, stainless steel, Stelite® or Inconel®. This coating type is usually incorporated into the design of various parts, starting with simple components, like bolts for agriculture combines, and ending with very complex components, just as high-tech medical devices used in complex surgeries.

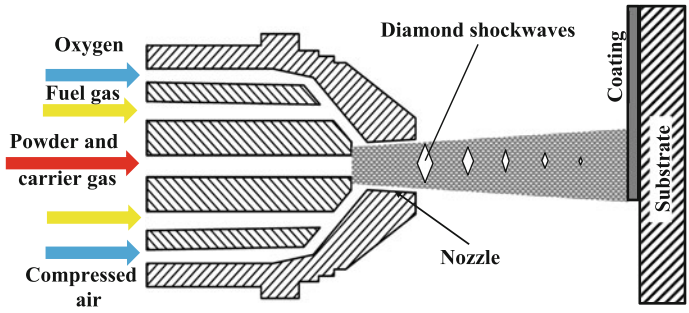

Fig. 8 Schematic diagram of the high velocity oxy-fuel spray process (HVOF)

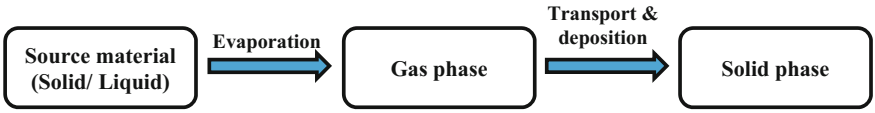

Fig. 9 Process flow diagram of PVD

4.4 Vapour Deposition (VD)

Vapour deposition (VD) refers to any process in which materials are reduced from gaseous to a liquid state by condensation or by a chemical reaction. These processes are carried out to obtain coatings for improving corrosion resistance and optical, thermal, electrical, mechanical and wear properties of the substrate. Vapour deposition processes are usually accomplished in a high-vacuum chamber, where the coating material is heated electrically and evaporated, and formed vapours being deposited on the surface to be coated.

The most common VD technologies are:

- Physical vapour deposition (PVD);
- Chemical vapour deposition (CVD).

(a) *Physical vapour deposition (PVD)* describes the process in which, first, a source material goes by evaporation from the solid or liquid phase to the vapour phase and, then, after transport and deposition, back, to a thin film condensed phase (see Fig. 9), which covers the entire surface of a workpiece, rather than just certain areas. The primary PVD methods are sputtering, evaporation, ion implantation, ion plating and laser surface alloying.

PVD is used to deposit thin films for mechanical, chemical, optical or electronic functions, such as for semiconductor devices, solar panels, food packing or cutting tools. The most common coating materials applied by PVD are titanium nitride (TiN), chromium nitride (CrN), zirconium nitride (ZrN) and titanium aluminium nitride (AlTiN).

Compared to other coating technologies, PVD has following advantages:

- PVD is more environment-friendly than traditional coating technologies, such as electroplating or painting.
- Ability to use a various range of organic and inorganic coatings on diverse substrates, using different finishing classes.
- A given film can be applied by more than one technique.
- PVD coatings are more corrosion resistant and harder than the coatings obtained by electroplating methods.
- Most of the PVD coatings maintain their strength at high temperature and under impact conditions.
- Excellent abrasion resistance and durability, so that protective topcoats are almost never necessary.

The method is associated with a few disadvantages too:

- The deposition rate is usually quite slow.
- PVD needs a cooling system to dissipate a large amount of heat.
- Some PVD technologies work at very high temperatures and vacuums, which require skilled operating personnel.
- The technology involves high capital costs.

(b) *Chemical vapour deposition (CVD)* was initially considered a subset of PVD, but over time, as new technologies have been developed, the distinction between CVD and PVD has blurred.

In typical CVD coating processes, reactive gases, often diluted in so called carrier gases, are brought at ambient temperature in a reaction chamber. This gas mixture is heated as it nears the workpiece surface which is placed upon a heated substrate. Depending on the operating conditions, the reactive gases may be subjected to homogeneous chemical reactions in the vapour phase before impacting the surface. Adjacent to the surface, momentum, thermal and chemical concentration boundary layers form as the gas flow heats, which then decrease due to viscous drag and the chemical composition changes. Heterogeneous reactions of the source gases occur at the workpiece surface, forming the coating deposition. During this process, volatile by-products, which are removed by gas flow through the reaction chamber, are also produced. The steps involved in the chemical vapour deposition process and a typical CVD reactor are shown in Fig. 10.

CVD is used to deposit various materials including carbide, nitride, oxynitride, titanium nitride, carbon or tungsten, in ways that traditional coating technologies are not capable of.

CVD has following advantages:

- The technology allows high purities and growth rates.
- The process is economical, since more parts may be coated at the same time.
- CVD can deposit materials which are hard to evaporate.

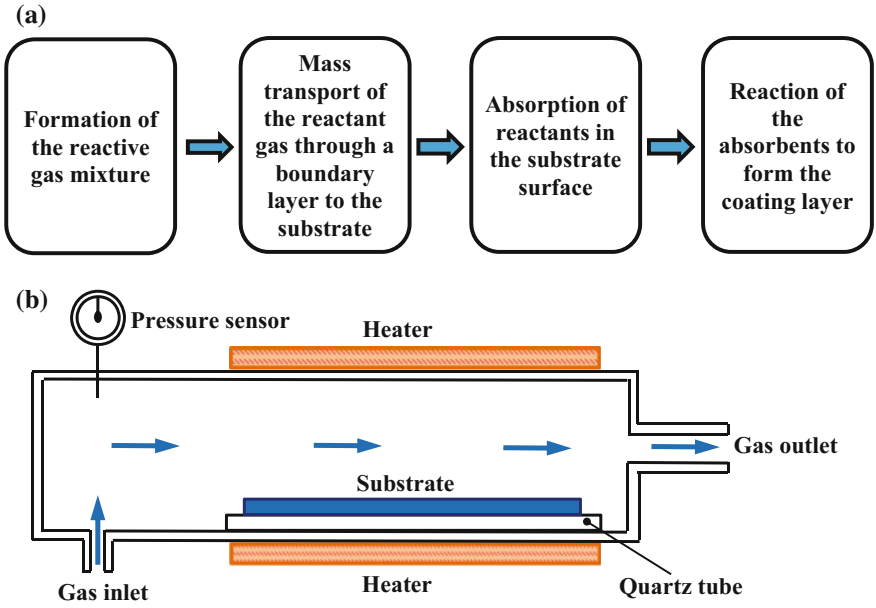

Fig. 10 **a** Process flow diagram of CVD and **b** typical CVD reactor

- The technology is versatile (any element or compound can be deposited) and has a good reproducibility.

Disadvantages may be mentioned as follows:

- The process is toxic and corrosive.
- CVD involves, as well as PVD, high temperatures.
- Being a complex process, it needs high-skilled operators.
- The start-up costs are high.

4.5 Cladding

Cladding is the process in which two different metals are bonded together. It is different from gluing or fusion welding, being achieved by extruding two metals trough a die or rolling two layers of different metals under high pressure. For example, an ordinary steel sheet is hot-rolled together with a thin nickel sheet for improving the properties of the steel substrate. Another example is that in which a high-strength aluminium alloy is often clad with a thin layer of commercial pure aluminium, in order to provide a corrosion barrier, because the alloy is vulnerable to stress corrosion. Materials such as aluminium, copper, nickel, titanium or stainless steel are the most common cladding materials used for steel.

This coating technology offers a high economic advantage by using, for example, for the construction of a high-pressure vessel, an inexpensive steel cladded with a relative thin layer of high-corrosion resistant material. In this case, the very high material costs, if the entire wall of the vessel would be made from corrosion resistant material, can be significantly reduced by using the cladded ordinary steel.

4.6 Fluoropolymer Coatings

A fluoropolymer is a chemical compound based in fluorocarbon which has many strong carbon-fluoride bonds. As the fluorine in a fluoropolymer is electrically negative, it provides the chemical compound the characteristic of not bonding lightly with other materials. This gives the fluoropolymers the non-stick property.

A fluoropolymer is an umbrella term which includes many products having trademarks like Algoflon®, Excalibur®, Fluon®, Kynar®, Maxcoat®, Solef®, Teflon® or Xylan®. Each of the above-mentioned brands represents a family of coatings specially designed to meet various engineering requirements, such as environment, expected loads, temperature, prescribed tolerances and other significant factors. For aesthetic or identification purposes, these fluoropolymer coatings are available in different colours.

The main features of the fluoropolymer coatings can be summarized as follows:

- coating thickness range: 5–20 μm;
- temperature range: −130–260 °C;
- hydrophobic surface;
- chemically inert;
- low friction coefficient;
- anticorrosive properties;
- wear resistant;
- flame retardant;
- electrically resistive;
- lower risk of hydrogen absorption, compared to electroplating coatings.

Fluoropolymer coatings are in a high demand for industrial applications because of the advantages they offer. Besides the advantages previously presented, fluoropolymers reduce the friction and increase the corrosion resistance, being suitable for the use at high temperatures, too. They are good insulators, meaning that they do not conduct electricity and also they do not absorb water. All these unique factors or combinations of them make fluoropolymer coatings ideal for use in automotive, aeronautics, electronics and many other applications.

Thus, in airplanes, fluoropolymer coatings are applied to the wiring insulation for protecting them and to reduce the fire risk. Furthermore, they are replacing cadmium in corrosive environments, by being applied on high use surfaces from

aircraft cabin interiors, actuators, gears, bearings, wheels or landing gear components.

A significant portion of high demand of fluoropolymer coatings comes also from the automotive industry, because they improve friction and help to treat corrosion of car parts. Lifespan of components like bearings and gears, which must withstand intensive wear and tear processes, can be significantly improved by applying fluoropolymer coatings. Pistons, cylinder blocks, cylinder liners, fuel pumps, engine block covers, swivels or splines are other automotive components whose lifetime can be extended by adopting this coating technology.

Fluoropolymers are also widely used in many other industrial settings, such as packing and printing factories. They use fluoropolymer coatings to apply thin protective layers on parts such as rolls, frames or ink trays. The coating prevents moving parts to stick to items that pass through and also make them easier to clean.

In medical and pharmaceutical applications, fluoropolymers are used to coat bone prostheses, turbo-molecular pumps, dental and pill moulds, mandrels, needles, scalpels, stents, surgical instruments and many other tools.

Even if the request for fluoropolymer coatings is already extensive, new uses and applications are constantly being developed, resulting in a continuous increase of the demand.

Without claiming to be presented all the painting techniques, Table 2 synthesizes the main advantages and disadvantages of the precision coating technologies summarized in the previous sections, enabling the reader to find the proper coating system for his application.

5 Precision Coatings—a Matter of Quality

Quality is most often defined as the sum of properties and characteristics that a product or service must have to meet all the requirements stipulated and assumed. In practice, the full potential of a special coating can be ensured only if the following conditions are simultaneously met:

- the coating materials have a proven quality;
- the necessary pretreatments of the substrate were properly fulfilled and controlled;
- the application method was correctly chosen, performed and checked.

Therefore, one of the most important aspects of special coating technologies involves an adequate quality control, in order to ensure the compliance with the requirements and the agreed specifications. The quality control activities may be divided into the following actions [9]:

(a) visual inspection;
(b) chemical composition;

Table 2 Advantages, disadvantages and typical application fields of the presented precision coatings

Coating technology	Advantages	Disadvantages	Typical applications
Electrochemical deposition	- versatile and inexpensive - low-temperature operating conditions - good corrosion resistance - improves the mechanical properties of the substrate	- non-uniform plating - time-consuming process - pollution potential - the electroplating solution has to be disposed safely after use	- car parts - bath taps - kitchen gas burners - wheel rims
Electroless plating	- method is suitable for non-metallic substrates - process does not require a DC power source - can be coated deeply recessed areas and parts with a complex geometry - uniform thickness of the coating	- limited lifespan of the chemicals - high cost of waste treatment due to speedy chemical renewal - porous nature of the plating, leading to inferior material structure	- aeronautics - car parts - food industry - cutting tools - chemical and oil industry - electronics (hard drive substrates, printed boards)
Thermal spraying			
Conventional flame spray	- simply in design and easy to operate - little operating training - dust, fume and noise level lower than at other thermal spraying processes - lower equipment costs compared to other thermal spraying processes	- high porosity (10-20 vol.%) - low density and high oxide level - very difficult to achieve deposition on inner surfaces - requires special health and safety measures	- repair procedures to restore components to their initial dimensions
Electric arc wire spray	- highest deposition rate of the thermal spraying processes - lower operating costs then plasma and HVOF spraying - low heating of the substrate	- very difficult to achieve deposition on inner surfaces - lower coating quality compared to plasma and HVOF spraying	- gas turbine components - textile machine components
Plasma spray	- higher quality compared to flame and electric arc spraying - wide range of coating materials - suitable for spraying of refractory metals	- equipment is not suitable for manual operating - inner electrodes of the spray gun need to be often replaced - high investment costs	- orthopaedic implants - paper industry (calendar rolls) - aluminium engine blocks

(continued)

Table 2 (continued)

Coating technology	Advantages	Disadvantages	Typical applications
High-velocity oxy-fuel spray (HVOF)	- high density and hardness - thicker coatings due to less residual stress	- requires qualified personnel - very difficult to achieve deposition on inner surfaces	- landing gears - jet engine components
Vapour deposition			
Physical vapour deposition (PVD)	- more environment-friendly than traditional coating technologies - ability to use a various range of organic and inorganic coatings on diverse substrates, using different finishing classes - a given film can be applied by more than one technique - more corrosion resistant and harder than the coatings obtained by electroplating methods - good strength at high temperatures and under impact conditions - excellent abrasion resistance and durability, so that protective topcoats are almost never necessary	- slow deposition rate - dissipates a large amount of heat - require skilled operating personnel - high capital costs	- cutting tools - automotive components - punching and forming tools - injection moulding tools - optical components
Chemical vapour deposition (CVD)	- high purities and growth rates - economical - can deposit materials which are hard to evaporate - versatile - good reproducibility	- toxic and corrosive -involves high temperatures - needs high-skilled operators - start-up costs are high	- forging tools - stamping tools - extrusion dies - semiconductors and related devices
Cladding	- material costs reduction - provides a good corrosion barrier		- high-pressure vessels - boiler tubes - pipelines - valve components
Fluoropolymer coating	- hydrophobic surface - chemically inert - flame retardant - low friction coefficient - good damping properties	- limited resistance to contact pressure	- automotive and aircraft components - fasteners - medical devices - pharmaceutical devices - gears and bearings

(c) thickness;
(d) porosity;
(e) adhesion;
(f) stress;
(g) ductility;
(h) strength;
(i) hardness;
(j) wear resistance.

The number and method of tests to be adopted depend on the coating material, the substrate characteristics and the deposition technology. Given the theme/scope of this chapter, some relevant aspects regarding precision control issues of the coatings are presented.

Hardness and thickness are important quality issues of each coating process, as they are significantly influencing not only the appropriate selection of the coating material, but also the longevity, the final texture of the surface and the final cost of the product.

5.1 Hardness Measurement

Hardness is the property of a material to resist against permanent deformations. In the coating industry, hardness measurements are performed to determine the resistance of the coating to wear and tear, to scratching or to find out if the coating is fully cured. Therefore, depending on the requirements and the type of the coating (metallic or non-metallic), various methods to test the coatings hardness are available.

For metallic coatings, the usual method to achieve the hardness value is to measure the area or the depth of an indentation left by an indenter having a specific shape, after applying a specific force, for a specific time period. There are four main scales for expressing the association between hardness and the size of the penetration, these being Brinell, Rockwell, Vickers and Knoop (for microhardness).

For non-metallic coatings, the following testing methods are being used in practice:

– pendulum test;
– Buchholz indentation test;
– pencil hardness test.

The pendulum hardness test evaluates the hardness by measuring the damping time of an oscillating pendulum. The testing method conforms to the standards ISO 1522 and ASTM D4366. Two types of pendulums (Koenig and Persoz) were standardized for this testing method.

The Buchholz indentation test method is applicable only on coatings with plastic deformation, consisting of a double con block, which is placed for 30 s on the

coating. The occurred indentation is measured with a precision microscope. The length of the indentation mark in the coating indicates the hardness of the coated surface. The method complies with the standard ISO 2815.

The pencil hardness test, also known as Wolff–Wilborn, is ideal for a quick evaluation of smooth coating surfaces, the hardness being evaluated with pencils in the hardness range of 8B to 10H, which are drawn over the coating surface, under a 45° angle with a constant pressure, in order to determine which pencil causes indentation. The testing method complies with the standards ISO 15184 and ASTM D3363.

As the hardness testing can directly affect the appearance of the part being evaluated, by causing unnatural imperfections on the evaluated surface, the measurement is regularly performed on coating samples.

5.2 Thickness Measurement

For reasons of functionality or economy, the coating thickness has to be precisely measured, in order to ensure the stipulated requirements. Together with the progress of various precision coating technologies, a variety of equipment and methods for testing the coatings thickness have been developed over the years. Most of them are non-destructive and cover a wide range of applications. These non-destructive methods are mostly used in commercial applications, while the destructive methods are rarely used outside the laboratories. As a single standard measuring procedure does not suite the measurement of all type of coating thicknesses, a basic understanding of these methods is essential when selecting the appropriate equipment.

(a) *Magnetic induction method* measures both non-magnetic coatings over metallic substrates and magnetic coatings over non-magnetic substrates, being ruled by the standards ISO 2178 and ASTM B499. The method is suitable for individual coating layer with thicknesses from 1 to 1000 μm and relative smooth surface.

Measurement principle of the method is graphically displayed in Fig. 11. As it can be observed, by placing the probe on the sample, the magnetic flux density of this field is modified either by the magnetic substrate or by the thickness of the magnetic coating. This change in the magnetic inductance is measured by a secondary coil, which is placed inside the probe. The output tension $U = f(\mathrm{Th})$ is transmitted to a microprocessor, where it is viewed on a display as a coating thickness (Th).

The method is quick and can be used for liquid or powder coatings, as well as cadmium, chrome or zinc plating applied on metallic substrates.

(b) *Eddy current method* is used to measure the thickness of electrically non-conducting coatings applied on non-magnetic metallic substrates, such as, for example, fluoropolymer applied on aluminium or copper. The method is ruled by the standards ISO 2360 and ASTM B244.

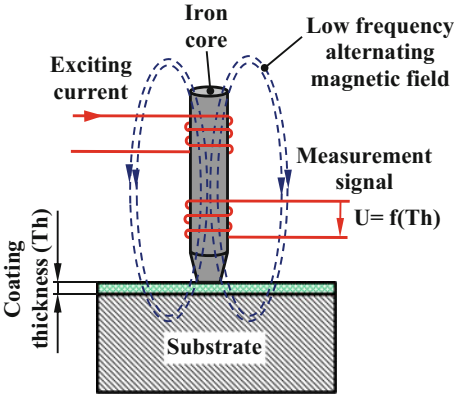

Fig. 11 Principle of magnetic induction method

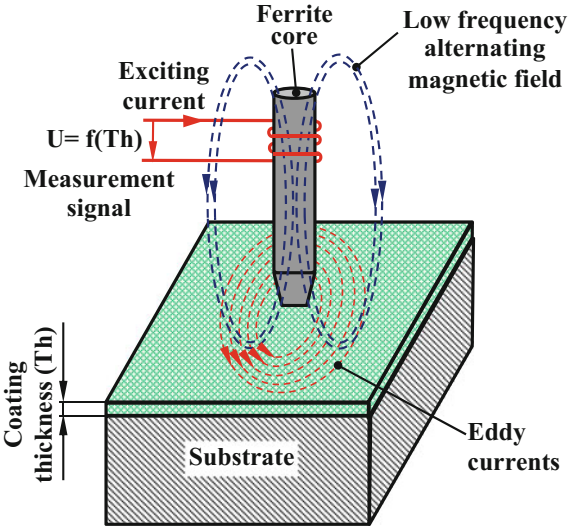

Fig. 12 Principle of eddy current method

The technique is similar to the previous one, quite often using the same probe design. As shown in Fig. 12, the probe contains only one coil, but this time it has a dual function: excitation and measurement. By bringing the probe close to the sample, eddy currents are generated in the metallic substrate, which will cause an impedance modification in the probe coil. This modification depends on the distance between the probe coil and the conductive substrate, i.e. the coating thickness. Measurement results are shown on a display, the typical tolerance being ± 1%.

(c) *X-ray fluorescence method* is a non-contact method used for measuring very thin multilayers of coatings applied on small substrates which have complex shapes. The standards ISO 3497 and ASTM B568 are regulating this procedure.

The method is performed by exposing the sample part to X-radiation, which is focused by a collimator onto an exactly defined surface of the part (Fig. 13).

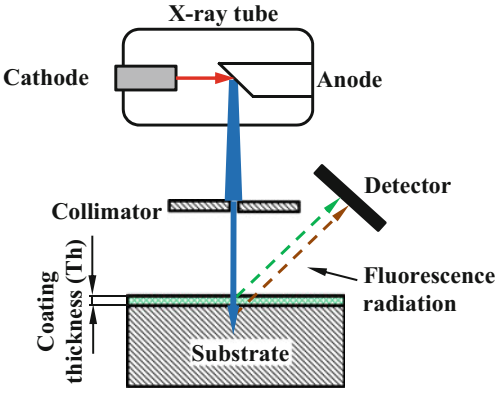

Fig. 13 Principle of X-ray fluorescence method

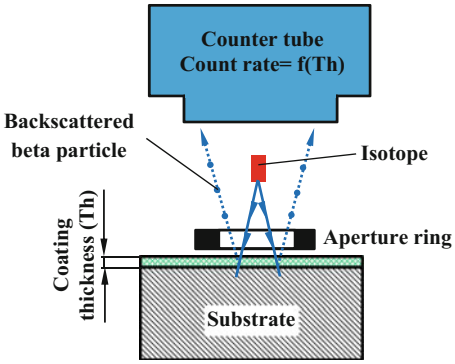

Fig. 14 Principle of beta backscatter method

This radiation is generating a characteristic X-ray fluorescence emission from both the substrate and the coating, which is identified by an energy-dispersive detector. The energy level or wavelength of the fluorescent X-rays is proportional to the atomic number of the material being specific for a particular substrate or coating. The amount of the released energy depends on the thickness of the coating being measured.

(d) *Beta backscatter method* uses a beam of beta particles from a beta-emitting isotope, which are directed through an aperture onto the test specimen. The particles penetrate the coating layer and are reflected back ("backscattered") towards the source, being collected and counted with a Geiger–Mueller tube for conversion to coating thickness. Measurement principle of the method is shown in Fig. 14.

The technique is in compliance with the standards ISO 3543 respective ASTM B5610 and is used to measure thicker coatings, where eddy current and magnetic induction methods are not suitable. Typical applications include thickness measurements of gold plating on nickel, silver on copper and titanium nitride (TiN) on steel.

6 Examples of Precision Coatings

Precision coating technologies have been significantly improved in the last decades, which allowed critical industrial parts to have a higher protection against failures and, consequentially, to prove a better reliability. Gears are critical parts to complex systems and machinery, and any unanticipated gear-related failure can cause interruptions in the work of the whole driving system, and generate thus auxiliary costs which are most often higher than the gear replacement cost. Therefore, the gear industry has also implemented gear coating technologies, for which a variety of coating methods and materials are used. Purposes for applying coatings on gears are various: lowering pitting and micropitting, preventing fatigue and corrosion, improving wear resistance, reducing friction respective decrease of vibration and noise levels. The following two sections are presenting two practical applications of gear coatings.

6.1 Effect of Tungsten Carbon Carbide (WC/C) Coating on the Wear Resistance of Gears

The tungsten carbon carbide (WC/C) is a metallic-hydrocarbon coating (Me–C:H), which is increasingly used in the gear manufacturing industry [10, 11]. These coatings are applied using a PVD technology, which permits the coating and the substrate to reach temperatures below 200 °C, making this deposition process suitable for case-hardened gears too. Usually, the coating has a thickness in the range 1–4 μm.

The purpose of this section is to present the results of research regarding the effect of a WC/C coating on the wear resistance of gears. The main properties of this coating type are presented in Table 3.

In this research [12], first a gear pair with uncoated teeth was checked, and then a WC/C coating with a thickness of about 2 μm was deposited on the teeth of the gearwheel. The testing (with coated and uncoated gears) was performed both on a laboratory back-to-back test rig, under dip lubrication conditions, and also using an industrial gear stand (chain conveyor).

During the tests, the loading torque was sequentially increased, covering 12 load stages. After running the test at a certain load stage, the teeth of the pinion were checked against scuffing. Afterwards, the load was increased to the next stage, and the test was run for the same specific duration (= 15 min). The load stage at which the first signs of scuffing have appeared is designated as “Failure Load Stage” (FLS) and describes the resistance against scuffing of the investigated gears.

During the laboratory test, it was observed that the uncoated gears showed a scuffing resistance corresponding to FLS = 8, while the WC/C coating significantly improved the scuffing resistance of the tested gears to FLS = 10. It was also noticed

Table 3 Main properties of PVD coating WC/C

Microhardness	1000–2200 HV
Maximum working temperature	400 °C (750 °F)
Friction coefficient against steel	0.2–0.25
Coating thickness	1–4 μm
Colour	charcoal
Low-temperature method	available
Main areas of use	- reduced friction when elements move against each other - precision components - punching and metal forming - plastic injection moulding

that the measured oil temperatures were significantly lower during the tests performed with the coated gearwheel, than in case of testing uncoated gears.

The improved scuffing resistance of the pinion when driving with the WC/C coated gearwheel was attributed to a smaller affinity by using different kinds of materials, than when both of them were identical (i.e. uncoated). Another conclusion of the study was that, if one of the gears (the coated gearwheel) is much harder than the matting part (pinion of case-hardened steel), there is a reduction in the friction tendency and adhesive bonding, thus scuffing. The same effect was observed when testing bevel gears and spur gears [12, 13].

Similar results were obtained by using the industrial gear stand (chain conveyor). It was concluded that the investigated gear coating can be applied to increase the wear resistance and to reduce the oil temperature in the transmission, resulting thus in improved reliability of the gears.

6.2 Fluoropolymer Coating of Gears for Noise Reduction

Along with the economic development, noise levels have become an important factor when determining quality of life [14]. High levels of noise can cause not only hearing loss, but also reduced concentration, having a direct effect on decreasing productivity and raising the risk of accidents. For this reason and given that employees tend to spend more time at work then in previous years, in many visited sites, including the workplaces, maximum levels of noise have been imposed.

Gearboxes are widely used in mechanical systems for transferring rotation into a wide range of conditions and with different transmission ratios. In these transmissions, gear meshing is a complex process involving vibration and noise emission. Therefore, in the last decades, a significant number of researchers have investigated the possibilities to reduce the noise level associated with the gears.

A special method of reducing the intensity of the sound field generated by gears consists of applying precision coating on the teeth flanks. These coatings are made of complex metal alloys or polymeric materials.

This section aims to present the results of research conducted on reducing the noise level of gears, by applying a fluoropolymer coating of Xylan 1052 (produced by Whitford Plastics Ltd, U.K.), on the teeth flanks. Two layers of coating, each having a thickness of 12–20 μm, were applied on the gears flank surfaces. The coating technology is described in detail in [14, 15] and consists essentially in following operations:

- degreasing of the gears;
- blasting of the teeth flanks;
- degreasing;
- application by spraying of the first coating layer;
- drying;
- inspection of the first coating layer;
- application by spraying of the second coating layer;
- drying;
- inspection of the second coating layer;
- crosslinking heat treatment of the coating;
- final inspection.

For a better visual perspective regarding this coating technology, Fig. 15 shows the comparison between coated and uncoated pinions, and gearwheels, respectively.

The research was performed on an earlier developed test rig [16], with an open energy circuit, where a hydraulically pump was adopted as a break; for load variation, a spherical valve mounted on the pressure pipe of the pump was used.

Results showed that, by applying this coating technology, the noise produced by a gearbox can be reduced, on average, and corresponding to the sound pressure level (SPL) values, by 7.76 dB, which represents 11.25% from the initial level of noise [14]. This fact implies a lower risk of exposure to noise pollution for the workers who operate the gearboxes.

The obtained noise reduction was attributed to the following parameters:

- improvement of the teeth flank roughness;
- an additional damping during the gear meshing process, facilitated by the applied fluoropolymer layers;
- a reduction of friction during the teeth meshing.

Besides noise reduction, the fluoropolymer coating of gears has another significant benefit: it can be used both on new surfaces and on worn out ones. Therefore, this coating technology can be applied for salvage purposes in the case of used gears or to recondition undersized respective worn parts.

Fig. 15 Coated and uncoated pinions and gearwheels [15]

7 Summary

- The coating process refers to covering the surfaces of an object referred to as the substrate and has a protecting scope against the direct and indirect costs of corrosion.
- The main functions of coatings are substrate protection, improving the wear resistance as well as the friction, sealing, changing adhesion properties, reducing vibration and noise levels, thermal insulation and facilitating optical, magnetic or electrical properties.
- Coating technologies are available in a wide range, being classified depending on the substrate on which the coating is applied, as well as on the material applied on the substrate (metallic vs. non-metallic), but also according to the chemical composition of the applied metallic material and the technological process used for covering the substrate.
- A variety of precision coating technologies are available for different applications. Electrochemical deposition requires a metal solution to be applied on a metallic substrate based on the Faraday laws. Electroless plating comes with a few advantages over the electrochemical deposition, such as suitability for both metallic and non-metallic substrates, but also disadvantages, for example, high cost of treatment. Thermal spraying involves applying any melted material which does not decompose during melting (i.e. pure metals, carbides, ceramics)

on a prepared surface. The substrates as well as the coating material vary depending on the spraying technology. Through vapour deposition, the substrate is coated using materials which are reduced from gaseous to liquid state, the most common technologies being physical or chemical vapour deposition, both of which present specific advantages as well as disadvantages. Two additional technologies are cladding, the process through which two metals are bonded together and fluoropolymer coating, a popular choice which holds a large number of advantages.

- Coating technologies having diverse industrial applications undergo a quality control process, which influences the appropriate selection of the coating material, as well as the longevity, the texture or the coated surface, and the associated costs. Hardness and thickness of the coating material represent two important quality issues.
- The tungsten carbon carbide (WC/C) coating and the fluoropolymer coating of gears are given as practical examples of precision coatings which prevent fatigue and corrosion, reduce friction and decrease the gear's vibration and noise levels.

References

1. Lambourne R, Strivens TA (1999) Paint and surface coatings. Theory and practice. Second Edition, Woodhead Publishing Ltd, Cambridge
2. Hays GF (2010) Now is the time. World Corrosion Organization. NACE Europe Board, CORRODIA, Fall 2010, available at: http://corrosion.org/wco_media/nowisthetime.pdf
3. Schmitt G et al. (2009) Global needs for knowledge dissemination, research, and development in materials deterioration and corrosion control. World Corrosion Organization, available from: http://corrosion.org/wco_media/whitepaper.pdf
4. Grainger S, Blunt J (1998) Engineering coatings: design and application, 2nd edn. Woodhead Publishing Ltd, Cambridge
5. Gamburg YD, Zangari G (2011) Theory and practice of metal electrodeposition. Springer, New York, Dordrecht, Heidelberg, London
6. Fauchais PL, Heberlein JVL, Boulos MI (2014) Thermal spray fundamentals. Springer, New York, Heidelberg, Dordrecht, London
7. Pratap B, Bhatt V, Chaudhary V (2015) A review on thermal spray coating. Int J Sci Eng Res 6(5):53–59
8. Fauchais PL, Vardelle A (2012) Thermal sprayed coatings used against corrosion and corrosive wear, advanced plasma spray applications In: Jazi H (ed), Tech, available from: http://www.intechopen.com/books/advanced-plasma-spray-applications/ thermal-sprayed-coatings-usedagainst-corrosion-and-corrosive-wear
9. Tracton AA (2007) Coating technology: fundamentals, testing and processing techniques. CRC Press, Taylor & Francis Group L.L.C., Boca Raton, London, New York
10. Krzan B (2016) Load-carrying capacity of WC/C-coated gears lubricated with a low-viscosity oil. Lubr Sci 28(3):127–139
11. Fujii M, Ski M, Yoshida A (2010) Surface durability of WC/C-coated case-hardened steel gear. J Mech Sci Tech 24(1):103–106
12. Tuszynski W et al (2015) The Effect of WC/C coating on the wear of bevel gears used in coal mines. Mater Sci 21(3):358–363

13. Tuszynski W et al (2012) A New scuffing shock test method for the determination of the resistance to scuffing of coated gears. Arc Civil and Mech Eng (ACME) 12:436–445
14. Korka Z, Gillich GR, Mituletu IC, Tufoi M (2015) Gearboxes noise reduction by applying a fluoropolymer coating procedure. Environ Eng Manage J 14(6):1433–1439
15. Korka Z (2009) Cercetari privind reducerea vibratiilor in functionarea reductoarelor cu roti dintate cilindrice (Research on reducing the vibration of cylindrical gearboxes). PhD Thesis. "Eftimie Murgu" University of Resita
16. Korka Z, Vela I (2008) Design and execution of a test rig for studying the vibrations of a gearbox. Annals of "Eftimie Murgu" University of Resita, Eng Fascicle 15(1): 134–140

Erratum to: Nano-Machining, Nano-Joining, and Nano-Welding

Kush Mehta, Munish Gupta and Priyaranjan Sharma

Erratum to:
Chapter "Nano-Machining, Nano-Joining, and Nano-Welding" in: K. Gupta (ed.), *Micro and Precision Manufacturing*, Engineering Materials,
https://doi.org/10.1007/978-3-319-68801-5_4

In the original version of the book, the incorrect author name "Priyanranjan Sharma" has been corrected to read as "Priyaranjan Sharma" in Chapter "Nano-Machining, Nano-Joining, and Nano-Welding" and TOC, which is a belated correction.

The updated online version of this chapter can be found at
https://doi.org/10.1007/978-3-319-68801-5_4

K. Gupta (ed.), *Micro and Precision Manufacturing*, Engineering Materials,
https://doi.org/10.1007/978-3-319-68801-5_9

Index

K. Gupta (ed.), *Micro and Precision Manufacturing*, Engineering Materials,
https://doi.org/10.1007/978-3-319-68801-5